Cobalt toxicity mechanisms in neural cells and brain tissue: understanding the implications for patients with cobalt-chromium alloy orthopaedic implants

A thesis submitted in partial fulfilment of the requirements for the degree of Doctor of Philosophy at the Department of Biomedical Engineering University of Strathclyde

by

Sara Gómez-Arnaiz

2022

Declaration of Authenticity and Author's Rights

This thesis is the result of the author's original research. It has been composed by the author and has not been previously submitted for examination which has led to the award of a degree.

Signed: 

Date: 8 December 2022

Previously Published Material

This thesis contains previously published material from the paper referenced below. The thesis has been authored by the same first author, Sara Gómez-Arnaiz. The first author performed the experiments and wrote the papers. M. Helen Grant and Rothwelle J. Tate assisted with the design of experiments, as well as with corrections to the final manuscripts as PhD supervisors:

Gómez-Arnaiz, S., Tate, R.J., Grant, M.H., 2020. Cytotoxicity of cobalt chloride in brain cell lines - a comparison between astrocytoma and neuroblastoma cells. Toxicology *In Vitro* 68, 104958. https://doi.org/10.1016/j.tiv.2020.104958

Gómez-Arnaiz, S., Tate, R.J., Grant, M. H., 2022. Cobalt Neurotoxicity: Transcriptional Effect of Elevated Cobalt Blood Levels in the Rodent Brain. Toxics, 10(2), 59. https://doi.org/10.3390/toxics10020059

Abstract

The most recent regulatory update on metal-on-metal (MoM) hip replacements (MDA/2017/018, 2017) has resulted in the monitoring of cobalt and chromium levels in circa 60,000 UK patients for signs of prosthesis failure and local toxicity (Matharu et al., 2018). Multiple medical reports have implicated cobalt in systemic toxicity in prosthetic patients. The consequences of elevated levels of cobalt range from severe cardiac symptoms to diverse neurological complications. In this thesis we have studied the consequences of systemic cobalt toxicity, aka cobaltism, with specific focus on the effect of cobalt in the brain through *in vitro* and *in vivo* studies.

We compared the effect of cobalt *in vitro* in neuroblastoma and astrocytoma cells via MTT and Neutral Red (NR) viability test and BrdU proliferation assay. The IC50s obtained indicated that the stalling of DNA synthesis preceded impaired viability. Cobalt effects in both cell lines was dose-dependent as measured by ICP-MS. Neurons appeared to be significantly more sensitive than astrocytes to the same cobalt doses. These investigations revealed cobalt to be toxic at very high concentrations (>100μM) *in vitro* after 24-72h treatment.

For *in vivo* rat dose and time-response experiments, rodents were injected i.p. with daily cobalt doses. Cobalt significantly accumulated in the hippocampus and pref. cortex of rats after 28 days treatment with 0.5 and 1m/kg B.W. $CoCl_2$. Through RNA-Seq of brain areas we identified a possible metal homeostasis dysregulation. Additionally, the transcripts of several metal-binding protein families such as nuclear receptors, cytochrome P540, carbonic anhydrases and phosphodiesterases were regulated. Mainly, RNA-Seq data showed choroid plexus transcripts, as well as changes in hormone and lipid metabolism. However, target protein levels did not follow gene expression fold change. Our research has found that the choroid plexus is an important target of cobalt toxicity in the rat brain with cobalt levels in blood similar to those of some MoM patients (4-38μg/l). Moreover, we developed new hypotheses about the mechanisms of cobalt toxicity which could be directly investigated in patients and contribute towards finding biomarkers of cobaltism.

Acknowledgments

I would like to thank my supervisors Prof Helen Grant and Dr Rothwelle Tate for giving me the opportunity to do a PhD and their unwavering support throughout these years. They have taught me science, been patient and understanding of my mistakes, and given me the confidence to take a leap into challenging research jobs. Their very generous references have opened me the door to pursue a career in neuroscience. I will forever be thankful to them, and I wish to reflect to others some of the enormous expertise and kindness they have shown me. There is now a part of my brain occupied by Helen's good advice and calming "it will be fine", and Roth's encouraging words and sense of humour. I consider myself very lucky to have had them as supervisors. I will keep them both close to my heart as my life mentors.

I am also deeply grateful to Katie Henderson, the soul of the lab. I wish every new PhD student could have someone as kind and intelligent as her to be introduced and guided through the multiple protocols and molar calculations they will face.

I would like to acknowledge the funders of my PhD, the University of Strathclyde Faculty of Engineering through the Engineering the Future Scholarship, as well as the Women in Science and Engineering studentship.

I would also like to thank my colleagues and good friends, Sarunya Laovitthayanggoon (Pae), Ibrahim Alanazi, Laura Beattie and Rachael Pirie. I wish Pae's and Ibrahim's stay in Scotland would have been longer than the duration of their PhDs as their company made every day in gloomy Glasgow so much brighter. I am glad that my initial admiration for my now buddy Pae became such a great friendship. She helped me in many experiments, and I learnt so much from her hands-on attitude. My friend Ibrahim was an invaluable emotional support. I also shared so many good times with Laura and Rachel, who are incredibly supporting and a great laugh. I treasure our cake celebrations in Helen's office with all the members of our team.

I am also grateful to my patient partner, Ian Holland, who has encouraged me during my experiments, particularly the ones that failed, as well as during the writing of this

manuscript. I would finally like to thank my family in Spanish so that this thesis contains something for them. Agradezco a mis padres, Miguel Ángel y Mari Flor, la libertad que me dieron para seguir un camino que me ha llevado lejos de ellos. A mis hermanos, Irene y Miguel, por su apoyo durante este tiempo. Quiero agradecer también su amistad y escucha a Blanca, Corina, Clara, Alba, Alicia y Olaia. Finalmente, me gustaría dedicar los esfuerzos de esta tesis a mis abuelos, Sara, Casimiro, Pilar y Sabiniano, a quienes admiro y que deseo estén orgullosos.

Contents

Declaration of Authenticity and Author's Rights 2

Previously Published Material 3

Abstract 4

Acknowledgments 5

Contents 7

List of Abbreviations 12

List of Tables 16

List of Figures 18

1. INTRODUCTION 22

1.1. Hip implant surgery 22

1.2. Motivation of this research 25

1.3. Systemic toxicity 26

1.3.1. A brief history of cobalt exposure 26

1.3.2. Cobalt systemic symptoms 28

1.3.3. Cobalt neurotoxicity 31

1.4. Current status of cobalt toxicity research in the brain 32

1.5. Experimental approach and model considerations 34

1.5.1. *In vitro* models: neuroblastoma and astrocytoma 34

1.5.2. *In vivo* rodent model: anatomy and function of the rodent brain 36

1.6. Potential role of chromium in the development of systemic toxicity 37

1.7. Immunogenic reactions to metal debris 40

1.8. Objectives of the present research 43

1.9. Thesis structure 44

2. IN VITRO METHODS 45

2.1. Cell cultures 45

2.2. MTT viability assay 45

2.3. Neutral Red (NR) viability assay 46

2.4. Proliferation assay 46

2.5. Calculation of IC50 values 46

2.6. Live/dead staining assay 47

2.7. Brightfield microscopy 47

2.8. Cellular cobalt uptake measured by ICP-MS 47

2.9. Statistics 48

3. IN VIVO MATERIALS AND METHODS *49*

3.1. Experimental animals and housing 49

3.2. Experimental design: control, treatment groups and sample sizes 49

3.3. Preparation of cobalt solutions and treatment of rats 50

3.4. Sacrifice of animals and tissue harvest 51

3.5. Tissue cobalt content measured by ICP-MS 54

3.6. RNA extraction and preparation for RNA-Seq and RT-qPCR analyses 54

3.6.1. Isolation of RNA 54

3.6.2. Quality check of RNA samples 55

3.7. RNA Sequencing (RNA-Seq) 55

3.7.1. Sample pooling for RNA-sequencing 55

3.7.2. RNA-Sequencing analysis by BGI 56

3.7.3. Gene Ontology (GO) and KEGG Pathway enrichment analysis 56

3.7.4. Identification of Differentially Expressed Genes (DEGs) and hierarchical clustering 57

3.8. Quantitative real-time polymerase chain reaction (RT-qPCR) 57

3.8.1. cDNA synthesis 58

3.8.2. Gene primer design 59

3.8.3. Performing PCR 62

3.8.4. Relative gene expression calculations 63

3.9. Protein immunoblotting 64

3.9.1. Lowry assay for determination of protein content 64

3.9.2. Protein sample preparation 65

3.9.3. SDS- Polyacrylamide Gel Electrophoresis (PAGE) 65

3.9.4. Western blotting 66

3.9.5. Western blot band signal analysis 68

3.10. Statistics 68

4. AN IN VITRO STUDY INTO COBALT TOXICITY IN BRAIN CELLS ***69***

4.1. Introduction 69

4.2. Results 71

4.2.1. Cobalt is toxic at high concentrations in *in vitro* viability tests 71

4.2.2. Proliferative activity is affected prior to MTT and NR viability 78

4.2.3. Cobalt induces vacuolisation of cytoplasm and cell death 82

4.2.4. Cobalt uptake is dose-dependent 85

4.3. Discussion 87

4.3.1. ROS and Hypoxia: partners in crime in cobalt toxicity 87

4.3.2. Cobalt alters metabolism. Implications for a demanding brain 88

4.3.3. Cobalt-induced DNA damage 92

4.3.4. Cobalt-induced cell death and calcium buffering - cobalt as a Trojan Horse 93

4.3.5. Cobalt uptake in CNS cells and differential resistance of neurons and astrocytes. 95

4.3.6. Limitations and recommendations for future research 97

4.4. Summary of Results 100

5. IN VIVO TIME-RESPONSE INVESTIGATION INTO COBALT TOXICITY ***101***

5.1. Introduction 101

5.2. Results 102

5.2.1. Body weight in control and treatment groups may vary with cobalt treatment 102

5.2.2. Cobalt accumulates in organs and in different brain structures 106

5.2.3. Accumulated cobalt induces a genetic response 111

5.2.4. Transcriptional changes in the cortex and cerebellum demonstrate a tissue-specific response 113

5.2.5. Common metal homeostasis dysregulation at the molecular level might underlie changes in biological processes 117

5.2.6. Divalent metal transporters: genetic regulation indicates ion competition 121

5.2.7. Metalloproteins could be targeted by cobalt: phosphodiesterase and carbonic anhydrase families 124

5.2.8. RT-qPCR *Pde* and *Car* gene expression follows RNA-Seq results 128

5.3. Discussion 133

5.3.1. Cobalt could influence body weight 133

5.3.2. Metal distribution pattern is consistent with previous research and cobalt accumulates significantly on the brain 134
5.3.3. Moderate transcriptional response to the accumulation of cobalt 140
5.3.4. Cobalt leads to tissue-specific transcriptional changes in the pref. cortex and cerebellum 140
5.3.5. Cobalt could alter metal homeostasis in the brain 142
5.3.6. Transporters as the main doors for cellular uptake 143
5.3.7. Hypothesis for a modified metalloenzyme activity 145
5.3.8. Limitations and recommendations for future research 147

5.4. Summary of Results 149

6. IN VIVO DOSE-RESPONSE INVESTIGATION INTO COBALT TOXICITY 151

6.1. Introduction 151

6.2. Results 152

6.2.1. Body weight gain might decline with increasing cobalt doses 152
6.2.2. Organ weight ratios do not change with cobalt dosage 155
6.2.3. Cobalt organ content increases significantly with higher doses of cobalt 156
6.2.4. The transcriptional response to the cobalt doses selected is non-proportional 162
6.2.5. Gene expression validated by RT-qPCR 183
6.2.6. Protein levels of target genes do not change significantly with cobalt treatment 187

6.3. Discussion 191

6.3.1. Could cobalt modulate weight gain or loss in patients? 191
6.3.2. The low range cobalt dosage used does not lead to a dose-response 196
6.3.3. What are the overall transcriptional effects of cobalt? 198
6.3.4. The choroid plexus as a target of cobalt toxicity 205
6.3.5. Validation of protein and gene expression in response to cobalt 210
6.3.6. The nucleus, a besieged organelle? 215
6.3.7. What we could not find: hypoxia and mitochondrial markers 221
6.3.8. Future work and recommendations 223

6.4. Conclusion 226

7. SUMMARY OF RESULTS AND FUTURE RESEARCH 228

7.1. Main *in vitro* and *in vivo* findings on cobalt toxicity in this thesis. 228

7.1.1. *In vitro* findings on brain cells exposed to cobalt 228
7.1.2. *In vivo* findings from time and dose-response rodent models of cobalt toxicity 230

7.2. Limitations of our research on systemic cobalt toxicity, and future directions. 234

7.3. Significance of our research for patients with MoM implants and arthroprosthetic cobaltism 241

References* *245

Appendices* *291

Appendix A: RNA quality of samples obtained from brain tissue 291

Appendix B: Selection of reference genes for the normalisation of target gene expression through RT-qPCR 300

Appendix C: MIQE checklist 305

Appendix D: Pathway mapping of genes obtained with PathView software 310

Appendix E: Comparison of number of DEGs with different cutoff values 314

List of Abbreviations

ALVAL	Aseptic lymphocyte-dominated vasculitis-associated lesion
ANOVA	Analysis of variance
ARMD	Adverse reactions to metal debris
ASR™	Articular Surface Replacement™
BBB	Blood-brain barrier
bp	Base pairs
BP	Biological Process
BPU	Biological Procedures Unit
BrdU	Bromodeoxyuridine
BSA	Bovine serum albumin
BW	Body weight
C.P.	Cardiac puncture
Ca	Carbonic anhydrase
Ca^{2+}	Calcium
cAMP	cyclic-Adenosine monophosphate
CC	Cellular component
cDNA	complementary DNA
CFDA	Carboxyfluorescein diacetate
cGMP	cyclic-Guanosine monophosphate
CNS	Central nervous system
Co	Cobalt
CO_2	Carbon dioxide
Co^{2+}	Cobalt
CoC	Ceramic-on-ceramic
$CoCl_2$	Cobalt chloride
CoCr	Cobalt Chromium
CoM	ceramic-on-metal
CoP	ceramic-on-polyethylene
CP-GluARs	Ca^{2+}-permeable AMPA receptors
Cr	Chromium
CSF	Cerebrospinal fluid

Ct	Cycle threshold
CYP	Cytochrome P450
DEG	Differentially expressed gene
DEPC	Diethyl pyrocarbonate
dH_2O	Distilled water
DMEM	Dulbecco's modified Eagle's medium
DMSO	Dimethyl sulfoxide
DNA	Deoxyribonucleic acid
DTH	Delayed-type hypersensitivity
ECACC	European collection of cell cultures
ECL	Enhanced chemiluminescent
ELISA	Enzyme-linked immunosorbent assay
EPO	Erythropoietin
FBS	Fetal Bovine Serum
Fig.	Figure
gDNA	Genomic DNA
GO	Gene Ontology
HIF-1α	Hypoxia-inducible factor alpha
i.p.	Intra-peritoneal
IC50	Half maximal inhibitory concentration
ICP-MS	Inductively coupled plasma mass spectrometry
IL6	Interleukin-6
In	Indium
kDa	Kilodalton
KEGG	Kyoto Encyclopedia of Genes and Genomes
MDA	Medical Device Alert
MF	Molecular function
mg/kg	Milligrams per kilogram
MHRA	Medicines and Healthcare products Regulatory Agency
MIQE	Minimum Information for Publication of Quantitative Real-Time PCR Experiments
mM	Millimolar
MoM	Metal-on-metal
MoP	Metal-on-polyethylene

mRNA	messenger RNA
MTT	3-(4,5-Dimethylthiazol-2-yl)-2,5-Diphenyltetrazolium Bromide
NCBI	National Center for Biotechnology Information
NEAA	Non-essential amino acids
ng/g	Nanograms per gram
NHS	National Health Service
NJR	National Joint Registry
NMDA	N-methyl-D-Aspartate
NO	Nitric oxide
NR	Neutral red
p	p-value (calculated probability)
P/S	Penicillin-Streptomycin
PAGE	Polyacrylamide gel electrophoresis
PBS	Phosphate buffer saline
PCR	Polymerase chain reaction
PDE	Phosphodiesterase
PI	Propidium iodide
PKA	cAMP-Protein kinase A
PKG	cGMP-Protein kinase G
ppb	Parts per billion
PPI	Protein-protein interaction
Pref. cortex	Prefrontal cortex
RNA	Ribonucleic acid
RNA-Seq	RNA sequencing
ROS	Reactive oxygen species
RT	Reverse transcriptase
RT-	No-reverse transcriptase control
RT-qPCR	Quantitative real-time polymerase chain reaction
RT+	Plus-reverse transcriptase
Sc	Scandium
SD	Sprague Dawley
SDS-PAGE	Sodium dodecyl sulfate-polyacrylamide gel electrophoresis
SEM	Standard error of the mean
SH-SY5Y	SH-SY5Y neuroblastoma cell line

THR	Total Hip Replacement
Tm	Melting temperature
TNFα	Tumor Necrosis Factor alpha
TRP	Transient Receptor Potential
U-373 MG	U-373 MG astrocytoma cell line
UoS	University of Strathclyde
v/v	Volume by volume
w/v	Weight by volume
WB	Whole blood
µg/g	micrograms per litre
µg/l	micrograms per litre (equivalent to parts per billion, ppb)
µl	microlitre
µM	micromolar

List of Tables

Table 1: Criteria for the design of the primers selected through NCBI Primer-BLAST tool. 59
Table 2: Primer sequences of prefrontal cortex and cerebellum-targeted genes designed for the in vivo time-response experiment. 60
Table 3: Primer sequences of prefrontal cortex-targeted genes designed for the in vivo dose-response experiment. 61
Table 4: Primer sequences of Hippocampus-targeted genes designed for the in vivo dose-response experiment. 61
Table 5: Fast PCR thermal cycling steps based on PowerUp™ SYBR™ Green Master Mix instructions for StepOnePlus Real-Time PCR system. 63
Table 6: Primer sequences of control genes, with gene symbol, accession number, amplicon length and calculated primer melting temperature (Tm) as supplied by NCBI Primer-BLAST. 64
Table 7: Resolving and stacking gel volumes for SDS-PAGE. 66
Table 8: Antibodies used and their characteristics (biological host, supplying company, clonality), as well as their dilution and predicted band size (kDa). 67
Table 9: IC50s of MTT and NR assays calculated as 50% of the control from trend-line equations at 24h, 48h, and 72h. 75
Table 10: Cobalt content values (ng/g) in heart, liver, kidney, lung, spleen and testes, as well as blood (μg/l) obtained from ICP-MS analysis. 107
Table 11: Cobalt content values (ng/g) in pref. cortex, cerebellum and hippocampus obtained from ICP-MS analysis. 108
Table 12: List with common DEGs between pref. cortex and cerebellum classified through hierarchical clustering ($|\log_2 Ratio| \geq 2$ and $p<0.05$). 115
Table 13: Summary of metalloprotein families within each of the ligand-associated child GO terms obtained from the significant GO term 'GO: metal ion binding' ($p<0.001$). 125
Table 14: Fold change in expression between the treated and untreated rats. 132
Table 15: Cobalt concentrations of whole blood (WB), brain and heart tissues in our research and another study that mimics gradual cobalt release 139
Table 16: ICP-MS cobalt analyses of heart, liver, kidney, lung, spleen, testes, and blood. 158
Table 17: Cobalt brain content of the pref. cortex, cerebellum, and hippocampus (ng/g) from ICP-MS metal content analyses. 159
Table 18: Gene Ontology (GO) enrichment of DEGs obtained from RNA-Seq analysis of the pref. cortex, cerebellum and hippocampus of rats treated with i.p. injections of 0.1, 0.5 or 1 mg/kg B.W. $CoCl_2$ during 28 days. 171
Table 19: Enriched GO terms obtained from DEGs of pref. cortex and hippocampus in response to cobalt treatment with 0.5 and 1 mg/kg B.W. $CoCl_2$ compared to control animals (dH_2O). 176

Table 20: Fold change (linear scale) gene expression of treated rats (n=4) compared with control group (n=4; dH_2O) after 28 days cobalt treatment with 1 mg/kg B.W. $CoCl_2$ in the pref. cortex and 0.5 mg/kg B.W. $CoCl_2$ hippocampus. 186
Table 21: Fold change and p-values of Insulin-like growth factor 1 (Igf1) in pref. cortex, hippocampus and cerebellum of 0.1, 0.5 and 1 mg/kg B.W. $CoCl_2$ treated rats. 193
Table 22: Growth Differentiation Factor 15 (Gdf15) fold change and p-value across brain parts analysed through RNA-Seq experiments after cobalt treatment: pref. cortex, hippocampus and cerebellum.. 194
Table 23: GDNF family receptor alpha-like (Gfral) fold change and p-values from RNA-Seq data obtained from pref. cortex, cerebellum and hippocampus of rats dosed with i.p. daily injections of 0.1, 0.5 and 1 mg/kg B.W. $CoCl_2$ or dH_2O (controls) during 28 days. 194
Table 24: Hmgn5 ($p<0.05$) fold change in the pref. cortex, cerebellum and hippocampus of rats dosed during 28 days with i.p. injections of 0.1, 0.5, and 1 mg/kg B.W. $CoCl_2$ or dH_2O (controls). 215
Table 25: Hypoxia-inducible factor 1-α (Hif1a) fold change and p-value in the pref. cortex, cerebellum and hippocampus of rats dosed during 28 days with i.p. injections of 0.1, 0.5 and 1 mg/kg B.W. $CoCl_2$ or dH_2O (controls). 222
Table 26: Quality check of RNA samples from the cerebellum tissue obtained from the in vivo time-response experiments (Chapter 5). 292
Table 27: Quality check of RNA samples from the pref. cortex tissue obtained from the in vivo time-response experiments (Chapter 5). 293
Table 28: Quality check of RNA samples from the pref. cortex tissue obtained from the dose-response in vivo experiments (Chapter 6). 294
Table 29: Quality check of RNA samples from the cerebellum tissues obtained from the in vivo dose-response experiments (Chapter 6). 296
Table 30: Quality check of RNA samples from the hippocampus tissues obtained from the in vivo dose-response experiments (Chapter 6). 298
Table 31: MIQE checklist from the MIQE guidelines (Bustin et al., 2009) for reproducibility and assessment of experimental RT-qPCR conditions. 305

List of Figures

Fig. 1: Percentage of uncemented primary hip replacements by bearing surface combinations calculated on a yearly basis. 24
Fig. 2: Design of in vivo time- and dose-response experiments showing group distribution and sample size. 50
Fig. 3: Cardiac puncture, dissection and harvest of tissue for metal content, protein and gene expression analysis. 52
Fig. 4: Processing of harvested tissue for long-term storage and further analysis. 53
Fig. 5: Cell viability determined by the MTT (a-c) and NR (d-f) assays (n=3) in the astrocytoma U-373 (blue) and the neuroblastoma SH-SY5Y (green) cell lines after 24 (a, d), 48 (b, e), and 72h (c, f) treatment with cobalt at different concentrations. 72
Fig. 6: IC50s calculations for MTT (upper panel) and NR (lower panel) assays in U-373 astrocytoma at 24, 48 and 72h. 73
Fig. 7: IC50s calculations for MTT (upper panel) and NR (lower panel) assays in SH-SY5Y neuroblastoma at 24, 48 and 72h. 74
Fig. 8: Brightfield of control SH-SY5Y neuroblastoma cells after 24h plating under MTT and NR treatments. 76
Fig. 9: Brightfield of control U-373 astrocytoma cells after 24h plating under MTT and NR treatments. 77
Fig. 10: Cell proliferation measured by BrdU at 72h time-point. Values are represented as percentage of the control (100%), which corresponds to untreated cells (0µM). 79
Fig. 11: IC50s calculations for BrdU proliferation assay in both U-373 astrocytoma (left) and SH-SY5Y neuroblastoma (right) at 72 hours. 80
Fig. 12: BrdU proliferation of SH-SY5Y neuroblastoma cells at 72h after treatment with low cobalt doses (0-25µM). 81
Fig. 13: Fluorescence microscopy micrographs of the U-373 (left) and the SH-SY5Y (right) cell lines after 48h exposure to 0µM (upper panels), 250µM (middle panels) and 500µM (lower panels) cobalt. 83
Fig. 14: Brightfield images at 24h exposure to cobalt of U-373 astrocytoma (a, c, e) and SH-SY5Y neuroblastoma (b, d, f) with cobalt concentrations of 0µM (a, b), 250µM (b, c) and 500µM (d, e). 84
Fig. 15: Cobalt ion uptake (µg/l) into U-373 MG human astrocytoma and SH-SY5Y neuroblastoma cell lines at 24, 48 and 72 h exposed to 0µM, 25µM, 50µM, 100µM, and 200µM $CoCl_2$. 86
Fig. 16: Body weight gain (mean ± SEM) of male SD rats during the course of 1 mg/kg B.W. $CoCl_2$ injection treatment during 7 and 28 days in control and treatment groups. 103
Fig. 17: Percentage of body weight gain (mean ± SEM) of male SD rats in relation to their weight before the start of the i.p. injections. 104
Fig. 18: Organ weights after dissection of rats given daily i.p. injections of 1 mg/kg B.W. $CoCl_2$ (treatment) and dH_2O (control) after 7 and 28 days of treatment. 106

Fig. 19: Cobalt content in SD male rats' tissues (ng/g) and blood (μg/l) at 7- and 28-days of daily i.p. $CoCl_2$ injection treatment as assessed by ICP-MS analysis. 110
Fig. 20: Cobalt content in pref. cortex, cerebellum, hippocampus (ng/g) and blood (μg/l) at 28 days of 1 mg/kg B.W. $CoCl_2$ treatment in SD male rats analysed by ICP-MS analysis. 111
Fig. 21: Number and distribution of Differentially Expressed Genes (DEGs) obtained through RNA-Seq in the pref. cortex and cerebellum of cobalt-treated SD male rats compared with controls. 112
Fig. 22: Hierarchical clustering of Differentially Expressed Genes (DEGs) in rats' pref. cortex and cerebellum after 28 days of i.p. $CoCl_2$ treatment ($log_2Ratio \geq 2$ and $p<0.05$). 114
Fig. 23: Molecular function Gene Ontology (GO) clustering of pref. cortex and cerebellum DEGs sorted by number of genes. 119
Fig. 24: Classification of metalloproteins from the pref. cortex and the cerebellum in the GO term 'GO: metal ion binding' (left) and its child term 'GO: transition metal ion binding' (right) by its metal ion ligands. 120
Fig. 25: DEGs ($p<0.05$) from the pref. cortex (a) and cerebellum (b) of the GO term 'GO: divalent inorganic cation transmembrane transporter activity'. 123
Fig. 26: Genes representing protein isoforms belonging to the phosphodiesterase family (Pde) with its corresponding expression level in the pref. cortex (up) or the cerebellum (down). 127
Fig. 27: Genes representing protein isoforms belonging to the carbonic anhydrase family (Ca or Car) with its corresponding expression level in the pref. cortex (upper panel) or the cerebellum (lower panel) (DEGs p-value <0.05). 128
Fig. 28: Fold change of target genes according to RNA-Seq (n'=1 of n=3 pooled samples) and RT-qPCR. 130
Fig. 29: ΔC_T values (C_T target gene – C_T internal control) obtained from RT-qPCR tests in pref. cortex and cerebellum. 131
Fig. 30: Male SD rats' weight throughout the 28 days $CoCl_2$ treatment with 0.1, 0.5 or 1 mg/kg B.W. $CoCl_2$ daily i.p. injections. 153
Fig. 31: Body weight percentage normalised to initial weight before the start of the 28-day treatment. 154
Fig. 32: Average daily growth of control, 0.1 mg/kg B.W., 0.5 mg/kg B.W. and 1 mg/kg B.W. $CoCl_2$ treated rats. 155
Fig. 33: Relative organ weight to final rat body weight (%) of $CoCl_2$ (0.1, 0.5 and 1 mg/kg B.W.) and dH_2O treated groups. 156
Fig. 34: Organ cobalt content (μg/g, tissue; μg/l, blood) obtained after tissue and blood collection through ICP-MS. 161
Fig. 35: Cobalt content of blood (μg/l) and separate brain areas (ng/g), pref. cortex, cerebellum and hippocampus, after 28 days of daily i.p. treatment with dH_2O, 0.1, 0.5, and 1 mg/kg B.W. $CoCl_2$. 162
Fig. 36: Number of up-regulated (red) and down-regulated (blue) DEGs in pref. cortex, cerebellum and hippocampus according to cobalt dose treatment: 0.1, 0.5 and 1 mg/kg B.W. $CoCl_2$. 164
Fig. 37: Fold-change distribution (logarithmic) of DEGs in the pref. cortex, cerebellum and hippocampus. 165

Fig. 38: Venn diagrams showing the number of overlapping DEGs between pref. cortex, cerebellum and hippocampus at the different cobalt treatment doses: 0.1, 0.5 and 1 mg/kg B.W. $CoCl_2$. ____ 166
Fig. 39: Hierarchical clustering of DEGs obtained from RNA-Seq comparison of cobalt-treated groups (0.1, 0.5, and 1 mg/kg B.W. $CoCl_2$) against controls (dH_2O). S.D. male rats were treated for 28 days with daily i.p. injections._____ 168
Fig. 40: Hierarchical clustering of DEGs over 2-fold-change (no significance considered) from RNA-Seq data obtained from the comparison of pref. cortex, cerebellum and hippocampus of rats treated with three concentrations of cobalt against those of controls treated with dH_2O. _____ 170
Fig. 41: Hierarchical clustering of DEGs from pref. cortex and hippocampus of rats dosed with 0.5 and 1 mg/kg B.W. $CoCl_2$ compared against control (dH_2O). _____ 173
Fig. 42: Hierarchical clustering of DEGs from brain tissues with significant accumulation of cobalt: pref. cortex and hippocampus from rats treated with 0.5 and 1 mg/kg B.W. $CoCl_2$. _____ 175
Fig. 43: Protein-protein interaction (PPI) network obtained from STRING web tool (https://string-db.org/) by analysing DEGs as their protein products. _____ 178
Fig. 44: DEGs obtained from the comparison of pref. cortex from rats dosed with 0.1, 0.5 and 1 mg/kg B.W. $CoCl_2$ against the control group (dH_2O)._____ 180
Fig. 45: DEGs expressed in hippocampus of rats treated via i.p. with daily injections of 0.1, 0.5, and 1 mg/kg B.W. $CoCl_2$ or dH_2O (control groups) for 28 days. _____ 181
Fig. 46: Gene fold change of cerebellum from rats of $CoCl_2$- treated groups (0.1, 0.5 and 1 mg/kg B.W.) compared with controls (dH_2O)._____ 182
Fig. 47: Fold change mRNA gene expression levels obtained from RNA-Seq (green) and RT-qPCR (blue) of Tnf, Spata18, Ttr, Akap14 (pref. cortex; n'=1 of n=4 pooled samples) and Kl (Klotho; hippocampus; n'=1 from n=4 control group, n=3 in 0.5 mg/kg B.W. $CoCl_2$ treatment group, or n=1 in treatment 1 mg/kg B.W. $CoCl_2$ pooled samples). _____ 184
Fig. 48: Quantification of Tnf, Spata18, Ttr, and Akap14 ΔC_T values (C_T target gene – C_T internal control) in the pref. cortex and Kl in the hippocampus through RT-qPCR._____ 185
Fig. 49: Immunoblot analyses of target proteins from pref. cortex (left panels) and cerebellum (right panels) tissue homogenates from rats treated with 1 mg/kg B.W. $CoCl_2$ or dH_2O (control)._____ 189
Fig. 50: Relative protein expression of target proteins in pref. cortex (top panel) and cerebellum (lower panel) of rats treated with 1 mg/kg B.W. $CoCl_2$ i.p. injections during 28 days. _____ 190
Fig. 51: Proposed mechanism of cobalt toxicity in the brain obtained from the RNA-Seq data of time and dose-response in vivo experiments in a rodent model of i.p. cobalt exposure._____ 233
Fig. 52: RefFinder ranking of three reference genes Ct values in pref. cortex samples from the in vivo time-response experiment. Only the samples from the rats dosed with i.p. injections for 28 days with dH_20 (controls) and 1mg/kg B.W. $CoCl_2$ (treatment group) were analysed. The candidate reference genes were Ywhaz, Pes1 and Tbp. The most stable and gene selected for further RT-qPCR assays in the pref. cortex samples of the time-response experiment is Ywhaz (Chapter 5). _____ 301
Fig. 53: RefFinder ranking of three reference genes Ct values in cerebellum samples from the in vivo time-response experiment. Only the samples from the rats dosed with i.p. injections for 28 days with dH_20 (controls) and 1mg/kg B.W. $CoCl_2$ (treatment group) were analysed. The candidate reference

genes were Ywhaz, Pes1 and Tbp. The most stable and gene selected for further RT-qPCR assays in the cerebellum samples of the time-response experiment is Tbp (Chapter 5). _____ 302
Fig. 54: RefFinder ranking of three reference genes Ct values in pref. cortex samples from the in vivo dose-response experiment. Only the samples from the rats dosed with i.p. injections for 28 days with dH_20 (controls) and 1mg/kg B.W. $CoCl_2$ (treatment group) were analysed. The candidate reference genes were Ywhaz, Pes1 and Tbp. The most stable and gene selected for further RT-qPCR assays in the pref. cortex samples of the time-response experiment is Pes1 (Chapter 6). _____ 303
Fig. 55: RefFinder ranking of three reference genes Ct values in hippocampus samples from the in vivo dose-response experiment. Only the samples from the rats dosed with i.p. injections for 28 days with dH_20 (controls) and 1mg/kg B.W. $CoCl_2$ (treatment group) were analysed. The candidate reference genes were Ywhaz, Pes1 and Tbp. The most stable and gene selected for further RT-qPCR assays in the hippocampus samples of the time-response experiment is Ywhaz (Chapter 6). _____ 304
Fig. 56: Mapped 'rno00140 Steroid hormone biosynthesis' pathway with common DEGs from the pref. cortex and hippocampus in response to cobalt treatment with 0.5 and 1 mg/kg B.W. $CoCl_2$ compared to the control samples from rats treated with dH_2O. _____ 311
Fig. 57: Mapped 'rno04640 Hematopoietic cell lineage' pathway with common DEGs from the pref. cortex and hippocampus in response to cobalt treatment with 0.5 and 1 mg/kg B.W. $CoCl_2$ compared to the control samples from rats treated with dH_2O. _____ 312
Fig. 58: Number of up-regulated (red) and down-regulated (blue) DEGs (cutoff |fold change|>2 and $p<0.05$) in pref. cortex, cerebellum and hippocampus according to cobalt dose treatment: 0.1, 0.5 and 1 mg/kg B.W. $CoCl_2$. _____ 315
Fig. 59: Number of up-regulated (red) and down-regulated (blue) DEGs (cutoff |fold change|>2 only) in pref. cortex, cerebellum and hippocampus according to cobalt dose treatment: 0.1, 0.5 and 1 mg/kg B.W. $CoCl_2$. _____ 316

1. INTRODUCTION

A decade ago consultants and regulatory bodies reported their concerns over the failures of fourth-generation metal-on-metal (MoM) hip implants. The early failure of MoM implants requires the continuous monitoring of patients with these prostheses and has left a burden to the health care system of several countries including the UK. Moreover, MoM implants made of CoCr alloy release cobalt and chromium ions into the bloodstream (Goode et al., 2012). In this work we aimed to explore the side effects of this arthroprosthetic challenge: systemic cobalt poisoning aka cobaltism. We will describe the origins of this healthcare crisis and our experimental approach to understand cobalt toxicity in the brain through the following sections.

1.1. Hip implant surgery

Total Hip Replacement (THR) is a successful procedure that has improved the lifespan and life quality of patients with degenerative bone conditions such as osteoarthritis (Evans et al., 2019; Learmonth et al., 2007). A THR surgery involves the excision of the head and neck of the femur and its substitution by a prosthetic ball with a stem that is fitted into the femur. The surgery is completed with the insertion with or without cement of a cup in the acetabulum to reproduce the ball-and-socket joint of the femur head with the hip. A resurfacing hip replacement surgery preserves more femur than THR since only the femoral head is sculpted to be covered by a ball-shaped prosthesis, but it also requires of the insertion of an acetabular cup (National Joint Registry, 2020). These prosthetic procedures lead to reduction of pain and improved mobility in patients suffering from joint diseases. Indeed, osteoarthritis was cited as the leading cause behind surgery according to the NJR's 2020 annual report, which indicated that the number of primary hip replacement surgeries from 2017 to the end of 2019 was 281,196 in England, Wales, and Northern Ireland (National Joint Registry, 2020). The median patient age for a primary hip replacement procedure is 69 years old. In this context, primary hip replacement refers to the first time a joint replacement is performed, subsequent procedures are referred as revision surgeries.

New designs and materials have been developed with the increased number of THR, and today, hip implants are expected to last for at least 15 years, with around half of hip replacements lasting over 25 years (Evans et al., 2019). The typical combinations of bearing materials for hip arthroplasty are metal-on-polyethylene (MoP), metal-on-metal (MoM), ceramic-on-polyethylene (CoP), ceramic-on-ceramic (CoC) and ceramic-on-metal (CoM), where the first letter indicates the material of the femoral head and the third of the liner or acetabulum (National Joint Registry, 2020). MoM implants were developed in response to the osteolysis and high wear rate induced by metal-on-polyethylene (MoP) prosthesis (Kovochich et al., 2018). However, even though newer MoM designs showed unmatched performance in the short term, earlier than expected failure was noted in the late 2000s. Several regulatory bodies raised concerns with regard to the high failure rate of these implants leading to the recall and market withdrawal of certain models. The most well-known case is the Articular Surface Replacement™ (ASR™) hip implant from DePuy Orthopaedics, which was recalled in 2010 after the Australian and the UK National Joint Registry (NJR) reported its poor performance compared to other prostheses (Cohen, 2011; Meier, 2010). At the time of the recall, DePuy stated the number of sold prostheses to be around 93,000 worldwide. Consequentially, DePuy's parent company, Johnson & Johnson, is facing multiple litigations in several countries with costs in the billions (Cohen, 2011).

More recently, the 2016 NJR report on implant devices revealed elevated rates of failure of prostheses and high incident rates of adverse soft tissue reactions for all MoM implants. Their research observed that patients with MoM implants have a higher risk of developing aseptic loosening and soft tissue pseudotumors around the prostheses than patients with other systems (National Joint Registry, 2016). These adverse reactions are produced in response to cobalt (Co) and chromium (Cr) wear debris from MoM implants. The debris damages soft and bone tissue, sometimes leading to irreversible conditions even in asymptomatic patients (Low et al., 2016; Pandit et al., 2008). Hence, the 2017 Medicines and Healthcare products Regulatory Agency (MHRA) directive increased the patient coverage from previous directives and over 60,000 patients with MoM hip implants were placed under health surveillance in England, Wales and Northern Ireland (Matharu et al., 2018; MDA/2017/018, 2017; National Joint Registry, 2016).

The problematic nature of these implants has also been reflected in the changing landscape of employed bearing materials with a drastic decline in the number of implanted MoM prostheses during the last decade. This effect can be observed in Fig. 1 extracted from the 2020 NJR Annual report, which shows the percentage of bearing materials employed in the case of uncemented primary hip implants.

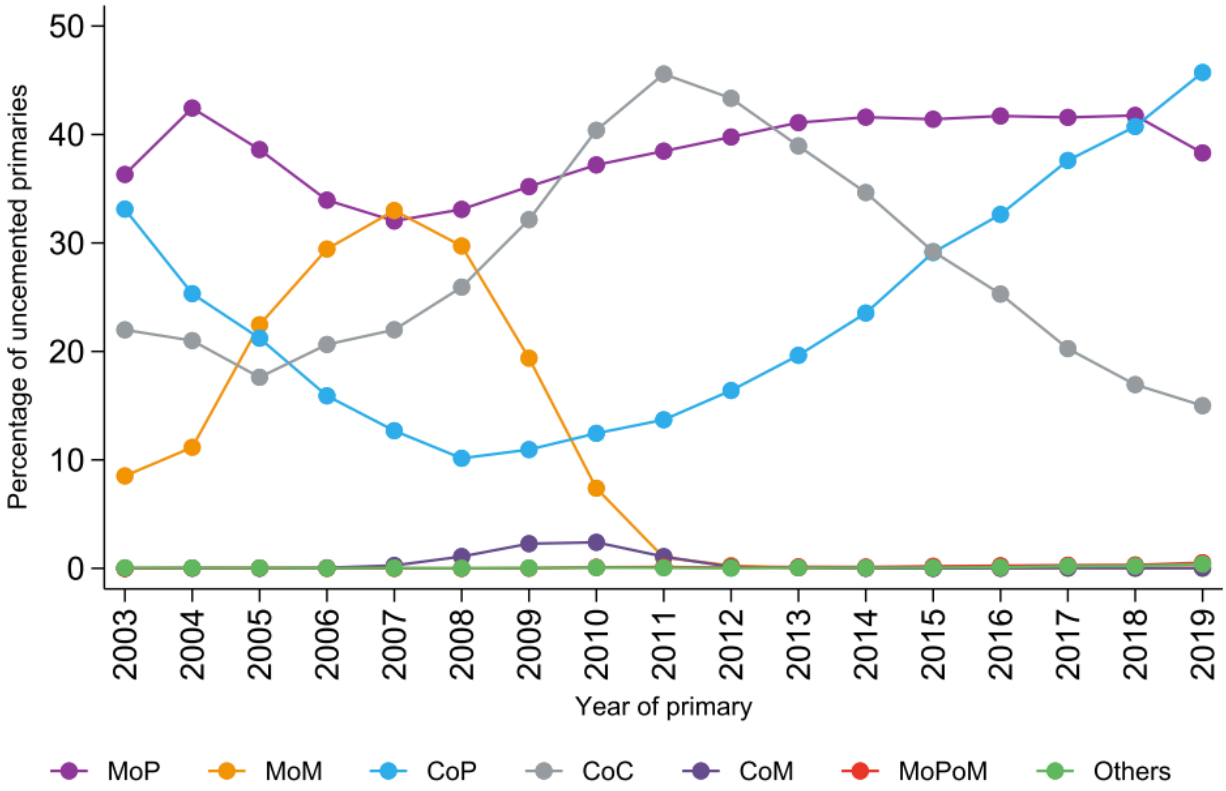

Fig. 1: Percentage of uncemented primary hip replacements by bearing surface combinations calculated on a yearly basis. Figure reproduced from the National Joint Registry 17th Annual Report with permission (National Joint Registry, 2020). MoM primary hip implant procedures are presented in orange. Their use starts declining after 2007. Abbreviations used: MoP, metal-on-polyethylene; MoM, metal-on-metal; CoP, ceramic-on-polyethylene; CoC, ceramic-on-ceramic; CoM, ceramic-on-metal; MoPoM, metal-on-polyethylene-on-metal. The first letter indicates the material of the femoral head and the third refers to the material of the liner or acetabulum.

However, the effect of Co and Cr particles is not limited to the surrounding prothesis area as debris from failed MoM articulations solubilises readily into the bloodstream in the form of metal ions (Cheung et al., 2016). The fact that Co and Cr ions have a systemic distribution through the bloodstream explains the systemic toxicity displayed by some MoM patients. Studies in animal models have shown that elevated levels of Co and Cr in blood lead to metal concentration in distant organs (Afolaranmi et al., 2012; Apostoli et al., 2013). Post-mortem analyses in MoM patients also showed metal accumulation in heart, spleen, liver, and lymph nodes, which were the only studied tissues (Abdel-Gadir et al., 2016; Martin et al., 2015; R M Urban et al., 2000; Urban et al., 2004; Wyles et al., 2017). An additional outcome arose from these studies since chromium, which was being extensively researched, appeared to be significantly less mobile than cobalt (Afolaranmi et al., 2012; Goode et al., 2012). Thus, it emerged that systemic toxicity in patients correlated with high Co levels in blood. The reference value of cobalt in blood is under 1 µg/l, however case reports of arthroprosthetic patients with symptoms of neurotoxicity have indicated values of up to 549 µg/l and 625 µg/l (Catalani et al., 2012). Another case report exceptionally described a MoP patient with a cobalt level in blood of 6521 µg/l who subsequently died of complications related to cobalt poisoning (Zywiel et al., 2013). In addition, the symptomatic similarities between previous cobalt poisoning cases like the Quebec Beer Drinkers suggest cobalt as the responsible ion (Cheung et al., 2016). Symptoms of cobaltism can involve a range of cardiac, nervous and endocrine conditions. The general agreement on the systemic effects of Co has led scientists and clinicians to coin the term arthroprosthetic cobaltism for systemic toxicity in MoM patients (Mao et al., 2011; Tower, 2010).

1.2. Motivation of this research

The disparate cobalt levels in blood and the sporadic nature of cobalt toxicity among patients with MoM implants complicates our understanding of the health risks that patients with elevated cobalt in blood endure. Cardiac toxicity has received more attention due to the severe nature of the symptoms, but the neurological consequences of elevated ions for otherwise healthy patients are still unknown. In addition, the information we have with regards to the mechanisms of action of cobalt in patients is still scarce, especially in the nervous system. Our research group is interested in the effects of Co in the brain. Case reports provide evidence that cobalt can affect cognitive

and sensory functions (Catalani et al., 2012; Green et al., 2017; Mao et al., 2011; Tower, 2010), however, even though the number of studies involving Co is slowly growing, there is little *in vivo* research at concentrations relevant for MoM patients. In addition, emerging High-Throughput technologies that have been recently incorporated into the field of Toxicology have not been applied to the study of cobalt to this date. In our *in vivo* study, we used a technique known as RNA-Sequencing (RNA-Seq) to evaluate the mechanisms of cobalt toxicity in the brain *in vivo*. This approach removes the bias of focusing in a specific pathway, as used in previous research literature by providing a screenshot of detectable transcripts in a given tissue, which allows for the identification of relevant pathways. Moreover, we coupled this technique with measurements of cobalt in the brain and in blood by inductively coupled plasma mass spectrometry (ICP-MS) in order to connect cobalt levels with mechanisms. At the same time, we also lack information at lower, perhaps more relevant, cobalt concentrations *in vitro*. Here, we evaluate the dose-response to cobalt in two CNS cell types, neurons and astrocytes from the SH-SY5Y neuroblastoma and the U-373 astrocytoma cell lines, respectively. We aim to obtain information about specific cell susceptibility and possible cobalt toxicity mechanisms in the brain through monitoring the differences in viability, proliferation, cobalt uptake, and morphology in both cell types. We hope that these *in vitro* and *in vivo* research studies will provide information about the toxic modes of action of cobalt ions.

In the next sections we will describe the overall symptoms of cobaltism and give a brief summary of previous *in vitro* and *in vivo* cobalt toxicity research. Within the context of this background we will explain why and how we defined our overall research design.

1.3. Systemic toxicity

1.3.1. A brief history of cobalt exposure

Cobalt utilisation by humans has a long history. Indeed, the word cobalt is derived from *kobold*, a spirit said to tease and madden the German miners who separated metals from the ore (Lindsay and Kerr, 2011). There are traces of cobalt in the hues from blue-and-white porcelain from 15th century in China, where international trading networks supported the import of cobalt mineral ores over Eurasia to produce blue dye (Jiang et al., 2020). However, the isolation and identification of cobalt as an element was not

accomplished until the eighteenth century by the chemists Georg Brandt and Torbern Bergman (Lindsay and Kerr, 2011). The decline in cobalt usage as a dying agent shifted with newer applications developed during the 20th century when cobalt started to be employed as a catalyst for chemical reactions and to manufacture metal alloys, although nowadays cobalt is mainly produced to fabricate rechargeable batteries (Dehaine et al., 2021). Even though the current production of cobalt is the highest in history, cobalt is a metal rarely found in the earth's crust and its exploitation is limited to a few countries such as the Democratic Republic of Congo (DRC), which currently has 70% of the worldwide production (Dehaine et al., 2021).

Cobalt toxicity has been linked to occupational activities previous to the problems derived from arthroprosthetic cobaltism. For example, Danish pottery makers using cobalt blue staining showed impaired lung function (Christensen and Poulsen, 1994). Moreover, asthma related to cobalt dust exposure is well known in welders and other industry metal workers (Al-abcha et al., 2020; Walters et al., 2014), although impairment to cardiac function does not appear to be induced in this setting (Linna et al., 2020). Recent studies in Congolese artisanal mining sites and the communities nearby have shown elevated levels of cobalt in urine and blood (Banza Lubaba Nkulu et al., 2018). A higher incidence of birth defects was found around mining areas but the effect of cobalt might be compounded with other extracted metals and follow up is required to understand the incidence in the population (Kayembe-Kitenge et al., 2020; Van Brusselen et al., 2020). In the last years of the 1960s a cardiotoxicity epidemic led to several fatalities in the city of Quebec as well as in Omaha and Minneapolis, in addition to Belgium (Seghizzi et al., 1994). It was discovered that cobalt had been added to stabilise the foam of some beers and was found to be the likely cause of the observed cardiac symptoms. In addition, the application of cobalt as a treatment for anaemia during the 1950s led to iatrogenic effects which included thyroid and neurological toxicity, although cardiotoxicity was not reported as a result (Catalani et al., 2012; Fisher, 1998; Paustenbach et al., 2013). More recently, concerns over doping with cobalt in a sport setting to increase red blood cell count have been ignited, although understandably there is little evidence about its actual use among athletes (Knoop et al., 2020).

In summary, humans have been exposed to cobalt through inhalation, ingestion and directly through the blood such as the case of patients with MoM implants. Different exposure routes may lead to different levels and types of toxicity. The scientific literature indicates that the toxicity experienced by patients with MoM implants appears to parallel that of the Quebec beer drinkers and patients with iatrogenic exposure. In the following section we will describe the overall systemic symptoms of cobaltism focusing mainly on patients with MoM implants.

1.3.2. Cobalt systemic symptoms

Overall, haematological, cardiac, thyroid, hepatic, and neuropathic conditions have all been described and attributed to toxic effects of cobalt in arthroprosthetic patients (Cheung et al., 2016). For example, cobalt is known to reduce iodine uptake and has led to hypothyroidism and goitre in patients receiving oral doses of cobalt to treat anaemia (Paustenbach et al., 2013). The haematological purpose of cobalt in the treatment of anaemia was ultimately to induce polycythaemia (Paustenbach et al., 2013). This cobalt-induced increase in red blood cells is thought to be ultimately mediated by the enhancement of erythropoietin synthesis in the kidney through cobalt's ability to elicit the expression of hypoxia-inducible factor (HIF-1α), although this hypotheses has not been experimentally confirmed (Fisher, 1998; Simonsen et al., 2012a). Cobalt was only employed to treat anaemia for a few years in the 1950s but its use was quickly stopped due to the consequences for the thyroid gland (Fisher, 1998). It was substituted by safer and more effective recombinant human erythropoietin in the last decade of the twentieth century, therefore we do not have more up to date information of cobalt iatrogenic effects. Unfortunately, both hypothyroidism and polycythaemia have been reported with poisoning from CoCr hip implants, although the haematological and thyroid effects of cobalt appear to be reversible (Allen et al., 2014; Apel et al., 2013; Choi et al., 2019; Gilbert et al., 2013; Ho et al., 2017; Rizzetti et al., 2009).

Cardiac symptoms are the most prominent systemic symptoms of cobalt toxicity due to their severity among patients with CoCr implants and also because of the specific pathology observed in the heart such as the disappearance of myofibrils and loss of mitochondrial structure (Fung et al., 2018). Intracytoplasmic vacuolisation, lipid

droplets and lipofuscin accumulation are also a hallmark of cobalt-related pathology in the heart but, most importantly, interstitial fibrosis is generally described in the majority of histological reports (Allen et al., 2014; Bonenfant, J.L., Miller, G., Roy, 1967; Choi et al., 2019; Khan et al., 2015; Martin et al., 2015; Mosier et al., 2016). Fibrosis is a typical occurrence in cardiomyopathies (Fung et al., 2018), which shows as cardiac tissue remodelling in response to overproduction of extracellular matrix proteins such as collagen (Gibb et al., 2020). This process is triggered by injury and carried out by cardiac fibroblasts, which transdifferentiate and proliferate into myofibroblasts to assist with wound healing by secreting extracellular matrix proteins. This reactive environment is set into action by pro-inflammatory mediators like the TGFβ cytokine that is released by macrophages responding to injury (Gibb et al., 2020; Tallquist and Molkentin, 2017). Prolonged activation of fibroblasts into myofibroblasts eventually leads to excessive deposition of collagen and scaffolding proteins initially provoking tissue stiffening and further activation of fibroblasts (Distler et al., 2019).

As a whole, all these cobalt-induced microscopic changes observed in the heart appear to be macroscopically reflected as cardiomegaly or enlarged heart (Choi et al., 2019; Morin et al., 1969; Stepien et al., 2018; Sullivan et al., 1969), also described as dilated cardiomyopathy (Allen et al., 2014; Gilbert et al., 2013; Khan et al., 2015; Martin et al., 2015), although there are differences between dilated cardiomyopathy and cobalt-cardiotoxicity (Packer, 2016). Some other reported symptoms of cobalt cardiotoxicity involve reduced left ventricular ejection fraction (Gilbert et al., 2013; Machado et al., 2012; Mosier et al., 2016). Additionally, back in the 1960s, during an epidemic of cobalt poisoning caused by adulterated beer, several authors preponderantly reported pericardial effusions (Alexander, 1972; Kesteloot et al., 1968; Sullivan et al., 1969), which has also been mentioned in recent cases of cobaltism with arthroprosthetic patients (Choi et al., 2019; Gilbert et al., 2013). Cardiac cobaltism has been previously studied by one of our colleages (Laovitthayanggoon et al., 2019), and we will not focus on its study, although we will keep discussing cobalt cardiotoxicity reports throughout this thesis in the context of cobalt systemic toxicity.

Ultimately, the manifestation of these conditions is far from simple as it tends to show as a multisystem disease among sporadic patients exposed to variable levels of cobalt (Zywiel et al., 2016). In their review of the literature, Fung *et al.* discussed whether

cobalt was causative of cardiomyopathy or pre-existing factors could have influenced this etiology, which is difficult to establish given the limited number of reports on cobalt cardiotoxicity (Fung et al., 2018). They argued that blood cobalt levels under 100μg/l are unlikely to contribute towards cobalt-induced cardiomyopathy. Paustenbach *et al.* set the bar over 300μg/l cobalt in blood for the occurrence of reversible haematological and thyroid disturbances, and recommended monitoring patients over 100μg/l (Paustenbach et al., 2013). This 100μg/l cobalt in blood threshold was calculated with an uncertainty factor of 3 from the cited 300μg/l to account for differences between individuals. The same authors reiterated their views in a more recent review (Kovochich et al., 2018), however, the exposure data in which they based their conclusions was obtained during periods of cobalt exposure that lasted less than a year as they previously acknowledged (Paustenbach et al., 2013).

Circa 60% of patients can live with well-functioning hip prostheses for 25 years (Evans et al., 2019), but patients with MoM implants have earlier revision rates than alternative implants such as MoP or ceramic on ceramic (Hunt et al., 2018; Kovochich et al., 2018). A brief review of the case reports indicates that the time between first implant or revision to a CoCr implant and the onset of systemic symptoms due to cobaltism can range between months (Rizzetti et al., 2009; Zywiel et al., 2013), a year (Choi et al., 2019; Tower, 2010), and two to six years' time (Apel et al., 2013; Choi et al., 2019; Machado et al., 2012; Mao et al., 2011; Steens et al., 2006; Tower, 2010). Some mechanical and health risks factors could also accelerate cobalt toxicity. For example, the revision from damaged ceramic implants to CoCr bearings can cause accelerated fretting of the metal alloys by the microabrasion with small ceramic fragments left at the implant site, or implants with larger implant heads can lead to increased levels of cobalt in blood (Zywiel et al., 2016). The switch from ceramic to CoCr head is the suspected case of systemic toxicity in other case reports (Choi et al., 2019; Gilbert et al., 2013; Zywiel et al., 2013). Health handicaps discussed as risk factors in the cited reviews from Zywiel *et al.* and Paustenbach *et al.* are a deficient nutrition and renal impairment that could interfere with the patients ability to excrete and deal with cobalt (Paustenbach et al., 2013; Zywiel et al., 2016). Zywiel *et al.* indicated that most cobalt poisoning reports in patients with CoCr prostheses occurred over 100μg/l and that toxicity under this threshold was unlikely (Zywiel et al., 2016). However, other papers have reported systemic symptoms of cobaltism with serum cobalt levels of 23μg/l

(Tower, 2010) and 24μg/l (Mao et al., 2011), while patients with levels over 100μg/l can remain asymptomatic (Ho et al., 2017). Thus, despite the careful and thorough reviews of the literature, we should be cautious when defining thresholds since the information available is still limited.

1.3.3. Cobalt neurotoxicity

More specifically, neurological symptoms associated with cobaltism include memory loss, cognitive decline, progressive deafness, atrophy of the optical nerve, retinopathy, vertigo, peripheral neuropathy (Catalani et al., 2012), fatigue, depression, and ataxia (Mao et al., 2011). Despite the several medical reports citing neurological symptoms as a result of high Co levels due to MoM implants (Green et al., 2017; Mao et al., 2011; Rizzetti et al., 2009; Tower, 2010), a couple of recent observational studies looking for this association have failed to confirm a relationship between cobaltism and neurological symptoms in MoM patients (Kavanagh et al., 2018; van Lingen et al., 2014). They reported difficulties with regards to a low number of patients with high levels of cobalt in blood (van Lingen et al., 2014), in addition to deficient case descriptions (Kavanagh et al., 2018). Furthermore, in contrast to cardiac signs, neurological symptoms are often downplayed or even go unnoticed as they might be confused with typical signs of ageing.

In summary, there is little information about the actual effects of cobalt in the peripheral and the central nervous system, and the most appropriate response to diminish patients' symptoms to date is to remove the implant as the source of cobalt ions through a revision surgery (Machado et al., 2012; Paustenbach et al., 2013; Tower, 2010). However, the recovery process from cobaltism is not well documented and there is no unified action considered appropriate to treat these patients. Our lack of knowledge on cobalt actions in the body extends further since we also ignore the implications for asymptomatic patients with high levels of cobalt in blood (Ho et al., 2017). In the following sections we will describe some of the cobalt neurotoxicity studies to date, and try to find the gaps of knowledge where we will establish our research with the aim to answer the questions we have previously formulated.

1.4. Current status of cobalt toxicity research in the brain

Multiple non-neuronal cell types related to local exposure of MoM hip implants have been evaluated e.g. osteocytes (Shah et al., 2017), osteoblasts and osteoclasts (Andrews et al., 2011; Shah et al., 2015), fibroblasts (Sabbioni et al., 2014b, 2014a), monocytes (Posada et al., 2015, 2014), macrophages (Salloum et al., 2021), lymphocytes (Akbar et al., 2011), and red blood cells among others (Simonsen et al., 2011a, 2011b). Our team has also investigated cells affected systemically by cobalt ions such as hepatocytes (Afolaranmi et al., 2011), and heart fibroblasts (Laovitthayanggoon et al., 2019). Another team did look into the effect of cobalt in lung epithelial cells as a result of inhalation (Bresson et al., 2013).

The effect of cobalt in central nervous system (CNS) cells has already been investigated by several authors *in vitro*. Nevertheless, with few exceptions most studies have only focused on the effects of cobalt at very high cobalt concentrations (>100μM) with the aim to induce hypoxia *in vitro* and have ignored other toxic mechanisms and doses (Muñoz-Sánchez and Chánez-Cárdenas, 2019). Some studies have been carried out on astrocytes (Karovic et al., 2007; Wang et al., 2016), neurons (Chimeh et al., 2018; Kikuchi et al., 2018; Li et al., 2015; Naves et al., 2013), and glia (Fung et al., 2016; Mou et al., 2012). In general, cobalt provokes extensive apoptosis and necrosis (Karovic et al., 2007), with different studies describing caspase dependent (Hartwig et al., 2014; Zou et al., 2002) and independent (Karovic et al., 2007) cell death, and oxidative stress being strongly involved (Kotake-Nara and Saida, 2007). Apart from that, the protein p53 seems to play a key role in the development of cobalt toxicity *in vitro* (M. Lee et al., 2013; Ratinaud, 2011), as it does with other heavy metals (Phatak and Muller, 2015). Amyloid protein production is also increased by cobalt (Zhu et al., 2009), which could link with neurodegenerative diseases such as Alzheimer's disease (Li et al., 2017). Mitochondria seem to be the main target of cobalt toxicity in neurons and astrocytes with ATP depletion and loss of transmembrane potential (Karovic et al., 2007; Ratinaud, 2011). Most of these CNS studies have used cobalt as a way to elicit hypoxia at high concentrations. Thus, it is difficult to evaluate the relevance of these studies when it comes to studying the effect of cobalt in MoM patients. Since it is difficult to equate the *in vitro* concentrations with the exposure in

patients with MoM implants, we decided to investigate cobalt across a range of doses in our studies.

There are fewer *in vivo* studies, but cobalt has also been applied to animal models such as rodents and zebrafish. Oral administration of 40 mg/kg BW of $CoCl_2$ led to increased levels of hypoxia and decreased activity of antioxidant enzymes in the cerebral cortex of treated mice. Pregnant female rats dosed orally with 350 mg/l also delivered pups with impaired levels of antioxidant proteins in cerebrum and cerebellum (Garoui et al., 2013). In zebrafish embryos the application of concentrations over 100 µg/l led to abnormal morphology, bradycardia and behavioural changes thought to be caused by increased oxidative stress and apoptosis (Cai et al., 2012). In addition, some groups have directly injected cobalt into the brain of rats (Caltana et al., 2009) or applied cobalt dust directly into the dura mater (cobalt epileptic focus model) (Kajiwara et al., 2008). The latter group discovered elevated expression of transthyretin (TTR) and phosphoglycerate mutase 1 (PGM) which are involved in thyroid transport and regulation of glycolysis respectively. Caltana *et al.* observed that the direct cortical injection of cobalt leads to histological changes consistent with focal ischemia involving neuronal and astrocytes morphological changes (Caltana et al., 2009). The cited papers are a sample of the available literature, and more studies have been described throughout the discussion sections of the thesis. Nevertheless, as with the previous *in vitro* literature, it is difficult to establish the relevance of these studies for patients with MoM implants and elevated levels of cobalt in blood due to the high dosage of cobalt used, the different types of cobalt delivery methods, such as oral administration or direct tissue application, and also due to the missing information on the resulting cobalt concentrations in blood or plasma. Our research will try to mimic the conditions that MoM implant patients endure to obtain a better representation of relevant cobalt toxic mechanisms for them.

Studies that have tried to image brain changes in response to systemic cobalt in MoM patients are limited by the low number of participants and confounding variables such as aging (Bridges et al., 2020; Clark et al., 2014). Clark *et al.* suggested small structural changes in the visual pathways and the basal ganglia but their observations lack statistical power, and Bridges *et al.* found several hypometabolic brain areas such the inferior temporal cortex of patients with MoM implants. Given that the location of

neurotoxicity is difficult to predict (Rao et al., 2014), we selected three neuroanatomical structures to study within the brain for our *in vivo* studies, the prefrontal cortex, hippocampus and cerebellum, which are within the list of brain areas advised by the Society of Toxicologic Pathology to be screened for clues of neurotoxicity (Morrison et al., 2015). These brain areas are easy to locate in a rodent brain and yield sufficient biological material for molecular and protein expression analysis. Most importantly the correlation between their structure and function could be associated with some of the symptoms experienced by patients with cobaltism. For example, the cerebellum is known to control motor coordination (Rao et al., 2014), while the hippocampus is involved in learning and memory formation, in addition to spatial navigation and emotional regulation (Strange et al., 2014). The pref. cortex is in charge of the executive function and integrating connections from other brain parts (Le Merre et al., 2021). Symptoms from patients with cobaltism such as sensorimotor impairment, hand tremor, coordination difficulty, depression, and cognitive decline could relate to a deterioration of these brain functions (Catalani et al., 2012; Green et al., 2017; Mao et al., 2011; Tower, 2010).

1.5. Experimental approach and model considerations

To better understand the effects of cobalt, we opted for a complementary approach by studying both human *in vitro* and rodent *in vivo* models. Both approaches have their advantages and disadvantages which will be discussed in the following sections.

1.5.1. *In vitro* models: neuroblastoma and astrocytoma

In vitro models such as cell lines or dissociated primary cells have the potential to reveal mechanistic pathways (Barbosa et al., 2015). In this way, the cellular response to a toxin can be monitored in real time, and there are several cytotoxicity assays specifically developed for their use *in vitro* which provide valuable information about the modes of action of toxins (Astashkina et al., 2012). Moreover, it is possible to use cells derived from human tissues, which facilitate the extrapolation of results for therapeutic applications. However, *in vitro* cell culture has its limitations. Given the lack of tissue structure and complex environment in cultured *in vitro* monolayers, *in vitro* tests can either underestimate or overestimate the metabolism of xenobiotics (Barbosa et al., 2015). Additionally, the blood-brain barrier (BBB) and blood-CSF barrier

introduce a level of uncertainty about the real toxin concentration that cells in the CNS endure in an *in vivo* setting or in patients. This makes the selection of appropriate *in vitro* doses even more challenging when attempting to design relevant models for patients (Barbosa et al., 2015). Thus, we should also be cautious when trying to extrapolate results obtained from *in vitro* neurotoxicology models to the clinic.

Our chosen *in vitro* models are the neuroblastoma SH-SY5Y and the astrocytoma U-373 cell lines. Both types are immortalised cell lines of human origin meaning that they have unlimited capacity to proliferate. SH-SY5Y cells were originally obtained from a 4-year old female patient through a bone marrow biopsy but have adrenergic ganglia origin and are considered to have an immature phenotype (Barbosa et al., 2015; Forster et al., 2016). There are several protocols available to differentiate SH-SY5Y neuroblastoma cells into growth arrested neuron-like cells (Forster et al., 2016; Simões et al., 2021)

U-373 MG astrocytoma cells are less researched than SH-SY5Y cells. However, they are still a widely used *in vitro* model. Originally, U-373 MG cells from the European Collection of Authenticated Cell Cultures (ECACC) were actually misidentified and were later declared to be U-251 MG cells, another human astrocytoma cell line (Timerman and Yeung, 2014). ECACC corrected the error and the cells used for the experiments in this thesis were U-373 MG (Uppsala) directly obtained from the laboratory of origin in Uppsala (ECACC, 2021). Astrocytes are a type of glial cells with important support functions for the functioning of neurons, as well as for the endothelial cells of the blood-brain barrier (BBB) (Barbosa et al., 2015). Similar to SH-SY5Y cells, U-373 MG astrocytoma cells are neoplastic and therefore, the toxicity observed in response to cobalt might be different from that of primary cells. However, the use of cell lines also has its advantages which we will describe.

Immortalised cell line populations can be easily expanded by sub-culturing, which allows the generation of high number of cells. In this way researchers are able to perform extensive time and dose-response assays. However, there are disadvantages when using cell lines. It is not clear whether the phenotype of immortalised cells represents that of non-cancerous cells from the original tissue since several differences have been detected with regards to genomic content, cell morphology,

contact inhibition behaviour, etc. (Astashkina et al., 2012). Moreover, given that cells keep dividing during the experiment it also becomes difficult to observe whether the toxin affects proliferation or cell death first (Barbosa et al., 2015). In spite of these drawbacks, cell lines are highly reproducible tools due to the homogeneity of cells obtained through sub-culturing, and both neuroblastoma SH-SY5Y and astrocytoma U-373 cell lines have a human origin. The latter is important because the results obtained *in vitro* through human cells can complement the knowledge obtained by researching animal models, and contribute towards a better understanding of cobalt poisoning in humans.

1.5.2. *In vivo* rodent model: anatomy and function of the rodent brain

Rodents have been the leading *in vivo* model of research, primarily rats and mice. Rats are easier to handle and have a larger size which helps with drug administration and dissection (Ellenbroek and Youn, 2016). There are obvious differences in size and functional capabilities between human and rodent brains, but they have similar neuroanatomy thus allowing cross-species extrapolation to an extent (Morrison et al., 2015). In addition, the structure of blood brain barrier (BBB), and blood-CSF barrier corresponding to the vascular endothelium and the epithelium of the choroid plexus respectively is similar between human and rodent studies (Engelhardt et al., 2017). Moreover, the diffusion of different fluorescent tracers across the BBB and the blood-CSF barrier shares features in both species, although the obvious brain size differences leads to reduced trafficking distances. Nevertheless, the correlation between rodent and human brains is far from ideal. There are important differences in the gyrification and number of cells in the cortical layers (DeFelipe, 2011), the orientation and connectivity of the hippocampus (Strange et al., 2014) and the transcriptional makeup of brain areas (Hodge et al., 2019) among others. Therefore, caution is needed when attempting to translate findings obtained in rodents to the clinic.

1.6. Potential role of chromium in the development of systemic toxicity

Although cobalt is thought to be the main culprit of systemic toxicity in MoM patients, literature is also accumulating with regards to the synergistic role that chromium could play. The percentage composition of the most common alloy used in MoM hip prostheses, the ASTM F75, is 5-7% Molybdenum (Mo) and 27-30% Cr balanced with Co up to 100%, which forms a metal composite of 2:1 Co:Cr ratio (Fleming et al., 2020). Thus, chromium is the second most abundant metal in the alloy. However, Cr is less mobile than Co, which readily solubilises (Goode et al., 2012; Koronfel et al., 2018). This separation of Co and Cr alloy from the metal debris is thought to follow a mechanism similar to de-alloying where CoCr particles become structurally porous due to cobalt solubilisation (Koronfel et al., 2018). In that regard, although solubilised ionic cobalt distributes easily through the blood stream, it is also rapidly excreted through urine, while the clearance of chromium from the organism is slower (Daniel et al., 2009; Newton et al., 2012) with Co excretion peaking six months and Cr one to two years after the patients received MoM resurfacing implants (Daniel et al., 2009). Our team also confirmed the faster mobility of Co in comparison to Cr by assessing the metal content in tissues from a rodent air pouch model injected with MoM wear (Afolaranmi et al., 2012). The lower mobility of Cr in contrast to Co is reflected in the higher concentration of chromium in synovial fluid and soft tissues of MoM hip implant patients. Chromium concentration is much higher than cobalt around the prostheses despite the 2:1 Co:Cr original ratio of the ASTM F75, while this relationship is inverted in blood, meaning that chromium is preferentially retained in local tissues (Nousiainen et al., 2020). Thus, it is possible that, once transported in blood, chromium stays in organs distant from the prosthesis for longer periods of time, and with unknown consequences for the host. CoCr particles were found co-localised within macrophages in the liver of a patient with a failed hip implant and very high metal levels in blood through micro X-ray fluorescencence, but there were not isolated Cr or Co particles detected (Abdel-Gadir et al., 2016). Cr has also potentially been found in macrophages of prosthetic patients within the liver and spleen in the portal tracts and lymphatic sheaths respectively, although the composition of the particles was not confirmed analytically, and they tended to appear in patients with failed prostheses (R.M. Urban et al., 2000; Urban et al., 2004). However, contrary to this hypothesis, myocardial Cr levels were not elevated in postmortem tissue of patients with THR CoCr

components after six years post-implantation (median) with a couple of exceptions, while average Co levels were (Wyles et al., 2017). Similar results were found by Swiatkowska *et al.* in postmortem cardiac samples from CoCr MoP patient samples (Swiatkowska et al., 2018). These are few studies and further metal analyses of tissues distant from the prosthesis will be necessary to determine whether chromium ions accumulate long-term in other vital organs such as the brain and the heart, and if Cr could play a role in systemic toxicity together with Co.

In addition to metal distribution, the chemistry of metal ions should also be considered, particularly in the case of chromium. While cobalt tends to dissolve from its metallic form to be released into the medium as divalent ions, the chemical form of chromium is more diverse as it can still be found in its metallic form but also as trivalent, Cr(III), and hexavalent, Cr(VI), ions (Swiatkowska et al., 2018). The clinical research on the speciation of chromium to date has established that most chromium found around the prostheses is in the form of Cr III phosphate ($CrPO_4$) (Hart et al., 2010, 2009; Morrell et al., 2019; Swiatkowska et al., 2018). Fortunately, the trivalent state of chromium is not particularly toxic and is thought to be a nutritionally valuable element while hexavalent chromium is, instead, a known carcinogen (Zhu and Costa, 2020). A higher amount of chromium detected in erythrocytes than in plasma is a concerning implication for patients because Cr(VI) crosses the cell membranes of red blood cells, while Cr(III) accumulates in the serum fraction. Thus, a few studies on CoCr implants have investigated the partition of chromium in blood (Finley et al., 2017; Langton et al., 2019; Merritt and Brown, 1995; Sidaginamale et al., 2013). In effect, *in vitro* spiking of samples with trivalent and hexavalent chromium demonstrated that a higher portion of hexavalent chromium was bound to erythrocytes while trivalent chromium had affinity for serum (Sidaginamale et al., 2013). In patients with CoCr implants, a couple of analysis of samples found chromium preferentially bound to serum indicating ionic chromium was likely trivalent (Finley et al., 2017; Sidaginamale et al., 2013). However, early research by Merritt and Brown *et al.* found hexavalent chromium in the blood of patients with CoCr corroded wear originating from implants (Merritt and Brown, 1995). More recently, Langton *et al.* revisited this topic and worryingly detected more chromium in blood than in serum samples in some of their MoM patients, and these cases were associated with failed head-stem taper junctions (Langton et al., 2019). Other studies have been able to directly study the ionic form of chromium in patients.

In 2010, Hart *et al.* reported no evidence of hexavalent chromium in the soft tissue surrounding MoM prostheses when evaluated by advanced elemental analysis with X-ray spectroscopy (Hart et al., 2010). However, more recently, Swiatkowska *et al.* found the presence of hexavalent chromium ions in a couple of diabetic patients with CoCr implants (Swiatkowska et al., 2018). The authors suggested that, rather than the generation of Cr(VI) from the implant, the oxidative cellular environment generated by diabetes could lead to re-oxidation of trivalent chromium leading to the generation of hexavalent chromium. The reports by Swiatkowska *et al*. in periprosthetic tissue and Langton *et al.* in blood have worrying implications for patients with co-morbidities as well as patients with failed CoCr implants due to corrosion (Langton et al., 2019; Swiatkowska et al., 2018). Despite the limited evidence of the presence of hexavalent chromium in patients with CoCr implants, further research is needed to understand the concentrations of Cr(VI) that some at-risk patients could be exposed to. To date, no association between cancer and MoM implants has been found (Brewster et al., 2013; Hailer et al., 2022), however, the results by Langton *et al.* and Swiatkowska *et al*. (Langton et al., 2019; Swiatkowska et al., 2018) point towards increased risk of only certain patients. Thus, patient-wide studies of cancer incidence should perhaps be reviewed to take into account co-morbidities and the corrosion state of current or previous prostheses that an implant patient has been exposed to.

A particular consideration with regards to resulting chromium chemistry and Co:Cr ratios should also be given to modular junctions, such is the case of the taper junctions of THR prostheses. A taper junction is a part of MoM THRs formed by a CoCr adapter sleeve, and resurfacing implants lack this interface. Therefore, THR prostheses have an additional metallic surface that is a source of metallic debris and ions. Recent research has shown that prostheses with stem-taper junctions have a higher Co:Cr ratio in blood than resurfacing implants (Ilo et al., 2021), 2.3:1 compared with 1.3:1 Co:Cr ratio. This relationship is inverted in the synovial fluid, where the concentration of Cr is expected to be higher than cobalt (Langton et al., 2019). Moreover, a CoCr joint fluid ratio > 1 is indicative of reduced Co clearance from the synovial compartment and taper failure. In addition, samples obtained from patients with MoM total hip replacements have revealed an additional chromium chemical form, Cr(III) oxide (Cr_2O_3), in the soft tissue around taper junctions (Di Laura et al., 2017). It is also known that a larger number of heterogeneous particles are generated in this interface by

corrosion, which is aggravated by the abrasive action of titanium particles (Di Laura et al., 2017; Xia et al., 2017), and this has been associated with more severe immunologic reactions (Xia et al., 2017). The authors speculated that macrophages present in the taper junction interface could generate higher oxidative stress due to the exfoliation of necrotic macrophages in the interface. The generation of oxidative stress in these conditions is particularly concerning since, as previously explained, it has been suggested that oxidative conditions induced by the corrosion in the taper junction could give rise to hexavalent chromium ions (Langton et al., 2019).

Our current knowledge about the distribution or the chemistry of chromium do suggest an important role around the prostheses, where it concentrates (Nousiainen et al., 2020), rather than in distant tissues such as the heart (Swiatkowska et al., 2018; Wyles et al., 2017). Thus, we have focused on cobalt to explain systemic toxicity in patients with MoM implants and consider that the topic of systemic chromium toxicity needs to be developed before implications for MoM implants can be drawn. A vast body of research has focused on the effects of metal debris around the prostheses but, further investigating the local concentrations of chromium on tissues affected by systemic toxicities such as the heart, brain or thyroid could help us define the impact of chromium species in these tissues. Deposition of chromium in these organs could potentially trigger damage. In this regard, the multiple previous studies about the detrimental effect of the local immune response to metal debris surrounding the prostheses are particularly relevant and could also shed light into systemic reactions to both cobalt and chromium.

1.7. Immunogenic reactions to metal debris

In patients with malfunctioning implants, periprosthetic metallic particles induce local innate and adaptive immune reactions that lead to severe inflammation and eventually aseptic implant failure (Hallab and Jacobs, 2017). Macrophages are considered to initiate the immune cascade by engulfing the metallic particles which, when phagocytosed, damage lysosomes releasing reactive oxygen species and triggering danger signals such as the inflammasome (Hallab and Jacobs, 2017). Specifically, CoCr alloy debris has been demonstrated to elicit inflammasome activity in macrophages both *in vitro* and *in vivo* (Samelko et al., 2016). Samelko *et al.* further

discovered that the NLRP3 inflammasome and caspase-1 danger signals induced by metal sensitization with cobalt ions activate T-cells *in vitro* and *in vivo* after re-exposure, and showed that the blockade of these danger signals reduced human lymphocyte activation (Samelko et al., 2019). The authors hypothesised that T-cell activation by inflammasome/caspase danger signals was the cause of metal induced delayed-type hypersensitivity (DTH) responses in implant patients. Moreover, metal-DTH responses, aka metal sensitivity or metal allergy, are thought to accelerate implant failure over macrophage-induced osteolysis (Hallab, 2017).

Adverse reactions to metal debris (ARMD) in an umbrella term that encompasses all inflammatory reactions derived from implant metallic debris from the perspective of the patient. This pathology includes pseudotumors, presence of metallic wear debris (metallosis), as well as aseptic lymphocyte-dominated vasculitis-associated lesion (ALVAL) aka perivascular lymphocytic cuffing (Natu et al., 2012; Perino et al., 2021). ALVAL is a specific immune response within periprosthetic tissues from metal implant patients that is histologically defined by lymphocytic cell neogenesis and infiltration. This lymphoid histological feature is consistent with metal induced DTH defined in the previous paragraph (Campbell and Takamura, 2020; Hallab, 2017), and its occurrence and severity appears to depend on the individual sensitivity to metal of a patient's immune system. For example, Ebramzadeh *et al.* observed that the level of wear is not proportional to the severity of ALVAL reactions, thus they suspected individual metal-DTH in patients (Ebramzadeh et al., 2015). Moreover, an study of bilateral MoM hip implant patients found symmetry of ARMD pathology despite differences in implant wear volume between hip sides, thus confirming intrinsic host factors that condition the inflammatory response (Lehtovirta et al., 2019). If systemic symptoms such as the cognitive decline reported in patients affected by cobaltism were to be related to an immune response it might explain the lack of dose response to cobalt levels in blood.

We should take into account that the referenced studies mainly refer to the micro- and nano-particulate metallic debris found in periprosthetic tissues, and that the debris is different from that detected in organs distant from the hip implant, which are divalent ions transported by the bloodstream (Simonsen et al., 2012b). The immune response elicited by debris with different size and shape will differ (Zare et al., 2021), thus the local and the systemic immune reactivity scenarios require individual assessment.

Langton *et al.* studied the reason behind why in spite of lower wear rates in the THR group, patients with THR implants showed higher metal concentrations in the synovial fluid (Langton et al., 2018). The increased Cr and Co concentrations in synovial fluid were associated with large fluid collection and worse ALVAL outcomes. From these results, the authors suggested that poor clearance of metal ions from the synovial fluid led to severe immunogenic reactions due to protein leakage from the synovial membrane. The authors also speculated that an increase in the amount of metal ions bound to proteins such as albumin and transferrin would delay the clearance of metal ions from the synovial fluid and work as haptens triggering the immune system. The excretion of ionic Cr through urine has been suggested to be slower than that of Co due to Cr higher affinity for proteins (Newton et al., 2012), while the hypothesis of protein-bound ions acting as haptens and inducing an immune response has also been mentioned in the MoM literature (Hallab, 2017). However, there is still little research with regards to the binding of Co and Cr ions and how it associates with the type of immune reaction or overall toxicity. In this thesis we will hypothesise about the potential implications of protein metal bonding aka metalation but, due to our research limitations it will not be possible for us to confirm these hypotheses.

Immunological responses related to cobalt exposure have also been observed in hard metal lung disease (HMLD). Hard metal, not to be confused with heavy metal, has a specific composition of 90% tungsten carbide and 10% cobalt powders, and it is a composite found in certain occupational industrial settings (Zheng et al., 2020). People affected breathe in the dust, and the metallic particles are pushed towards the alveoli. HMLD is also considered to be a rare disease, with symptoms ranging from occupational asthma to fibrosis in the most severe cases (Zheng et al., 2020). Cobalt has also been indicated as the culprit of toxicity in HMLD (Cirla, 1994). Pathological examinations in patients have found a predominant activation of lymphocytes and multinucleated giant cells showing emperipolesis, which is why they have also been named cannibalistic giant cells (Adams et al., 2017; Zheng et al., 2020). An *in vivo* study in rodents found cytokine release in response to cobalt inhalation, which was further accentuated by cobalt dermal application (Tsui et al., 2020). Similarly to what has been found in the cobalt literature, the authors reported that individual mice responses varied widely to cobalt application. Microarray analysis of *in vitro* epithelial cells exposed to cobalt showed altered expression of a number of immune-related

genes (Verstraelen et al., 2014). However, the authors did not extend their research to other cells relevant for the immunity within the lungs and there is little research with regards to the transcriptional response elicited by cobalt in this organ.

1.8. Objectives of the present research

The symptoms of cobalt neurotoxicity are varied and cobalt poisoning might remain an elusive diagnosis in patients with MoM implants as there is not a linear association between cobalt ions in blood and symptoms. Given the lack of knowledge about the effects of cobalt on the CNS, our main objective is to increase our understanding about the cellular and molecular systems by which cobalt could interfere with CNS function in patients with MoM implants. This aim was divided into the following sub-objectives:

- Obtain cell viability and proliferation profiles *in vitro* for main CNS cell types, neurons and astrocytes, through neuroblastoma and astrocytoma cell lines treated with cobalt.
- Establish a comparison between cellular cobalt uptake levels through ICP-MS in astrocytoma and neuroblastoma cell lines and viability profiles.
- Estimate metal content for main organs and brain parts with relevant concentrations of cobalt in blood for MoM patients via extrapolation from time and dose-response experiments *in vivo* with a Sprague Dawley rat model.
- Identify mechanisms of cobalt toxicity *in vivo* through RNA-Seq technology and validate results via gene and protein expression analyses using RT-qPCR and western blot techniques.
- Establish new avenues for research of cobalt poisoning effects on the CNS for patients with MoM implants.

1.9. Thesis structure

This thesis is divided into seven chapters:

- Chapter 2 and Chapter 3 describe the methods followed for the *in vitro* and the *in vivo* experiments respectively.
- Chapter 4 contains the results and discussion from the *in vitro* experiments using neuroblastoma and astrocytoma cell lines.
- In Chapter 5 we present the results from an *in vivo* time-response experiment. Main results refer to gene expression analyses through RNA-Seq and RT-qPCR, as well as organ and blood cobalt metal content obtained via ICP-MS analyses.
- In Chapter 6 we show the results from the *in vivo* dose-response experiment. Results also involve RNA-Seq in addition to validation of gene expression through RT-qPCR and investigation of target proteins through western blot.
- Finally, in Chapter 7 we summarise the main results obtained throughout this project and propose new avenues for research.

2. *IN VITRO* METHODS

2.1. Cell cultures

Human U-373 MG (Uppsala) astrocytoma cells and SH-SY5Y neuroblastoma cells (Culture Collections of Public Health England, UK) were cultured in either Dulbecco's Modified Eagle Medium (DMEM; Lonza, UK) supplemented with 10% (v/v) foetal bovine serum (FBS) (Biosera, UK) or DMEM/F-12 (GIBCO, Life Technologies, UK) with 15% (v/v) FBS in astrocytes or neurons respectively, as well as 5ml of antibiotics to a final media concentration of 50IU penicillin and 50µg streptomycin (Sigma-Aldrich, UK) and 1X non-essential amino acids (NEAA; Lonza, UK). Cells were incubated at 37^{o}C and in a 5% (v/v) CO_2 air atmosphere. Cells were subcultured when reaching 70-80% confluency. Old medium was removed and cells were washed with 10 ml of versene twice in a T75 flask, then 2ml of 0.05% (w/v) trypsin in versine were added for cell detachment. After 2 minutes, 5ml medium was mixed in to inhibit trypsin, and cells were centrifuged at 800rpm for 5 min (MSE Mistral 2000; Fisher Scientific, UK) to remove media solution. Then, cells were resuspended in 6ml of complete media and passaged in a 1:2 or 1:4 ratio every 2 or 3 days depending on confluency. All reagents were prewarmed beforehand. Passage number did not exceed 30.

2.2. MTT viability assay

Cell viability was assessed by both 3-(4,5-dimethylthiazol-2-yl)-2,5-diphenyl-tetrazolium bromide (MTT) and Neutral Red (NR) assays. Cells were grown in 96-well plates (Thermo Fisher Scientific, UK) at a density of $5x10^4$ cells/cm^2 in 200µl of the appropriate complete medium for the cell type. After an incubation period of 24h, the medium was removed and newly prepared 0-500µM dilutions of cobalt (II) chloride hexahydrate ($CoCl_2$; Sigma-Aldrich, UK) in 200µl corresponding medium were added. After 24h, 48h, or 72h of Co treatment, 50µl of 10mM MTT (Sigma-Aldrich, UK) were added to each well and the cells were incubated for 4h at 37^{o}C and 5% CO_2. The liquids were then removed, and 200µl DMSO per well were applied, and absorbance was measured at 540nm using the Multiskan GO Microplate spectrophotometer (Thermo Fisher Scientific, UK).

2.3. Neutral Red (NR) viability assay

Cells were grown as described before, and in this case 200µl of 0.4mg/ml NR (Sigma-Aldrich, UK) was added for 3h. The wells were then washed with phosphate-buffered saline (PBS), followed by 100µl NR destain (50% (v/v) ethanol, 1% (v/v) glacial acetic acid, and 49% (v/v) distilled water all mixed), with the absorbance recorded at 540nm.

2.4. Proliferation assay

The Cell Proliferation ELISA, BrdU (colorimetric) kit (Roche, Germany) was used to identify cell proliferation changes after 72h exposure to cobalt. BrdU labelling solution (20µl/well) was added and cells were incubated for 4 hours at 37ºC to allow incorporation of BrdU. The cells were fixed and their DNA denatured after the 4h incubation period by removing the medium and incubating the cells with a fixative/denaturing reagent supplied for 30 minutes. An anti-BrdU antibody solution (100µl/well) was added for 90 minutes. After washing with PBS buffer and adding the tetramethyl-benzidine (TMB) chromogenic substrate solution (100µl/well), the final absorbance was detected at 370nm in the plate reader spectrophotometer (the reference wavelength used was 492nm).

2.5. Calculation of IC50 values

A sigmoidal function was considered to be the most adequate mathematical model to fit the experimental MTT, NR, and BrdU curves. The following 4-parameter Hill formula (Gadagkar and Call, 2015) was used to fit the data to estimate the cobalt dosage at which there is 50% viability or proliferation:

$$y = A + \frac{(B - A)}{[1 + (C/x)^D]}$$

Where *x* is the cobalt concentration, *y* is the Hill function value, A and B are respectively the minimum and maximum values of the Hill function, C is the calculated IC50 and D reflects the steepest slope of the function. A least-squares Matlab software fitting function was used for solving the process after an initial estimation of the parameters (*lsqcurvefit.m*; Matlab R2017b, The MathWorks Inc.). The hormetic responses interfere

with the matching process and because of that, the lowest concentrations of cobalt have been excluded to obtain suitable curve fittings.

2.6. Live/dead staining assay

Propidium iodide (PI) and carboxyfluorescein diacetate (CFDA) dyes (Molecular Probes, Life Technologies, UK) were used as markers for dead cells (red) and viable cells (green) respectively. The medium was removed and cells washed twice with PBS, after which 1ml (20µg/ml) of PI was added to the Falcon® 35mm^2 petri dishes (Corning, UK). After a one-minute incubation, PI was discarded and the dishes were rinsed again with PBS three times to remove the excessive dye. Finally, the cultures were incubated at room temperature with 1ml of CFDA (25µM in PBS pH 6.75) for 5 minutes. CFDA was removed and the dishes were washed a further three times (PBS pH 6.75). After adding 2ml PBS, pictures were taken with a Carl Zeiss Axio Imager microscope using a water lens (x20) together with the AxioVision software (Zeiss, UK).

2.7. Brightfield microscopy

Morphology of viable and dying cells was also assessed through brightfield imaging with the ZOE™ Fluorescent Cell Imager with a x20 objective (Bio-Rad, UK).

2.8. Cellular cobalt uptake measured by ICP-MS

To avoid metal contamination during cobalt uptake analysis, all the equipment was soaked in 1% (v/v) nitric acid (HNO_3) (TraceSELECT® Ultra; Fluka, Sigma-Aldrich, UK) overnight and then rinsed twice with HPLC grade water (Thermo Fisher Scientific, UK) to be finally dried in a 37^{o}C incubator.

The cells were seeded in 35 mm^2 Falcon® Petri dishes (Corning, UK) with 2ml of their corresponding complete media at a density of 5x10^4 cells/cm^2. After a 24h period that allows cells to reach 70% confluency, the medium was substituted by 500µM, 200µM, 100µM, 50µM, 25µM, and 0µM Co concentrations.

At the 24h, 48h, and 72h time-points the Petri dishes were washed with PBS (1ml/Petri dish), and the cells scraped and centrifuged for 5 minutes at 350xg, after which the

supernatants were discarded and the pellets sonicated to obtain the cobalt content of the cells. The lysates were then resuspended in 1ml of HPLC grade water and stored at -20^{o}C.

The samples were thawed on the day of the ICP-MS analysis and then centrifuged during 15 minutes at 13,200rpm. The supernatant was then diluted 5-fold in 1% (v/v) nitric acid. The Agilent 7700x octopole collision system ICP-MS (Agilent Technologies; Wokingham, UK) in helium gas mode using scandium (Sc) as internal standard processed the samples taking the maximum signal (peak height) as quantification mode.

2.9. Statistics

All the analyses were performed using one-way analysis of variance (ANOVA) followed by Dunnett's multiple comparison post-hoc test. Normality was assessed by the Shapiro-Wilk test, and homogeneity of variances was tested by Levene's test. For comparison between only two groups, an independent two-sample t test was used. Results were considered to have a significant level at $p<0.05$. Statistical analyses were performed using IBM SPSS Statistics 25.

3. *IN VIVO* MATERIALS AND METHODS

3.1. Experimental animals and housing

Experiments were performed in adult male Sprague Dawley (SD; body weight range at the start of the experiments: 210-280g) rats obtained from Charles River (UK). All animal procedures were conducted in accordance with the United Kingdom Animal (Scientific Procedures) Act 1986 under valid UK Home Office project licenses, 60/4341 and PDE5626B67, and took place at the University of Strathclyde Biological Procedures Unit (BPU). Rats were randomly housed in groups of 2 or 3 with food and water provided *ad libitum*. Their body weight and general aspects of health were monitored daily during the length of the treatment to guarantee that they remained in good health conditions.

3.2. Experimental design: control, treatment groups and sample sizes

Two separate *in vivo* experiments were performed successively. The first experiment was a time-response experiment in which we sought to compare a 7-day cobalt treatment against a 28-day treatment at a fixed cobalt dose. Animals were treated with either 1ml/kg body weight distilled water (controls) or 1mg/kg body weight (BW) $CoCl_2$ injected i.p. (treated groups). Six groups were arranged, each with n=3 rats, and 3 groups were allocated to each time point, one destined to be a control and the other two to be cobalt-treated groups. Fig. 2 depicts this information diagrammatically. The second *in* vivo experiment was a dose-response experiment. The animals were given 1ml/kg distilled water i.p., in the case of the control group, or a range of cobalt solutions- 0.1, 0.5 or 1mg/kg BW i.p. injections. Each of the four groups had n=4 rats and the total duration of this procedure was 28 days for all animals.

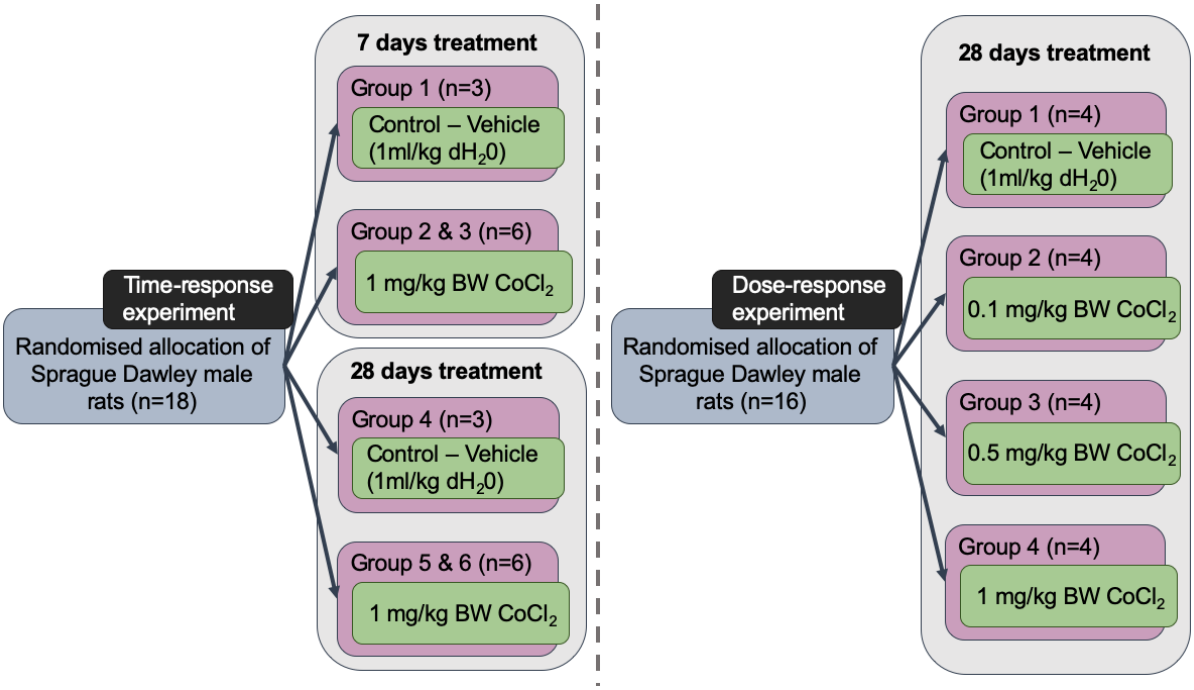

Fig. 2: Design of *in vivo* time- and dose-response experiments showing group distribution and sample size. All injections, both control and Co treated rats, were carried out intraperitonially.

3.3. Preparation of cobalt solutions and treatment of rats

Cobalt chloride hexahydrate ($CoCl_2.6H_2O$; Sigma-Aldrich, UK) was dissolved in distilled water (dH_2O) to a concentration of 0.1, 0.5 and 1 mg/ml for the intraperitoneal 0.1, 0.5 or 1mg/kg BW injections, respectively. Cobalt solutions and deionised water were sterilised into separate vials for each day through a 0.22µm syringe-driven filter (Merck Millipore, UK). The solutions were freshly made every week and the vials kept at 4^{o}C until the day of the injection, when they were pre-warmed to room temperature before being injected. The injections were performed by trained staff from the BPU and opened individual vials were discarded after being used for the one daily set of injections.

3.4. Sacrifice of animals and tissue harvest

At the end of the exposure time, animals were killed by carbon dioxide (CO_2) asphyxiation in a CO_2 chamber to obtain the tissues, which were quickly extracted after death. Blood samples were collected through cardiac puncture immediately before death with the help of a BPU licensed technician and mixed with 200µl heparin (1000 IU/mL diluted 1:10; Sigma- Aldrich; UK) to avoid clotting. The dissection and collection of tissues was carried out rapidly by a small team of BME colleagues and the student according to the experimental plan presented in Fig. 3, prioritising the organs of interest, i.e. brain and heart. From the brain, prefrontal cortex, cerebellum and hippocampus were identified and dissected separately. Each organ was weighed and sections of tissue stored appropriately until its corresponding further analysis to preserve its metal content, molecular RNAs or proteins (Fig. 4). The processing of samples is described later in each dedicated Methods section.

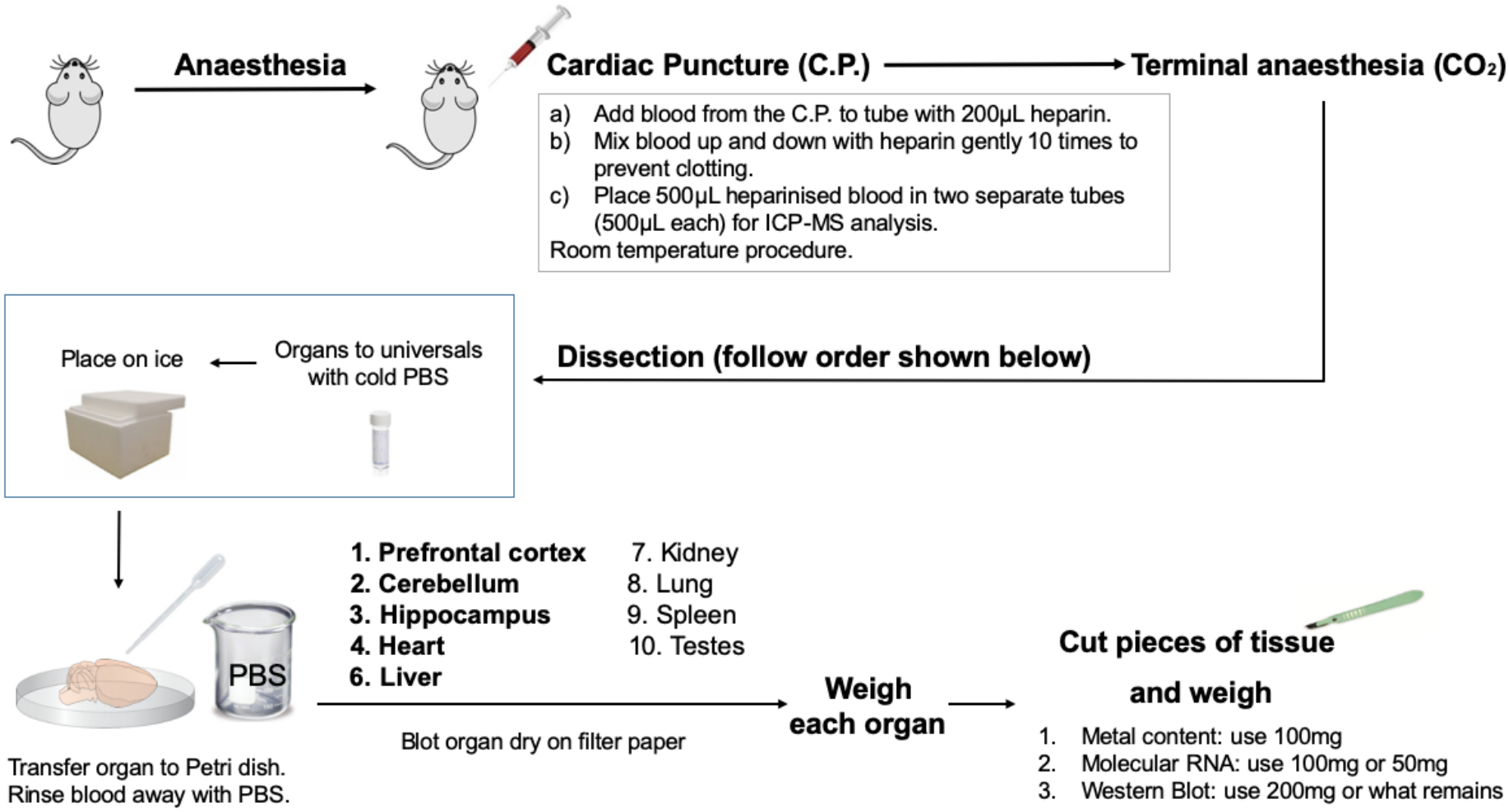

Fig. 3: Cardiac puncture, dissection and harvest of tissue for metal content, protein and gene expression analysis.

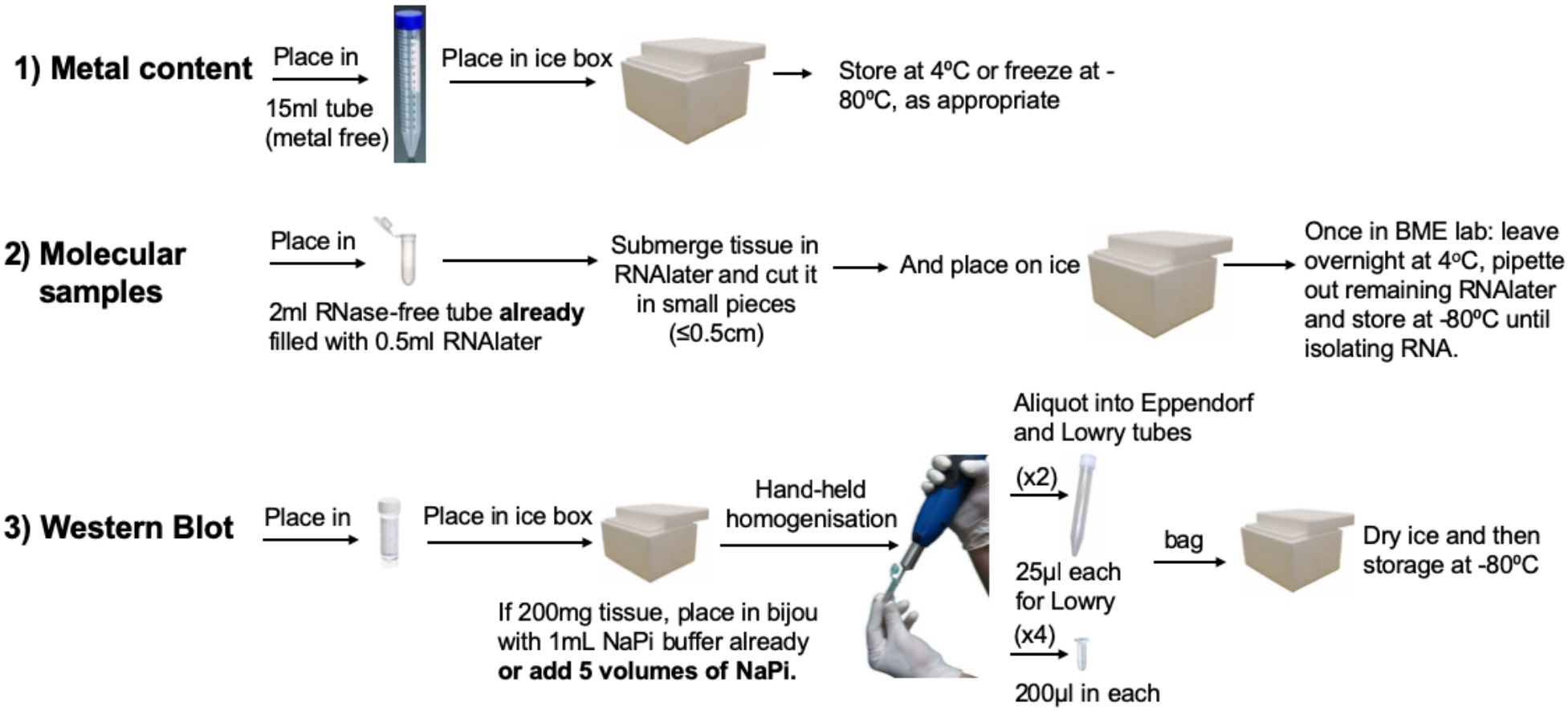

Fig. 4: Processing of harvested tissue for long-term storage and further analysis.

3.5. Tissue cobalt content measured by ICP-MS

Quantification of cobalt content in the prefrontal cortex, cerebellum and hippocampus was obtained via ICP-MS analysis. For that, 100mg of tissue from each brain part were taken and stored at -80ºC until further sample digestion. To obtain a liquid solution of the samples suitable for metal detection 0.5ml concentrated nitric acid was used per sample (HNO_3; TraceSELECT^{TM} Ultra, Sigma-Aldrich (Fluka), UK) followed by 0.25ml 30% hydrogen peroxide (w/w) (H_2O_2; Sigma-Aldrich, UK). Each reagent was left to act for 20 minutes at 100ºC in a hot block to ensure that the decomposition of the matrix was complete. A quantity of 0.25mL was transferred together with 9.75mL ultrapure water into acid-washed tubes to avoid trace metal contamination (see section 2.8 for details of material decontamination). Standard dilutions were prepared from Cobalt Standard for atomic absorption spectrometry stock (TraceCERT®, Sigma-Aldrich (Fluka), UK). The 1:40 dilution samples were serially introduced to the Agilent 7700x octopole collision ICP-MS system (Agilent Technologies, UK). Scandium or Indium were used as internal standards and data were obtained from the maximum signal with the ICP-MS operating in the Helium mode. The analysis by the ICP-MS equipment is a service provided by the Department of Pure and Applied Chemistry of the University of Strathclyde.

3.6. RNA extraction and preparation for RNA-Seq and RT-qPCR analyses

3.6.1. Isolation of RNA

For the sample preparation, 50 or 100mg from specific segments of brain tissue were dissected and placed in RNAse-free tubes with 0.5ml of RNAlater (Ambion, UK) to stabilise the RNA content and reduce degradation. RNase-free aerosol-resistant filter tips were used for all pipetting steps in the RNA work. The tissue was further cut into thin pieces and completely submerged on the stabilization solution for overnight storage at 4ºC. The next day, the RNAlater reagent was removed from each of the tubes and the tissues were frozen at -80ºC until the RNA extraction took place.

On the day of the RNA isolation, the tissue was resuspended in 1ml QIAzol lysis reagent (QIAGEN, UK) and a cone ball steel bead was placed inside the tube. The tissue was disrupted with a horizontal Retsch MM200 Mixer Mill (Retsch GmbH,

Germany) set at 30Hz, for 1 minute intervals, which shook the conical bead inside the tube. The process was repeated up to three times until complete tissue homogenisation was achieved, then the lysate was transferred to another tube with 4ml of QIAzol lysis reagent and the contents were mixed by vortexing. The pre-processed samples were further prepared according to the protocol RNeasy Plus Universal Midi Kit (Qiagen, UK) provided by the manufacturer.

3.6.2. Quality check of RNA samples

After RNA isolation, a 5µl aliquot was taken to quantify the nucleic acid concentration with the Nanodrop-2000c spectrophotometer (Labtech International, UK). RNA purity was characterised by the absorbance at 260 nm and the ratio of the absorbances 260/280nm using the same equipment. The integrity of the sample was assessed with another 5µl aliquot through microfluidic chip-based analysis (Experion RNA StdSensChip; Bio-Rad, UK) in the Experion Automated Electrophoresis System (Bio-Rad, UK). This last analysis calculates the RNA Quality Indicator (RQI) number, a standard index score ranging from 0 to 10, formulated to indicate the degradation of RNA in a sample (Denisov et al., 2008). The results of these analyses for all the samples are displayed in Appendix A.

3.7. RNA Sequencing (RNA-Seq)

3.7.1. Sample pooling for RNA-sequencing

In order to reduce the RNA-Sequencing cost, three (time-response exp.) or four (dose-response exp.) biological samples for each comparison group were pooled into a single sample. The RNA concentration of the individual samples may vary depending on the type and amount of tissue from which the RNA was isolated e.g. 100mg were used in the time-response experiment while only 50 mg were used in the dose-response experiment. Therefore, the necessary volume from each sample was adjusted to obtain an RNA quantity of 5-20µg depending on the brain area yield. At this stage, the individual sample volumes were pooled into the corresponding RNAse-free tubes for each group and the final contents were briefly vortexed. Purity and integrity of pooled samples were analysed by the Nanodrop and Experion equipment as previously described in section 3.6.2. Finally, 20-25µL aliquots of the pooled samples were sent

to BGI Tech Solutions (Hong Kong), who were entrusted with the RNA-sequencing analysis. The remainder of the pooled samples were retained for further in-house analysis.

3.7.2. RNA-Sequencing analysis by BGI

RNA-sequencing of the pooled samples was performed by BGI Tech Solutions (Hongkong) Co. Ltd. using a BGISEQ-500 sequencing platform with depth of 20 million base pairs (Mb) clean reads per sample and 50 single-end bases (50SE) read length. Filtering of clean reads and their mapping to the UCSC rn6 rat reference genome were carried out by BGI, in addition to the quantification of gene fold-change.

3.7.3. Gene Ontology (GO) and KEGG Pathway enrichment analysis

The software tool Cytoscape and its plugin ClueGO were used to conduct the Gene ontology analysis of the DEGs. Enrichment analysis on the transcriptome was performed to connect gene expression data with functional activity of the specific genes that could point towards cobalt toxicity induced pathologies. ClueGO allowed the comparison to different reference ontology sets, such as Molecular Function (GO MF; 08/04/2016), Biological Process (GO BP; 08/04/2016), Cellular Component (GO CC; 08/04/2016), which describe specific gene function and cellular location aspects of gene activity, as well as the Kyoto Encyclopedia of Genes and Genomes (KEGG; 14/06/2016) for the specific enrichment of known pathways. The DEGs were mapped to the symbols (Symbol ID) of the *Rattus norvegicus* gene list to generate the enrichment with the different GO or KEGG sets.

Additionally, two other online software programmes were used to complement enrichment analyses: STRING (https://string-db.org/) and PathView Web (https://pathview.uncc.edu/). STRING creates protein-protein interaction (PPI) networks of gene-protein products (Szklarczyk et al., 2021), while PathView Web creates graphs with enriched KEGG pathways and marks the represented DEGs on the pathway (Luo et al., 2017).

3.7.4. Identification of Differentially Expressed Genes (DEGs) and hierarchical clustering

Further bioinformatic analyses were performed in Matlab software. Different fold change and p-value threshold criteria were considered for the selection of DEGs, since too stringent or permissive conditions can alter the interpretation of transcriptomic results (Dalman et al., 2012). The fold change is a description of the difference of expression level in a certain gene between control and treatment samples. The ratio is scaled using the binary logarithm, i.e. $\log_2$ Ratio (Treatment/Control gene expression level), and the absolute value is taken (Zhao et al., 2018). This is used as a way to measure the change in the expression levels of a gene. The Matlab *clustergram* toolbox was used to perform the hierarchical clustering of the selected DEGs with the corresponding dendrogram. The genes were clustered following the Euclidean distance metric and complete linkage over the DEGs' fold change.

3.8. Quantitative real-time polymerase chain reaction (RT-qPCR)

RT-qPCR was used to obtain the expression of genes of interest in individual samples in order to validate RNA-Seq results. RT-qPCR is a molecular technique that uses the DNA-based technique of polymerase chain reaction (PCR) to amplify complementary DNA (cDNA) created from the mRNA transcripts in the samples. In this workflow, cDNA is synthesised from the mRNA templates through a first-strand synthesis reaction with reverse transcriptase enzyme, therefore the cDNA becomes a proxy for mRNA amplification. We are interested in mRNA as gene expression levels will directly impact the expression of proteins that might respond under cobalt poisoning. To assess the gene expression, we employed quantitative PCR (qPCR), a technique that incorporates a fluorescent reporter through the thermal cycling that allows us to track the fluorescence levels during the amplification process making possible to quantify gene expression.

All RT-qPCR experiments were performed in accordance with the minimum information for publication of quantitative real-time PCR experiments (MIQE) guidelines. The MIQE guidelines specify a list with 85 items that should be provided when publishing, with the aim of increasing reproducibility and evaluating the validity of published quantitative PCR assays (Bustin et al., 2009; Taylor et al., 2010). It

accounts for topics such as research design, sample procurement, storage, RNA extraction, quality control, reverse transcription protocol details, primer design, selection of reference genes and validation of RT-qPCR results. The guidelines indicate essential or desirable technical information that should be included with the submission of manuscripts to journals in order to improve the quality of publications. We have worked accordingly with the MIQE guidelines and followed the recommendations. The checklist for RT-qPCR assays performed with samples from our *in vivo* experiments is fully displayed in Appendix C.

3.8.1. cDNA synthesis

In order to obtain cDNA from our RNA samples we used the Tetro cDNA Synthesis Kit (Bioline, UK) for the *in vivo* time-response experiment. Following the pack instructions, RT+ and RT- solutions for each sample were made with 4μl 5x RT buffer, 1μl of a mix of primer Oligo$(dT)_{18}$, 1μl of 10mM deoxynucleoside triphosphates (dNTPs) for cDNA synthesis material and 1μl of RNAse inhibitor protein (10u/μl). RT- samples are established 'no reverse transcriptase' controls generated to detect genomic DNA (gDNA) contamination of the isolated RNA that could lead to overestimation of mRNA expression. Therefore, 1μl reverse transcriptase (200u/μl) was added only to the RT+ tubes, and the same volume was substituted by DEPC water in the RT- solutions. In the tube for each sample, 1μg RNA concentration in DEPC water was added, as well as RT- or RT+ solutions to a final volume of 20μl. A thermal cycler (Model 480, Perkin Elmer, UK) was set to 45°C for 30 minutes to catalyse the reverse transcription reaction in the sample tubes, and to 85°C for 5 minutes to inactivate the RT enzyme. After cooling down the samples, they were diluted with x1 RT buffer and vortexed to obtain 100μL total volume. The cDNA samples were stored at -20°C until further use for RT-qPCR reactions.

For ease of use and supplier issues, the LunaScript RT SuperMix Kit (New England Biolabs, UK) was utilised to generate cDNA for the dose-response experiment samples instead of the Tetro cDNA Synthesis Kit. The RT SuperMix and the No-RT control mix already contain dNTPs, RNase inhibitor, and a combination of Oligo (dT) and random hexamer primers to improve annealing. The RT SuperMix additionally includes reverse transcriptase. The reagent concentrations are not provided by the company. To each

RT+ or RT- reaction, 4μL of RT SuperMix and the No-RT control mix were respectively added, in addition to enough volume of each sample to attain 1μg RNA, and RNAse-free water to make up 20μL in each tube. The cycler was pre-heated at 25ºC, and primers were allowed to anneal for 2 minutes at this temperature, continuing at 55ºC for cDNA synthesis during 10 minutes, and the final RT inactivation at 95ºC for 1 minute.

3.8.2. Gene primer design

The primer sequences were designed to span an intron or exon-exon junction through the NCBI Primer-BLAST tool (https://blast.ncbi.nlm.nih.gov/Blast.cgi) to selectively amplify cDNA and not contaminant genomic DNA (gDNA) which may give a false positive signal. The primer design criteria followed is in displayed in Table 1.

Table 1: Criteria for the design of the primers selected through NCBI Primer-BLAST tool. Bp refers to base pairs.

Primer design condition	Design criteria
PCR primer size (bp)	130-150
Primer melting temperature (Tm)	59-61°C
Max. melting temperature difference between forward and reverse primer	≤ 1°C
Stability at 3' primer end	Max. 3 Gs or Cs bases in the last 5bp
Long runs of repeated bases	Max. 4 contiguous repeated bases
Conditions for genomic DNA exclusion	Exon junction span (forward primer or reverse primer) or intron inclusion
GC content (%)	40-60%
Specificity	Specific to targets, only predicted transcript variants of targets allowed when no option.

Oligos were synthesised and purchased from Integrated DNA Technologies (IDT, Belgium). The genes with their accession number and primer sequence, amplicon length and melting temperature are presented in the tables below (Table 2, Table 3 and Table 4). Table 2 shows the primers selected for the time-dose response experiment, while Table 3 and Table 4 refer to the designs for the dose-response experiment, Table 3 presents the primers selected for the pref. cortex and Table 4 for hippocampus respectively.

Table 2: Primer sequences of prefrontal cortex and cerebellum-targeted genes designed for the *in vivo* time-response experiment. Gene symbol, accession number, amplicon length and calculated primer melting temperature (Tm) are supplied as obtained from NCBI Primer-BLAST.

Pref. Cortex and Cerebellum primers – Cobalt time-response experiment primers					
Gene	Accession no.		Primer sequence (5'-3')	Length (bp)	Tm
Nos1	NM_052799.1	F	TGACCCAAGGTCTTTCCAATGT	131	59.82
		R	CTGATTCCCGTTGGTGTGGA		59.96
Car2	NM_019291.1	F	GCTGCAGAGCTTCACTTGGT	149	60.89
		R	TGCAGTGCTTCAGTGATTTTCTG		60.00
Car4	NM_019174.3	F	ATGCAGCTCCTTCTTGCTCT	133	59.38
		R	AGTCTCCAGTCCATTGTTCAGG		59.70
Car5b	NM_001005551.2	F	GTTTTGAGGATGCAGCACTGG	132	60.07
		R	CCAGGGTATCCTTGTGCTTAATTG		59.66
Pde2a	NM_031079.2	F	GACACGCAAGTGCTGGTCATA	135	60.94
		R	CACCAGAGCATGCTTCTCCA		60.04
Pde5a	NM_133584.1	F	TGGAGCCCGCTGATCTAATG	132	59.61
		R	GCAGGGGCAAACAGTCTTCT		60.54
Pde8b	NM_199268.1	F	AAGCCGTGTGCAGGTCAAT	134	60.23
		R	TCTCCGGTTAAAGCCTGCAT		59.38
Prkg1 (Pkg)	NM_001105731.3	F	CACCTTTCTCAGGCCCAGAT	137	59.38
		R	TTCTGATGGGTTGTCCCTGC		59.96
Prkar2b (Pka)	NM_001030020.1	F	ACCCCCAGTAAGGGTGTCAA	144	60.40
		R	TTCTGCACATACCGAGGCAC		60.39

Table 3: Primer sequences of prefrontal cortex-targeted genes designed for the *in vivo* dose-response experiment. Gene symbol, accession number, amplicon length and calculated primer melting temperature (Tm) are supplied as obtained from NCBI Primer-BLAST.

Pref. Cortex - Cobalt dose response *in vivo* experiment primers					
Gene	Accession no.		Primer sequence (5'-3')	Length (bp)	Tm
Ttr	NM_012681.2	F	GGCTCACCACAGATGAGAAGT	149	59.72
		R	GGTGTAGTGGCGATGACCAG		60.46
Tnf	NM_012675.3	F	ACGTCGTAGCAAACCACCAA	132	60.18
		R	AGATAAGGTACAGCCCATCTGC		59.63
Akap14	NM_021703.1	F	TCAGTTTGTGGAAGAAGCCAGA	141	59.83
		R	GCATAGTACACCCAGCGGTT		60.11
Spata18	NM_199374.2	F	CCCAGGTTCAAGACGATCTGAC	139	60.68
		R	TCCTCCTGGGCTTGAAGAGAT		60.27

Table 4: Primer sequences of Hippocampus-targeted genes designed for the *in vivo* dose-response experiment. Gene symbol, accession number, amplicon length and calculated primer melting temperature (Tm) are supplied as obtained from NCBI Primer-BLAST.

Hippocampus - Cobalt dose response *in vivo* experiment primers					
Gene	Accession no.		Primer sequence (5'-3')	Length (bp)	Tm
Kl	NM_031336.1	F	TCCCTGTGACTTTGCTTGGG	141	60.18
		R	TTGGCTACAACCCCGTCTAC		59.39
Cxcl13	NM_001017496.1	F	TGTAGGTGTTCCAAGGTGAGC	150	59.93
		R	TCTGGCAGTAGGATTCACACAT		59.16
Sry	NM_012772.1	F	TCATCGAAGGGTTAAAGTGCCA	133	59.96
		R	AGCTCTAGCCCAGTCCTGTC		60.69
Trpv5	NM_053787.2	F	ACGAACTCTGGAGAGCACAG	138	59.40
		R	GGTGTTCAACCCGTAAGAACC		59.12

3.8.3. Performing PCR

PCR experiments were performed with triplicate RT+ per sample, one no-reverse transcriptase control (RT-) per sample and one no-template control (NTC) per gene and with the corresponding reference gene controls. The SYBR green detection method was used for the detection of amplification with the kit PowerUp™ SYBR™ Green Master Mix (Applied Biosystems, Thermo Fisher Scientific, UK). This kit already contains an optimised mix of Taq DNA polymerase, SYBR™ Green Dye, dNTPs, Uracil-DNA Glycosylase (UDG) to remove carryover PCR amplicon contaminants, and ROX™ passive dye as a reference to normalise the SYBR Green fluorescent signal, in addition to optimised buffers. To avoid PCR contamination, we used RNase-free aerosol-resistant tips throughout all the process.

The forward and reverse primers (10pM/μL) and molecular grade water were mixed with Master Mix (2X). Samples consisting of 1μL cDNA were pipetted in MicroAmp Fast Optical 96-well reaction Plates (Applied Biosystems, UK) and the previous mix was added up to a final volume of 20μL per well. The plate was covered with MicroAmp Optical Adhesive Film Kit (Applied Biosystems, UK) to avoid contamination and evaporation during the PCR process. After a short centrifugation, the plate was introduced in the StepOnePlus Real-Time PCR system (Applied Biosystems, UK). The specific thermal cycling parameters were set according to the optimised PowerUp™ SYBR™ Green Master Mix for Fast cycling mode in the StepOnePlus Real-Time PCR system (Table 5). The initial holding steps shown in the Table 5 allow for the activation of UDG and Taq polymerase. This is followed by the cyclical denaturation and annealing of cDNA. During denaturation the RNA-cDNA hybrid separates in the first cycle, once cDNA is in the form of single strands the temperature drops allowing for the annealing of the primers of interest to their complementary sequences in the single cDNA strands, and then the polymerase proceeds to extend the sequences. The cDNA region from our gene of interest that is located between the primers is therefore duplicated over the cycle and SYBR™ Green can bind to the double stranded DNA giving a fluorescent signal. This cycling process is repeated 40 times. At the end of the cycling process, a melt curve was produced and inspected for the occurrence of primer dimers and possible contamination of reagents or genomic DNA.

Table 5: Fast PCR thermal cycling steps based on PowerUp™ SYBR™ Green Master Mix instructions for StepOnePlus Real-Time PCR system.

	Step	T (°C)	Duration	Cycles
Holding stage	UDG activation	50	2 minutes	Hold
	Dual-Lock DNA polymerase	95	2 minutes	Hold
Cycling stage	Denature	95	3 seconds	40
	Anneal/extend (data collection)	60	30 seconds	
Melting curve	Denature	95	15 seconds	1
	Anneal/extend	60	1 minute	
	Denature (data collection)	95	15 seconds	

3.8.4. Relative gene expression calculations

The method used to calculate the fold-change is the comparative C_T method (Schmittgen and Livak, 2008), C_T (or Ct) being the threshold cycle detected over the 40 run cycles. The threshold cycles of target genes are normalised to the C_Ts of the chosen reference gene from Table 6, which is used as an internal control. The following formula shows how the relative mRNA expression change between treatment and control samples has been calculated:

Fold change= $2^{-\Delta\Delta C_T}$

Where ΔΔCt =

[(C_T gene of interest – C_T internal reference gene) $_{\text{treatment sample}}$

– (C_T gene of interest – C_T internal reference gene) $_{\text{control sample}}$]

For gene normalization, we studied the expression of typical brain reference genes *Ywhaz*, *Tbp*, and *Pes1*. Primer sequences are shown in Table 6. After quantification the RefFinder web-based tool: https://www.heartcure.com.au/reffinder/ (Xie et al., 2012) was used to define the most stable reference gene for each tissue. Full results of RefFinder analyses for each tissue are shown in Appendix B.

Table 6: Primer sequences of control genes, with gene symbol, accession number, amplicon length and calculated primer melting temperature (Tm) as supplied by NCBI Primer-BLAST.

Primers of Control genes for both dose and time-response *in vivo* experiments					
Gene	Accession no.		Primer sequence (5'-3')	Length (bp)	Tm
Ywhaz	NM_013011.3	F	GAGTCGTACAAAGACAGCACG	131	59.29
		R	AAAGGTTGGAAGGCCGGTTA		59.52
Tbp	NM_001004198.1	F	ACTTCGTGCCAGAAATGCTGA	140	60.54
		R	TGGATTGTTCTTCACTCTTGGCT		60.18
Pes1	NM_001044228.1	F	GTACAAGGTGTTTGTCCGGAAG	148	59.45
		R	GTCACGCAACGCATCGATAA		59.36

3.9. Protein immunoblotting

3.9.1. Lowry assay for determination of protein content

Immediately after dissecting tissue destined for blotting, 200mg tissue samples were homogenised with 1mL sodium phosphate buffer (Na_3PO_4; 0. 1 M Sodium Phosphate buffer pH 7. 6), or 5 proportional volumes of sodium phosphate buffer if less tissue is available with a T8 Ultra Turrax hand-held homogeniser (IKA, UK). In order to quantify protein concentration in the homogenised samples, the Lowry protocol was used (Lowry et al., 1951). Bovine Serum Albumin (BSA) was utilised as standard. Aliquots of homogenised brain samples were diluted 1:10 in sodium phosphate buffer and briefly vortexed. From that 50μL were taken and mixed with 950μl of 0.5M NaOH. Solution A was made of 2% (w/v) $NaCO_3$, 1% (v/w) $CuSO_4$ and 2% NaK (w/v) Tartrate following a 98:1:1 ratio. For the solution B, Folin was diluted at 1:4 with dH_2O. Reagents for solutions A and B were all purchased from Sigma-Aldrich. In each tube, 5 mL of solution A were added to each tube and well mixed with the sample protein solutions. After 10 minutes, 0.5mL solution B was mixed in the tubes. Thirty minutes later, the resulting solutions were measured at a wavelength of 725nm against a water blank in the UV-2401PC spectrophotometer (Shimadzu, UK).

3.9.2. Protein sample preparation

Homogenised tissue samples were prepared at a final protein concentration of 1mg/mL in 2x Laemmli buffer (Sigma-Aldrich, UK) following the results from the Lowry assay. A 1:10 dilution with sodium phosphate buffer was carried out first and the solution was aliquoted into Eppendorf safe-lock tubes. The amount of 2X Laemmli buffer needed to attain 1mg/mL per tube was added and mixed with the diluted sample solution. Samples were then boiled for three minutes and later frozen at -20^{o}C for preservation.

3.9.3. SDS- Polyacrylamide Gel Electrophoresis (PAGE)

To create gel stacks, short and long glass plates were clipped and assembled on the casting chamber from the Mini Protean Tetra Cell (Bio-Rad, UK). After checking for leaks, 12.5% (acrylamide) resolving gel and stacking gel were made. The proportions of 40% acrylamide, 1.5% APS, and TEMED needed are presented in Table 7 (all Sigma-Aldrich, UK). The resolving buffer was poured, in addition to some water on top of the gel to avoid drying. After 15 minutes, water was dried with filter paper and the newly made stacking gel was poured on top. The combs were inserted into the stacking gels to create the lanes.

The plate-gel sandwiches were taken from the chamber and securely positioned into the electrode from the Mini Protean System. The chambers were filled with 1X Tris/Glycine/SDS Buffer (Sigma-Aldrich, UK). Then, the combs were removed from the stacking gel and the remaining wells were loaded with 10μg Laemmli sample per well with gel-loading tips (Thermo Fisher Scientific, UK). One of the wells was reserved to the Novex Sharp pre-stained marker standard (Thermo Fisher Scientific, UK). The electrode cores were filled with running buffer and placed inside the Mini Protean Tetra buffer tank. Similarly, the space between the cores and the tank borders was filled with running buffer up to the manufacturers' indicated levels. The cabled lid was placed on the tank and the voltage was set at 150V with the highest current (initially 400mA). The gels were run for an hour and 10 minutes.

Table 7: Resolving and stacking gel volumes for SDS-PAGE.

Solutions	Resolving Gel (12.5%)	Stacking gel
Stacking gel buffer (0.5M Tris (pH 6.8))	-	2.5ml
Resolving gel buffer (1.5m Tris buffer pH 8.8)	5.625ml	-
Acrylamide (40%)	7.03ml	1ml
1.5% Ammonium persulfate (APS)	1.125ml	0.5ml
Distilled water	8.72ml	6ml
TEMED*	17.5µl	10µl

3.9.4. Western blotting

Gels were lifted from the glass plates at the end of the run and positioned appropriately in between the Trans-Blot Turbo Mini 0.2 µm PVDF Transfer Packs from Bio-Rad (UK), the membrane of which has a pore size more convenient for transfer of lower molecular weight protein. The sandwich was placed on top of the cassette from the Trans-Blot Turbo Transfer System (Bio-Rad, UK) and the transfer of proteins was carried out through the Mixed MW (Turbo) program (7 minutes up to 25V).

The membrane was removed and soaked in blocking buffer made with 5% BSA (Sigma-Aldrich and Fisher Scientific, UK) in TBST (20 mM Tris, 150 mM NaCl and 0.1% (w/v) Tween-20 (pH 7.5); all Sigma-Aldrich, UK) for 2 hours at room temperature. Then it was washed for 5 minutes in TBST. The primary antibody (Table 8) was diluted in 0.5% BSA in TBST. The membrane was left submerged in the antibody dilution overnight at 4^{o}C. The next morning it was washed with TBST 3 times for 5 minutes and finally placed in the orbital shaker covered with diluted HRP–conjugated goat anti-rabbit secondary antibody (Table 8) for 90 minutes at room temperature. The antibody was collected and the membrane washed 3 times in TBST. In the dark room, washing buffer was discarded and Enhanced chemiluminescent (ECL) reagents were added (all Sigma-Aldrich, UK) to the membrane in the same proportions and mixed for 2 minutes to detect immunoreactivity. The membrane was transferred to the autoradiography cassette (Fujifilm), covered with cling film and the X-ray film on top (Santa Cruz Biotechnology, Inc., UK) leaving it enough time for signal detection.

Finally, the films were inserted into the JP-33 X-ray Film Processor for automatic development (JPI Healthcare, Korea).

Some of the primary antibodies had similar molecular weight to beta-actin (ACTB), the loading control. In these cases, rather than cutting the membrane and separating the incubation of target and loading control primary antibodies, the blot membrane was first incubated with the primary antibody of interest following the same protocol presented before. Then, the blot membrane was submerged in 15mL stripping solution (206.5mM Tris-HCl and 87mM SDS in 0.4L of dH_2O (pH 6.7), later adding 0.5L dH_2O) with 105μL β-mercaptoethanol. The membrane was placed in the orbital shaker at 60°C during 30 minutes. Then it was washed with TBST four times, and was re-probed with beta-actin.

Table 8: Antibodies used and their characteristics (biological host, supplying company, clonality), as well as their dilution and predicted band size (kDa).

Name	**Hosts**	**Supplier (Cat. #)**	**Clonality**	**Dilution**	**Expected size (KDa)**
Primary antibody					
SPATA18	Rabbit	Abcam (ab180154)	Monoclonal	1/1000	61
TTR	Rabbit	ThermoFisher (PA5-80196)	Polyclonal	1/1000	Homotetramer: 14, 30 and 55
AKAP14	Rabbit	Abcam (ab180160)	Monoclonal	1/1000	23
TNF	Rabbit	Bio-Rad (AAR33)	Polyclonal	1/1000	17
Angiogenin (ANG)	Rabbit	Abcam (ab189207)	Polyclonal	1/1000	17
Actin (ACTB)	Rabbit	Abcam (ab227387)	Polyclonal	1/20000	42
Secondary antibody					
HRP-anti-Rabbit	Goat	Sigma-Aldrich (A6154)	Polyclonal	1/5000	-

3.9.5. Western blot band signal analysis

Autoradiography films were scanned at 600 dpi resolution in TIFF format. The band of interest was identified for each primary antibody based on the source information and the Novex marker stains. All bands were quantified through the image analysis software FIJI by densitometry analysis, subtracting background and normalising to beta-actin.

3.10. Statistics

As described for the *in vitro* methods (see section 2.9 for details).

4. AN *IN VITRO* STUDY INTO COBALT TOXICITY IN BRAIN CELLS

4.1. Introduction

Cobalt is very soluble in blood and tends to travel systemically reaching organs far from the originating MoM prosthesis (Bijukumar et al., 2018), such as the brain. Several studies have looked into its toxic effects on the CNS, however, the information we have is still scarce with regards to the mechanisms of action. Although *in vitro* conditions do not replicate the complexity of the brain, *in vitro* models of neurotoxicity are a valuable tool to observe cellular processes and determine the mechanisms of action of toxins (Barbosa et al., 2015).

The main purpose of the work detailed in this section is to characterise cobalt toxicity in brain cell lines across a wide range of concentrations and time-points. In particular, to observe how cobalt affects the viability, proliferation, and morphology of neuronal cells, as well as to see how much cobalt they are able to assimilate. To better encompass the complexity of the brain, we inspected the similarities and differences between two human brain cell lines of different origins, neuroblastoma SH-SY5Y and astrocytoma U-373, which we used as representatives of neurons and astrocytes respectively. Neurons are specialised in the transfer of information, while astrocytes have a supportive and defensive function. As we previously mentioned in the Introduction, cobalt has been frequently used at high concentrations (>100μM) to induce hypoxia *in vitro* (Muñoz-Sánchez and Chánez-Cárdenas, 2019), but we lack information at lower cobalt doses, which perhaps may better correspond with the levels found in MoM patients. In order to model the release of a high number of cobalt ions we used cell medium as an *in vitro* proxy for plasma and neural cell lines to understand how cobalt may impact cells in the brain directly. Although 1μM equates to 58.93 μg/l (Co MW = 58.93), which could correspond to a very elevated level of cobalt in blood in patients with a MoM implant, the composition of plasma and cell medium differs considerably (Ackermann and Tardito, 2019). It is known that free cobalt ions are not made available to cells cultured in DMEM until 40μM Co due to the complexation of cobalt with albumin and histidine in the media (Sabbioni et al., 2014b). Thus, the dose

range selected covered between 25μM and 500μM to account for situations in which cobalt ions would be bound to these proteins, as well as free, in addition to also involving doses known to induce hypoxia and further toxicity (>100μM). The information we aim to obtain about cell susceptibility and possible cobalt toxicity mechanisms in the brain could give insights into the modes of action of cobalt toxicity. In addition, it could provide a future model to explore the susceptibility of other cells to the harmful effects of cobalt associated with systemic conditions in MoM patients.

The techniques used in this study were presented and described in Chapter 2. In brief, cells were cultured and treated with cobalt concentrations ranging from 0 to 500μM. MTT and NR assays were applied to evaluate viability, and BrdU to measure proliferation. Changes in morphology through cobalt addition were observed by brightfield and fluorescence microscopy. Inductively coupled plasma mass spectrometry (ICP-MS) was employed to detect the metal content of the cells. The results to these tests are presented in the next section and have been published (Gómez-Arnaiz et al., 2020).

4.2. Results

4.2.1. Cobalt is toxic at high concentrations in *in vitro* viability tests

MTT and Neutral Red (NR) viability tests were used to investigate the metabolic and lysosomal activity of neurons and astrocytes. Fig. 5 shows the viability results across 24, 48, and 72h time points at different cobalt concentrations, revealing a decrease in cellular activity in response to cobalt ions across time points. It can be observed that *in vitro* cobalt treatment leads to dose- and time- dependent toxicity in both astrocytes and neurons. Post-hoc tests show that cobalt significantly impairs viability at high concentrations compared to the control groups ($p<0.05$). Moreover, neurons show greater susceptibility to cobalt as they follow a steeper trend towards cell death than astrocytes.

There is also an increase in viability at the lowest cobalt concentrations, though only significant in certain cases (Fig. 5a, b, f). Interestingly, the doses at which these increases appear are inconsistent across time points and between cell lines. It is possible that this effect is part of a homeostatic reaction to mild cobalt toxicity, however, we cannot conclude whether it is fully representative of the cobalt response due to its variable presence across the cobalt concentrations and time points studied.

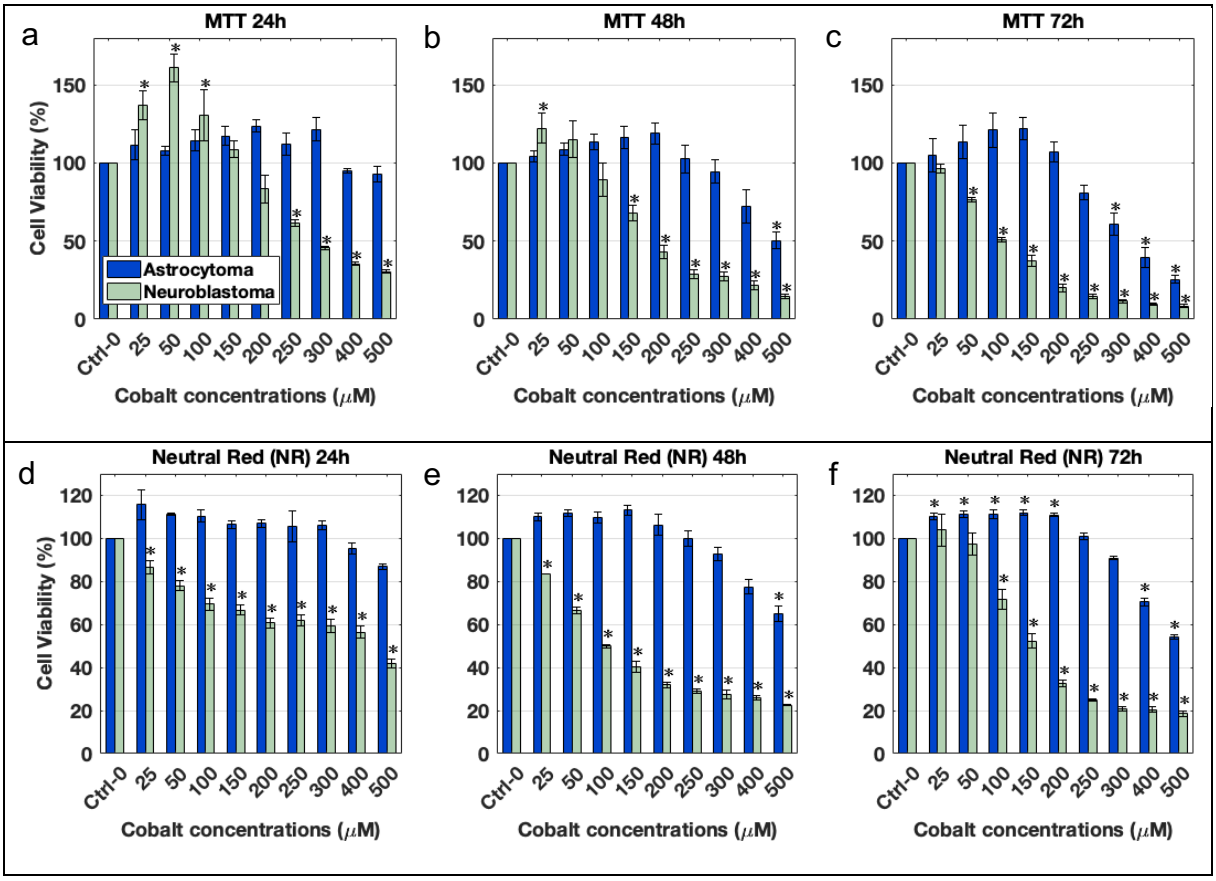

Fig. 5: Cell viability determined by the MTT (a-c) and NR (d-f) assays (n=3) in the astrocytoma U-373 (blue) and the neuroblastoma SH-SY5Y (green) cell lines after 24 (a, d), 48 (b, e), and 72h (c, f) treatment with cobalt at different concentrations. * significantly different from control groups (0μM cobalt) by one-way ANOVA with Dunnett's multiple comparison ($p<0.05$).

As mentioned in the *in vitro* methods section 2.5 , the Hill function was chosen to model the dose-response curves and calculate the IC50s. Fig. 6 and Fig. 7 show the fitted Hill curves and the calculated IC50s. In some cases, it was not possible to calculate these concentrations as there were no viability values recorded beyond a 50% viability drop. Table 9 shows the final IC50 values from MTT and NR assays, significantly different at 72h between SH-SY5Y and U-373 ($p=0.001$), which suggests that neurons are more vulnerable to cobalt than astrocytes.

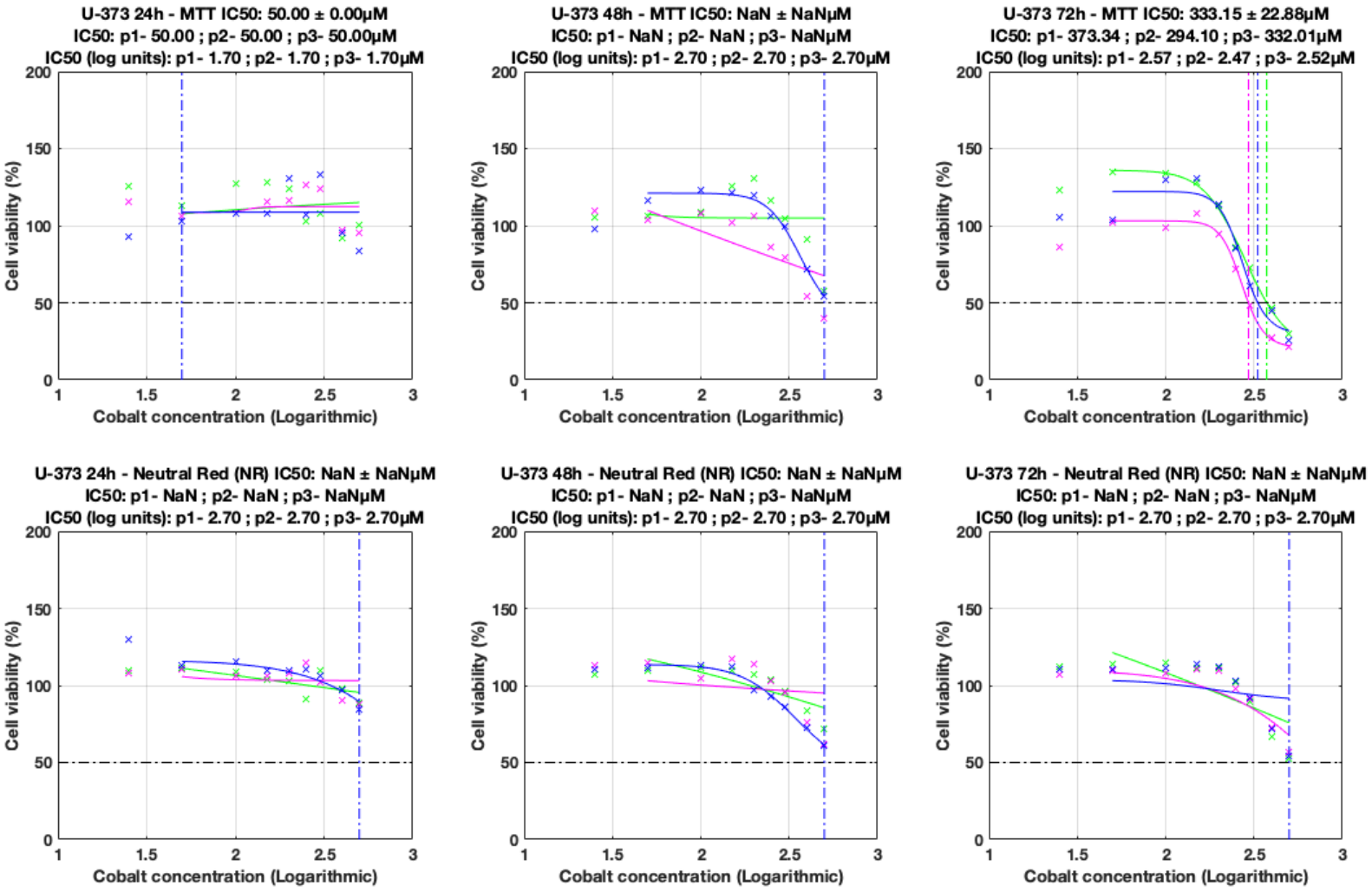

Fig. 6: IC50s calculations for MTT (upper panel) and NR (lower panel) assays in U-373 astrocytoma at 24, 48 and 72h. Data fit was achieved through the Hill function (NaN stands for 'Not a Number', and shows in cases where it was not possible to retrieve a solution for the IC50 calculations).

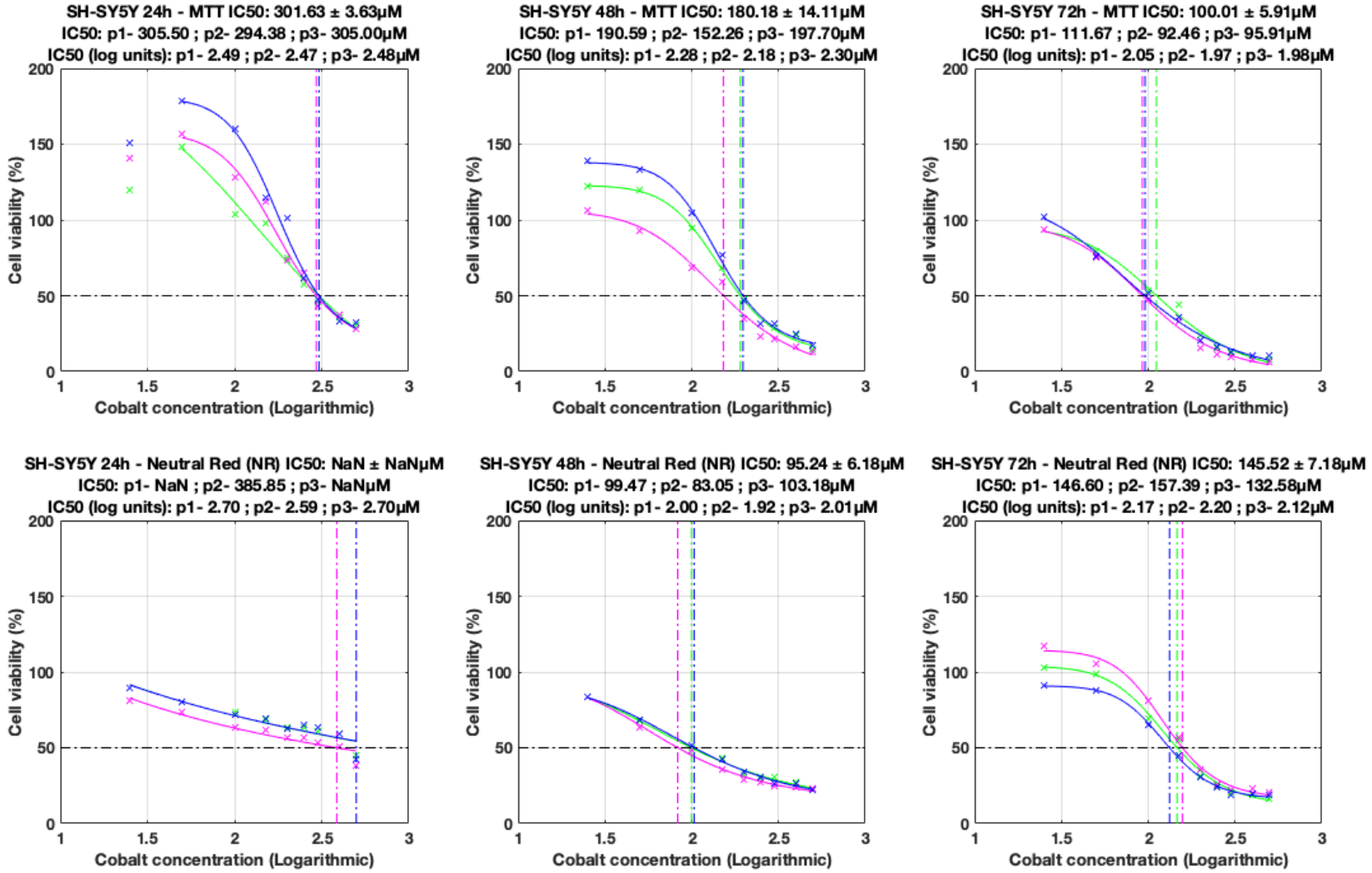

Fig. 7: IC50s calculations for MTT (upper panel) and NR (lower panel) assays in SH-SY5Y neuroblastoma at 24, 48 and 72h. Data fit was achieved through the Hill function.

IC50s (μM)		24h	48h	72h
MTT	Astrocytoma (U-373)	-	-	333.15 ± 22.88
	Neuroblastoma (SH-SY5Y)	301.63 ± 3.63	180.18 ± 14.11	100.01 ± 5.91 *
NR	Astrocytoma (U-373)	-	-	-
	Neuroblastoma (SH-SY5Y)	-	95.24 ± 6.18	145.52± 7.18

Table 9: IC50s of MTT and NR assays calculated as 50% of the control from trend-line equations at 24h, 48h, and 72h. Results are cobalt concentration values expressed in μM (mean ± SEM, n = 3). * Significant difference between the two cell lines at that time-point calculated by two sample t-test (p=0.001).

MTT appears to be a more sensitive viability assay than Neutral Red, but the latter could be more robust. Sample screening under the brightfield microscope during the MTT and NR assays showed important changes of morphology during MTT tests and large needle-shaped formazan crystals in SH-SY5Y cells (Fig. 8) suggesting that MTT could be especially toxic for this cell type in comparison to astrocytes (Fig. 9). While Fig. 9 shows that astrocytes maintain their structure throughout the assay, neurons have lost their elongated morphology and become rounded. MTT has been reported to produce this effect specifically in SH-SY5Y neurons (Lü et al., 2012). The NR assay does not interfere with morphology in any case. Therefore, viability comparisons between SH-SY5Y neurons and U-373 astrocytes will be made carefully.

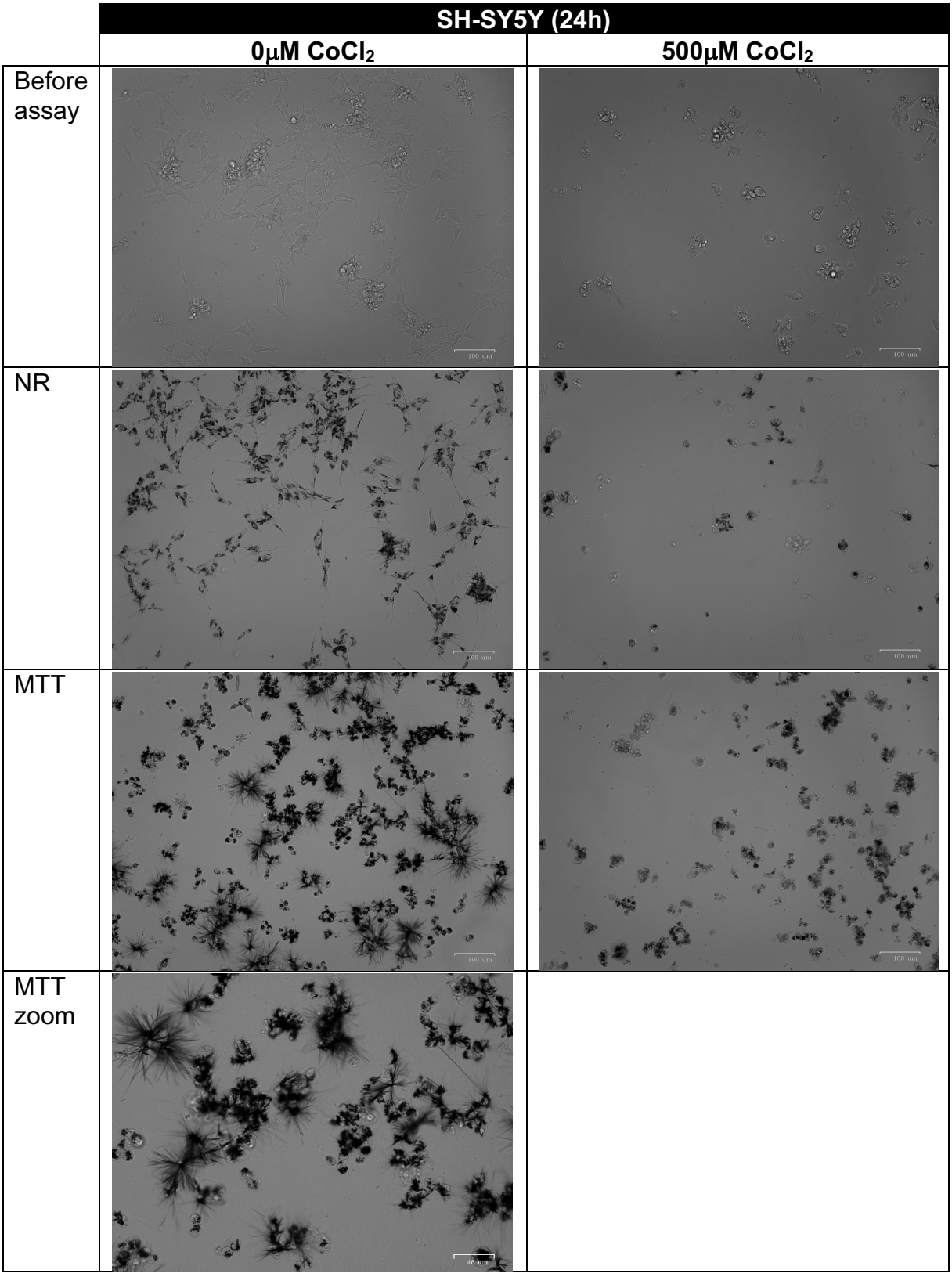

Fig. 8: Brightfield of control SH-SY5Y neuroblastoma cells after 24h plating under MTT and NR treatments.

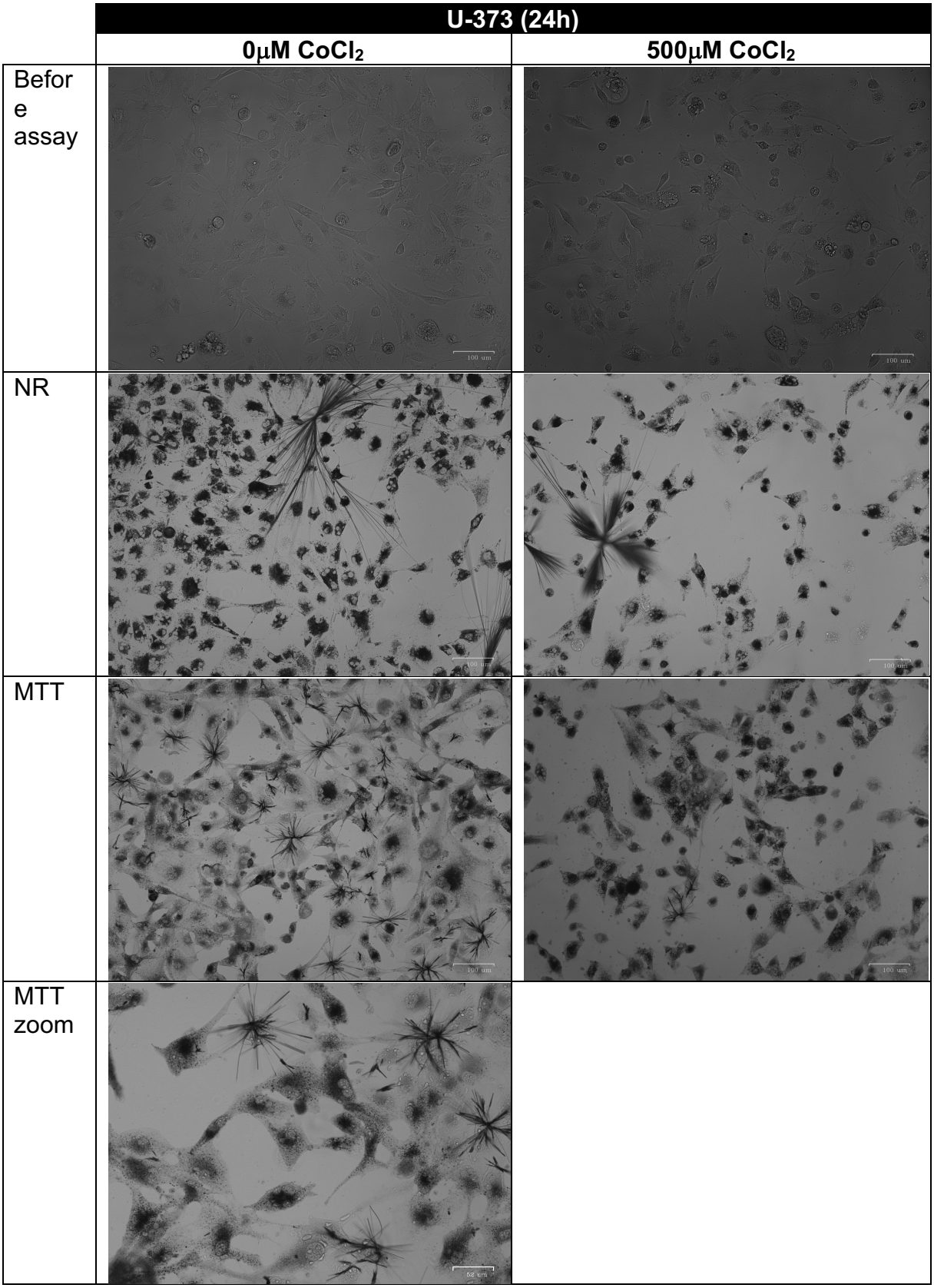

Fig. 9: Brightfield of control U-373 astrocytoma cells after 24h plating under MTT and NR treatments.

4.2.2. Proliferative activity is affected prior to MTT and NR viability

Cell proliferation under cobalt exposure was measured by BrdU incorporation into the cells after 72 hours treatment with cobalt. As seen in Fig. 10, cobalt significantly reduced the proportion of proliferating cells compared to the controls from 50μM for the neuroblastoma cells ($p=0.012$) and from 200μM for the astrocytoma ($p=0.005$). The IC50s resulting from BrdU incorporation were also significantly different ($p=0.004$): 88.86±19.03μM and 212.89±9.84μM for the neuroblastoma and astrocytoma, respectively (see Fig. 11 for IC50s curve fitting).

As for the viability results, a slight increase in proliferation (not significant) can be observed for astrocytes at 25μM, and not for neurons. Incidentally, this could have been related to the viability increase previously mentioned. Therefore, we searched to evaluate the effect of cobalt at lower concentrations to see whether the increase in metabolism could be due to an increase in proliferation.

Fig. 12 shows the changes in proliferation at low cobalt doses after 72h treatment in SH-SY5Y. We could not establish an increase of proliferation at low concentrations after long term treatment with cobalt. Nevertheless, more in depth experiments at all time points would be needed to determine the frequency and the underlying cause of the increase in metabolism and its real relevance for humans.

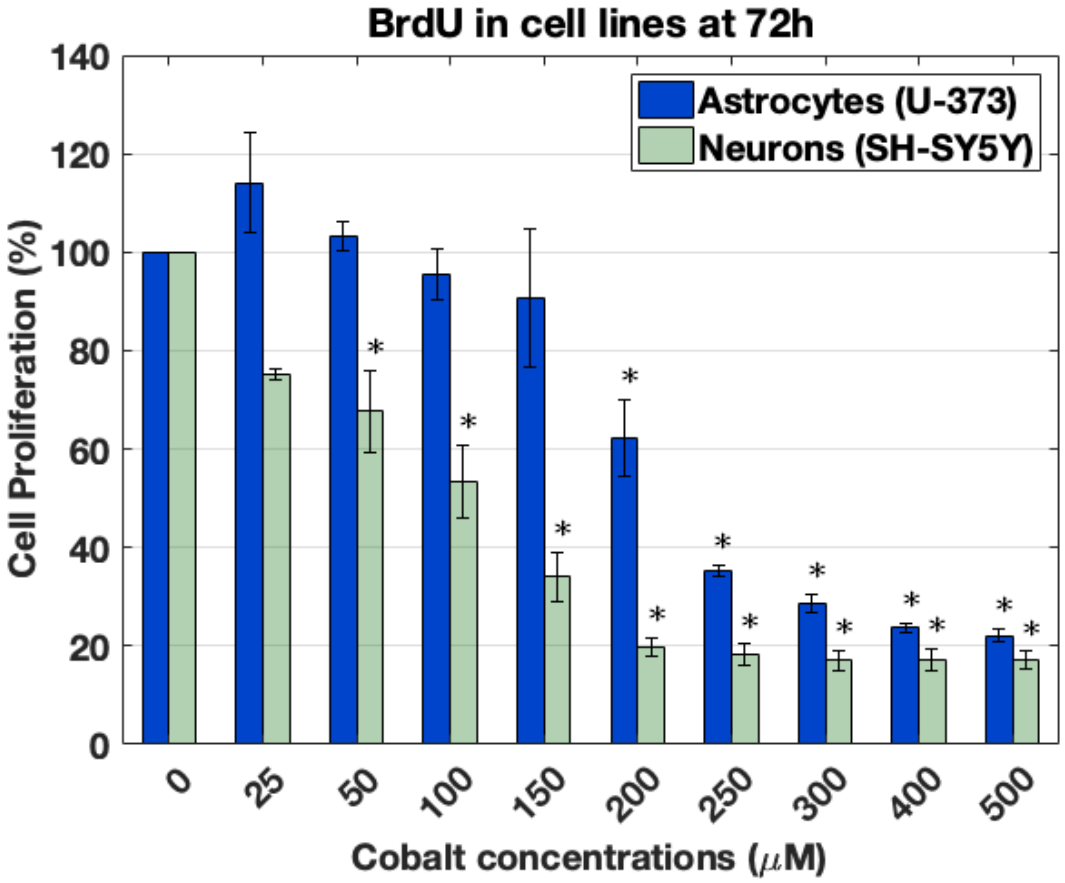

Fig. 10: Cell proliferation measured by BrdU at 72h time-point. Values are represented as percentage of the control (100%), which corresponds to untreated cells (0μM). Data are presented as mean ± SEM of n = 3 samples. *Significantly different from the control group for SH-SY5Y neuroblastoma (p=0.012) and for U-373 astrocytoma (p=0.005) by one-way ANOVA with Dunnett's multiple comparison.

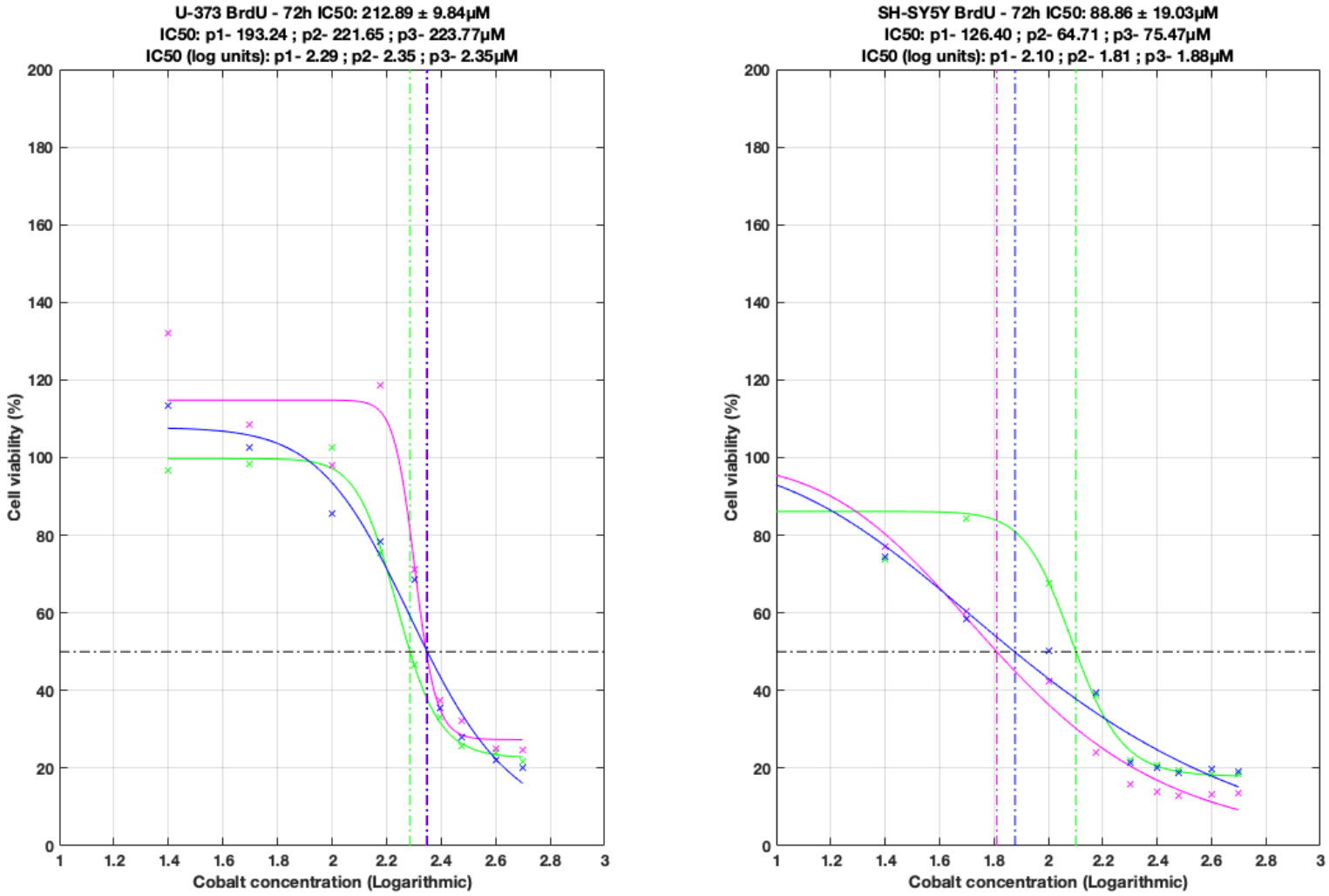

Fig. 11: IC50s calculations for BrdU proliferation assay in both U-373 astrocytoma (left) and SH-SY5Y neuroblastoma (right) at 72 hours. Fit to data was achieved through the Hill function.

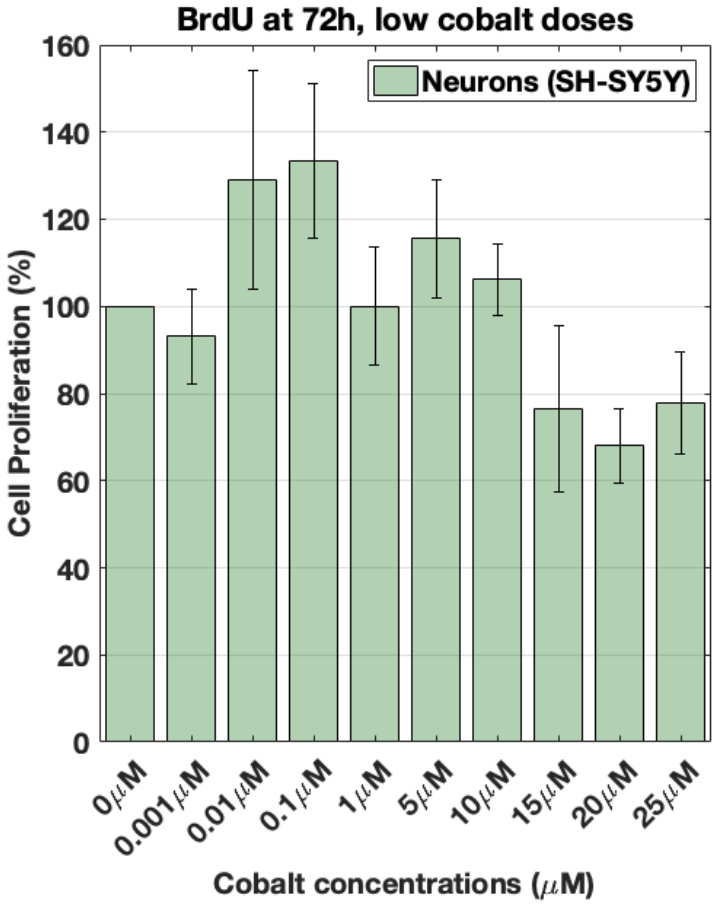

Fig. 12: BrdU proliferation of SH-SY5Y neuroblastoma cells at 72h after treatment with low cobalt doses (0-25μM). Percentage values are calculated with respect to the control (0μM) as mean ± SEM (n = 3).

4.2.3. Cobalt induces vacuolisation of cytoplasm and cell death

Samples exposed to 250μM $CoCl_2$ after 48 hours were imaged under the epifluorescence microscope to observe live and dead cells with CFDA and PI fluorescent dyes, respectively. Cobalt elicits morphological changes, mainly intracytoplasmic vacuoles and cell membrane fragmentation (blebbing), in addition to progressive cell shrinking (Fig. 13). There is a noticeable decrease in cell density at this concentration, especially in neuroblastoma cells. SH-SY5Y inherently tended to grow in cell clumps as shown in Fig. 13b.

The cell washes necessary for the procedure appear to wash away most dead cells, which explain why PI stained cells rarely appear. However, brightfield images at 24h reveal massive blebbing in neuroblastoma cell groups after treatment with 250 and 500μM cobalt (Fig. 14d, f), which are indicative of cell death. Vacuoles can also be observed (Fig. 14e).

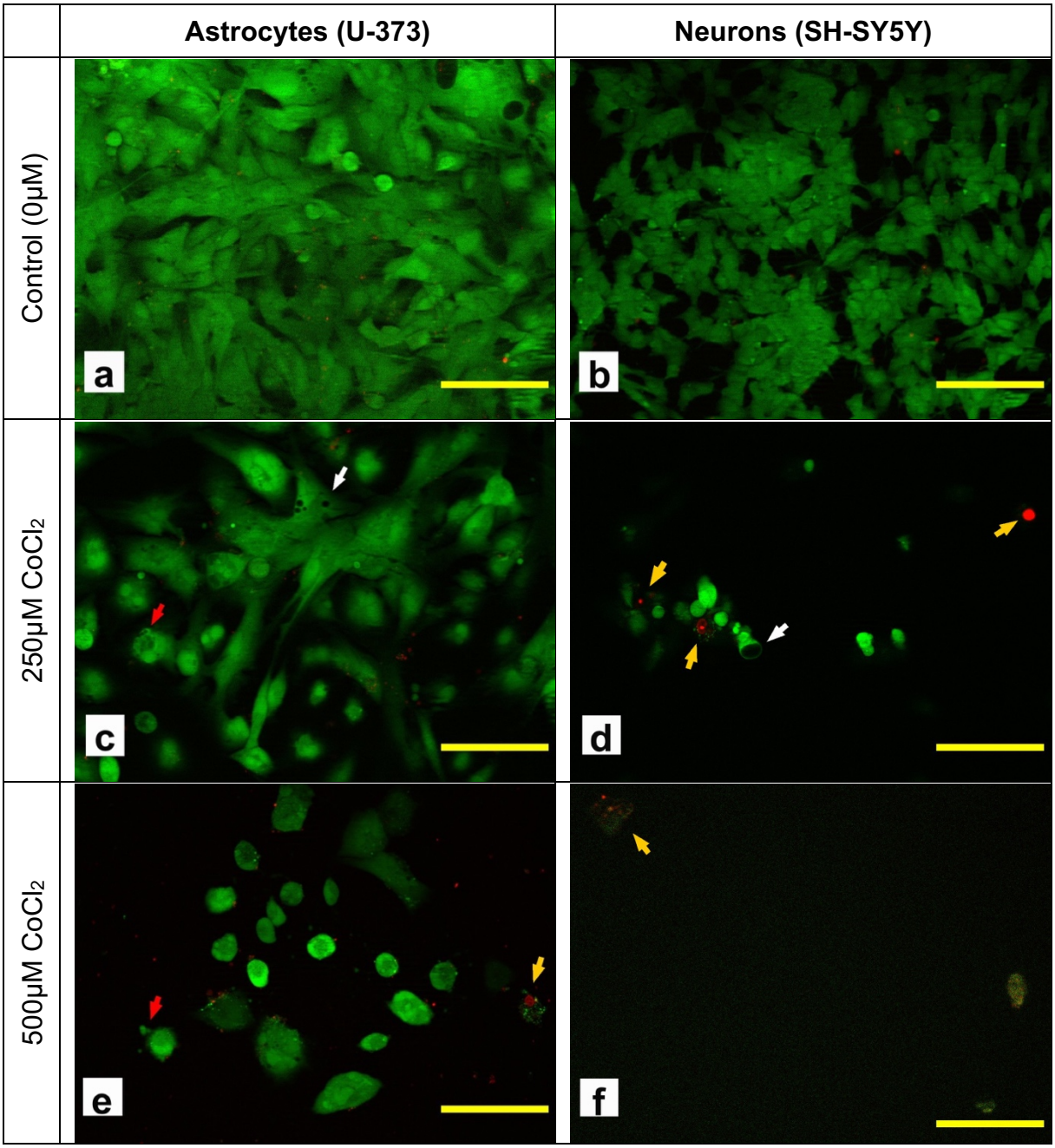

Fig. 13: Fluorescence microscopy micrographs of the U-373 (left) and the SH-SY5Y (right) cell lines after 48h exposure to 0µM (upper panels), 250µM (middle panels) and 500µM (lower panels) cobalt. Results of dead/live staining (live cells, green and dead cells, red). Lower cell density is observed after exposure, with the presence of membrane fragmentation (red arrow), vacuolization of the cytosol (white arrows), and cell death (yellow arrows). Scale bars represent 100µm.

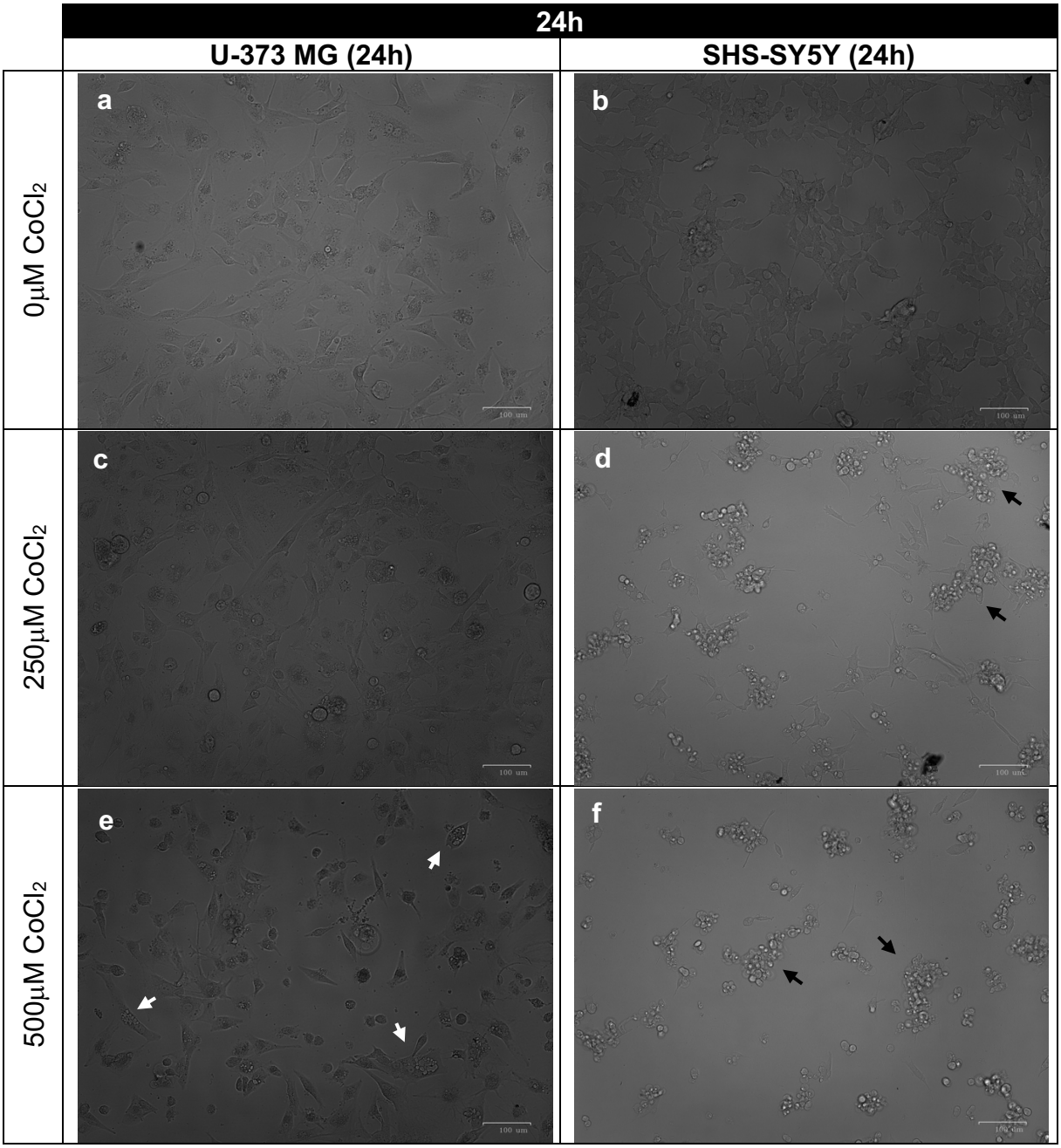

Fig. 14: Brightfield images at 24h exposure to cobalt of U-373 astrocytoma (a, c, e) and SH-SY5Y neuroblastoma (b, d, f) with cobalt concentrations of 0µM (a, b), 250µM (b, c) and 500µM (d, e). There is vacuolisation of some cells (white arrows) and SH-SY5Y show extensive cell blebbing (black arrows).

4.2.4. Cobalt uptake is dose-dependent

ICP-MS analysis after 24, 48, and 72-hours exposure to cobalt reveals accumulation of cobalt in both neurons and astrocytes (Fig. 15). Metal uptake is dose-dependent and it appears that at higher cobalt concentrations astrocytes are more capable of metal uptake than neurons. From the results we have collected, it cannot be concluded that astrocytes have an inherently higher capacity for assimilating cobalt than neurons. Neurons, being more sensitive to cobalt, undergo cell death more intensively and therefore the neuronal culture could lose uptake ability. Thus, the astrocytes innate resistance to toxicants such as cobalt could confer them with higher uptake capability.

The uptake of cobalt is significant in neurons and astrocytes after 100μM compared to controls ($p<0.05$), however, cobalt content is inconsistent across time points, most likely due to cell viability interference in the two cell lines. This deviant decrease in Co cellular incorporation across time points is especially noticeable in SH-SY5Y neuroblastoma cells, although the decremental change can also be observed between the 48 and the 72 hour time points in astrocytes.

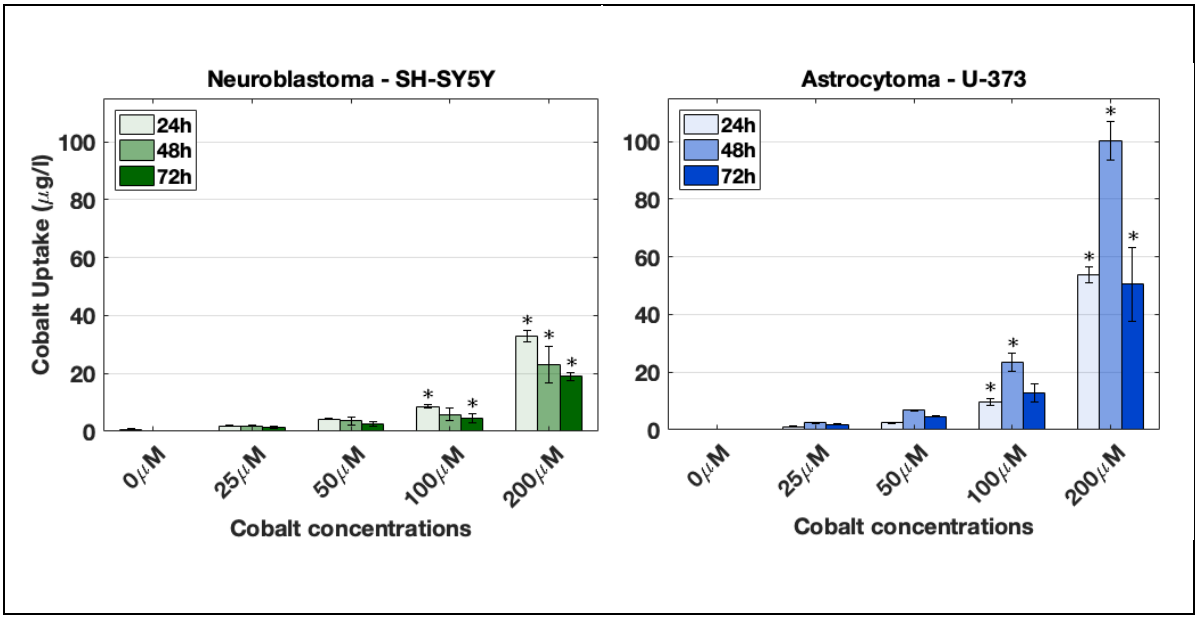

Fig. 15: Cobalt ion uptake (µg/l) into U-373 MG human astrocytoma and SH-SY5Y neuroblastoma cell lines at 24, 48 and 72 h exposed to 0µM, 25µM, 50µM, 100µM, and 200µM $CoCl_2$. ICP-MS was used to measure cobalt content. Results correspond to the mean ± SEM, with n = 3 samples. * significantly different from that of a control group by one-way ANOVA with Dunnett's multiple comparison post-tests ($p<0.05$).

4.3. Discussion

Our aim through these experiments was to investigate and identify toxic cobalt concentrations *in vitro*, as well as to understand the mechanisms of cobalt toxicity in the brain by exposing neuroblastoma and astrocytoma cell lines to different cobalt doses. Changes in viability, proliferative activity, morphology, and uptake under cobalt exposure will be discussed in this section to evaluate cellular susceptibility to cobalt.

4.3.1. ROS and Hypoxia: partners in crime in cobalt toxicity

Reports on systemic cobalt toxicity caused by MoM implants are relatively recent, however, many *in vitro* studies have previously published the effects of cobalt to cause hypoxia in cells (J.-H. Lee et al., 2013; Muñoz-Sánchez and Chánez-Cárdenas, 2019). Cobalt induces chemical hypoxia through stabilising hypoxia-inducible factor α (HIF-1α) in a concentration and extent of exposure dependent manner (Muñoz-Sánchez and Chánez-Cárdenas, 2019). Our results show a dose- and time- dependent loss of viability in both neurons and astrocytes (Fig. 5 and Table 9), which is consistent with other toxicological studies on cobalt (Chimeh et al., 2018; Fung et al., 2016; Kikuchi et al., 2018). In mice, cobalt induced HIF-1α gene and protein expression in the cerebral cortex of mouse at different high $CoCl_2$ oral dosing concentrations (10-50 mg/kg BW) for 15 days (Rani and Prasad, 2014). Antioxidant proteins superoxide dismutase and catalase were significantly reduced indicating ROS involvement. However, the protein expression of hypoxia diminished after 50 mg/kg BW. Unfortunately, this study did not report external changes on the health of the animals or directly evaluated the effect of cobalt in tissues, therefore, the reduction on hypoxia at high concentrations remains unexplained.

Nonetheless, not only hypoxia, but also other factors such as the generation of reactive oxygen species (ROS) contribute significantly to induction of cell death following cobalt treatment at high concentrations (Chimeh et al., 2018; Li et al., 2015). A colleague tentatively studied the correlation between ROS and cobalt in the neuroblastoma and astrocytoma cell lines through the use of the oxidative stress indicator, Carboxy-H_2DCFDA (unpublished PhD thesis, I. M. Alanazi, 2019, University of Strathclyde). Cobalt concentration was above 200μM at 24h for ROS to be significant. This goes in line with other work in primary astrocytes (Karovic et al., 2007), in which application of

different antioxidants did not rescue the ATP loss induced by cobalt. There is a general agreement in the literature about the contribution of ROS to cobalt toxicity, however, its role in the initiation of cell death is still ambiguous. According to a number of studies, the cytotoxic effects of either hypoxia or cobalt addition seem to begin around 200-300μM depending on the distinct sensitivity of different cell types to cobalt (Muñoz-Sánchez and Chánez-Cárdenas, 2019). In our study, SH-SY5Y neuroblastoma cells appear to be more vulnerable to cobalt than U-373 astrocytoma cells in the viability assays (Table 9) and under cell microscopic observation (Fig. 13 and Fig. 14), but the observed IC50s in both cell types approximate the known range of toxic concentrations previously mentioned: 200-300μM. Cobalt has been reported to mimic hypoxia by the inhibition of prolyl-hydroxylases (Muñoz-Sánchez and Chánez-Cárdenas, 2019), however, in the case of cobalt, hypoxia can also be concomitantly enhanced through the action of ROS by a mitochondrial independent mechanism (Chandel et al., 1998). Therefore, the double activation of ROS and stabilisation of HIF-1α could be closely interconnected in cobalt cytotoxicity.

4.3.2. Cobalt alters metabolism. Implications for a demanding brain

Early mitochondrial damage in cobalt toxicity has also been reported *in vitro* and is among the first reports of cobalt toxicity (Alexander, 1972). Recent research on neurons exposed to cobalt revealed disruption of mitochondrial fusion and fission dynamics (Chimeh et al., 2018), as well as a significant dose-dependent decrease in the number of motile mitochondria in axons together with fragmentation and destruction of mitochondrial inner membrane and cristae (Kikuchi et al., 2018). Although the MTT assay has been commonly used as a tool for measuring mitochondria metabolic activity, new studies have refuted the notion of the mitochondrial reduction of MTT. It is now understood that the endoplasmic reticulum and cytoplasm are the sites that produce the formazan product. Indeed, glycolytic enzymes such as NADH or NADPH in these cellular locations are responsible for MTT reduction (Stockert et al., 2018). Taken together, the MTT assay could act as an overall measurement of cell metabolism, particularly of glycolysis, appearing to be more sensitive to cobalt toxicity than the NR assay, an estimate of lysosomal integrity (Repetto et al., 2008) (Table 9). However, MTT might not be able to pick up early

mitochondrial damage due to the reasons previously explained and therefore cobalt toxic effects could possibly start at lower concentrations in a subtle manner.

In contrast, cobalt effects at lower concentrations appear to mildly increase viability in MTT and NR results (Fig. 5a, b, f). This viability boost as part of a biphasic response has been observed before in a study where primary astrocytes were both cobalt treated and deprived of oxygen, thus the authors attributed the cobalt outcome to a reactive response to mild hypoxia (Fang et al., 2008). However, given that MTT is a measure of glycolytic metabolism, this effect might reflect an increase in aerobic glycolysis rather than increased cell populations. Indeed, we should be careful with the interpretation of these results as cancer cells preferentially employ this type of energy production, aka the Warburg effect (Liberti and Locasale, 2016), which refers to the generation of ATP in the cytoplasm through glycolysis resulting in lactate in the presence of oxygen, rather than utilising mitochondrial respiration. Aerobic glycolysis occurs naturally when ATP is required rapidly and energy requirements exceed oxygen reserves as happens during exercise. Our cells were cultured in conditions of abundant media and with adequate levels of oxygen, therefore this increase in glycolysis might reflect a homeostatic reaction to either the induction of hypoxia by cobalt or a failure in cellular respiration involving the citric acid cycle or oxidative phosphorylation. Macrophages exposed to cobalt at similar concentrations as in our studies switched from cellular respiration to lactate-producing glycolysis, and this process was thought to be mediated by HIF-1α (Salloum et al., 2021). In our experiments this increase in glycolysis precedes the reduction of cell viability.

Cobalt at low concentrations has also been used as a pre-treatment to protect neurons and astrocytes against further ischemic insults, in an adaptive process thought to be mediated by erythropoietin (EPO) (Jones et al., 2013). Fairly recently, cobalt doping has been suspected in athletes and illicitly used in equine sport to stimulate erythropoiesis, but evidence is lacking to support its use (Mobasheri and Proudman, 2015). It is unknown whether the activation of aerobic glycolysis is enhanced under these circumstances. However, fifty years ago several cases of lactic acidosis were seen in Quebec Beer Drinkers (Alexander, 1972), where tissue microscopy showed damaged mitochondria indicative of a possible link between injured mitochondria and increased rates of lactate production. This pathology was thought to be produced by

cobalt, which had been added to the beer as a foam stabiliser. Nevertheless, these patients drank high quantities of alcohol, which can lead to other metabolic problems such as thiamine deficiency (Berg et al., 2015). The possibility that cobalt could exacerbate problems of alcohol drinkers who could be metabolically challenged already was discussed at the time (Alexander, 1972). In any case, the concentration or exposure threshold between hormetic and deleterious responses has yet to be determined and, as it can be observed, the increase in MTT metabolisms is inconsistent across time points. Any energy-generating process occurs within each cell and therefore a heterogenous cellular response is expected. Transient metabolic variations might not be detected in a set time-point by an averaging assay e.g. MTT, NR or BrdU, which are used to detect overall population changes and drastic estimates such as IC50s. Live cell imaging techniques with GFP reporters or other protein tags able to resolve time dynamics at the single cell level could be useful to determine the early effects of cobalt in metabolism (Reyes and Lahav, 2018). There is also a long-standing debate in Toxicology regarding the frequency and meaning of hormetic events, and whether they are a relevant part of the toxic profile of a substance (Mushak, 2013). New targeted studies in this area might settle the controversy regarding hormesis, however it is important to consider that the underlying motives for adaptive homeostatic mechanisms might not necessarily be beneficial or long-lasting.

Brain energy requirements are said to be around 20% of total body glucose reserves (Magistretti and Allaman, 2015). The interference of cobalt with energy metabolism is therefore expected to have a relevant impact on brain function. Symptoms like fatigue and anorexia have been reported through cobalt poisoning (Mao et al., 2011) (Kesteloot et al., 1968; Zywiel et al., 2013). Cerebrospinal fluid (CSF) collected from three individuals with cobalt-related neurological symptoms had cobalt levels of 2.2 (Tower, 2010), 3.2 (Steens et al., 2006), and 4.4μg/l (Rizzetti et al., 2009), which are more than 20 - 40 times higher than reference CSF levels for cobalt (Gerhardsson et al., 2008), thus indicating that cobalt had most likely passed through the blood-CSF barrier. Consequently, cell populations in close proximity with the CSF could be at risk of cobalt toxicity. The optic nerve, whose atrophy has been reported in cobalt poisoning (Lim et al., 2015), is also surrounded and permeated by the CSF (Mathieu et al., 2017), and as a matter of fact, cobalt was found in the vitreous and aqueous eye humor of rabbits dosed with high concentrations of cobalt (Apostoli et al., 2013).

Moreover, tanycytes, a special glial cell in direct contact with both the CSF and blood vessels, transfers metabolic signals such as glucose levels from the CSF to the hypothalamic neurons. These hypothalamic cells have been seen to directly influence appetite and body weight (Langlet, 2014), and are able to self-renew after damage. Could cobalt interfere with body energy balance by hindering tanycyte metabolism? It is possible that tanycytes glucosensing function could predispose them to toxicity due to higher exposure to chemicals. Indeed, anorexia was thought to have triggered some of the symptoms in Quebec beer drinkers (Kesteloot et al., 1968). If cobalt already interferes with metabolism, limiting glucose pools through anorexia could have accelerated some of the symptoms. Similarly, brain circumventricular organs have fenestrated capillaries that allow for sensing of blood or CSF molecules. These capillaries are surrounded by subsequent layers of astrocytic feet and neuronal dendrites with the neuronal somas at a farther distance (Morita et al., 2016). Border cells such as the glia limitans allow the passage of CSF solutes through the astrocytic feet forming the CNS-barriers around the meninges and blood vessels, therefore cobalt could, in principle, cross these barriers and reach neurons in the parenchyma (Engelhardt et al., 2017).

Astrocytes not only act as a barrier with blood and CSF through their astrocytic feet, they also play an active role in metabolism through both the neurovascular and the astrocyte-neuron metabolic coupling. The process of neurovascular coupling involves the release of chemicals by the wrapping astrocytes to alter the tone of the capillaries and increase blood flow to support increased neural activity. It is also known that astrocytes, through their own glycolysis, are able to fuel neurons with lactate, a process known as astrocyte-neuron metabolic coupling. In addition, only glial cells are able to transfer glucose to glycogen stores for later mobilisation in glycolysis when neuronal activity increases metabolic requirements. The importance of the astrocyte-neuron metabolic coupling has been debated as neurons are also able to use glycolysis to support activity (Díaz-García et al., 2017), which has been confirmed by the high turnover of glycolytic proteins in neurons (Dörrbaum et al., 2018). Regardless, astrocyte metabolism is important for brain functioning and cobalt interference with energy metabolism could lead to serious impairment of neurological functions. Consequently, the relevance of energy metabolism in brain functional cells could make

them susceptible to cobalt toxicity. Indeed, energy metabolism and apoptosis are intrinsically associated through the glucokinase protein, and therefore, a metabolic failure could lead to cell death (Danial et al., 2003; Jensen et al., 2006).

4.3.3. Cobalt-induced DNA damage

Nevertheless, cell proliferation, as measured by BrdU, appears to be affected before MTT reduction at 72h suggesting that other toxic mechanisms such as DNA or mitochondrial damage could be involved earlier on in cobalt toxicity. The genotoxic effect of cobalt has been extensively investigated, and although in principle it does not generate mutations, there is a general agreement that cobalt induces micronuclei, chromosomal aberrations, and DNA-damage *in vitro*, although these results have not been observed *in vivo* (Kirkland et al., 2015). In addition, cobalt accumulation in osteoblast (Shah et al., 2015), keratinocytes (Ortega et al., 2009), and lung epithelial cells (Bresson et al., 2013) occurs mainly in the nucleus, also presenting a homogeneous distribution within the cytosol with exception of the perinuclear area. Ortega *et al.* compared cobalt content in keratinocytes and found perinuclear cobalt-rich areas in half of the cells, with their cobalt content almost doubling that of the nucleus (Ortega et al., 2009). The authors ventured that these cobalt-rich perinuclear areas could be colocalised with the endoplasmic reticulum and the Golgi apparatus, although mitochondria have also been seen to surround the nucleus under hypoxic conditions (Al-Mehdi et al., 2012). Indeed, in rats dosed with very high cobalt doses, the myofibrils from myocytes had been displaced from the perinuclear area and nuclei were deformed (Zadnipryany et al., 2017). The perinuclear cytoplasm of cortical cells was also found edematous and distinct indentations appeared in nuclei after intracerebral cobalt injections (Caltana et al., 2009). Nevertheless, divalent cobalt does not significantly associate with DNA in fibroblasts (Sabbioni et al., 2014b), thus it is still unclear how cobalt interferes with cell nucleus functions.

It is difficult to translate our proliferation findings to mature neurons and astrocytes. Whether cobalt induces DNA repair stalling or chromatin reorganization in post-mitotic cells is unknown, and it would be necessary to establish the pathological effects of these changes *in vivo* and in patients. With regard to proliferating cells in the human CNS, a few stem cells are still able to proliferate through adulthood. In rats exposed to

toxic levels of glucokinase inhibitor, hypothalamic tanycytes, which retain self-renewal capacities, were able to repopulate and restore feeding behaviour and body weight following almost complete depletion 14 days after treatment (Sanders et al., 2004). Hence, under cobalt exposure, stalling of proliferation in neural stem cells may further impact recovery after cellular toxicity.

In our results, lowered proliferation and increased fractional cell death are the likely reason behind the drop in glycolytic metabolism at higher concentrations (Fig. 5, Fig. 10, and Fig. 13). However, in neuroblastoma cells, lower cobalt doses at 72h exposure did not induce any consistent or significant proliferation increase that could result in incremental aerobic glycolysis (Fig. 12). It is not known whether the increased viability of the biphasic response corresponds to early disturbances of cellular respiration, which could ultimately lead to cell cycle arrest and prevent cell proliferation, or if earlier nuclear damage could influence energy metabolism resulting in increased glycolytic rates. Further research is needed to identify the toxicity initiating events of cobalt.

4.3.4. Cobalt-induced cell death and calcium buffering - cobalt as a Trojan Horse

Under the microscope, cobalt treated neurons and astrocytes revealed cell body retraction, vacuolisation of the cytosol, and ultimately blebbing before cell death (Fig. 13 and Fig. 14). We know from *in vivo* studies that high doses of cobalt in rabbits induce depletion of retinal and cochlear ganglion cells (Apostoli et al., 2013) and that intracerebral injection of cobalt leads to necrosis of brain tissue (Caltana et al., 2009). Mentions of cobalt-induced cell death in humans are limited to central vein necrosis in livers of Quebec Beer Drinkers (Alexander, 1972), and recent reports of cobalt poisoning in patients with hip prostheses have solely investigated the effects of cobalt on the heart, where cell death does not seem to occur. Hence, we still ignore whether cobalt cell death *in vivo* and *in vitro* follow similar mechanisms, and if these mechanisms are relevant for patients.

In summary phenotypic changes in cardiac cells include hypertrophic myocytes together with interstitial fibrosis and damaged contractile elements, as well as abnormal mitochondria, lipofuscin deposits and cytoplasmic vacuolation (Gilbert et al., 2013; Martin et al., 2015). In our results, vacuolisation of the cytoplasm occurred both

in neurons and astrocytes (Fig. 13 and Fig. 14), and cobalt toxicity reports have linked it with autophagy, which appears to be a rescuing mechanism under stress, but can also participate in cell death (Chimeh et al., 2018; Fung et al., 2016). A number of commercial autophagy detection kits are available and could be used, in combination with immunoblot analysis of LC3-I/II conversion or Beclin-1 increase over time to observe autophagic flux (Klionsky et al., 2016). However, these experiments, are very time-consuming and beyond the scope of our work. Whether the cytoplasmic vacuolization phenotype corresponds to autophagy (Aki et al., 2012), and the potential cytoprotective effects of inhibiting or enhancing autophagy under our specific experimental conditions will remain to be established.

Apoptosis has already been reported as cobalt induces cell death *in vitro*, possibly triggered through mitochondria. Previous studies in SH-SY5Y cells and mouse embryonic stem cells with cobalt confirmed mitochondrial-triggered apoptosis through the tumour suppressor protein p53 associated with the loss of mitochondrial transmembrane potential (J.-H. Lee et al., 2013; Ratinaud, 2011). Karovic *et al.* also blamed cobalt toxicity on the loss of mitochondrial membrane potential, as well as the disruption of calcium signalling in a hypoxia model of primary astrocytes. The prevention of cobalt-induced ROS by antioxidants did not limit ATP depletion, and HIF-1α stabilisation did not induce apoptosis when using the hypoxia inducer DMOG (Karovic et al., 2007). Thus, the authors suspected that other mechanisms different from ROS and hypoxia led to cobalt-induced apoptosis. Calcium is implicated in energy metabolism in the mitochondria, and dysregulation of mitochondrial calcium can lead to cell death (Giorgi et al., 2018). Indeed, calcium raises are necessary for glycogenolysis through the activation of glycogen phosphorylase (Berg et al., 2015). If cobalt was impersonating calcium, cells might fail to elicit calcium transients and be unable to breakdown glycogen, thus explaining the glycogen deposits in heart muscle of Quebec beer drinkers (Alexander, 1972; Bonenfant, J.L., Miller, G., Roy, 1967). Other enzymes in energy pathways such as glucokinase (Markwardt et al., 2016) and pyruvate dehydrogenase (Berg et al., 2015) are also regulated by calcium dynamics. A paired failure of oxidative respiration and glycogenolysis would oblige cells to continuously rely in aerobic glycolysis, leading to increased levels of lactate. In addition, calcium acts as a second messenger in signalling cascades through many

calcium-dependent kinases, phosphatases, and other intracellular messengers (Berg et al., 2015). This theme will be explored further in Chapter 5.

4.3.5. Cobalt uptake in CNS cells and differential resistance of neurons and astrocytes.

While astrocytes seemed to be less susceptible to the toxic effects of cobalt, their cobalt content was, in general, higher than in neurons (Fig. 15). The differential resistance of astrocytes in comparison to neurons under low oxygen conditions has already been reported and is thought to be necessary to protect neurons in the face of hypoxia (Jones et al., 2013). Fang *et al.* showed that upon exposure to either cobalt or hypoxia, astrocytes can transform into reactive cells as assessed by the increased expression of bystin protein (Fang et al., 2008). This reactive gliosis was also detected *in vivo* through glial fibrillary acidic protein (GFAP) expression in a rat model of ischemic brain injury that used intracerebral injections of cobalt (Caltana et al., 2009). Both increased viability and cobalt uptake lead us to believe that astrocytes may assume a neuroprotective role against cobalt toxicity. Reactive astrocytes are able to increase their iron uptake by quenching excess ions and therefore maintain the extracellular homeostasis for neurons (Pelizzoni et al., 2013), and it is possible that this mechanism may have been activated under our experimental conditions.

Diminished viability is associated with increased cellular cobalt content (Fig. 5 and Fig. 15). Recent reports comparing astrocytes of different origin indicate that intracellular labile zinc is a burden that increases the vulnerability to oxidative stress, and that cells that are able to maintain lower zinc levels under stress remained viable (Furuta et al., 2019). In our research, neurons had a lower cobalt content than astrocytes but the latter might be innately more resistant for the reasons mentioned in the previous paragraph. To our knowledge no study has yet specifically researched cobalt uptake in neurons and astrocytes. The few *in vitro* published examples have quantified cobalt accumulation in fibroblast (Sabbioni et al., 2014b), bone (Shah et al., 2015) and red blood cells (Simonsen et al., 2011b), revealing some interesting findings in the context of cellular cobalt toxicity. For example, cobalt irreversibly accumulates through calcium channels in red blood cells (Simonsen et al., 2011b), and osteoblast influx partially traverses through a P2X7R-dependent transporter, while osteoclast cobalt uptake likely relies on endocytosis (Shah et al., 2015). Moreover, a cobalt-labelling technique

has been in use for years to study calcium-permeable AMPA receptors in neurons and certain TRP channels (Aurousseau et al., 2012). Although this protocol is a general divalent cation permeability test, it cannot be used to observe all divalent channels e.g. NMDA and voltage-gated calcium channels because they are impervious to cobalt. It appears that cobalt uptake depends on the actions of specific transporters, making some cell-types more vulnerable than others. Careful election of cell models should be undertaken in future *in vitro* studies of cobalt toxicity, since certain subpopulations in the nervous system could be more sensitive, e.g. retinal ganglion cells (Apostoli et al., 2013), due to either a higher uptake of cobalt or a reduced ability to eliminate it.

As mentioned before, cobalt gathers in the nuclear and perinuclear areas in osteoblast (Shah et al., 2015), keratinocytes (Ortega et al., 2009) and lung epithelial cells (Bresson et al., 2013), although cobalt is also homogeneously dispersed in the cytosol. Instead, in fibroblasts treated with low cobalt concentrations ($<$50μM) accumulation occurred mainly in cytoplasm, followed by nucleus and mitochondria (Sabbioni et al., 2014b), while cobalt localisation in osteoclast was found near the basolateral membrane (Shah et al., 2015). Electron-dense material thought to be cobalt was found within the mitochondria with electron microscopy techniques (Alexander, 1972; Rona, 1971; Zadnipryany et al., 2017). Shah *et al.* suggested that the differential distribution of cobalt in osteoblast and osteoclast could be related to the mode of cobalt transport from the extracellular medium to the cell (Shah et al., 2015), however, this hypothesis still needs to be researched.

Similar to what has been noted in other *in vitro* studies (Kikuchi et al., 2018; Li et al., 2015), the cobalt concentrations needed to elicit a toxic response in astrocytoma and neuroblastoma are very high compared with the blood and serum content of MoM patients. The range 25 to 500µM equates to 1,473–29,465 µg/l (Co MW = 58.93). To our knowledge the highest level of measured cobalt in patients' blood is 6,521µg/l (Zywiel et al., 2013), equivalent to 110µM cobalt concentration, similar to some of the IC50s obtained in this study. However, the level of 300µg/l Co in blood equates to 5µM and is above which systemic toxicity usually develops (Kovochich et al., 2018). While this last concentration seems low, translational challenges exist as cell culture medium and conditions do not properly model the human physiological environment. Previous research has established that cobalt ions bind to albumin and histidine, and that free

cobalt is not made available to cells until protein saturation is achieved at around 40µM Co (Sabbioni et al., 2014b). This could influence the amount of free ions available and the associated impact on cytotoxicity. Indeed, this is the concentration treatment level after which cobalt uptake is significant in our results (Fig. 15). In addition, our time points only extend to 72h cobalt-exposure while MoM implants reside in patient for months to years, leading to a cumulative effect. Nevertheless, we ensured our Co concentration range was also similar to other *in vitro* models (Kikuchi et al., 2018). Cobalt is transported into the neurons and astrocytes (Fig. 15), and the intracellular content may increase with exposure duration. Cobalt may slowly accumulate in cells and tissues for an extended period of exposure until its toxic effects become evident and affect cell function or viability. Then it may cause the neurological symptoms observed in patients with prostheses. Our research offers new clues into the modes of action of cobalt and supports previous investigations. However, more research is needed to identify what underlines these symptomatic manifestations, and further *in vivo* and *in vitro* work should carefully choose cell models, assays, and cobalt concentrations.

4.3.6. Limitations and recommendations for future research

The biological materials and research methods used in this study were selected for its ease of standardisation, high-throughput yield, as well as to establish comparisons with the available literature. We are satisfied with the results obtained, however, these protocols have their own limitations that impede us reaching further conclusions regarding cobalt toxicity in the CNS. Our methods have been able to identify major toxicological modes of action, but the details of cobalt toxicity are still evasive. Protein or gene expression experiments would be valuable to identify the precise metabolic cues that are being impacted by cobalt before irreversible cell death.

Calcium appears to be a key player in cobalt toxicity, and it would be interesting to see how cobalt concentrations within cells impact calcium intracytoplasmic levels. Especially interesting would be to pair cobalt uptake with functional studies of action potential firing or mitochondria respiration. Neuroblastoma SH-SY5Y cells are proliferating cells of immature phenotype (Pezzini et al., 2017), therefore they do not fully present the functions or phenotypic characteristics of specialised neurons, which limits our ability to fully understand the consequences of cobalt toxicity for mature CNS

cells. Other methods requiring fewer cells could substitute cancer cell lines for primary cells to perform functional studies and research the antagonistic effect of cobalt over other ions such as calcium in the mitochondria or the nucleus.

Regarding the calcium/cobalt ratio, it is possible to characterise two different ions simultaneously through ICP-MS, however, it requires finely tuned equipment. The instruments used here were too exposed to variations from other experiments, which made cobalt quantification challenging even with the specialised help of the UoS Chemistry technicians. As discussed previously, cobalt transport seems to be dependent on cell type and coupled with the array of transporters the cell uses to function. Questions about the number of metal ion transporters contributing to cobalt uptake in different cell types, as well as whether cobalt accumulation in different cellular compartments is related to the form of uptake remain to be explored. Cobalt uptake and intracellular accumulation could explain the sensitivity disparities between different cell types, and perhaps further research would help identify therapies to block cobalt entry in vulnerable cells.

Techniques such as ICP-MS could become useful to quantify differences in intracellular cobalt uptake after application of the drugs of interest. Our work analysing cobalt uptake in different cell types via ICP-MS could be easily extended by screening various uptake inhibitors such as calcium channel blockers or other suppressors of cellular transport systems such as endocytosis, the latter of which has been previously done with gold nanoparticles (Ng et al., 2015). However, some important factors must be considered to improve the accuracy of such assays. We evaluated the viability of the cells under cobalt exposure, however, we did not perform normalisation of ICP-MS cobalt levels with the number of live cells. Although cells were seeded at the same density, cell viability appears to modulate cobalt uptake (Fig. 15) and, in hindsight, our work would have greatly contributed from normalisation to the number of viable cells through imaging or protein quantification. Both ICP-MS and fluorescence experiments required a number of washes in the procedure. In our conditions, high concentrations of cobalt induce cell death, and washes detach weakly attached cells or apoptotic membrane blebs, which could impact the results. Disparities between cell proliferation rates in U-373 and SH-SY5Y cells, as well as their different sensitivity to cobalt could bias uptake levels. Our approach would be more suitable for sub-lethal cobalt

concentrations. Future research would benefit either from normalisation or the use of other techniques that do not require washes.

In addition, due to time and cost limitations, we only compared a couple of CNS cell lines, i.e. neurons and astrocytes, which represent the brain functional constituents. However, other less known brain cells that form CNS barriers could be in contact with cobalt and be affected by its toxicity. For example, cells from the choroid plexus, which form the CSF-blood barrier, or endothelial and pericyte cells that wrap the capillaries of the BBB could be considered a route of entry of heavy metals (Schmitt et al., 2011). The functional significance of cobalt toxicity over these cells would be less clear but their roles as routes of access to the CNS make them crucial to understand cobalt toxicity in the brain. Other groups have investigated the effect of cobalt on visual and auditory organs (Apostoli et al., 2013) as cobalt patients report vision and hearing related problems (Catalani et al., 2012), however, sensory tissues are incredibly complex and out with the scope of our work. To date, the extend of cobalt toxicity in the brain is still unclear. Patients' symptoms offer clues as to which systems could be affected by cobalt, however we are still ignorant of the full extent of cobalt poisoning. Advance imaging techniques that combine ICP-MS technology or silver staining of brain tissue sections or explants would be valuable to detect cell populations at risk of enduring cobalt toxicity. Although challenging, this work would clearly benefit patients, and help focus the attention towards more relevant hypothesis.

4.4. Summary of Results

In this chapter, we investigated the effects of cobalt on viability, proliferation, morphology and uptake in CNS cell lines. The following conclusions resulted from this research:

- MTT and NR assays show that cobalt ions are toxic at high concentrations *in vitro*. IC50s demonstrate that neurons are more susceptible to cobalt than astrocytes.
- Viability increase in biphasic response might indicate a compensatory response related to aerobic glycolysis and early disruption of metabolism by cobalt. This response is inconsistent across time points and requires further validation.
- MTT and BrdU sensitivity suggests that Co impedes metabolism and DNA synthesis at high concentrations. Although proliferation is impacted by cobalt, our methods cannot determine the mechanism and extent of mitochondrial damage. Further research will be needed to elucidate if mitochondrial disruption precedes or follows nuclear damage.
- Cobalt metal uptake is dose-dependent in neuroblastoma and astrocytoma cells.
- Astrocytoma exhibit greater resistance to cobalt toxicity despite a higher uptake.

The results of this chapter have been recently published in Toxicology *in Vitro* (Gómez-Arnaiz et al., 2020)

5. *IN VIVO* TIME-RESPONSE INVESTIGATION INTO COBALT TOXICITY

5.1. Introduction

Neurological conditions caused by high levels of cobalt ions in blood have been demonstrated in several clinical reports in relation to patients with MoM implants (Mao et al., 2011; Tower, 2010). As highly soluble cobalt disseminates from the CoCr debris in periprosthetic tissues through the blood stream, patients with elevated levels of cobalt in blood might display a plethora of systemic conditions (Bijukumar et al., 2018). Symptoms appear to cease once the patient has a revision surgery and the blood metal levels reduce (Catalani et al., 2012). Nevertheless, revision surgeries are not always to be recommended for every patient and health concerns regarding the safety of patients with Metal-on-Metal (MoM) hip implants have increased in the last 10 years. The lack of understanding about cobalt toxicity and its treatments, suggest that research is needed to find better medical care for patients.

In vitro models such as the human cell lines used in the previous experiments are valuable tools to understand the modes of action of cobalt toxicity in the brain. *In vitro* research is used to study individual cells or groups of cells under controlled experimental conditions, and this can diminish an organism's complexity. Previous toxicogenomic analyses have demonstrated that *in vitro* systems fail to fully represent relevant processes occurring in rat liver tissues after exposure to toxic compounds (McMullen et al., 2019). Molecular and functional events occurring *in vivo* at tissue and organ levels could be crucial mechanisms in the physiological response to cobalt. We search to integrate both *in vitro* and *in vivo* studies to uncover mechanisms of cobalt-induced toxicity and progress towards the clinical translation of results to MoM patients.

The aim of this *in vivo* work was to identify how cobalt accumulated in tissues after long-term systemic circulation, and specifically answer whether cobalt concentration increased in the brain. We also sought to understand the underlying molecular changes in the brain at the transcriptional level in laboratory rats after the

aforementioned exposure. Research on MoM cobalt-induced systemic toxicity is scarce and to our knowledge, there are few publications addressing neurological manifestations *in vivo*. We hope to generate and test hypotheses through RNA-sequencing (RNA-Seq) to gain mechanistic insights into the modes of action of cobalt. This high-throughput technique quantifies changes in mRNA production in tissue samples and is able to identify genes or pathways with altered expression compared to the controls. Transcriptomic applications have already been proven effective to toxicology, not only by understanding mechanisms but also, by finding early end-points for detection of toxicity and identification of biomarkers (Joseph, 2017).

Male SD rats were treated with sub-toxic intraperitoneal doses of cobalt (1mg/kg B.W.) for 7 and 28 days. After animals were sacrificed, organs were dissected, weighed and pieces of tissue were appropriately preserved for experiments. The prefrontal (pref.) cortex, cerebellum and hippocampus were taken separately from the brain. Tissue cobalt content was analysed through ICP-MS. RNA was isolated from the pref. cortex and cerebellum and RNA-Seq was performed. RT-qPCR was used to validate RNA-Seq results (refer to *in vivo* methods in Chapter 3 for more details on these methods).

5.2. Results

5.2.1. Body weight in control and treatment groups may vary with cobalt treatment

Rat weights were monitored during the duration of the treatment as an indicator of general health. Fig. 16 shows the recorded weights in control and treatment groups throughout the 7- or 28-day treatments. Body weight increases constantly across time points, and both control and treatment growth trends are *a priori* undistinguishable. However, when the weight is presented as a percentage of the rat body weight before the start of treatments, a difference in growth rate emerges (Fig. 17). At 7 days, there is an average 2.22% weight gain difference (median; range: 0.67 - 2.96%), which increases up to 6.77% (median; range: 0.46 - 11.57%) at 28 days. Statistical analysis reported significance only at certain time points ($p \leq 0.05$) that have been indicated in Fig. 17. Therefore, cobalt-treated rats may possibly have been affected by the treatment and have reduced growth rates. Given that rats were fed *ad libitum*, it is possible that either the student or the BPU technicians failed to notice changes in food

consumption. Nevertheless, the rats' general aspect was good, and as Fig. 18 shows, organ weight did not indicate noticeable differences between controls and treatment. The prefrontal cortex is an exception in this regard. We are certain that the reason behind the decrease in weight of the prefrontal cortex across experimental doses and time points is the difficulty involved in the dissection of individual isocortical areas rather than a consequence of cobalt toxicity.

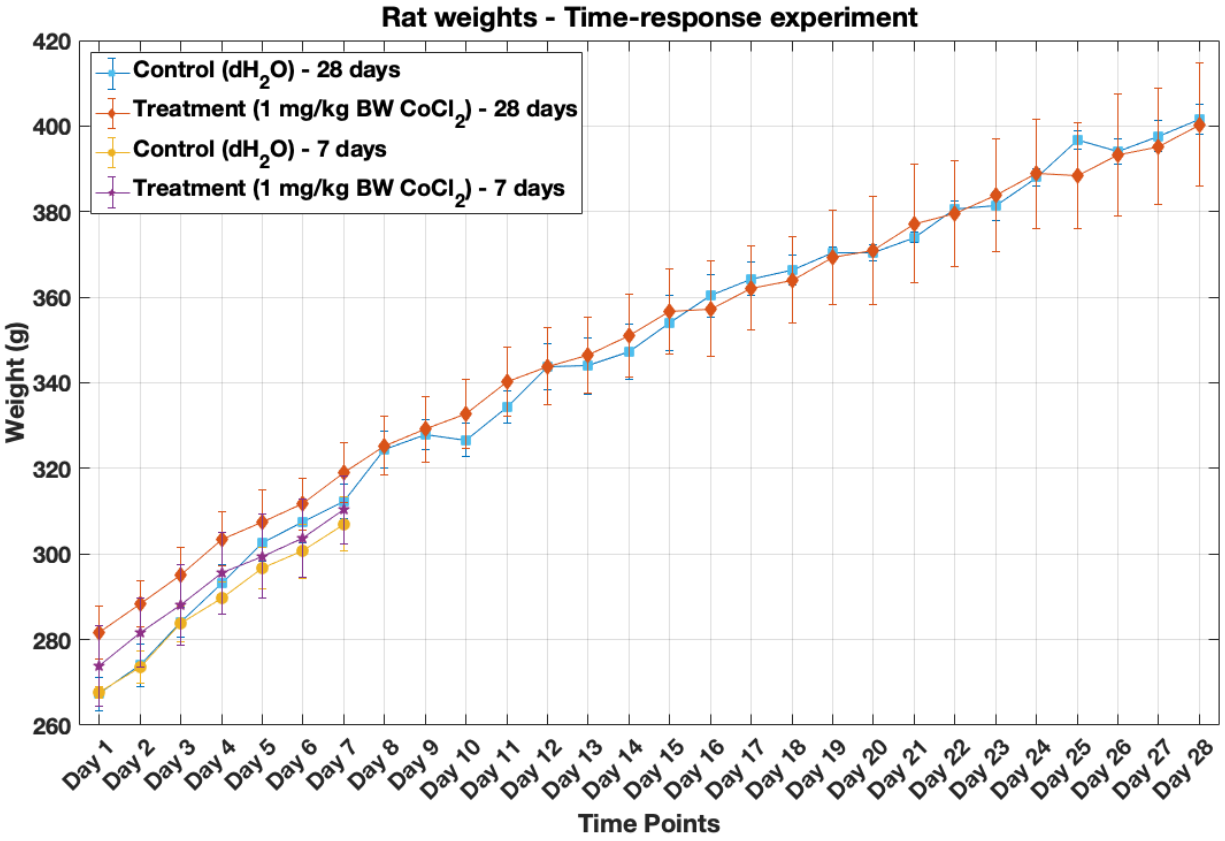

Fig. 16: Body weight gain (mean ± SEM) of male SD rats during the course of 1 mg/kg B.W. $CoCl_2$ injection treatment during 7 and 28 days in control and treatment groups. Daily i.p. injections of dH_2O were given to control rats (n=3) and 1 mg/kg B.W. $CoCl_2$ to the treatment groups (n=6). The markers used are squares for the control group at 28 days, and rhombus for the treatment, while at 7 days the circles represent the control and the stars the treatment, colour details are presented on the figure legend.

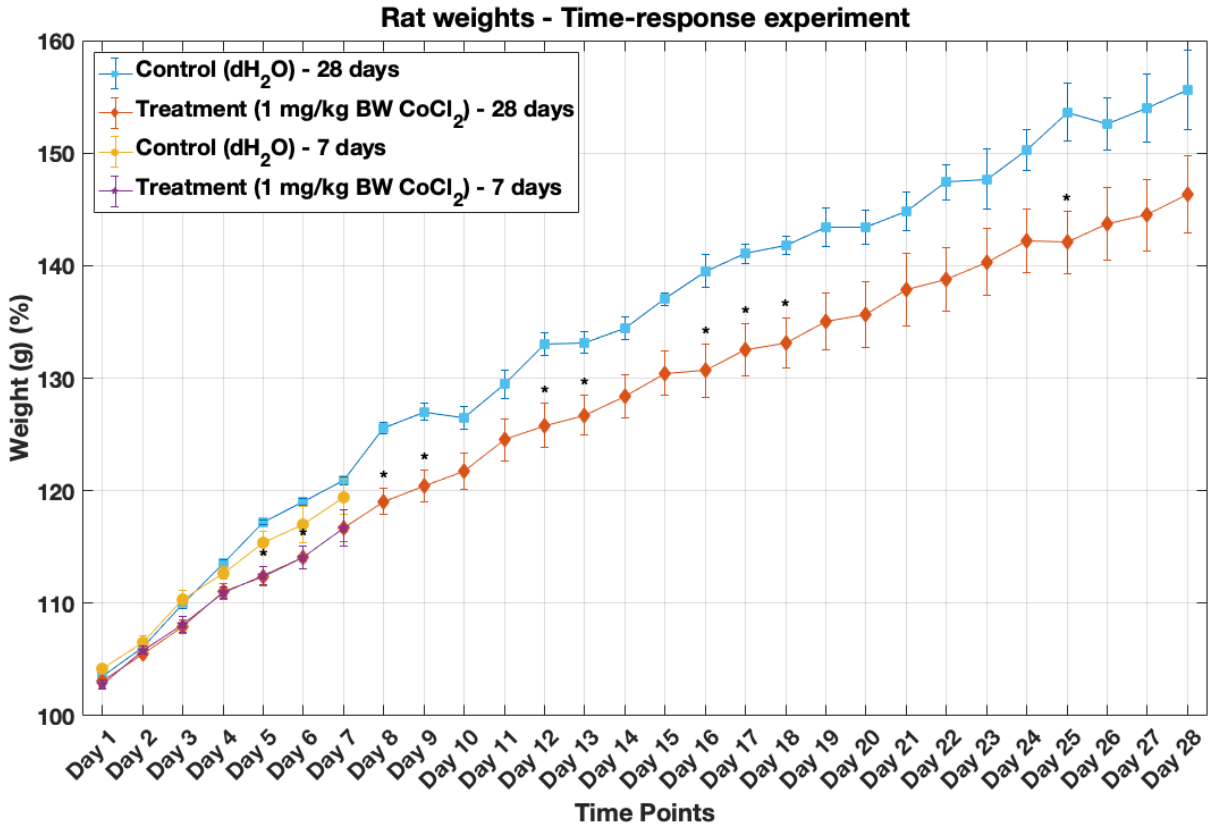

Fig. 17: Percentage of body weight gain (mean ± SEM) of male SD rats in relation to their weight before the start of the i.p. injections. Daily i.p. injections of dH_2O were given to control rats (n=3) and 1 mg/kg B.W. $CoCl_2$ to the treatment groups (n=6). *Significantly different from the control groups at that time-point calculated by two sample t-test ($p \leq 0.05$). The figure legend indicates the colour of the markers. Marker shapes are squares and rhombus for the control and treatment groups respectively at 28 days, circles and stars represent the control and the treatment respectively at 7 days.

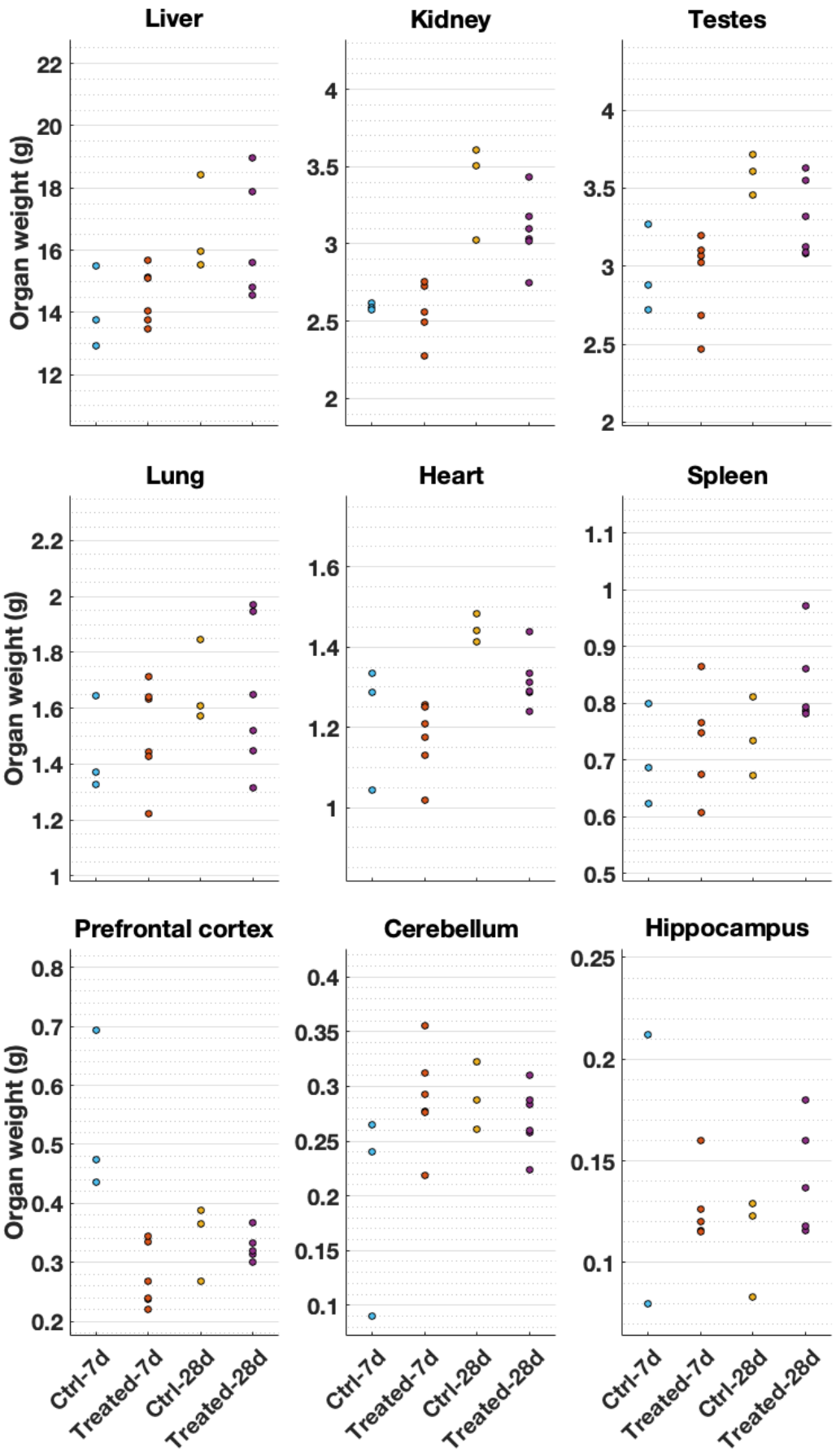
Liver
Kidney
Testes
Lung
Heart
Spleen
Prefrontal cortex
Cerebellum
Hippocampus
Organ weight (g)
Ctrl-7d
Treated-7d
Ctrl-28d
Treated-28d

Fig. 18: Organ weights after dissection of rats given daily i.p. injections of 1 mg/kg B.W. $CoCl_2$ (treatment) and dH_2O (control) after 7 and 28 days of treatment. The weights of rats' organs were recorded and are displayed separately according to control (n=3) and treatment groups (n=6) at 7 and 28 days of treatment. Weights were presented individually to display data variability. No incremental or detrimental trends with cobalt treatment are observed in organ weight data.

5.2.2. Cobalt accumulates in organs and in different brain structures

Our ICP-MS results reveal that kidney, liver and heart incorporated the highest Co content among the rats' organs in that order: Table 10 presents cobalt concentration values, and Fig. 19 displays cobalt accumulation in all tissues tested and blood after 7- and 28-days treatments. ICP-MS measurements of the 28-day cobalt-treated rats (Fig. 20) demonstrate that the pref. cortex, cerebellum and hippocampus assimilated lower but significant amounts of cobalt ($p<0.01$, compared with control rats). This was not the case at 7-days treatment (Table 11). Co levels detected in blood from the treated rats by ICP-MS were within the range found in MoM patients. Co detected in rat blood was 27.14±2.70µg/l, compared with the average levels, 1-2µg/l (Sidaginamale et al., 2013), and the maximum concentrations found in patients with CoCr prostheses, 6521µg/l (Zywiel et al., 2013). For reference, the MHRA has indicated in medical device alerts that patients with cobalt blood levels over 7µg/l should be further evaluated for peri-prosthetic adverse tissue reactions to metal debris (MDA/2010/033, 2010; MDA/2017/018, 2017).

Several tissues in Fig. 19 present increased cobalt accumulation from 7 to 28-days, indicating possible cobalt time-dependent accumulation in heart, liver, kidney, spleen, pref. cortex and blood. However, almost all of the control samples at 7-days treatment indicate high levels of cobalt (heart, liver, kidney, lung, spleen, testes, pref. cortex and cerebellum). This augmentation is likely an artefact of ICP-MS measurements., probably leading to a lack of differential statistical significance with respect to the treatment group in some tissues at 7-days cobalt treatment. Cobalt levels measured here are very low compared with other experimental set-ups applied to the ICP-MS system from the University of Strathclyde Chemistry Department e.g. elemental analysis in soil samples. This makes instrument calibration difficult and, in this case,

the first samples to be introduced to the ICP-MS could have deviated values from the internal standards recovery (0-500 ppb). For values closer to the Co detection limit, it could mean that cobalt content is slightly pushed to higher values. The metal content values obtained from the controls at 28 days are similar to those obtained by a previous study conducted by our team using the same research design (Laovitthayanggoon et al., 2019). In this study cobalt accumulation in all tissues tested at 7 days was significant, i.e. in heart, liver, kidney, lung, spleen, testes, brain and blood. Consequently, the build-up of cobalt at 7 days in the organs we studied is also expected to be relevant, and should not be dismissed in future investigations.

Table 10: Cobalt content values (ng/g) in heart, liver, kidney, lung, spleen and testes, as well as blood (μg/l) obtained from ICP-MS analysis. Mean ± SEM are calculated for n = 3 samples in control groups and n=6 in 1 mg/kg B.W. $CoCl_2$ groups for both 7- and 28-days treatment duration. * significantly different between control and treatment group as assessed by independent-samples t-test ($p \leq 0.05$).

Duration	7 days cobalt content (ng/g)		28 days cobalt content (ng/g)	
Treatment	Control	1 mg/kg B.W.	Control	1 mg/kg B.W.
Heart	152.4 ± 60.8	182.5 ± 31.1	54.1 ± 6.9	341.3 ± 25.6*
Liver	121.8 ± 33.8	525.8 ± 67.2*	57.8 ± 2.8	785.9 ± 97.4*
Kidney	252.9 ± 36.8	768.9 ± 62.3*	229.8 ± 30.4	1144.2 ± 74.7*
Lung	80.9 ± 17.3	104.6 ± 23.2	30.6 ± 4.4	123.3 ± 11.9*
Spleen	48.0 ± 8.8	123.1 ± 19.8*	28.4 ± 5.4	179.5 ± 16.7*
Testes	66.8 ± 16.7	30.6 ± 4.3	6.8 ± 1.4	39.3 ± 2.1*
	7 days cobalt content (μg/l)		28 days cobalt content (μg/l)	
Blood	1.0 ± 0.1	13.8 ± 2.9*	0.9 ± 0.0	27.2 ± 2.7*

Table 11: Cobalt content values (ng/g) in pref. cortex, cerebellum and hippocampus obtained from ICP-MS analysis. Results are presented as mean ± SEM, with n = 3 samples in control groups and n=6 in 1 mg/kg B.W. $CoCl_2$ treatment groups. Treatments were 7 or 28 days long. * significantly different from control group by independent-samples t-test ($p<0.01$).

Duration	7 days cobalt content (ng/g)		28 days cobalt content (ng/g)	
Treatment	Control	1 mg/kg B.W.	Control	1 mg/kg B.W.
Pref. Cortex	44.6 ± 24.6	42.7 ± 5.2	14.5 ± 0.1	57.5 ± 3.7*
Cerebellum	20.1 ± 14.4	36.4 ± 5.5	14.8 ± 0.8	44.2 ± 5.2*
Hippocampus	6.0 ± 1.6	46.9 ± 21.6	5.4 ± 0.8	38.7 ± 1.8*

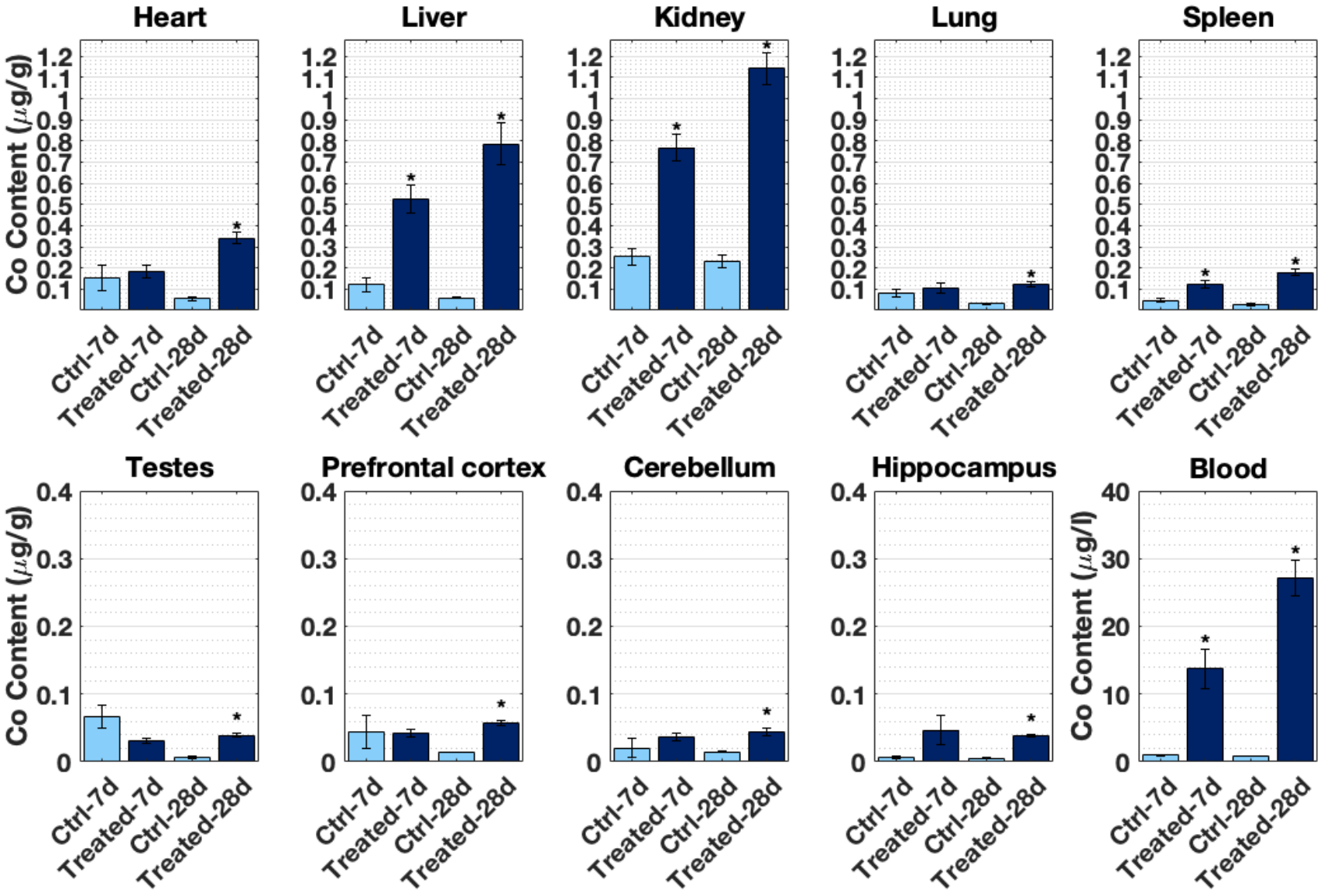
Heart
Liver
Kidney
Lung
Spleen
Testes
Prefrontal cortex
Cerebellum
Hippocampus
Blood
Co Content (μg/g)
Co Content (μg/l)
Ctrl-7d
Treated-7d
Ctrl-28d
Treated-28d

Fig. 19: Cobalt content in SD male rats' tissues (ng/g) and blood (μg/l) at 7- and 28-days of daily i.p. $CoCl_2$ injection treatment as assessed by ICP-MS analysis. Control groups were instead injected with distilled water following the same procedures. Figure presents mean ± SEM calculated from n = 3 samples in control groups (dH_2O) and n=6 in treatment groups (1 mg/kg B.W. $CoCl_2$). * significantly different between control group and treatment group at a given time-point as assessed by two sample t-test ($p \leq 0.05$).

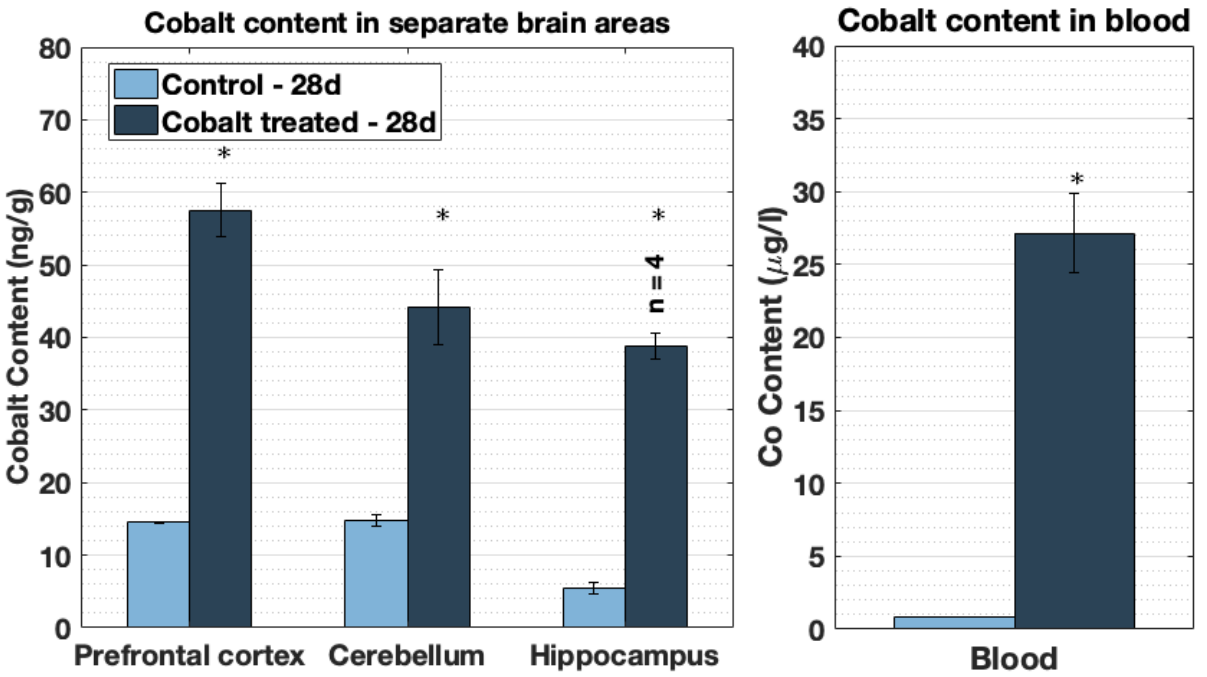

Fig. 20: Cobalt content in pref. cortex, cerebellum, hippocampus (ng/g) and blood (μg/l) at 28 days of 1 mg/kg B.W. $CoCl_2$ treatment in SD male rats analysed by ICP-MS analysis. Mean ± SEM shown are calculated from control groups (n = 3), which were treated with dH_2O, and $CoCl_2$ treatment groups (n=6 unless stated). *significantly different between control and treatment group at 28 days by two sample t-test statistical analysis ($p<0.01$).

5.2.3. Accumulated cobalt induces a genetic response

To observe changes in gene expression, RNA-Seq analysis was performed in pref. cortex and cerebellum from the 28 days-treatment groups, which were the ones reporting significant cobalt tissue accumulation. Unfortunately, there was not enough tissue to research the hippocampus due to its small size. Fig. 21 shows the number and distribution of differentially expressed genes (DEGs) with p-value <0.05. The number of significantly expressed messenger RNA (mRNA) transcripts is higher in the pref. cortex (3564 up-regulated genes, 2694 down-regulated) than in the cerebellum (2037 up, 1568 down). A fold-change threshold is an arbitrary condition commonly set at $|\log_2(\text{Ratio})| \geq 2$ to filter only the most highly up-regulated or down-regulated genes with respect to the control (ratio), which are supposed to be more meaningful in the transcriptomic response to a drug (see section 3.7.4. from the *in vivo* methods chapter for a description of the fold change). The number of DEGs over this boundary is still

more for the pref. cortex (264 up, 84 down) than for the cerebellum (254 up, 37 down). From the distribution of gene expression in Fig. 21, it can be appreciated that most genes have low expression values ($|\log_2 \text{Ratio}| < 2$).

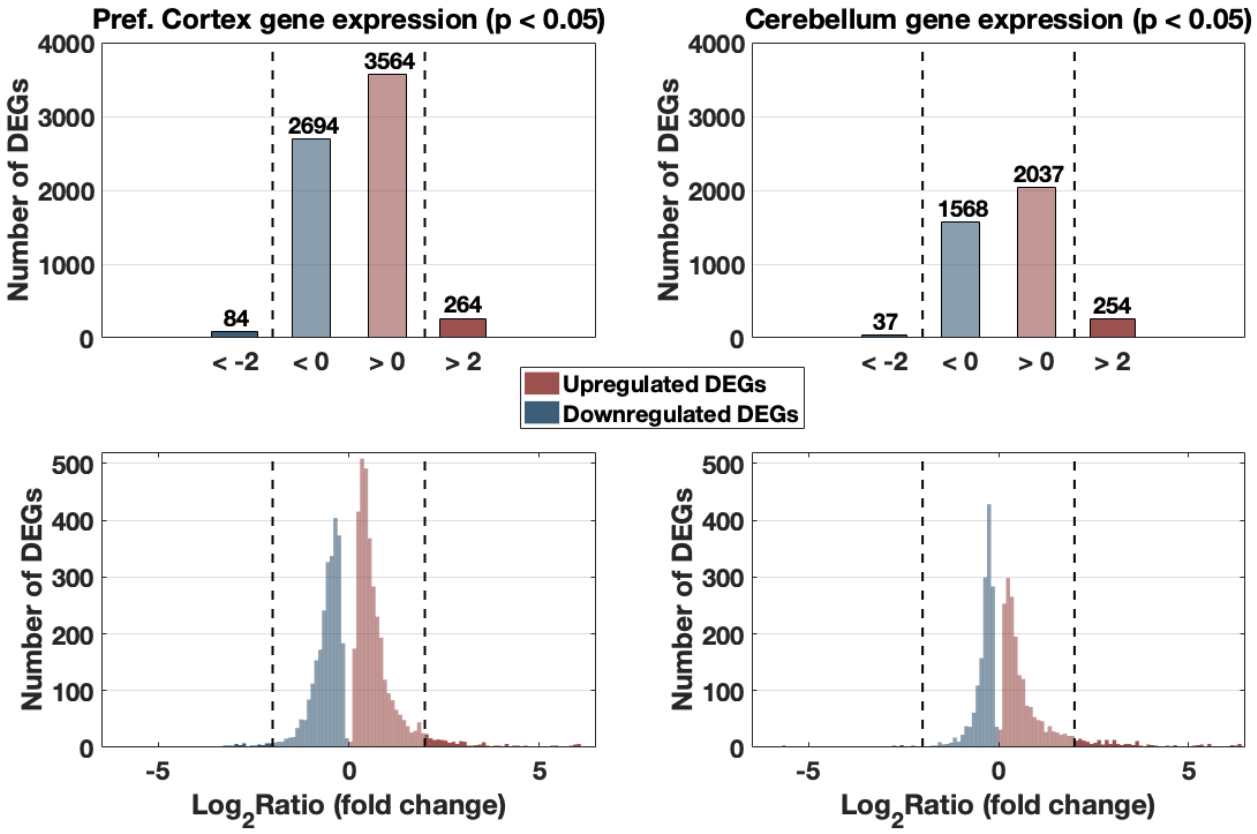

Fig. 21: Number and distribution of Differentially Expressed Genes (DEGs) obtained through RNA-Seq in the pref. cortex and cerebellum of cobalt-treated SD male rats compared with controls. Treated rats (n'=1 of n=3 pooled samples) were dosed during 28 days with 1 mg/kg B.W. Cobalt Chloride ($CoCl_2$), and controls with dH_2O (n'=1 of n=3 pooled samples). The DEGs considered were those with p-value <0.05, and the threshold condition applied to capture highly expressed genes was $|\log_2(\text{Ratio})| \geq 2$.

5.2.4. Transcriptional changes in the cortex and cerebellum demonstrate a tissue-specific response

In order to observe gene expression patterns, which could unveil functional gene groups in both pref. cortex and cerebellum, a hierarchical clustering of the DEGs was performed. The hierarchical clustering of DEGs ($|\log_2 \text{Ratio}| \geq 2$, $p<0.05$) from the cerebellum and the pref. cortex presents only 16 coinciding genes between the two gene expression sets. The heatmap (Fig. 22) shows the name of these genes and its fold-change expression value as indicated by the colour bar. The hierarchical classification of genes performed through the dendrogram returned three groups: C1, which are genes up-regulated in the cerebellum and in the pref. cortex, C2 refers to gene transcripts that are down-regulated in the cerebellum and up-regulated in the pref. cortex, and finally C3 formed by most genes, which are up-regulated in the cerebellum and down-regulated in the pref. cortex.

The Gene Ontology (GO) enrichment analysis of the 16 hits through the Cytoscape software did not return any functional aspect. This could be explained by the low number of genes used to perform the analysis, as well as the fact that some of these genes have only been superficially researched and are poorly annotated as a result. The main functions of each specific gene are commented on Table 12 with information found in the scientific literature, the NCBI Entrez Gene (Gene [Internet]. NCBI Entrez Gene Database, 2004) and UniProtKB (The UniProt Consortium, 2017) databases. It can be appreciated that *a priori* there is no obvious functional relationship between them, and none of the genes seem particularly critical for the development of cobalt toxicity. However, very little research has been carried out in most of these genes and perhaps future investigations will uncover functional relationships.

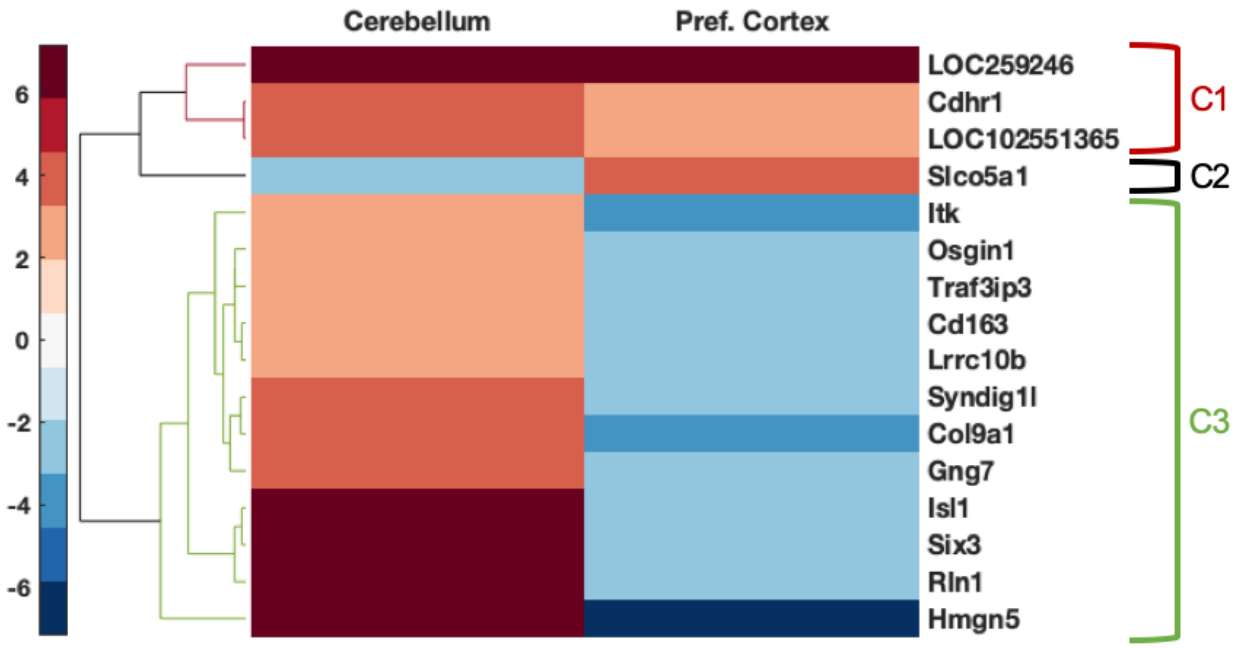

Fig. 22: Hierarchical clustering of Differentially Expressed Genes (DEGs) in rats' pref. cortex and cerebellum after 28 days of i.p. $CoCl_2$ treatment ($log_2Ratio \geq 2$ and $p<0.05$). On the left side, the colour bar reflects the fold-change expression and the dendrogram heights display the Euclidean distance between pref. cortex and cerebellum DEGs pairs. On the right, three brackets have been used to denote the DEGs' groups categorised by the hierarchical clustering. The clustergram function from MATLAB software was used to produce the hierarchical clustering and the graphic. DEGs were obtained through RNA-Seq by comparing the gene expression of pref. cortex and cerebellum of 1 mg/kg B.W. $CoCl_2$-treated rats (n'=1 of n=3 pooled samples), against that of the controls dosed with dH_2O (n'=1 of n=3 pooled samples).

Table 12: List with common DEGs between pref. cortex and cerebellum classified through hierarchical clustering (|log$_2$Ratio|≥ 2 and p<0.05). Descriptions were obtained from NCBI Entrez Gene (Gene [Internet]. NCBI Entrez Gene Database, 2004) and UniProtKB (The UniProt Consortium, 2017) databases unless otherwise cited.

Cluster	Gene / protein name	Fold change		Comments
		Crbm	Crtx	
C1	*LOC259246* alpha-2u globulin PGCL1	6.555	6.672	Male rat-specific protein that accumulates in kidneys causing toxicity (Hamamura et al., 2017).
	Cdhr1 cadherin-related family member 1	3.794	2.003	Role in the structure of photoreceptor cells in the outer segment disc. Belongs to cadherin family, which is calcium dependent. It is involved in retinopathies.
	LOC102551365 stress response protein nst-1-like	3.638	2.070	Unreviewed.
C2	*Slco5a1* solute carrier organic anion transporter family, member 5A1	-2.536	3.561	Its function is still not well known but appears to play a role in cell shape reorganization and migration (Sebastian et al., 2013).
C3	*Hmgn5* high mobility group nucleosome binding domain 5	6.977	-8.109	Modifies chromatin and nucleosome architecture influencing transcription and RNA polymerase II activity. Oncogene.
	Rln1 relaxin 1	6.728	-3.126	Involved in stress and depressive disorders in the brain. Activates G-protein coupled receptors. Also involved in collagen turnover and insulin regulation (Bathgate et al., 2003).

	Six3 SIX homeobox 3	7.180	-2.205	Transcription factor associated with eye and brain development. Disruption leads to holoprosencephaly.
	Isl1 ISL LIM homeobox 1	6.794	-2.116	RNA polymerase II transcription factor. Regulates insulin gene expression. Essential for retinal and heart cells development.
	Gng7 G protein subunit gamma 7	4.133	-2.141	Signal transmembrane transductor involved in adenylyl cyclase activity and cAMP in certain regions of the brain. Influences mice fear response (Schwindinger et al., 2003).
	Col9a1 collagen type IX alpha 1 chain	3.426	-3.400	Encodes part of structural constituent type IX collagen. Linked to ophthalmic, sensorineural and heart defects. Disrupted in Stickler syndrome. Metal ion binding.
	Syndig1l synapse differentiation inducing 1-like	3.442	-2.902	Downregulated in rodent models of Huntington Disease. Very limited research.
	Lrrc10b leucine rich repeat containing 10B	3.097	-2.404	Found as a marker for poor prognosis in lung carcinoma.
	Cd163 CD163 molecule	2.716	-2.555	The encoded protein protects from free haemoglobin oxidative damage. It is secreted in macrophages and can be found in plasma.
	Traf3ip3 TRAF3 interacting protein 3	2.176	-2.022	Activates JNK signalling system that controls several cell functions. Also regulates T cell differentiation (Zou et al., 2015).

	Osgin1 oxidative stress induced growth inhibitor 1	2.277	-3.000	Regulates cell death by responding to oxidative stress together with p53. It can regulate mitochondrial structure (Hu et al., 2012).
	Itk IL2-inducible T-cell kinase	2.399	-4.358	Adaptive immune response. Controls T-cell differentiation. Binds to zinc.

5.2.5. Common metal homeostasis dysregulation at the molecular level might underlie changes in biological processes

In order to find potential toxic mechanisms, GO enrichment analysis of both pref. cortex and cerebellum DEGs ($p<0.05$; no fold change threshold considered) were performed against the Molecular Function reference ontology set (GO MF; 08/04/2016). Fig. 23 shows a graphical representation of this classification with the GOs organised from highest to lowest populated terms. The GO term that comprised most DEGs were 'GO: cation binding' and 'GO: metal ion binding', with a total of 769 genes for the cerebellum and 1292 for the cortex respectively. A further analysis of the DEGs from the 'GO: metal ion binding' term returned its child terms with a thorough classification of metalloproteins by its metal ligands (Fig. 24). Proteins bound to zinc, calcium, magnesium and iron are clearly represented in the spectrum. These results could point out to a possible metal dysregulation in the brain.

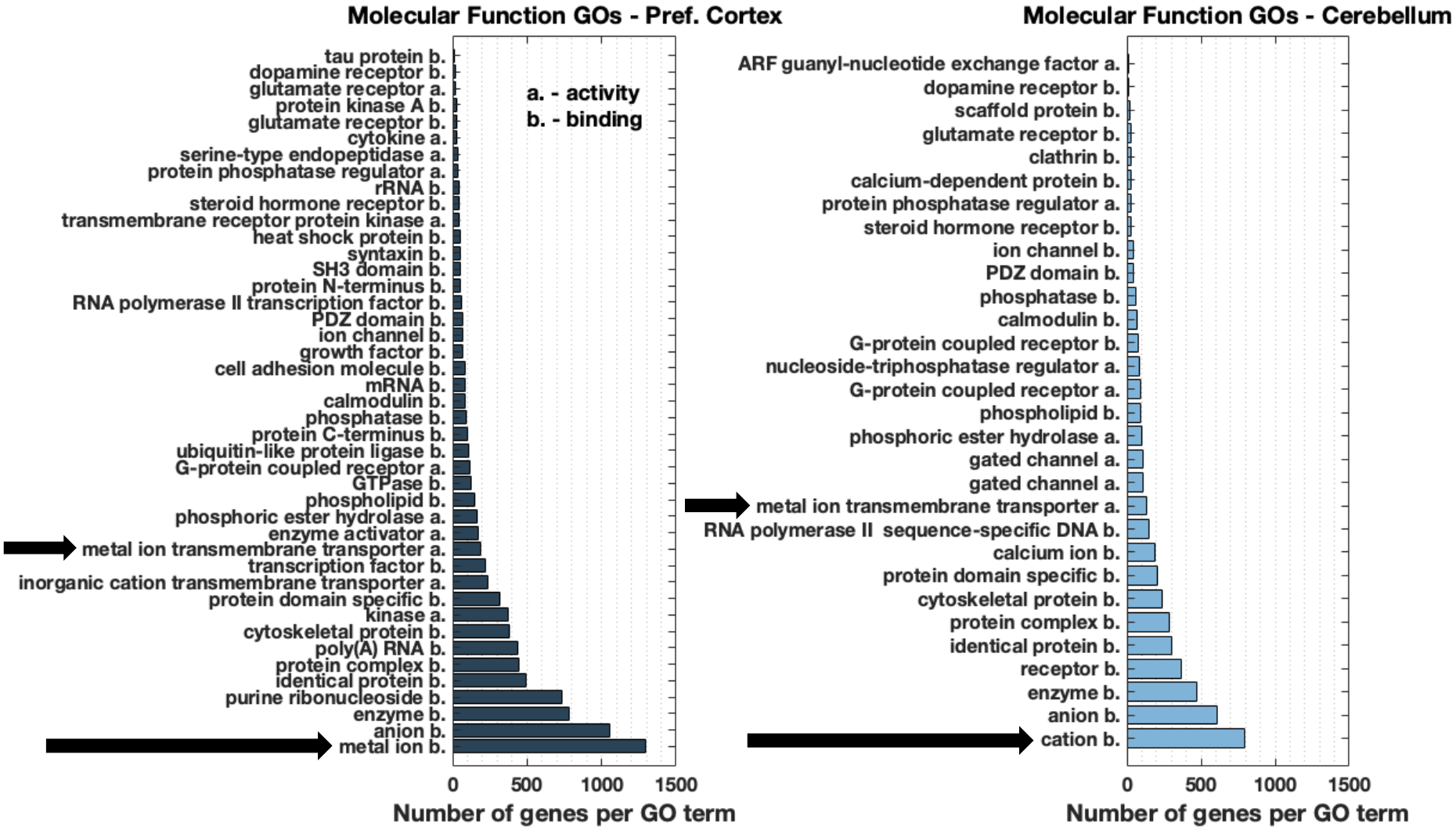
Molecular Function GOs - Pref. Cortex
tau protein b.
dopamine receptor b.
glutamate receptor a.
protein kinase A b.
glutamate receptor b.
cytokine a.
serine-type endopeptidase a.
protein phosphatase regulator a.
rRNA b.
steroid hormone receptor b.
transmembrane receptor protein kinase a.
heat shock protein b.
syntaxin b.
SH3 domain b.
protein N-terminus b.
RNA polymerase II transcription factor b.
PDZ domain b.
ion channel b.
growth factor b.
cell adhesion molecule b.
mRNA b.
calmodulin b.
phosphatase b.
protein C-terminus b.
ubiquitin-like protein ligase b.
G-protein coupled receptor a.
GTPase b.
phospholipid b.
phosphoric ester hydrolase a.
enzyme activator a.
metal ion transmembrane transporter a.
transcription factor b.
inorganic cation transmembrane transporter a.
protein domain specific b.
kinase a.
cytoskeletal protein b.
poly(A) RNA b.
protein complex b.
identical protein b.
purine ribonucleoside b.
enzyme b.
anion b.
metal ion b.
a. - activity
b. - binding
0
500
1000
1500
Number of genes per GO term
Molecular Function GOs - Cerebellum
ARF guanyl-nucleotide exchange factor a.
dopamine receptor b.
scaffold protein b.
glutamate receptor b.
clathrin b.
calcium-dependent protein b.
protein phosphatase regulator a.
steroid hormone receptor b.
ion channel b.
PDZ domain b.
phosphatase b.
calmodulin b.
G-protein coupled receptor b.
nucleoside-triphosphatase regulator a.
G-protein coupled receptor a.
phospholipid b.
phosphoric ester hydrolase a.
gated channel a.
gated channel a.
metal ion transmembrane transporter a.
RNA polymerase II sequence-specific DNA b.
calcium ion b.
protein domain specific b.
cytoskeletal protein b.
protein complex b.
identical protein b.
receptor b.
enzyme b.
anion b.
cation b.
0
500
1000
1500
Number of genes per GO term

Fig. 23: Molecular function Gene Ontology (GO) clustering of pref. cortex and cerebellum DEGs sorted by number of genes. Metal ion binding GO term and cation binding are the most populated terms for the pref. cortex and cerebellum respectively. Arrows indicate to GO terms of interest: ‘metal ion binding’, ‘cation ion binding’ and ‘metal ion transmembrane transporter activity’. DEGs classification was produced by Cytoscape and GO term display was obtained with MATLAB.

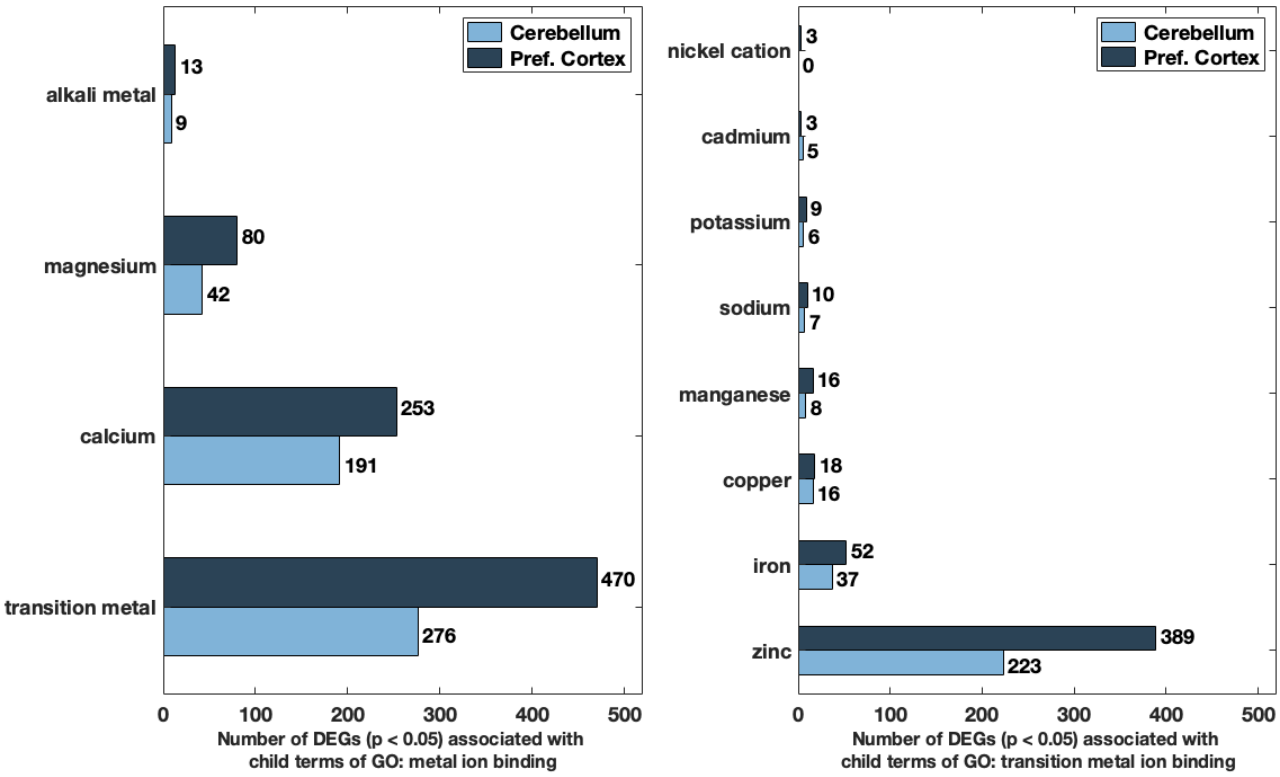

Fig. 24: Classification of metalloproteins from the pref. cortex and the cerebellum in the GO term 'GO: metal ion binding' (left) and its child term 'GO: transition metal ion binding' (right) by its metal ion ligands. DEGs were obtained through RNA-Seq by comparing the gene expression of pref. cortex and cerebellum of cobalt-treated rats (n'=1 of n=3 pooled samples) (1 mg/kg B.W. $CoCl_2$), against that of the controls dosed with dH_2O (n'=1 of n=3 pooled samples). The number of DEGs in each group is roughly indicated in the x-axis and precisely at the right of the bars. DEGs classification was produced by Cytoscape and GO term display was obtained with MATLAB.

5.2.6. Divalent metal transporters: genetic regulation indicates ion competition

Another GO term represented in the molecular functional analysis in both cerebellum and pref. cortex data sets is ‘GO: divalent inorganic cation transmembrane transporter activity’ (Fig. 23). A closer look into the genes that compose this group in Fig. 25 reveals that in the pref. cortex there are 81 divalent transporters, of which 63 are estimated to be calcium (Ca^{2+}) channels, 24 of them active by voltage. Meantime, 47 divalent transporters were found in the cerebellum, of which 40 are calcium (Ca^{2+}) channels, and 18 of them are also activated by voltage ($p<0.05$). These channels could be directly or indirectly regulated by cobalt, but the elevated number of calcium channels might indicate a crucial role of calcium transporters in cobalt toxicity. In addition, other GO terms such as ‘GO: glutamate receptor binding’ in the pref. cortex or ‘GO: extracellular ligand-gated ion channel activity’ in the cerebellum ($p<0.05$) also have implications for the transport of Ca^{2+} ions through ligand gated-operated channels (Bardsley et al., 2018). They involve genes encoding Glutamate ionotropic receptor AMPA type subunits (Gria), Glutamate ionotropic receptor NMDA type subunits (Grin) or the Gamma-aminobutyric acid type subunit (Gabra).

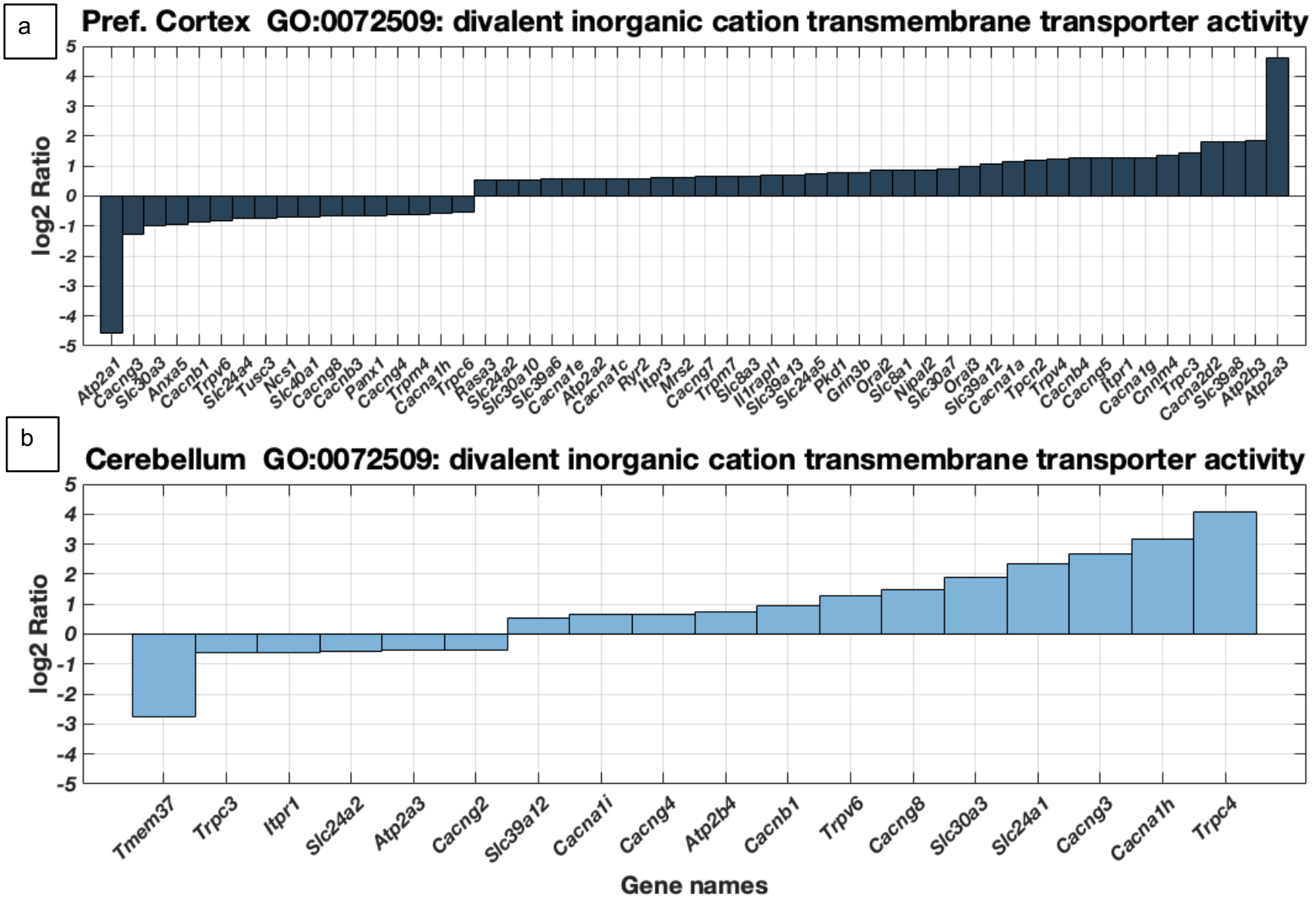
a
Pref. Cortex GO:0072509: divalent inorganic cation transmembrane transporter activity
log2 Ratio
5
4
3
2
1
0
-1
-2
-3
-4
-5
Atp2a1
Cacng3
Slc30a3
Anxa5
Cacnb1
Trpv6
Slc24a4
Tusc3
Ncs1
Slc40a1
Cacng8
Cacnb3
Panx1
Cacng4
Trpm4
Cacna1h
Trpc6
Rasa3
Slc24a2
Slc30a10
Slc39a6
Cacna1e
Atp2a2
Cacna1c
Ryr2
Itpr3
Mrs2
Cacng7
Trpm7
Slc8a3
Il1rapl1
Slc39a13
Slc24a5
Pkd1
Grin3b
Orai2
Slc8a1
Nipal2
Slc30a7
Orai3
Slc39a12
Cacna1a
Tpcn2
Trpv4
Cacnb4
Cacng5
Itpr1
Cacna1g
Cnnm4
Trpc3
Cacna2d2
Slc39a8
Atp2b3
Atp2a3
b
Cerebellum GO:0072509: divalent inorganic cation transmembrane transporter activity
log2 Ratio
5
4
3
2
1
0
-1
-2
-3
-4
-5
Tmem37
Trpc3
Itpr1
Slc24a2
Atp2a3
Cacng2
Slc39a12
Cacna1i
Cacng4
Atp2b4
Cacnb1
Trpv6
Cacng8
Slc30a3
Slc24a1
Cacng3
Cacna1h
Trpc4
Gene names

Fig. 25: DEGs ($p<0.05$) from the pref. cortex (a) and cerebellum (b) of the GO term 'GO: divalent inorganic cation transmembrane transporter activity'. The transporter gene name is indicated in the x-axis and the fold-change ($|\log_2 Ratio|$) is on the y-axis. Due to the high number of genes the figure only presents genes with $|\log_2 Ratio| \geq 0.5$.

5.2.7. Metalloproteins could be targeted by cobalt: phosphodiesterase and carbonic anhydrase families

To further investigate the possible metal dysregulation, the DEGs classified in the metal ion GO child terms (indicating metal ligand/substrate) from 'GO: metal ion binding' represented in Fig. 24 were re-evaluated against the Molecular Function reference ontology set (GO MF; 08/04/2016). Terms which were mainly composed by the isoforms of a protein family are reported in Table 13 (as observed by visual inspection). The rationale for this analysis is that proteins sharing structural similarities, such as in protein families, might be affected in a similar way by increased concentrations of cobalt, thus showing altered activity, e.g. protein inactivation. In our analysis, if a set of isoforms belonging to a protein family is consistently regulated at the transcriptional level, we hypothesise that it might indicate molecular activity changes, which could eventually lead to relevant pathologies. In this case, GO terms involving the families of phosphodiesterases (Fig. 26) and carbonic anhydrases (Fig. 27) were found to be significantly affected among others.

Table 13: Summary of metalloprotein families within each of the ligand-associated child GO terms obtained from the significant GO term 'GO: metal ion binding' (p<0.001). Fields listed are the ligand type -zinc (Zn^{2+}), calcium (Ca^{2+}), magnesium (Mg^{2+}), etc.-, the possible metalloprotein families whose activity could be targeted by cobalt, the significance of the GO term that family was present in (GO term name if different from the protein family name) in the pref. cortex and in the cerebellum. Colour code indicates the biological aspect of the proteins – signalling (orange), metabolism (green), formation of synapses and axons (yellow), genetic or protein regulation (blue) and metalloproteinases or other functions (grey).

Ion	Metalloprotein family potentially targeted by cobalt	Term significance within Metal binding term (from reanalysis)	
		Pref. Cortex	Cerebellum
Zn^{+2}	Carbonic anhydrase/carbonate dehydratase (*Ca*)	0.00	0.06
	S-acyltransferases/palmitoyltransferase activity (*zDHHC*)	**0.04**/0.17	1.00/1.00
	Phosphodiesterases (*Pde*): Site one binds Zn^{+2}, site two Mg^{+2} and/or Mn^{2+}.	0.00 (GO: 'cyclic-nucleotide phosphodiesterase activity')	0.00
	Zinc finger protein 3: mRNA decay enzymes (*Zfp3*)	1.00 ('mRNA 3'-UTR binding')	1.00
	Nuclear, Estrogen and Thyroid receptor superfamily (*Nrxyz, Esr, Thr*).	0.01/0.15 ('steroid hormone receptor activity', 'RNAII transcription factor')	0.00/0.00
	Ring finger and Tripartite motif families (*Rnf* and *Trim*).	0.00 ('ubiquitin-like protein transferase activity')	0.02
	Ubiquitin specific peptidases (*Usp*)	1.00 ('ubiquitin-like protein-specific protease activity')	1.00
	Ubiquitin specific peptidases (*Usp*) and Calpain (*Capn*)	1.00 ('cysteine-type peptidase activity or peptidase act. with Adam')	1.00
	A Disintegrins and Metalloproteinases (*Adam* and *Adamts*)	**0.00** ('metalloendopeptidase activity')	0.23

Ca^{+2}	Diacylglycerol kinase activity (*Dgk*) / Diacylglycerol binding (*Unc13*)	0.20/0.18	1.00/0.47
	Alpha-Mannosidase (*Man*)	1.00	1.00
	Phospholipase C (*Plc*)	1.00	0.03
	Actin filament binding/ligand-dependent nuclear receptor (*Actn*)	1.00/1.00	1.00/1.00
	Synaptotagmin (*Syt*)	0.00/0.00 ('clathrin binding', 'syntaxin binding' or 'SNARE binding' too)	0.00/0.00
	Slit guidance ligand	1.00 ('Roundabout binding')	0.08
Mg^{+2}	G protein alpha subunit (*Gna*)	0.38/0.00	0.76/0.19
	Serine/threonine PP (*PPM/PPP*) families	0.33 ('phosphatase activity')	1.00
	Adenylate cyclases (*Adcy*)	1.00	0.62
	Polypeptide N-acetylgalactosaminyltransferase (*GALNT*).	1.00	0.14
	Serine/threonine-protein kinase C (*PrkC*)	0.07 ('protein kinase C activity')	0.00
	Testican/SPOCK & Tissue inhibitors of metalloproteinases (*TIMP*s).	1.00 ('metalloendopeptidase inhibitor activity')	0.00
Heme	Cytochromes P450 (*CYP*s)	1.00 ('oxidoreductase activity, acting on paired donors')	1.00
Varied	ATPase/GTPAse	1.00/1.00	1.00/1.00

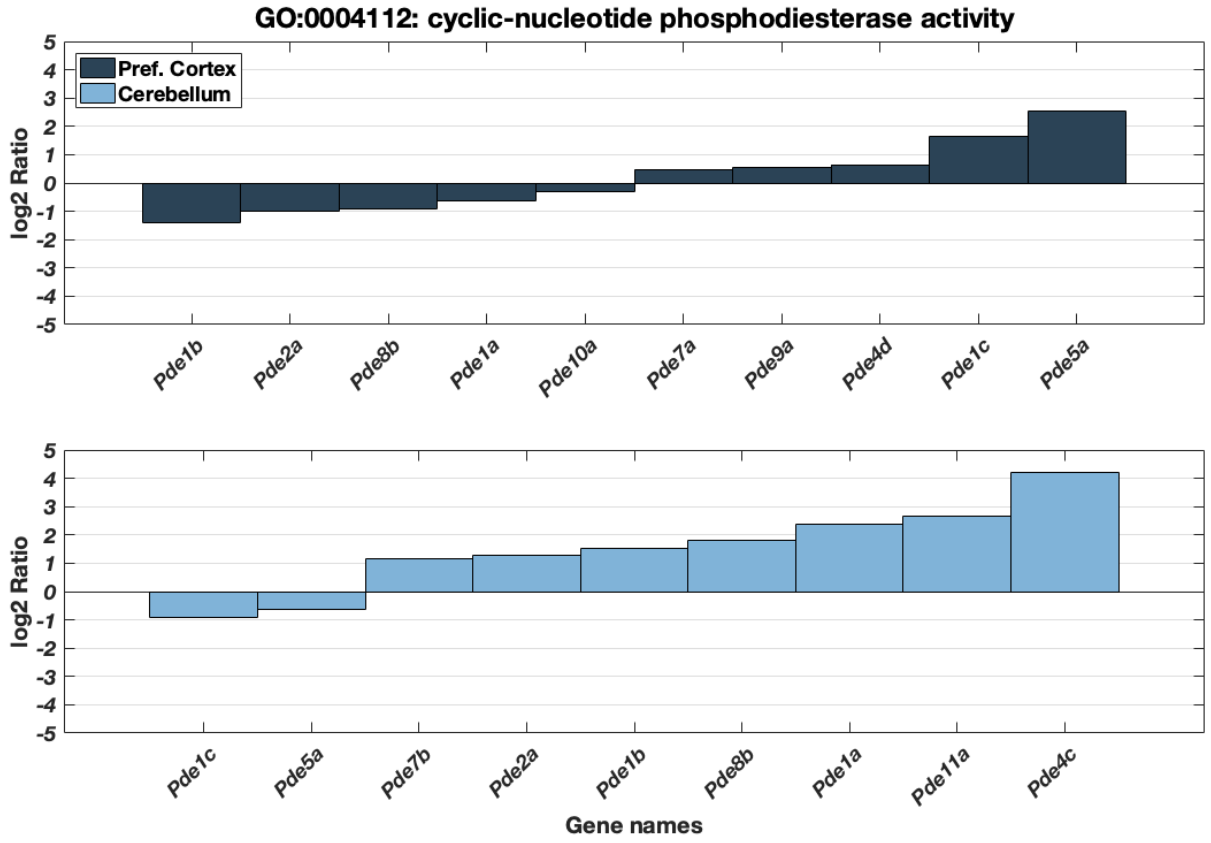

Fig. 26: Genes representing protein isoforms belonging to the phosphodiesterase family (Pde) with its corresponding expression level in the pref. cortex (up) or the cerebellum (down). Usual ligands are zinc or magnesium. The GO term they belong to is indicated over the figures (DEGs p-value <0.05). The DEGs found are from an RNA-Seq experiment in pref. cortex and cerebellum of 1 mg/kg B.W. $CoCl_2$-treated rats (n'=1 of n=3 pooled samples), compared against that of the controls (dH_2O; n'=1 of n=3 pooled samples).

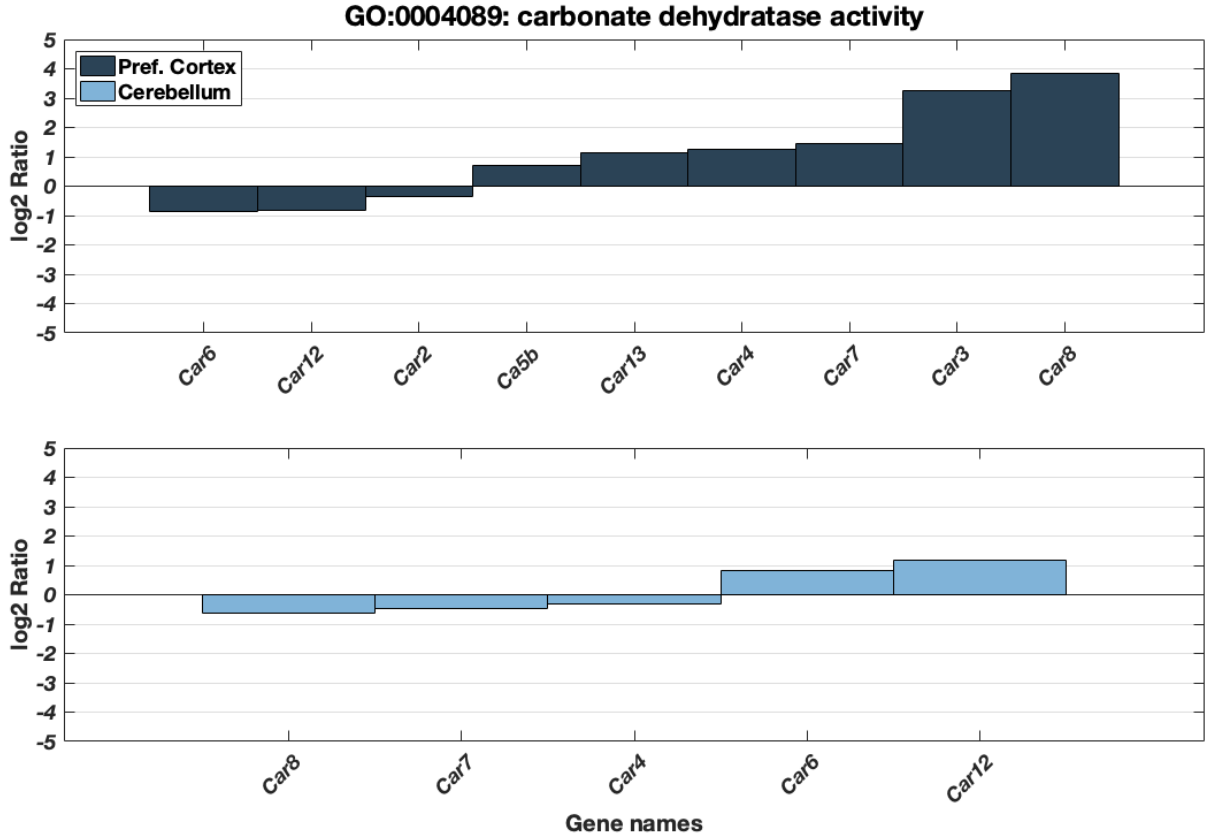

Fig. 27: Genes representing protein isoforms belonging to the carbonic anhydrase family (Ca or Car) with its corresponding expression level in the pref. cortex (upper panel) or the cerebellum (lower panel) (DEGs p-value <0.05). The usual ligand is zinc. The GO term they belong to is indicated over the figures. DEGs were obtained by performing RNA-Seq in pref. cortex and cerebellum of 1 mg/kg B.W. $CoCl_2$-treated rats (n'=1 of n=3 pooled samples), and comparing against that of controls dosed with dH_2O (n'=1 of n=3 pooled samples) for 28 days.

5.2.8. RT-qPCR *Pde* and *Car* gene expression follows RNA-Seq results

Carbonic anhydrases control the conversion of carbon dioxide (CO_2) to bicarbonate, thus regulating pH balance and are also involved in cellular respiration and electrolyte secretion. Phosphodiesterases are mainly involved in second messenger cyclic-AMP and GMP (cAMP and cGMP) signalling. Moreover, the carbonic anhydrase and phosphodiesterase pathways are thought to be connected by the bicarbonate activation of soluble adenylyl cyclase (sAC) to generate cAMP (Tresguerres et al., 2011), and phosphodiesterase activity inhibitors have been shown to activate several isoforms of carbonic anhydrase (Abdülkadir Coban et al., 2009). To test whether these

pathways were possibly affected we studied the expression of genes from the carbonic anhydrase (*Car2, Car4*) and phosphodiesterase (*Pde2a, Pde5a, Pde8b*) families. From the phosphodiesterase family, we selected *Pde2a, Pde5a, Pde8b* which are expressed in RNA-Seq results from both pref. cortex and cerebellum samples (Fig. 26). *Pde2a* and *Pde8b* are widely expressed in the rat pref. cortex while *Pde5a* is expressed in the cerebellum (Kelly et al., 2014). These isoforms are also widely expressed in the human CNS (Lakics et al., 2010). The protein PDE2A catalyses the hydrolysis of both cAMP and cGMP, while PDE5A has substrate specificity for cGMP, and PDE8 only hydrolyses cAMP, which covers both cGMP-PKG and cAMP-PKA pathways (Heckman et al., 2018). Moreover, the three proteins are involved in cognition (Heckman et al., 2018), and their expression suffers age-related changes in the CNS (Kelly et al., 2014). We also selected cGMP-dependent protein kinases genes, *Prkg1*, and the brain nitric oxide, *Nos1*, which are both activated by cGMP, in addition to the cAMP-dependent protein kinase (PKA), *Prkar2b*, which is activated by cAMP. The selected carbonic anhydrase genes, *Car2* and *Car4*, are also present in the RNA-Seq data but their expression is low (Fig. 27). Other carbonic anhydrase genes such as *Car8* and *Car3* have a high expression, but they are either acatalytic or have very low activity. Carbonic anhydrase II (CA2) is a cytosolic protein present in oligodendrocytes, astrocytes, the choroid plexus epithelial cells, in addition to a few neuronal subsets, while CA4 is a membrane-bound protein located in the BBB and cerebral cortex (Provensi et al., 2019).

Fig. 28 shows the expression of these genes according to the results of RNA-Seq and RT-qPCR. The fold-change reported by the two techniques is fairly similar, and the direction of fold change expression is only different for *Car2* in the pref. cortex (Fig. 28). However, only the expression of *Car4* ΔC_T values was significantly different between the control and the treatment groups as assessed by RT-qPCR (Table 14). Fig. 29 displays the ΔC_T values, where it can be observed that the relative gene expression does not undergo important changes in most target genes.

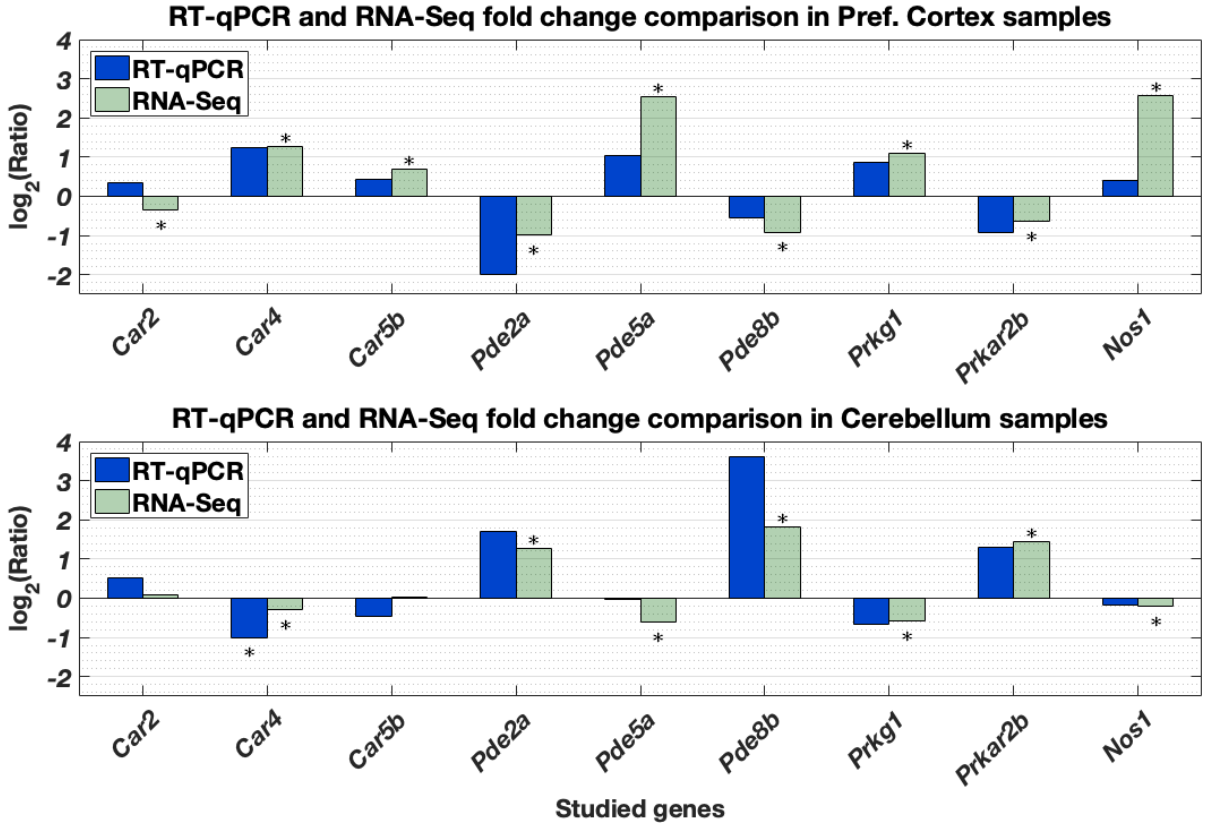

Fig. 28: Fold change of target genes according to RNA-Seq (n'=1 of n=3 pooled samples) and RT-qPCR. * significant difference with reference to the control group (n=3) at 28 days treatment (1 mg/kg B.W. $CoCl_2$; n=3) independent-samples t-test ($p \leq 0.05$), it does not represent a significant difference between RNA-Seq and RT-qPCR results. Target genes: *Car2*, *Car4*, *Car5b*, *Pde2a*, *Pde5a*, *Pde8b*, *Prkg1*, *Prkar2b* and *Nos1*, where internal controls were *Ywhaz* (pref. cortex) and *Tbp* (cerebellum).

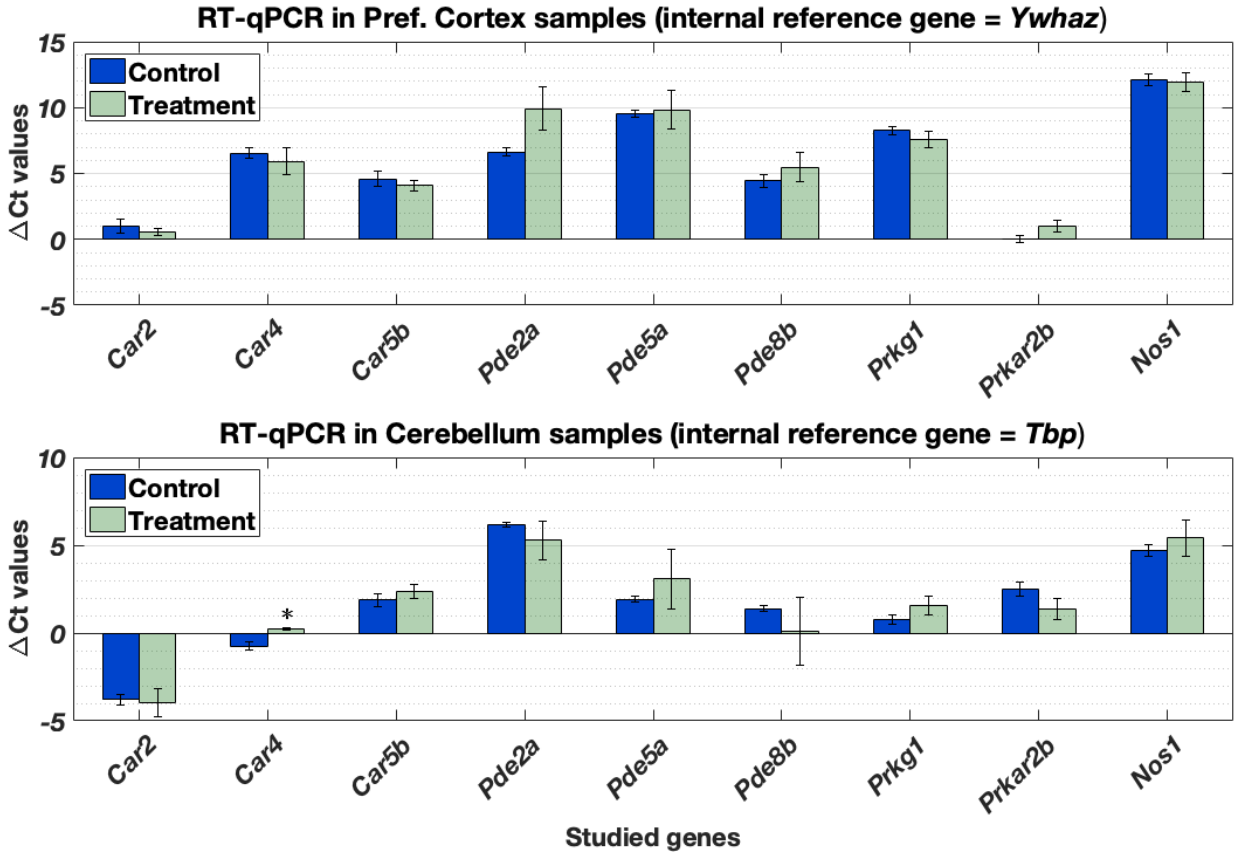

Fig. 29: ΔC_T values (C_T target gene – C_T internal control) obtained from RT-qPCR tests in pref. cortex and cerebellum. Target genes are *Car2*, *Car4*, *Car5b*, *Pde2a*, *Pde5a*, *Pde8b*, *Prkg1*, *Prkar2b* and *Nos1*, while internal controls were *Ywhaz* and *Tbp* for pref. cortex and cerebellum respectively. Mean ± SEM (n=3) at 28 days. *significantly different control group (n=3) from 1 mg/kg B.W. $CoCl_2$ treatment groups (n=3) for 28-days treatment duration independent-samples t-test ($p \leq 0.05$).

Table 14: Fold change in expression between the treated and untreated rats. *significant difference between control group (n=3) and treatment groups (n=3) (1 mg/kg B.W. $CoCl_2$) at 28 days treatment duration independent-samples t-test ($p \leq 0.05$).

Symbol	Pref. Cortex		Cerebellum	
	Fold-change	p-Value	Fold-change	p-Value
Ca2	1.26	0.454	1.44	0.861
Ca4	2.37	0.59	-2.00*	0.017
Ca5b	1.35	0.489	-1.38	0.408
Pde2a	-3.96	0.116	3.25	0.463
Pde5a	2.068	0.842	-1.02	0.57
Pde8b	-1.48	0.446	12.28	0.565
Prkg1	1.82	0.379	-1.60	0.408
Prkar2b	-1.89	0.137	2.47	0.176
Nos1	1.34	0.795	-1.13	0.533

5.3. Discussion

With these experiments we searched to investigate the *in vivo* effects of cobalt at the molecular level and its accumulation in different organs. Male SD rats were dosed intraperitoneally with 1mg/kg B.W. cobalt chloride for 7 or 28 days. Their weights were assessed during the treatment period. Once the treatment was finished, cobalt content was obtained from several organs and brain areas. In addition, we also looked at the gene expression levels in the brain through RNA-Seq, and validated these results through RT-qPCR.

5.3.1. Cobalt could influence body weight

Animals were weighed daily during the treatment period to evaluate their general health. We observed constant weight gain in the rats, which, in principle, appeared to follow similar rates across control and treatment groups (Fig. 16). However, after normalising to initial body weight, an average 6.77% (range: 0.46 - 11.57%) weight difference is observed between treated and control animals at 28 days (Fig. 17). As rats were fed *ad libitum* no differences in food intake between the control and treatment groups were noted by the student or technicians. Indeed, the animals were healthy and kept playing with their cage mates throughout the experiment. Organ weights were also assessed and no obvious changes were observed in this parameter (Fig. 18), hence confirming that rats had not experienced severe toxicity.

This slightly delayed growth between control and treatment groups was also noted by our colleagues using the same cobalt treatment conditions (Laovitthayanggoon et al., 2019). Moreover, other researchers who dosed rats with 0.75mg/kg cobalt intraperitonially for three weeks also observed a significant weight drop in comparison to rats treated with saline (control) or hydroxocobalamin (Houeto et al., 2018). Several recent reports have cited anorexia as a symptom of cobaltism in hip prostheses patients (Mao et al., 2011; Zywiel et al., 2013). This effect was also prevalent in Quebec Beer Drinkers (Kesteloot et al., 1968; Morin et al., 1969). The brain has a dominant role in energy balance and control of body weight and appetite through the feeding circuits in the hypothalamus (García-Cáceres et al., 2019). Thus, it is possible that cobalt toxicity in the brain may directly or indirectly hinder metabolism and cause cobalt-treated animals to lose nutrient sensing abilities and change their food

consumption behaviour. Hypothalamic tanycytes, which were discussed in section 4.3.2. from the previous chapter, are involved in inflammation-induced anorexia (Böttcher et al., 2020), and insult to tanycytes in the third ventricle led to significant decrease of food intake after 4 days and total body weight loss of 10% after 14 days (Sanders et al., 2004). Tanycytes are in contact with both blood and CSF, therefore, they could easily be exposed to cobalt. Nevertheless, whether cobalt interferes with the brain metabolic centres such as the hypothalamus and affects food intake and body weight in treated animals is a hypothesis that should be evaluated further.

5.3.2. Metal distribution pattern is consistent with previous research and cobalt accumulates significantly on the brain

Fig. 19 and Table 10 present cobalt content at 7 and 28 days in different organs. Cobalt distribution follows the same pattern as previous experiments from our research group (Afolaranmi et al., 2012; Laovitthayanggoon et al., 2019) and other teams investigating cobaltism (Apostoli et al., 2013). Liver, kidney and heart visibly accumulated more metal than other organs (Fig. 19), which correlates with cobalt organ concentration in humans following cobalt radioisotope distribution (Paustenbach et al., 2013). Most cobalt is excreted through urine (Daniel et al., 2010; Paustenbach et al., 2013), and given that both kidney and liver are in charge of toxin and waste detoxification, it is not surprising that cobalt is predominantly concentrated in these tissues. The few post-mortem examinations in MoM patients also reveal metal accumulation in heart, spleen, liver, and lymph nodes, these being the only tissues analysed to date (Abdel-Gadir et al., 2016; Martin et al., 2015; R M Urban et al., 2000; Urban et al., 2004; Wyles et al., 2017). *In vitro* studies of cobalt in hepatocytes revealed damage to mitochondria (Battaglia et al., 2009) and partial glucuronidation inhibition (Afolaranmi et al., 2011), a pathway which is necessary for the excretion of xenobiotics. *In vivo* research showed increased antioxidant activity of hepatic catalase and glutathione peroxidase (Afolaranmi et al., 2012). However, it is worth noticing that even though the preferential accumulation of cobalt occurs in the liver and kidney, patients' symptoms do not indicate major toxicity in these two organs (Apostoli et al., 2013; Paustenbach et al., 2013), aside from the implant patient with the highest levels of cobalt reported (6521 µg/l) (Zywiel et al., 2013), and some Quebec Beer Drinkers (Sullivan et al., 1969). Instead, in cobaltism the heart and nervous system organs emerge as the main targets of toxicity (Cheung et al., 2016). The toxicity of each metal is unique, yet most heavy

metals have moderate or even severe adverse effects on the kidney and the liver. Metal toxicity depends on several characteristics such as the chemical state of the metal, i.e. their speciation, the complexation with proteins, if interference with other essential metals exists, the availability of metal transporters, and the specific host conditions (Goyer and Clarkson, 2008), as well as their redox cycling characteristics (Valko et al., 2016). Thus, the particular mode of action of cobalt toxicity will depend on the relative importance of these factors, which will make cobalt effects different from those of other metals.

To our knowledge, there is no information about cobalt concentrations of MoM patients in the brain, probably due to the difficulty of obtaining samples from patients. As mentioned in section 4.3.2. from Chapter 4, cerebrospinal fluid in patients with very high cobalt levels could be 20-40 times the reference CSF cobalt content. A recent study on MoM patients showed that higher concentrations of cobalt in plasma were associated with increased concentrations in CSF, although they were unable to find a threshold for cobalt neurotoxicity (Harrison-Brown et al., 2020). In our study, the brain parts dissected from the brain, the pref. cortex, cerebellum and hippocampus, had significant cobalt accumulated at 28 days (Fig. 20 and Table 11). A study by Apostoli et al. with rabbits dosed with cobalt during 18 days intravenously reported elevated brain levels, 0.2 ± 0.2 µg/g, from average control levels, 0.06 ± 0.04µg/g dry weight, and cobalt whole blood， 420.9 ± 154.5 µg/l, see Table 15 for reference. Although we should be cautious with their ICP-MS cobalt analysis given the large standard deviations reported, the histology in several organs only reported damage to the eyes and the auditory systems. Our model had much lower cobalt blood concentration (27.1± 2.7 in contrast with the 420.9 ± 154.5 µg/l of rabbits), and animals remained in good health, while Apostoli et al. described balance disturbance in rabbits owing to vestibular damage. Given the literature and our own observations, we expect cobalt to induce nothing more than subtle or moderate neurotoxicity in our study even when cobalt has significantly accumulated in the rats' brains.

There are a couple of studies investigating brain functions in MoM patients through PET (Bridges et al., 2020) and MRI (Clark et al., 2014). They reported hypometabolism and changes in the structure of several brain areas, however, these studies investigate patients with blood concentrations at the lower end of cobalt poisoning (<20 µg/l) and

present methodology problems. The same occurs with studies investigating the auditory (Leyssens et al., 2020) and visual functions (Unsworth-Smith et al., 2017). Blood cobalt levels in patients with well-functioning MoM hip resurfacing implants are expected to be lower than 2 µg/l (reference range <1 µg/l), with values over 5.6 µg/l suggestive of abnormal wear (Sidaginamale et al., 2013). Case reports indicate that systemic symptoms typically appear with cobalt levels above 300µg/l, provided there is no comorbidity and that it is likely unnecessary to suspect systemic concerns in patients with blood cobalt levels under 100µg/l (Kovochich et al., 2018). For instance, a review cites values of 549 µg/l and 625 µg/l cobalt in blood of hip prostheses patients with neurotoxic symptoms (Catalani et al., 2012). Various investigations of MoM patients with cobalt blood levels under 100µg/l found no correlation between cobalt blood levels and symptoms of systemic cobaltism (Ho et al., 2017; Leikin et al., 2013; van Lingen et al., 2014), although systemic symptoms of cobaltism have also been reported in arthroprosthetic patients with serum cobalt levels of 23µg/l (Tower, 2010) and 24µg/l (Mao et al., 2011). It has been hypothesised that certain patients with metal allergy might be hypersensitive to cobalt (Kovochich et al., 2018). Langton *et al.* found that the presence of ALVAL increased concentrations of Co in fluid collections in a higher proportion than local volumetric wear (Langton et al., 2018). Thus, tissue damage could be associated with the immune response, and in that case, individual differences in immunity might predispose some patients to develop a reaction to cobalt. This could explain the inconsistent systemic responses to different Co levels in blood. In addition, patients with hip implants belong to an aged sector of the population (National Joint Registry, 2020), and are likely affected by other health conditions that might increase the risk of developing symptoms. The cobalt blood concentration at 28 days, 27.1 $\pm$ 2.7µg/l, is a relatively low concentration compared with the 100-300µg/l systemic toxicity threshold, and considering previously mentioned experiments and literature on patients, we expect weak or moderate brain changes in response to cobalt toxicity in our model. In this research we consider levels under 100µg/l cobalt in blood as moderate cobalt levels, while values under 20µg/l are regarded as low due to their diminished potential to induce cobalt systemic toxicity, rather than indicating local prostheses failure. These labels are based on the limited literature available rather than specific research due to the few numbers of patients with evident cobaltism (Kovochich et al., 2018). The blood cobalt levels associated with peri-prosthetic

damage and failure of MoM prostheses are understandably lower (>4.5 μg/) and have been extensively researched (Langton et al., 2013; Sidaginamale et al., 2013).

Only two papers have quantified cobalt content from MoM patients' tissues from hearts post-mortem and after transplant: 4.75 (Martin et al., 2015) and 8.32 μg/g (Allen et al., 2014) compared with 0.060 μg/g reference value of unexposed individuals (Wyles et al., 2017). In addition, other post-mortem analyses on patients with metal-on-polyethylene hip prostheses also revealed significantly elevated cobalt content averaging 0.12 μg/g (range: 0.006-6.299 μg/g), which was associated with lower cardiac ejection fraction, fibrosis and cardiomegaly (Wyles et al., 2017). Cobalt in the heart tissue of beer drinkers was also quantified, 0.48±0.24 μg/g (Sullivan et al., 1968), although the techniques used at the time might be unreliable today and we are unsure of the accuracy of these results because we could not access this paper directly, the values were taken from (Paustenbach et al., 2013). In our results, cobalt heart content in the control group at 28 days was 0.054± 0.01 (simplified 0.1 ± 0.01) μg/g, which is similar to the cited control values in humans: 0.060 μg/g (Wyles et al., 2017), see Table 15 for a compact presentation of these figures. The higher values of 0.2± 0.0 μg/g and 0.34± 0.0 μg/g in the rats' hearts at 7 and 28 days respectively are close to the average content in MoP patients (0.12 μg/g) (Wyles et al., 2017). These values have also been displayed in Table 15 for further comparison. Hence, the gradual dosing model used by our team here and in previous studies (Laovitthayanggoon et al., 2019) is comparable to the long-term systemic exposure of cobalt through circulating blood in patients in relation to blood cobalt levels, as well as in cobalt myocardial concentrations. Thus, our model is a relevant tool to characterise systemic cobalt toxicity in MoM patients, and more representative than bolus dosage or other *in vivo* modelling techniques used (Madl et al., 2015).

Fig. 19 shows that there is a time-dependent cobalt accumulation trend in most tissues. The increased cobalt content in some control tissues at 7 days cobalt-treatment likely appears as a result of a technical artefact in ICP-MS measurements as previously explained in section 5.2.2 of the Results. These time-dependent trend might indicate that the longer cobalt levels remain elevated in blood, the higher the deposition of cobalt in nearly all organs tested, particularly in heart, liver, kidney, and blood. However, it could be convenient to study more time points in the future to observe the

cumulative capacity of organs, given that patients may live with failed prostheses for years.

To conclude, our *in vivo* rodent model that emulates gradual cobalt release from MoM implants, reproduces cobalt systemic distribution in humans and other animal models, and therefore, the effects observed in rats could be assimilated to a moderate long-term response in MoM patients affected by cobaltism. In addition, cobalt levels were significantly increased in several brain parts at 28 days, although given that the blood cobalt levels are under 100µg/l we only expect subtle or moderate neurotoxicity.

Table 15: Cobalt concentrations of whole blood (WB), brain and heart tissues in our research and another study that mimics gradual cobalt release (Apostoli et al., 2013). The results of cobalt tissue analyses in the cardiac tissue and serum of MoM patients with cobaltism, as well as post-mortem heart tissue from metal-on-polyethylene (MoP) patients, and the Quebec Beer Drinkers (Sullivan et al., 1968). We were unable to obtain the reference (Sullivan et al., 1968), thus the value is quoted from (Paustenbach et al., 2013). Cobalt content values in unexposed human brain (<0.025 µg/g), heart (0.060 µg/g) and blood (<1 µg/l) were obtained from (García et al., 2001), (Wyles et al., 2017) and (Sidaginamale et al., 2013) in that order. The abbreviations are: Trt, Treatment; Ctrl, Control; avg., average.

Studies		Our study	(Apostoli et al., 2013)	(Martin et al., 2015)	(Allen et al., 2014)	(Wyles et al., 2017)	(Sullivan et al., 1968) in (Paustenbach et al., 2013)
Study outline / Tissues		$CoCl_2$ SD rats 28 days 1 mg/kg BW i.p.	$CoCl_2$ rabbits 18 days 1354 µg/ml intravenous	MoM patient	MoM patient	MoP patients	Quebec beer drinkers
WB or serum (µg/l)	Trt	27.15 ± 2.70* (WB)	420.9 ± 154.5 (WB)	192 (serum)	287.6 (serum)	Unknown	Unknown
	Ctrl	0.87 ± 0.00	11.7 ± 2.7	<1			
Brain (µg/g)	Trt	0.058 ± 0.004 * (pref. cortex)	0.2 ± 0.2	Unknown			
	Ctrl	0.015 ± 0.000	0.06 ± 0.04	<0.025			
Heart (µg/g)	Trt	0.341 ± 0.026 *	0.7 ± 0.5	4.75	8.32	0.12 (avg.); range: 0.006-6.299	0.48 ± 0.24
	Ctrl	0.054 ± 0.007	0.07 ± 0.1	0.060			

5.3.3. Moderate transcriptional response to the accumulation of cobalt

Histological investigations of Apostoli *et al.* only showed effects in the cochlea and visual system of rabbits with higher cobalt concentrations in brain and blood that in our model (Table 15) (Apostoli et al., 2013). We have recognised in the previous section that the cobalt treatment used in our study will most likely lead to a weak or moderate effect in the brain unlikely to manifest in histology. Previous Toxicogenomic studies have demonstrated higher sensitivity than histology or clinical chemistry (Joseph, 2017), therefore we expect to observe early toxicological events in the brain through RNA-Seq that could not be monitored with other techniques.

Fig. 21 shows the number of Differentially Expressed Genes (DEGs) ($p<0.05$) in the pref. cortex (3564 up-regulated, 2694 down) and cerebellum (2037 up, 1568 down), which indicates a transcriptional response to Co accumulation from the clinically relevant doses of Co used. The increased number of mRNA transcripts in the pref. cortex and the cerebellum is most likely a consequence of the significant amount of cobalt accumulated in these brain parts. However, most significant DEGs values are under 2-fold change indicating that the doses of cobalt used induced a mild response, which confirms our suspicions. This might be the reason why most patients with low (<20 µg/l) or moderate (<100 µg/l) levels of cobalt do not normally demonstrate any systemic symptoms derived from the circulating cobalt, although there are exceptions (Mao et al., 2011; Tower, 2010). Still, previous toxicogenomic analysis revealed that subtoxic mechanisms maintain the same mechanisms as with toxic doses but with the difference of increased fold-changes and numbers of genes affected (Heinloth et al., 2004), hence our model will be useful to generate hypotheses to further study cobalt toxicity.

5.3.4. Cobalt leads to tissue-specific transcriptional changes in the pref. cortex and cerebellum

In general, genes expressed in the pref. cortex and the cerebellum were very different between them as only 16 hits were found ($|\log_2 \text{Ratio}|$ aka fold change ≥ 2, $p<0.05$). Many of the genes displayed in Table 12 are involved in eye development and ear morphogenesis (e.g., *Cdhr1*, *Six3*, *Isl1* or *Col9a1*). Although the cerebellum and the pref. cortex are not directly involved in the structure of the visual and auditory systems,

many genes and proteins are ubiquitously present throughout the nervous system. The fact that cobalt ions induce transcriptional regulation of non-typical genes over these areas may suggest parallel effects of cobalt in the visual and auditory systems, which could connect back to arthroprosthetic cobaltism symptoms such as retinopathy or bilateral deafness (Catalani et al., 2012). Focusing on genes which could be linked with the cortex and cerebellum associated cognitive features, the Relaxin 1 protein encoded by *Rln1* is suspected to be involved in stress and depression processes (Bathgate et al., 2003), while G protein subunit gamma-7 (Gng7) knockout mice exhibited an accentuated startle response (Schwindinger et al., 2003). Several patients with MoM hip prosthesis have been reported to endure severe depression and anxiety (Green et al., 2017), and the connection of these genes with fear or related behavioural responses could point towards a direct implication of cobalt in these matters.

A few transcription factors (*Hmgn5, Six3* and *Isl1*) in charge of reprograming cell functions and regulating cell fate are also present. Two other genes, *Osgin1* and *Cd163*, are moreover oxidative stress markers (Yao et al., 2008). The protein encoded by *Traf3ip3* is known to activate the c-Jun N-terminal kinase (JNK) signalling system (Zou et al., 2015), and the expression of *Osgin1* is promoted by p53 after DNA damage (Yao et al., 2008). Both processes are involved in apoptosis (Rana, 2008). Therefore, the results shown here could indicate that cobalt generates free radicals that might induce oxidative DNA damage *in vivo* leading to transcriptional regulation of DNA repair or even apoptosis. These results are consistent with a previous study in the cerebrum and cerebellum of Suckling rats under cobalt treatment that demonstrated increased protein and lipid oxidation, in addition to DNA degradation (Garoui et al., 2013). Nevertheless, the genes presented in Table 12 had received limited attention and were poorly annotated in the software. It is possible that future research will uncover important functions for these genes that will help explain cobalt toxicity better.

Even if both cerebellum and pref. cortex are parts of the brain, there is a surprising difference in the genes found under the influence of cobalt ions. This contrast could be rooted to the brain's embryonic development in which the cerebellum emerges from the hindbrain, while the cortex develops from the forebrain area. Comprehensive research has shown that regional gene and protein expression in the cerebellum is markedly distinct from other brain areas such as the cerebral cortex and hippocampus

(Sjöstedt et al., 2020). However, although the majority of genes in the pref. cortex and cerebellum were different, GO enrichment analysis revealed several common GO Molecular Functions terms, e.g. enzyme and anion binding, cytoskeletal protein binding, calmodulin binding, as well as dopamine and glutamate receptor binding (Fig. 23). Thus, while both pref. cortex and cerebellum show little overlap at the individual gene level they share molecular ontology pathways, that is, common molecular changes induced by cobalt could give rise to tissue-specific responses due to the brain regional specialisation.

5.3.5. Cobalt could alter metal homeostasis in the brain

Furthermore, both pref. cortex and cerebellum brain parts have overlapping Molecular Functions terms involved in metal binding and transport (Fig. 23), and these brain parts have the largest number of genes from all GO terms. This suggest that long-term exposure to cobalt could lead to metal dyshomeostasis in the brain. Several studies have demonstrated that metal ion supplementation alters the mineral profile of the brain (Ciavardelli et al., 2012; Zhang et al., 2016), the kidney and liver (He et al., 2016). Although cobalt is also a micronutrient, it is not incorporated into the body as such, but in the form of vitamin B12. Only vitamin B12 and perhaps the protein methionine aminopeptidase require cobalt for their function (Simonsen et al., 2012b). Cobalt has been seen to decrease zinc and magnesium levels in human keratinocytes (Ortega et al., 2009) and zinc in bacteria (Osman et al., 2017), which is alarming given that these ions are the two most common metal ligands (Waldron et al., 2009). In addition, a computational algorithm that predicts cobalt replacement of Mg^{2+} and Mn^{2+} from the protein structure of enzymes has been developed to detect possible targets of cobalt toxicity (Khrustalev et al., 2019). Scharf et al. used immobilised metal ion affinity chromatography (IMAC) to detect cobalt-binding proteins from periprosthetic tissues, and discovered that the metalloproteins likely binding to cobalt were those with native calcium, zinc, iron, magnesium and manganese in that order (Scharf et al., 2014). Moreover, early studies in the Quebec Beer Drinkers also reported high zinc urine excretion (Sullivan et al., 1969), and zinc was also found to be protective of cobalt toxicity in a monocyte cell line *in vitro* (Zhu et al., 2017). We decided to investigate which were the native metal elements of the proteins involved in the metal ion binding GO term and obtained the profiles shown in Fig. 24. The metal binding transcripts

most abundant in our results encode proteins that bind to zinc, calcium, iron and magnesium mainly. Cobalt could thus displace other divalent metal ions leading to toxicity. Another metal-related GO term present in both the pref. cortex and the cerebellum is 'calmodulin binding' (Fig. 23). Calmodulin is a calcium sensor the impact of which goes as far as long-term potentiation in the brain, a necessary step for synaptic plasticity and thus memory formation (Sadiq et al., 2012). In summary, we hypothesise that metal pool imbalances at the molecular level could underlie the specific tissue transcriptional responses induced by cobalt in the rat pref. cortex and cerebellum.

5.3.6. Transporters as the main doors for cellular uptake

Although we hoped to spot specific channels through which cobalt could access the cytoplasm, the high diversity of transporters observed in Fig. 25 implies a homeostatic regulation of channels in the brain. Most of the observed divalent channels in both cerebellum and pref. cortex belonged to established calcium transporters (Fig. 25). The calcium (Ca^{2+}) transport system has already been hypothesised to be the access to the cell for Co^{2+} ions (Simonsen et al., 2012b). The calcium channels in the neuronal plasma membrane which could enable substantial Co^{2+} entry to the intracellular compartment are voltage-gated channels, receptor-operated/ligand-gated channels, store-operated calcium channels and Transient Receptor Potential (TRP) channels (Brini et al., 2014). The genes shown in the results (Fig. 25) can be broadly classified according to these channel types.

Cobalt ions have been used as inorganic blockers of voltage-activated Ca^{2+} channels in several studies (Díaz et al., 2005; Mitterdorfer and Bean, 2002; Schwarz et al., 1990). This block is thought to be due to occupation by cobalt of the intra channel pore site rather than by competition of Co^{2+} with Ca^{2+} ions. The bound ions can flow towards the inside of the cell when this is depolarised (Neumaier et al., 2015). Nevertheless, the rates of Co^{2+} entry by these means have not been defined yet, so the role of voltage-activated Ca^{2+} channels in cobalt-related toxicity is unknown.

It is worth mentioning that cobalt staining is an established imaging technique used to detect the expression of several divalent transporters in cells that stain Co^{2+}-positive.

This technique is not applicable to every divalent transporter. Such is the case for N-methyl-D-Aspartate (NMDA) receptors or voltage-gated calcium channels, which apparently do not allow for the entry of cobalt. It is typically applied to the study of Ca^{2+}-permeable AMPA receptors (CP-GluARs) in neurons, and potentially TRP channels. The inward flow of cobalt into the cell is triggered by either ligand application (e.g. L-glutamate) or changes in pH conditions (Aurousseau et al., 2012).

All the genes encoding the subunits of CP-GluARs (Gria1-4 i.e. AMPA GluA1-GluA4 subunits) are present in our RNA-seq data. However, it is the inclusion of GluA2 subunits within the channels what makes AMPA receptors permeable to Ca^{2+} (Brini et al., 2014), and confirming the presence of CP-GluARs only from the data is unfeasible. Given these conditions, we could hypothesise that certain neuronal cell subpopulations could be more susceptible to the effect of cobalt ions due to higher ionic permeability from these calcium channels. Postsynaptic CP-GluARs have been found in cortical neurons, basal forebrain cholinergic neurons, motor neurons, cerebellar Purkinje neurons, hippocampal neurons (Weiss and Sensi, 2000), an also in several retinal cells (Diamond, 2011) and auditory neurons (Eybalin et al., 2004).

The existence of especially cobalt-pervious channels would explain the selective loss of neuronal cell populations. For example. rabbits treated with high doses of cobalt manifest depletion of ganglion retinal and cochlear hair cells (Apostoli et al., 2013). Impairment of certain cell types could portray symptoms similar to cobaltism phenotypes involving vision and hearing loss, neuropathy, tremors or cognitive decline. On that note, our ability to detect important fold-changes in gene expression and associate them to small cell populations is limited, given that gene expression in RNA-Seq data is averaged with that of many other cells in the CNS. Ideally, if we determine a transporter that renders a cell population susceptible to cobalt, we may be able to block it and rescue cell viability. However, as observed in Fig. 25, several channels could be involved and it is possible that not only one channel allows the passage of cobalt depending on the cell type or tissue being studied (Laovitthayanggoon et al., 2019). We believe this information might be better obtained from research at the single-cell level.

5.3.7. Hypothesis for a modified metalloenzyme activity

Specific metal cofactors are needed for the catalytic activity of several enzymes. In that regard, the cellular environment provides restricted metal pools to avoid competition with non-native metals that could have high affinity for those proteins. There are many examples of incorrect metalation *in vitro*, although very few *in vivo*. The outcome from non-native metal binding to either the primary catalytic site or an alternative site is normally enzyme inactivation (Foster et al., 2014).

The analysis used (Table 13) hoped to expose metalloprotein families the activity of which could be jeopardised by cobalt ions through this mechanism. Two candidate families emerged: phosphodiesterases (PDEs) and carbonic anhydrases (CAs). The first regulates signalling, by hydrolysing cyclic nucleotides (Podda and Grassi, 2014), and the second controls pH homeostasis by hydrating CO_2 to bicarbonate (Lionetto et al., 2016). Both proteins have been observed to interact with metal ions before resulting in inactivation (Fox et al., 1998; Lionetto et al., 2016; Wa, 2001).

Early reports on cobaltism identified that metabolic acidosis seemingly correlated with patient mortality (Alexander, 1972). Pharmacological inactivation of CAs has led to this outcome on occasions (Hoffmanová and Sánchez, 2018). Furthermore, some patients with MoM hips complain about a metallic taste in their mouths (Leikin et al., 2013; Mao et al., 2011). The salivary isoform, CAVI, is known to produce this effect when inhibited (Köhler et al., 2007), although other conditions different from cobalt poisoning can also induce this symptom. In addition, CA is in the list of metalloproteins where the native metal has been replaced by cobalt in periprosthetic tissue (Scharf et al., 2014). Recent studies of CA function in the CNS also expose connections with cognition and memory (Canto de Souza et al., 2017; Yang et al., 2013). The effect of CA modulation in the brain has recently been evaluated with surprising results. While its direct enhancement in the brain improves spatial memory and object recognition in rats, its inhibition affects the consolidation of memory and induces amnesia (Canto de Souza et al., 2017). CA enhancement through drug activators has been recently researched and suggested as a treatment for fear disorders such as anxiety and PTSD as it modules the consolidation of fear memories in certain brain areas (Schmidt et al., 2020). It is understood that astrocytes carry energy metabolites to neurons through lactate when

energy is quickly needed for neuronal activity. Thus, astrocytes collect glucose from the blood vessels and either transform it into pyruvate or glycogen. Pyruvate is further processed into lactate by lactate dehydrogenase (LDH) and then the lactate is shuttled to neurons through monocarboxylate transporters (MCTs). This process is known as the Astrocyte to Neuron Lactate Shuttle or the astrocyte-neuron metabolic coupling, mentioned in section 4.3.2. from Chapter 4. Both the activity of CAs and the sodium bicarbonate cotransporter 1 (NBCe1) are necessary to equilibrate the ionic fluxes of hydrogen (H+), bicarbonate (HCO_3) and CO_2 to equilibrate the proton buffer needed to pump lactate through astrocyte MCTs (Deitmer et al., 2019). Thus, CAs and MCTs are said to form a metabolon, and the disruption of this system might disturb brain areas relying on aerobic glycolysis such as the prefrontal cortex (Vaishnavi et al., 2010).

Concomitant PDE gene expression implicates cAMP and cGMP-dependent pathways. With regard to PDE activity, its systemic inhibition due to high doses of the drug Sildenafil leads to sensorineural hearing loss, tinnitus (Antunes et al., 2013) vision and cardiac abnormalities (Schwarz et al., 2007). PDEs control both cAMP-Protein kinase A (PKA) and cGMP-Protein kinase G (PKG) pathways, which are in turn dependent on CAs (Tresguerres et al., 2011) and nitric oxide (NO) (also expressed; data not shown) (Podda and Grassi, 2014), respectively. The activity of several calcium channels is also controlled by PKA and PKG (Podda and Grassi, 2014). cGMP is also able to modulate AMPA GluA1 and GluA2 receptor subunits and glutaminergic transmission through the glutamate–nitric oxide–cGMP pathway (Cabrera-Pastor et al., 2017), which is ultimately implicated in learning (Cabrera-Pastor et al., 2016) and depression (Gerhard et al., 2016).

Certainly, it is possible that both PDEs and CAs are indirectly regulated through other pathways rather than directly by cobalt. For example, phosphodiesterases might be directly modulated through calmodulin (Sadiq et al., 2012) or adenylyl cyclase, which can, in some way, be regulated by the protein encoded by *Gng7*, found regulated in the RNA-Seq data (Table 12). These proteins are difficult to study because they are located to microdomains (Averaimo and Nicol, 2014).

It can be tempting to suggest that the lack of statistical significance between the genes ΔC_T values as assessed by RT-qPCR (Table 14 and Fig. 29) indicates that these genes might not be as strongly modulated by cobalt as hypothesised. However, we evaluated genes that had subtle transcriptional expression changes in response to cobalt treatment. Given that the response of tissue to mild or moderate interventions is not completely isogenic, it could be argued that the research is statistically underpowered to find significant changes in gene expression through RT-qPCR with the given number of biological replicates per group, n=3. Thus, it is still of interest to proceed investigating the effect of cobalt on PDEs, CARs, and cAMP/cGMP related pathways in future studies that can cover the cost of a sufficient number of samples, or that investigate them on cell lines which are genetically less heterogeneous. In addition, the fold changes obtained through RT-qPCR and RNA-Seq correlate, and the direction of fold change expression is only different for *Car2* in the pref. cortex (Fig. 28). Due to the intrinsic differences between RNA-Seq and RT-qPCR technology platforms, we do not expect both technologies to report the same fold changes for each target. In these comparisons, the correlation of calculated fold changes is used to confirm the concordance of results (Everaert et al., 2017). Thus, RT-qPCR validates the results obtained through RNA-Seq.

5.3.8. Limitations and recommendations for future research

While a time-response to cobalt accumulation is suggested from the data (Fig. 19), we only treated the rodents for 7 and 28-days. Future research would need to increase the number of time-points to confirm our findings. In addition, our longest treatment lasted for 28 days which, relative to the number of years MoM patients wear their prosthesis, can be considered a very short period of time.

It is understood that patients with low cobalt concentrations in blood (<20μg/l) will be unlikely to develop signs of toxicity, and that their reported symptoms are probably related to other conditions. A few studies report finding signs of further deterioration in the brain (Bridges et al., 2020; Clark et al., 2014), visual (Unsworth-Smith et al., 2017) and auditory systems of implant patients (Leyssens et al., 2020). In these papers, the number of patients being investigated is low (n<40), with most patients showing cobalt levels in the lower range, and some had methodology pitfalls. Nonetheless, factors

such as tissue retention could play a role in the development of toxicity in patients. Perhaps patients that maintain low or moderate levels of cobalt for long periods of time could eventually develop toxicity symptoms as cobalt builds up in organs. There are exceptions in the literature in which patients with very high cobalt levels remain asymptomatic (Ho et al., 2017). In the same way, the development of cobalt symptoms might not only depend on blood cobalt levels but also on the duration of exposure and the specific tissue retention. All these factors combined could eventually impact on the cobalt tissue concentration, and perhaps explain symptomatic variability. It is difficult to get a high number of patients with high levels of cobalt and there are many cofounding variables, such as age and gender, which make the design of these studies challenging, thus the concerns over patients with low or moderate levels of cobalt must not be downplayed. Research continuing to study these factors in adequate animal models would help settle public health concerns regarding cobalt toxicity in implant patients. In this regard, this work has focused on cobalt toxicity in the brain, but other studies (Apostoli et al., 2013) have demonstrated earlier damage to visual and vestibular areas. It would be necessary to analyse cobalt effects in these tissues through a model that represents patients with moderate cobalt concentrations to understand the implications for patients with MoM implants.

Additionally, from our RNA-Seq data it appears that cobalt affects metal homeostasis and either competes with or displaces other essential metals but we do not have the technologies to validate this hypothesis fully and identify target proteins in the brain. Other experienced teams in this field could more easily investigate this issue through immobilised metal affinity chromatography (IMAC), a technique able to measure protein affinity through columns loaded with metal ligands (Scharf et al., 2014) or other techniques. Part of this task will be to validate whether cobalt interferes with carbonic anhydrases and phosphodiesterases at different concentrations and how this could affect neuronal function. Moreover, due to its regional location in the brain and its microdomain activity (Averaimo and Nicol, 2014), cyclic nucleotides and the products of carbonic anhydrases need specific equipment to be assessed.

Finally, the interference of cobalt with zinc-modulated enzymes such as PDEs and some phosphatases that are important in immune signaling could perhaps explain the variability of individual responses to cobalt (Maywald et al., 2017).

5.4. Summary of Results

The results presented in this chapter are concerned with the accumulation of cobalt and its effects at two different time points after its systemic circulation through blood in a rodent model (1 mg/kg B.W. $CoCl_2$-treatment, or dH_2O-control group, i.p. dosing for 7 and 28 days). Our research has specifically investigated the toxicity of cobalt in the brain through two molecular techniques, RNA-Seq and RT-qPCR. We obtained the following conclusions:

- A small weight gain difference was found between treated and control rats. However, rats remained healthy and the organs tested did not vary their weight with the treatment used. Thus, cobalt might alter weight gain in treated rats but overall the treatment effect is mild.
- Kidney, liver and heart assimilated the highest amount of cobalt from all the organs tested as measured by ICP-MS.
- Cobalt showed a time-dependent accumulation in several organs, mainly heart, liver, kidney, and blood, and to a lesser extend in spleen and pref. cortex.
- Co content was significantly increased in the pref. cortex, cerebellum, and hippocampus ($p<0.01$, compared with control rats dosed with dH_2O).
- Co levels in blood were significantly elevated and within the range seen in MoM patients: 13.8 ± 2.9 µg/l at 7 days and 27.1±2.7µg/l at 28 days.
- The cobalt organ content and blood accumulation demonstrated here show that the treatment used is clinically relevant, and can be used to model systemic toxicity in MoM patients with low and moderate levels of cobalt in blood (<100µg/l).
- Transcriptional changes in the cortex and cerebellum demonstrate a tissue-specific response likely derived from cobalt accumulation: DEGs in the pref. cortex were 3564 up-regulated, and 2694 down, while in the cerebellum 2037 were up-regulated and 1568 down-regulated (DEGs selected with $p<0.05$).
- GO enrichment analysis of the RNA-Seq transcripts revealed metal ion terms as the most populated term: molecular classification shows a possible common metal homeostasis dysregulation in the pref. cortex and cerebellum due to cobalt interference with other ions.

- DEGs from the most populated functional group ‘metal ion binding’ transcribe for proteins binding to zinc, calcium, and magnesium.
- GO enrichment also revealed that ion channels and transporters that handle calcium and zinc were also significantly regulated in RNA-Seq data. Gene expression of calcium channels may indicate cobalt uptake through this system.
- Finally, investigation into metal ion binding protein families showed that gene expression of zinc binding phosphodiesterase and carbonic anhydrase families was significantly altered, suggesting that Co could modulate cyclic nucleotide signalling and pH balance, respectively. However, the changes in gene expression for individual PDE and CAR targets were not statistically significant, this might be because of the low number of biological replicates (n=3).
- RT-qPCR confirmed the validity of RNA-Seq results since the fold changes obtained with the different technologies followed corresponding expression levels.

6. *IN VIVO* DOSE-RESPONSE INVESTIGATION INTO COBALT TOXICITY

6.1. Introduction

The previous chapter, in which we studied the time-response of cobalt, left some unanswered questions. We evaluated the transcriptional response to cobalt at one time point, 28 days, and in two tissues, the pref. cortex and the cerebellum, but we were unable to identify highly expressed gene markers through RNA-Sequencing (RNA-Seq) that could be linked to the mechanisms of cobalt toxicity. The low number of conditions tested probably limited our ability to filter and identify important genes. However, we obtained valuable information about brain metal homeostasis in response to cobalt and found the PKA/PKG pathway to be possibly altered. In this new chapter, we have decided to widen our transcriptomic research and increase the number of conditions and tissues tested to explore the progression of cobalt toxicity in a dose-response manner.

To better understand the effect of cobalt in the brain, we envisage a more comprehensive transcriptomic analysis following a long-term dose-response to cobalt treatment. To investigate this, we included the hippocampus for RNA-Seq analysis as it is a relevant brain part involved in both memory consolidation, and loss of memory. Cognitive decline complaints are often heard from patients with arthroprosthetic cobaltism (Catalani et al., 2012; Green et al., 2017; Mao et al., 2011; Tower, 2010). Regarding dosage, the highest dose we employed in this study was 1 mg/kg B.W. of $CoCl_2$, which was also the fixed dose used in the previous time-response experiments. Patients display a range of cobalt concentrations in blood, and we expect the dosage range selected for this investigation to translate to patients with low (<20μg/l) to intermediate (<100μg/l) cobalt blood levels. This is the range where most patients are found to be (Langton et al., 2013; Sidaginamale et al., 2016, 2013; van Lingen et al., 2014). Our research interest is not only to understand cobalt toxicity but also to find markers to identify and prevent cobaltism in patients before symptoms occur i.e., patients with lower levels of cobalt. Previous microarray evaluations in the liver revealed similar signatures with other chemicals at both sub-toxic and toxic doses (Heinloth et al., 2004), thus we expect the transcriptional signatures of rats dosed at

lower concentrations of cobalt may reveal mechanisms of cobalt toxicity that also occur in patients with high cobalt concentrations (>100μg/l). The clues seeded by these transcriptomic studies could also assist future research to further explore cobalt toxicity in other tissues and at other concentrations.

In summary, animals were cobalt-treated with three different doses, 0.1, 0.5, 1 mg/kg B.W. $CoCl_2$. Controls were treated with distilled water (dH_2O). S.D. rats were weighed every day during the 28 days treatment period. After being sacrificed, pref. cortex, cerebellum and hippocampus, as well as other organs were dissected, weighed and appropriately processed and stored. Metal content of all organs and brain parts was determined by ICP-MS, while the RNA from the three brain parts was isolated and sent for discovery of DEGs. We carried out RNA-Seq analysis and validated some highly expressed genes through RT-qPCR. Western Blot was used to determine the corresponding protein expression. For more details about these procedures, please refer to the *in vivo* methods section in Chapter 3. In the following section we present the outcomes of these experiments.

6.2. Results

6.2.1. Body weight gain might decline with increasing cobalt doses

Fig. 30 shows the rats' weights during the 28-day treatment with 0.1, 0.5, and 1 mg/kg B.W. $CoCl_2$ or dH_2O in the case of the control. The rats' weight increased constantly for the 4-week treatment period confirming the good health of the animals. Nevertheless, growth trajectories diverged as the treatment progressed. This is even more noticeable after normalisation to initial weights (Fig. 31), where the relative weight of rats in treatment groups differed significantly from that of the control ($p \leq 0.05$). Average growth rates have also been plotted in Fig. 32. Although the growth rate seems to diminish with increasing doses of cobalt, growth rates are not significantly different (Fig. 32). This lack of significance is probably due to within-group variabilities as the groups consist of only n=4 animals each. New studies might be needed to increase the number of animals tested and thus confirm whether or not cobalt affects growth rates.

Rats were also examined daily for changes of behaviour or signs of toxicity. We determined that animals remained healthy and playful with their cage mates. Given that they were fed *ad libitum* it was not possible to detect changes in diet consumption. Yet, it is unlikely that feeding behaviour changes were noticeable since growth rate was still positive and no weight drop in any of the rats was observed during the treatment.

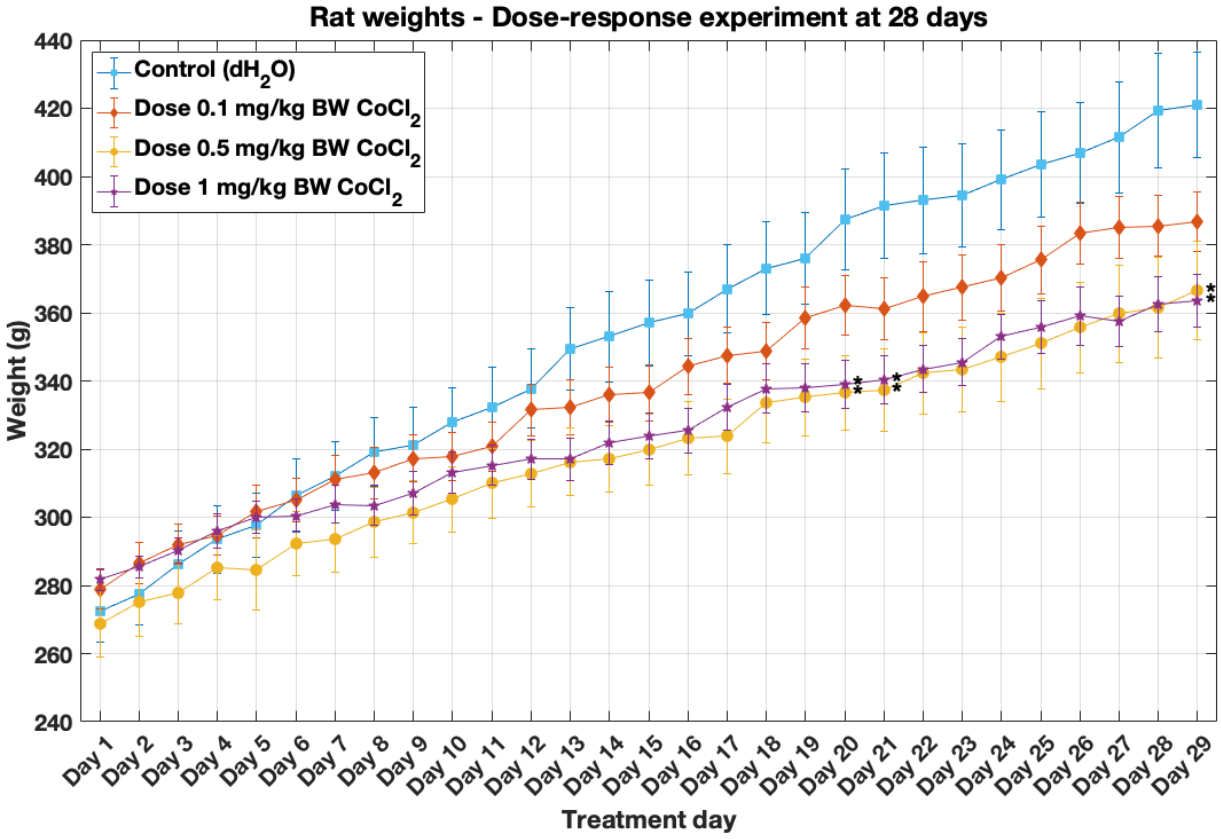

Fig. 30: Male SD rats' weight throughout the 28 days $CoCl_2$ treatment with 0.1, 0.5 or 1 mg/kg B.W. $CoCl_2$ daily i.p. injections. Controls were treated with dH_2O. Data are presented as mean ± SEM and all groups were n=4. Figure legend shows the colours and markers assigned to the groups: squares (control), rhombi (0.1 mg/kg B.W.), circles (0.5 mg/kg B.W.) and stars (1 mg/kg B.W.).

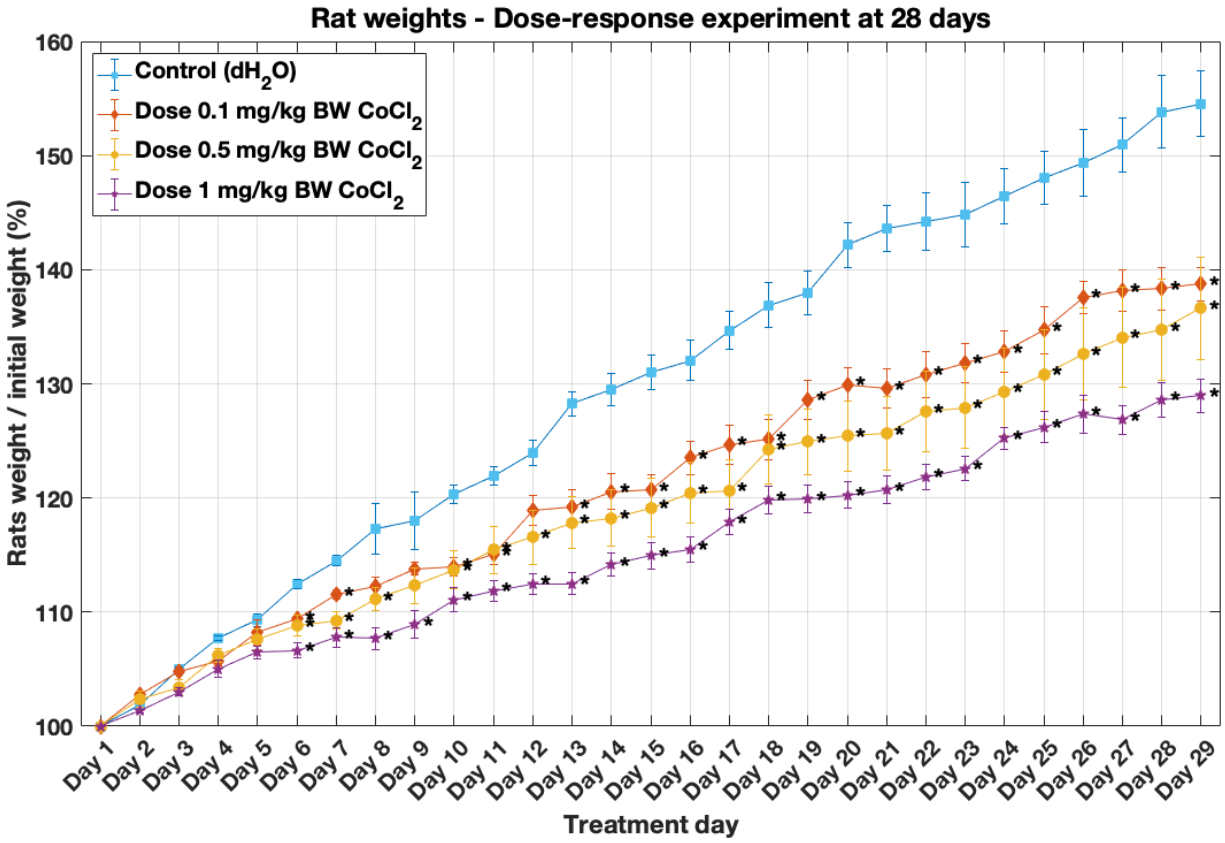

Fig. 31: Body weight percentage normalised to initial weight before the start of the 28-day treatment. Rats were given daily i.p. injections of dH_2O (controls), 0.1, 0.5 and 1 mg/kg B.W. $CoCl_2$ (n=4 in each group). Colours and shapes for the mean values are indicated in the legend: controls are represented by squares, 0.1 mg/kg B.W. by rhombi, 0.5 mg/kg B.W. by circles and 1 mg/kg B.W. by stars. *Significantly different from the control groups at that time-point calculated by two sample t-test ($p \leq 0.05$).

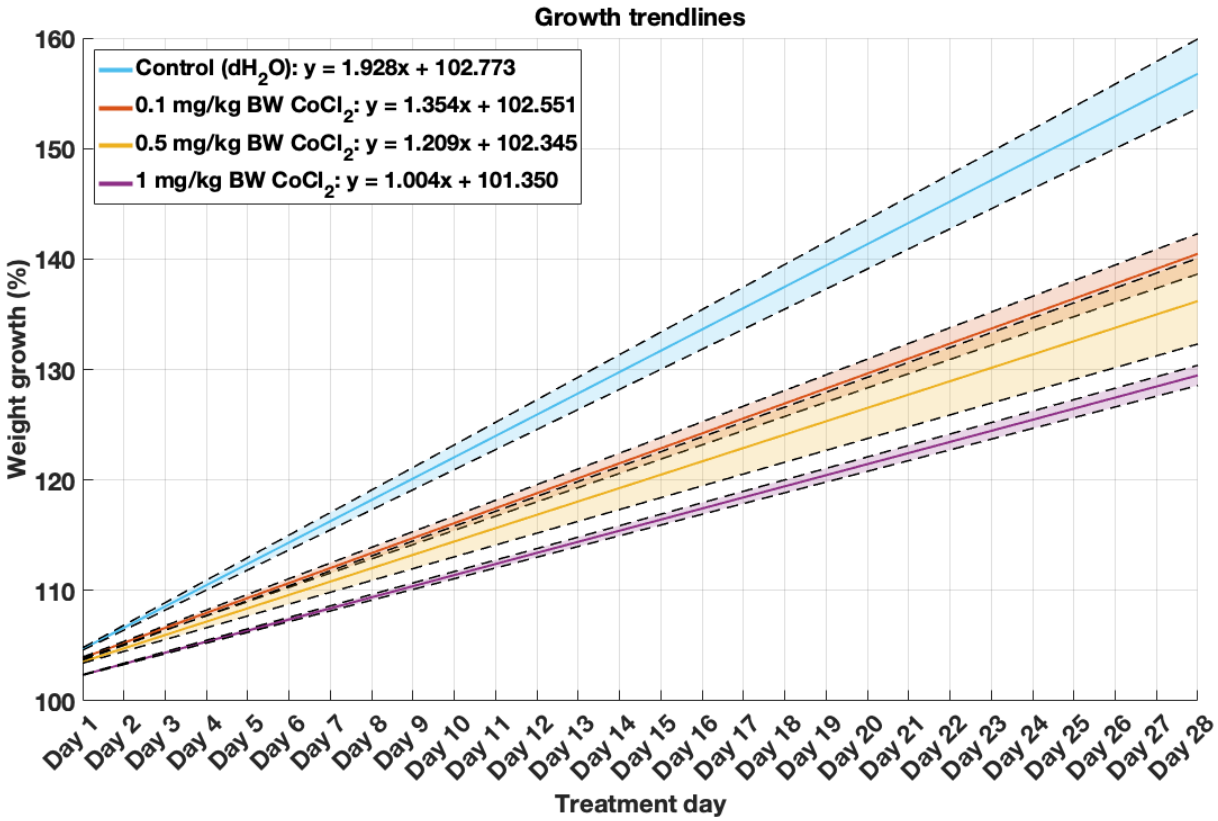

Fig. 32: Average daily growth of control, 0.1 mg/kg B.W., 0.5 mg/kg B.W. and 1 mg/kg B.W. $CoCl_2$ treated rats. Animals were dosed daily with i.p. injections for 28 days. Solid lines show the mean growth rate in blue for the control, red for 0.1 mg/kg B.W., yellow for 0.5 mg/kg B.W. and purple for 1 mg/kg B.W. $CoCl_2$. Lower and upper dotted lines represent the 25th and the 75th percentiles respectively. The growth rates were not found to be significantly different to each other by ANOVA test ($p<.05$). The graph was plotted with the help of MATLAB *plot_ci.m* function.

6.2.2. Organ weight ratios do not change with cobalt dosage

In addition to recording rats' weights daily, the weights of the main organs were also recorded post-mortem as a way to evaluate the health of the animals. Fig. 33 displays the organs' weight ratio by dosage group. The organ weights to body weight ratio of treated rats were not significantly reduced or increased as compared with the controls ($p \leq 0.05$).

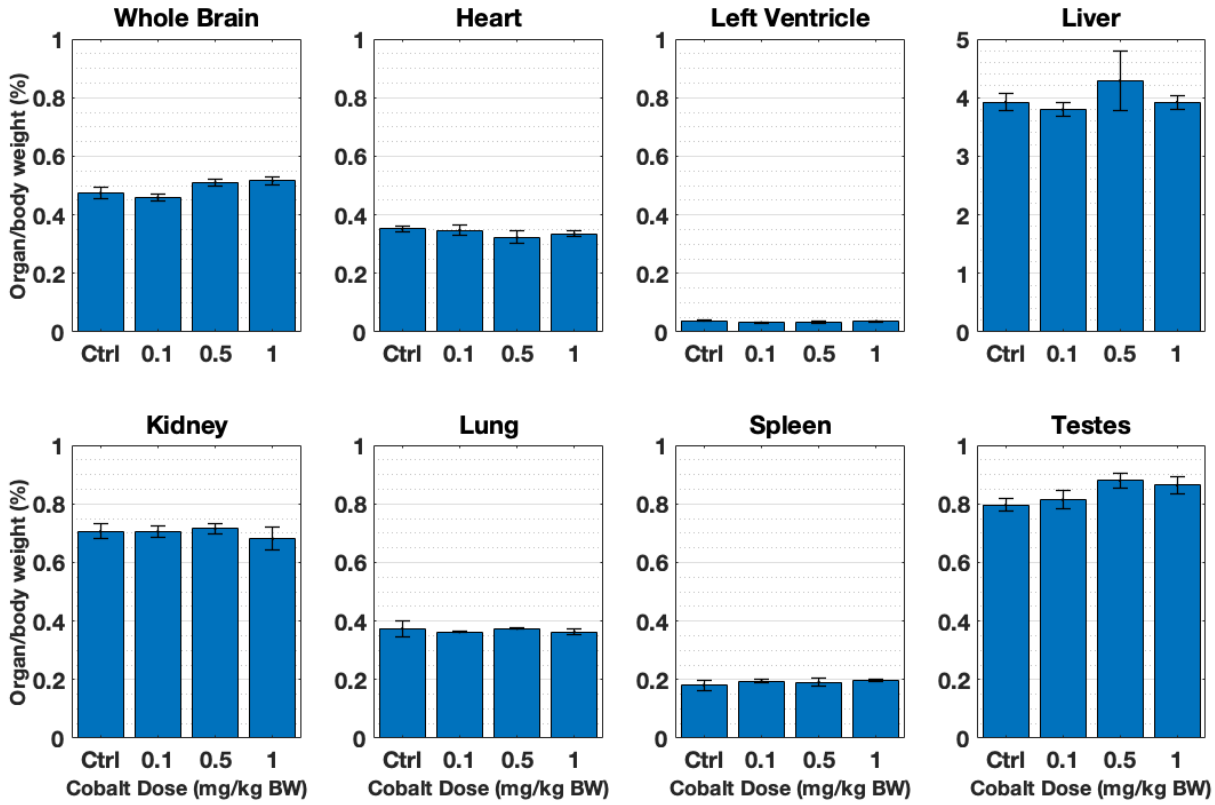

Fig. 33: Relative organ weight to final rat body weight (%) of $CoCl_2$ (0.1, 0.5 and 1 mg/kg B.W.) and dH_2O treated groups. Organs shown are whole brain, heart, left ventricle, liver, kidney, lung, spleen and testes. Rats were given i.p. injections with corresponding daily cobalt doses for 28 days (n=4). No significant differences between relative organ weights were detected with ANOVA statistical test ($p<.05$) between treatment groups.

6.2.3. Cobalt organ content increases significantly with higher doses of cobalt

Table 16 and Table 17 show the cobalt content values detected by ICP-MS in all organs. This metal content analysis revealed an incremental accumulation of cobalt concentrations in tissues with increased doses (Fig. 34). Thus, there is a dose-response accumulation of cobalt, which was significant after 0.5 mg/kg B.W. $CoCl_2$ in most tissues. Kidney, liver, and heart in that order accumulated most cobalt (Fig. 34 and Table 16). The pref. cortex and hippocampus also accumulated significant levels of cobalt ($p<0.01$; Fig. 35 and Table 17).

We also noticed the same issue described in section 5.2.2. of Chapter 5 with regards to the offset in the control samples, which are closer to the detection limit of the ICP-MS

due to their low cobalt content. This effect becomes obvious in the case of the cerebellum control group (Fig. 35). There is also a larger standard error (SEM) in the control groups of lung and spleen (Fig. 34). No tissues show significant differences at 0.1 mg/kg B.W. $CoCl_2$ dosage ($p<0.05$), which could be due to simply the low dosage not being enough for cobalt to significantly accumulate in tissues, or also due to detection thresholds and instability at lower concentrations.

Blood cobalt concentration is higher than in the section 5.2.2. from the previous chapter using the same dosage: 1 mg/kg B.W. $CoCl_2$ of daily i.p. injections for 28 days. In the time-response experiment presented in the last chapter the cobalt blood level of the control group after 28-day treatment with dH_2O was 0.9± 0.0 µg/l, while in the currently discussed dose-response experiment the level was 1.2±0.3 µg/l. With regards to the cobalt in blood after 28-day treatment with 1mg/kg B.W. the level was 27.1± 2.7 µg/l in the time-response experiment, while it is 38.2± 2.1 µg/l in the dose-response experiment. A potential reason for this maybe that, in contrast with the time-response experiment, the ICP-MS internal standard element had to be changed from scandium (Sc) to indium (In) because of calibration problems. Thus, comparisons between these metal content results and those of the previous chapter should be done with care. Finally, organs were not perfused, thus the cobalt content of organs such as heart, liver, kidney and brain could be compounded with that of the blood level. The latter is true for both time and dose-response cobalt accumulation experiments with ICP-MS.

Table 16: ICP-MS cobalt analyses of heart, liver, kidney, lung, spleen, testes, and blood. Cobalt content units are ng/g, except for blood cobalt levels where they are expressed as µg/l. Data are shown as mean ± SEM of n=4 samples from controls, 0.1, 0.5, and 1 mg/kg B.W. $CoCl_2$ treated groups. Blood from control group shows only n=3. Rats were treated with a daily dose during 28 days, and dH_2O was used for the controls. * significant difference between control and treatment groups tested by one-way ANOVA ($p \leq 0.05$).

Duration	28 days cobalt content (ng/g)			
Treatment	Control	0.1 mg/kg B.W.	0.5 mg/kg B.W.	1 mg/kg B.W.
Heart	85.8 ± 8.5	134.6 ± 19.5	302.4 ± 57.5*	443.6 ± 61.5*
Liver	175.1 ± 14.3	277.8 ± 22.8	697.8 ± 85.7*	1103.5 ± 128.4*
Kidney	270.3 ± 25.6	378.5 ± 46.3	974.4 ± 131.4*	1464.8 ± 96.4*
Lung	65.0 ± 30.4	56.1 ± 11.2	104.5 ± 6.3	138.3 ± 5.1*
Spleen	58.0 ± 25.3	75.1 ± 9.0	162.1 ± 18.7*	275.2 ± 38.3*
Testes	10.3 ± 3.2	28.3 ± 15.2	41.6 ± 7.1	65.6 ± 9.4*
	28 days cobalt content (µg/l)			
Blood	1.2± 0.3	4.4 ± 0.9	17.0 ± 2.8*	38.2 ± 2.1*

Table 17: Cobalt brain content of the pref. cortex, cerebellum, and hippocampus (ng/g) from ICP-MS metal content analyses. Data are presented as mean ± SEM (n=4). S.D. male rats were treated during 28 days with daily i.p. injections of dH_2O (control group), or 0.1, 0.5, and 1 mg/kg B.W. $CoCl_2$. * significantly different from control group by one-way ANOVA statistical test ($p<0.01$).

Duration	28 days cobalt content (ng/g)			
Treatment	Control	0.1 mg/kg B.W.	0.5 mg/kg B.W.	1 mg/kg B.W.
Pref. cortex	11.2 ± 0.8	16.2 ± 2.1	55.0 ± 4.1*	70.6 ± 7.3*
Cerebellum	20.9 ± 7.8	16.5 ± 6.1	28.2 ± 3.9	33.5 ± 2.8
Hippocampus	8.0 ± 1.9	8.1 ± 2.9	30.4 ± 6.5*	54.1 ± 3.6*

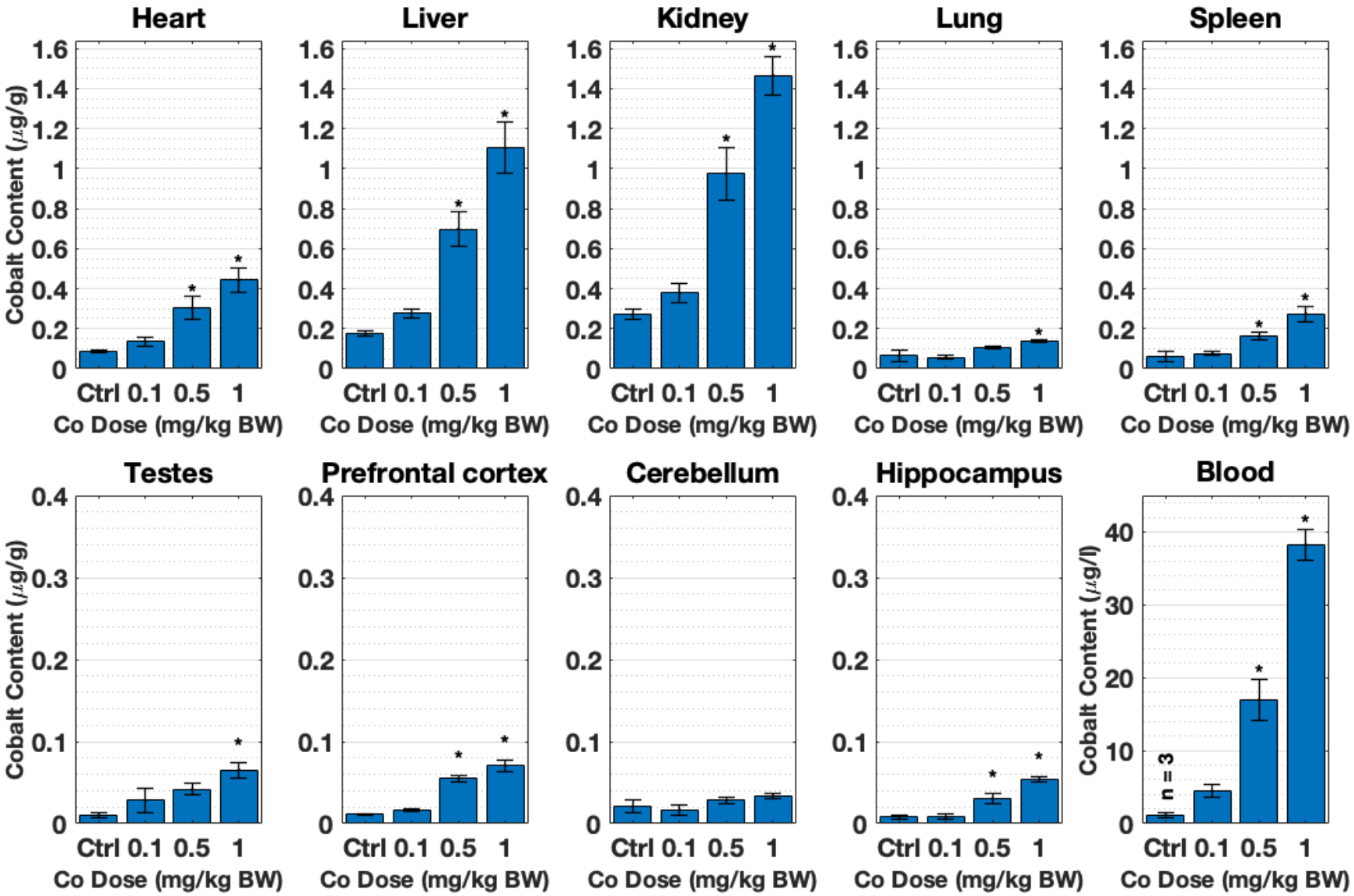
Heart
Liver
Kidney
Lung
Spleen
Testes
Prefrontal cortex
Cerebellum
Hippocampus
Blood
Cobalt Content (μg/g)
Cobalt Content (μg/l)
Ctrl 0.1 0.5 1
Co Dose (mg/kg BW)
n = 3

Fig. 34: Organ cobalt content (µg/g, tissue; µg/l, blood) obtained after tissue and blood collection through ICP-MS. SD male rats were treated with dH_2O (control group) or different doses of $CoCl_2$: 0.1, 0.5, and 1 mg/kg B.W. Animals were dosed daily with i.p. injections during 28 days. Each group presents mean ± SEM from n=4 rats, and * shows significantly different control and treatment means as tested by one-way ANOVA ($p \leq 0.05$).

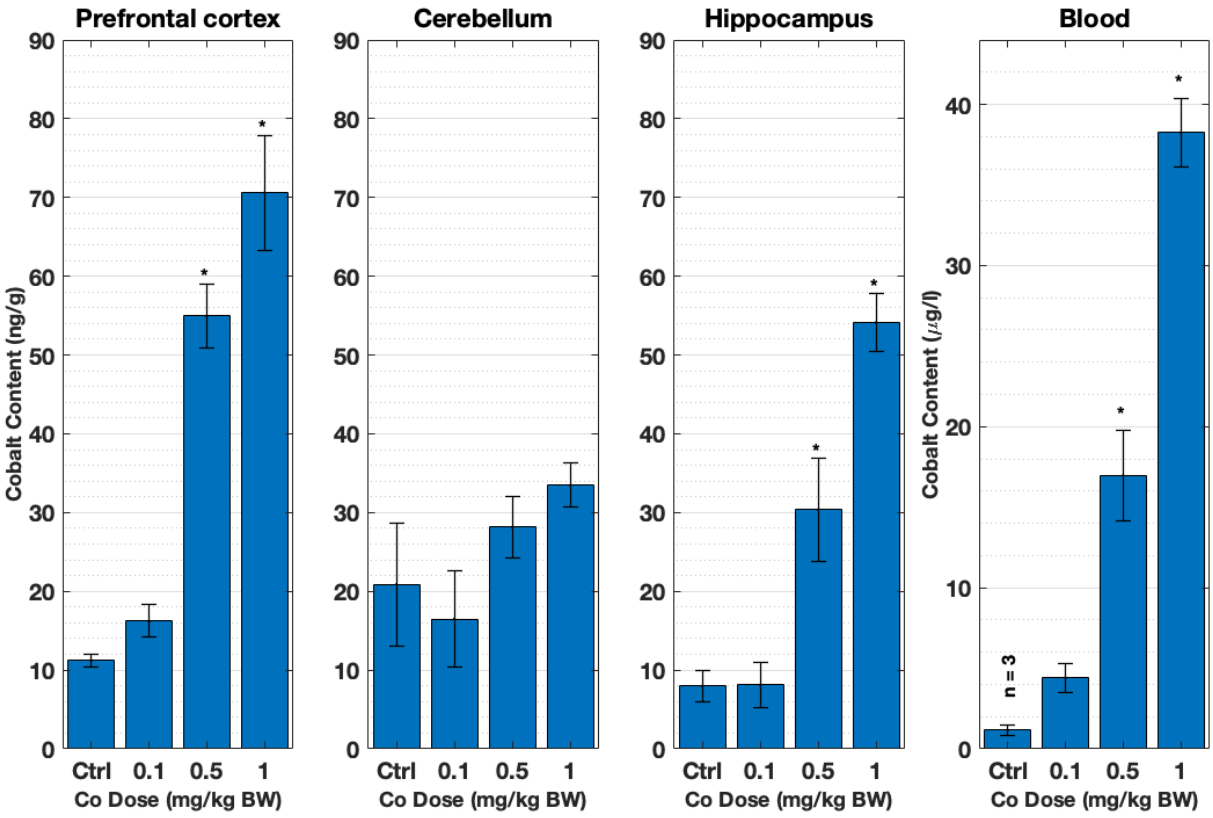

Fig. 35: Cobalt content of blood (μg/l) and separate brain areas (ng/g), pref. cortex, cerebellum and hippocampus, after 28 days of daily i.p. treatment with dH_2O, 0.1, 0.5, and 1 mg/kg B.W. $CoCl_2$. Figure shows mean ± SEM of n=4 per group, with * displaying statistical differences between control and treatment groups by one-way ANOVA analysis ($p<0.01$).

6.2.4. The transcriptional response to the cobalt doses selected is non-proportional

The cobalt tissue content measured through ICP-MS determined that the pref. cortex and hippocampus of 0.5 and 1 mg/kg BW $CoCl_2$-treated groups had significantly greater accumulated cobalt compared to their control groups (Fig. 35). Initially, we considered whether to analyse the transcriptome only brain areas from treated animals that had statistically significant levels of cobalt as obtained through ICP-MS. Nevertheless, RNA-Seq is a very sensitive technique that can outperform typical toxicology end-points (Joseph, 2017), and detect transcriptional changes in weakly treated samples (Wang et al., 2014). Thus, we also included brain tissues from the lower dose, 0.1 mg/kg B.W. $CoCl_2$, and carried out the RNA-Seq analysis of the three

cobalt treatments: 0.1, 0.5 and 1 mg/kg B.W. $CoCl_2$. To evaluate whether the incremental dose cobalt treatment resulted in a progressive transcriptomic response, the number of genes and the magnitude of gene expression were plotted for each dose in Fig. 36 and Fig. 37 respectively (DEGs $p<0.5$). Although the number of DEGs increased from 0.1 mg/kg B.W. $CoCl_2$ to the other two doses (0.5 and 1 mg/kg B.W. $CoCl_2$), there is no clear dose response in terms of the number of DEGs in pref. cortex and hippocampus (Fig. 36). Thus, perhaps the two higher doses (0.5 and 1 mg/kg B.W. $CoCl_2$) produce analogous responses in the brain since the amount of accumulated cobalt is similar in contrast to the differences between these two doses in other tissues such as liver, kidney or blood as can be observed in Fig. 34. The cerebellum, however, shows the number of DEGs to be directly proportional to the dose used (Fig. 36). Still, the fold change of the DEGs is in general very low. Fig. 37 shows the DEGs fold change distribution through boxplots, the median of which, as well as the 25^{th} and 75^{th} percentile, are close to zero both for up- and down-regulated genes. DEGs with higher fold-change (approx. > 1) are displayed as outliers for all tissues and doses. Thus, cobalt probably elicits a mild response at the concentrations used in this experiment.

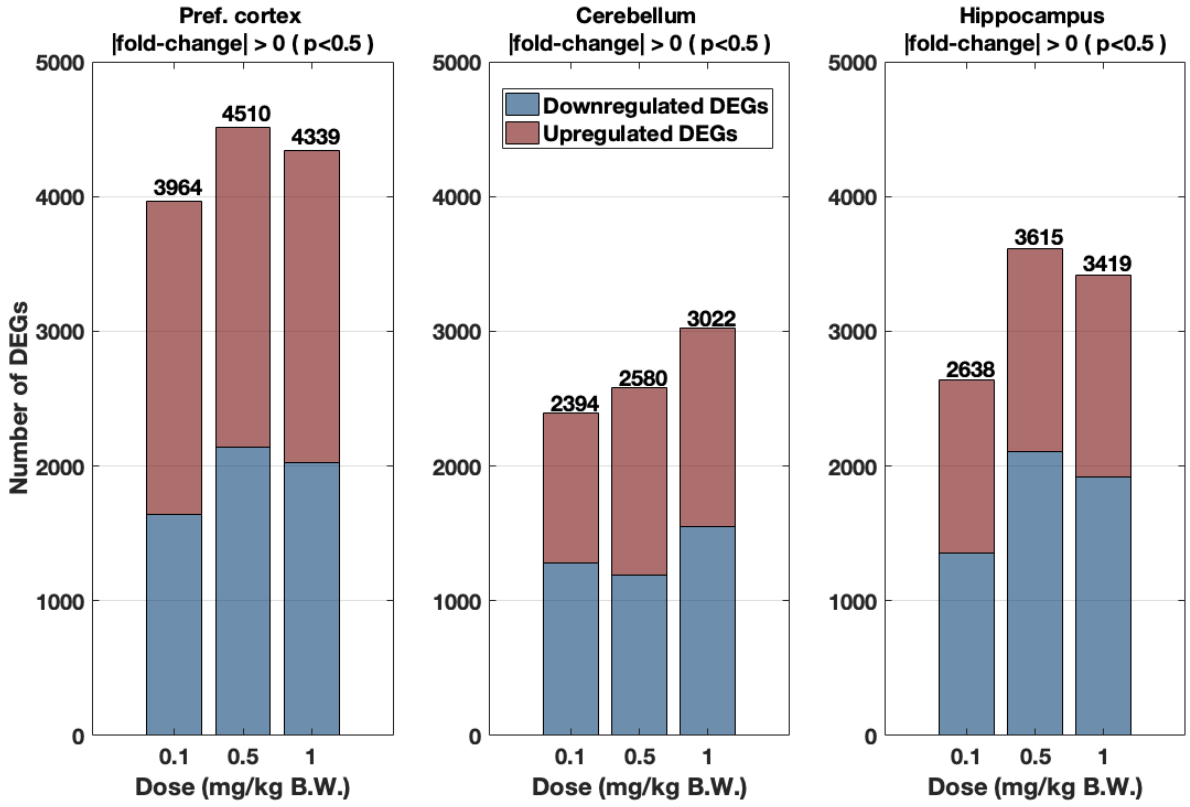

Fig. 36: Number of up-regulated (red) and down-regulated (blue) DEGs in pref. cortex, cerebellum and hippocampus according to cobalt dose treatment: 0.1, 0.5 and 1 mg/kg B.W. $CoCl_2$. Animals were dosed i.p. daily, for 28 days with the mentioned doses or dH_2O (controls). Data were extracted from RNA-Seq experiments in which n=4 samples were pooled to get n'=1, except in the case of the hippocampus treatment group 0.5 mg/kg B.W. $CoCl_2$ where n'=n=3, as well as for 1 mg/kg B.W. $CoCl_2$ where n'=n=1. Conditions imposed in the RNA-Seq data were p<0.5.

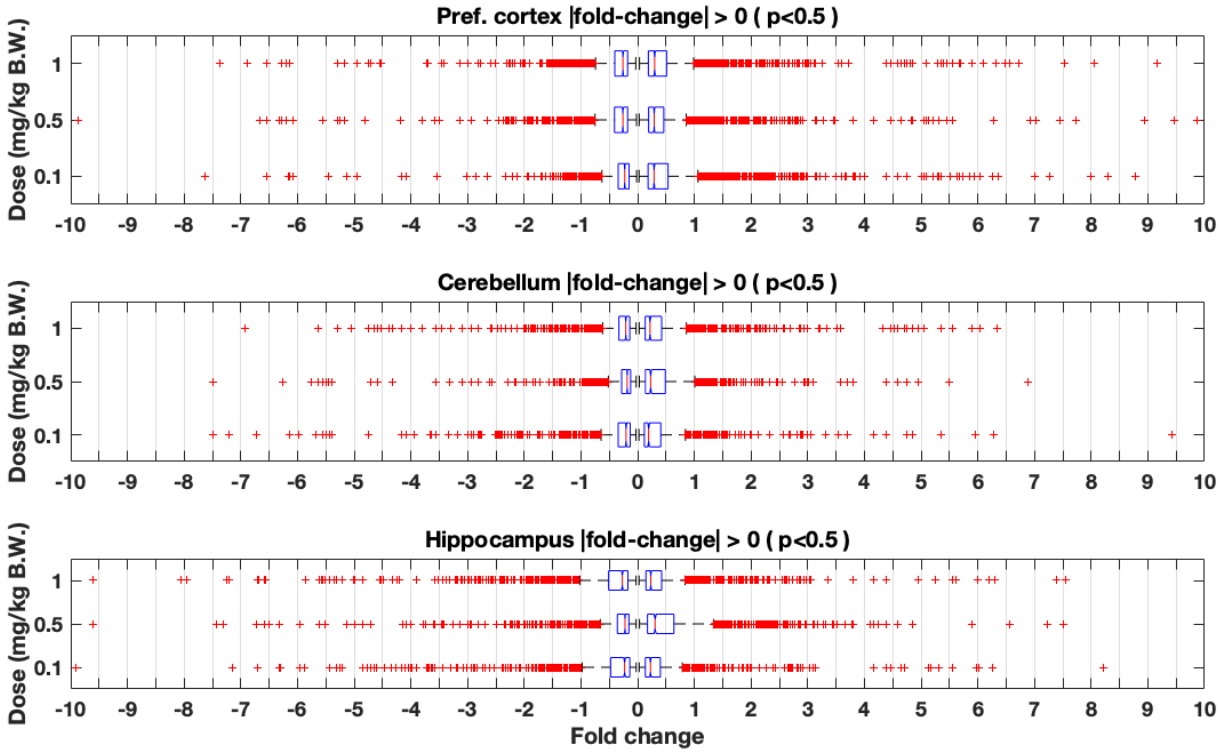

Fig. 37: Fold-change distribution (logarithmic) of DEGs in the pref. cortex, cerebellum and hippocampus. Rats were treated during 28 days with i.p. injections of dH_2O (control group), 0.1, 0.5 or 1 mg/kg B.W. $CoCl_2$. Data show DEGs fold changes of treatment groups compared against the control group (n'=1 from n=4 pooled samples; except for hippocampus 0.5 mg/kg B.W. $CoCl_2$ with only n'=n=3, and hippocampus 1 mg/kg B.W. $CoCl_2$ with n'=n=1). RNA-Seq data shown in the figure were filtered to obtain only DEGS with p-value<0.5. Boxplots were drawn with MATLAB displaying the median (red line) in between the 25th and 75th percentiles (blue edge enclosure) and 1.5x interquartile range (dashed black lines) after which DEGs were categorised as outliers (red crosses).

Fig. 38 shows the Venn diagram of DEGs found in pref. cortex, cerebellum, and hippocampus (p<0.05). The diagram intersections display common DEGs between groups, with pref. cortex and hippocampus demonstrating a higher number of common genes than the cerebellum for every dose. Although the number of overlapping genes between brain areas indicate that the hippocampus, cerebellum, and pref. cortex are all part of the same tissue, i.e. the brain, the different DEGs also point towards highly regionalised areas with specific functions. This was briefly discussed in section 5.3.4. from Chapter 5. It can also be appreciated that the doses 0.5 and 1 mg/kg B.W. $CoCl_2$ alter the expression of more common and tissue-specific genes than the 0.1 mg/kg

B.W. $CoCl_2$ dose, thus indicating a stronger impact of cobalt at elevated concentrations. However, there are little differences in the number of common genes between 0.5 and 1 mg/kg B.W. $CoCl_2$ dosages.

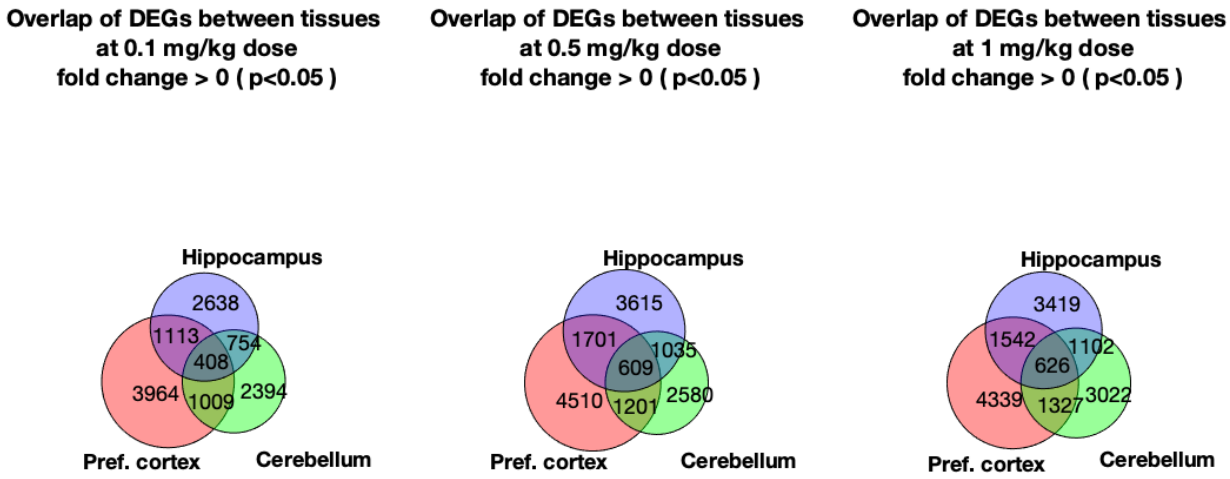

Fig. 38: Venn diagrams showing the number of overlapping DEGs between pref. cortex, cerebellum and hippocampus at the different cobalt treatment doses: 0.1, 0.5 and 1 mg/kg B.W. $CoCl_2$. Rats were treated by daily i.p. injection for 28 days. DEGs were obtained through RNA-Seq by comparing brain parts mRNA abundance of treatment groups against controls (dH_2O-treated). Diagrams were plotted using the MATLAB *venn.m* function.

To further explore the effects on gene expression according to the dosage, we performed the hierarchical clustering of common DEGs for all brain parts analysed as shown in Fig. 39 and Fig. 40. Fig. 39 displays common genes whose fold-change are over 2 and with $p<0.05$. However, only two genes comply with these conditions: membrane bound O-acyltransferase domain containing 7-like 1 (*Mboat7l1*) and transthyretin (*Ttr*). Yet, neither of them present a dose-response pattern. Moreover, two genes would not be representative of the dataset. Given that the number of common tissue genes fulfilling the criteria $p<0.05$ is too large for the software to process and analyse, we opted to remove the significance condition and produce the hierarchical clustering of DEGs over 2-fold change with no p-value considered. The resulting heatmap with common tissue DEGs over 2-fold is presented in Fig. 40. The number of up-regulated and down-regulated DEGs is presented in Appendix E.

The clustering from Fig. 40 shows that brain parts are consistently clustered together independently of the dose treatment group. Nevertheless, the doses used do not have the same organisation pattern within the brain parts, which reinforces the idea that the transcripts generated do not follow a dose-response in terms of their fold change. We could not identify an independent set of DEGs that followed a dose-response fold change in Fig. 40. Thus, we can conclude that the number and range of the doses used does not prompt a dose-response. This does not mean that the transcriptional response elicited is not relevant. Table 18 displays the result of the Gene Ontology enrichment analysis performed by Cytoscape software on the common DEGs shown in Fig. 40 (DEGs over 2-fold change from the three brain tissues with no p-value threshold considered). GO terms obtained from Biological Process (BP GOs) and KEGG ontologies of these common genes indicate that terms affected by cobalt are steroid hormone synthesis, bile and renin secretion, and response growth hormone among others. These terms could be related or fall under the umbrella of the activity of UDP-glucuronosyltransferases (UGTs) or sulfotransferases as outlined by the components of ‘transferase activity, transferring sulfur-containing groups’ Molecular Function (MF) GO term and ‘Steroid hormone biosynthesis’ KEGG terms. Glucuronidation and sulfonation processes are implicated in the clearance and transport of bile acids, thyroid and steroid hormones, as well as exogenous compounds such as drugs and xenobiotics.

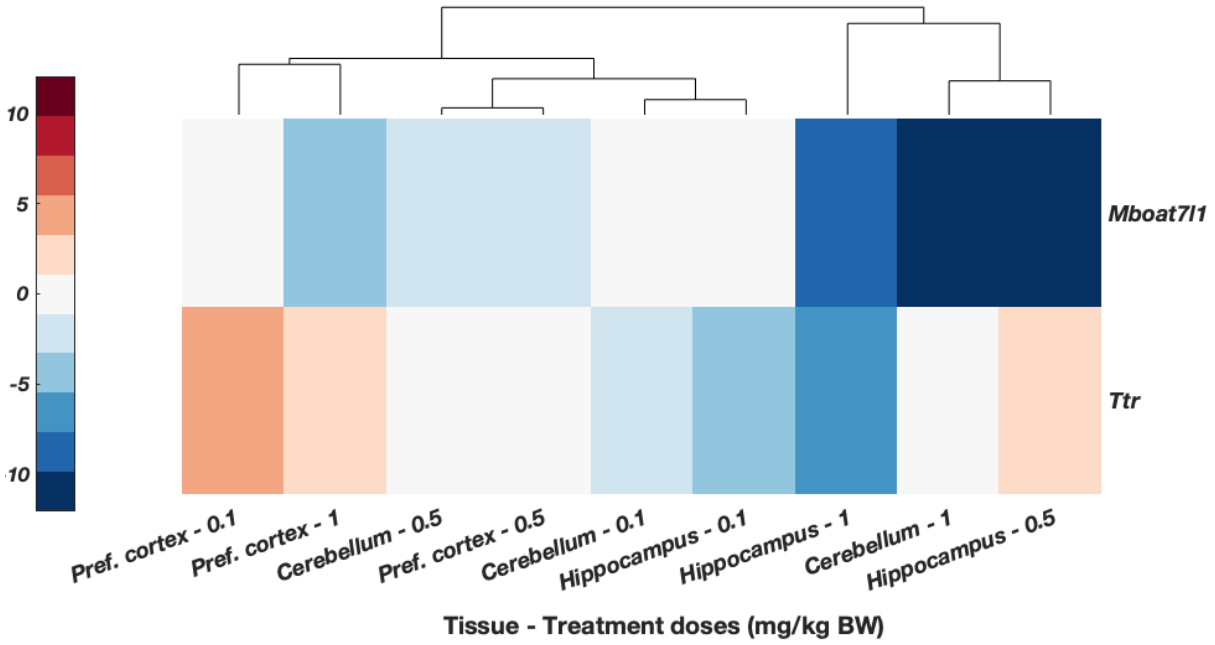

Fig. 39: Hierarchical clustering of DEGs obtained from RNA-Seq comparison of cobalt-treated groups (0.1, 0.5, and 1 mg/kg B.W. $CoCl_2$) against controls (dH_2O). S.D. male rats were treated for 28 days with daily i.p. injections. Tissues whose DEGs are displayed are pref. cortex, cerebellum and hippocampus. DEGs shown are common across tissues, have fold-changes over 2 and p<.05. Dendrogram heights represent the Euclidean distance between pairs of DEGs. Dendrogram connects tissues with similar gene expression patterns, although in this case only two genes gather these conditions and classification is unlikely to be representative. The graph was obtained with MATLAB clustergram.m function. Colour bar displays fold change of upregulated (red) and downregulated (blue) DEGs. One pooled sample was analysed per group (n'=1) from n=4 in all groups with the exception of hippocampus treatment group 0.5 mg/kg B.W. $CoCl_2$ with n=3 pooled samples, and 1 mg/kg B.W. $CoCl_2$ with n=n'=1.

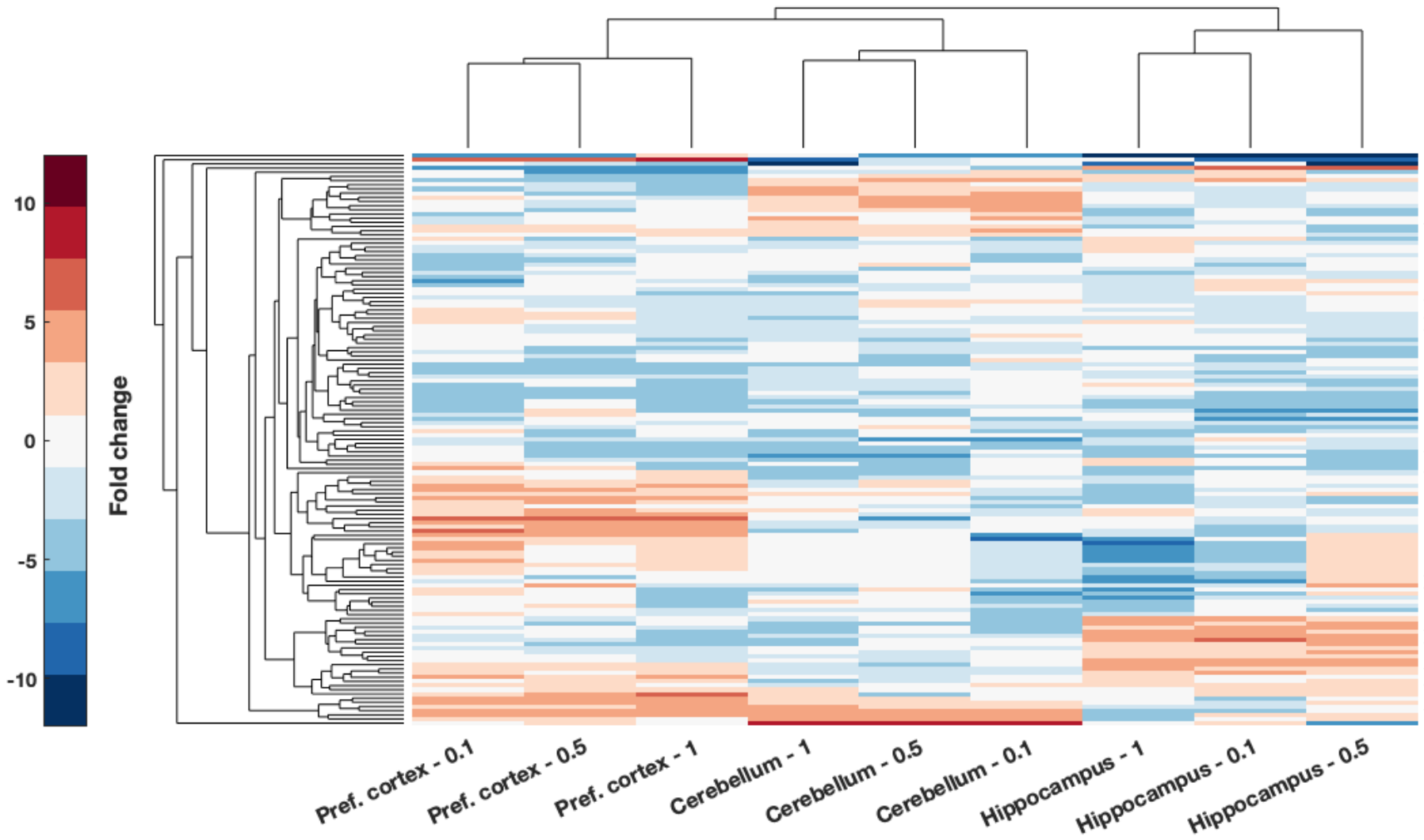
10
5
0
-5
-10
Fold change
Pref. cortex - 0.1
Pref. cortex - 0.5
Pref. cortex - 1
Cerebellum - 1
Cerebellum - 0.5
Cerebellum - 0.1
Hippocampus - 1
Hippocampus - 0.1
Hippocampus - 0.5

Fig. 40: Hierarchical clustering of DEGs over 2-fold-change (no significance considered) from RNA-Seq data obtained from the comparison of pref. cortex, cerebellum and hippocampus of rats treated with three concentrations of cobalt against those of controls treated with dH_2O. RNA was isolated from brain tissues of S.D. male rats treated with daily i.p. injections for 28 days with different concentrations of cobalt: 0.1, 0.5 and 1 mg/kg B.W. $CoCl_2$. Samples analysed in each group were pooled (n'=1) from n=4, except in the case of the hippocampus of rats treated with 0.5 mg/kg B.W. $CoCl_2$, n=3, and 1 mg/kg B.W. $CoCl_2$, n=1. Dendrogram heights display the Euclidian distance between DEGs pairs, and colour bar shows the fold change. Graph plotted with MATLAB *clustergram.m* function.

Table 18: Gene Ontology (GO) enrichment of DEGs obtained from RNA-Seq analysis of the pref. cortex, cerebellum and hippocampus of rats treated with i.p. injections of 0.1, 0.5 or 1 mg/kg B.W. $CoCl_2$ during 28 days. Controls were treated with dH_2O. DEGs analysed were common genes among tissues compared over 2-fold (no significance level imposed). GO databases employed for enrichment were Molecular Function (MF; 08/04/2016), Biological Process (BP; 08/04/2016), Cellular Component (CC; 08/04/2016) and Kyoto Encyclopedia of Genes and Genomes (KEGG) (14/06/2016) ontologies.

Gene Ontologies (GO) and GO terms	# genes with annotations in the ontology (%)	# genes represented in GO Terms (%)
Biological Process (BP) GO terms	96 (74.42%)	26 (20.16%)
hormone metabolic process	*Afp, Cyp17a1, Gh1, Ghrhr, Nt5c1b, Rbp2, Sult1e1, Ttr*	
response to growth hormone	*Fga, Orm1, Ugt2b17*	
secretion by tissue	*Agr2, Aqp1, Ghrhr, Slc4a5*	
response to retinoic acid	*Aqp1, Cyp17a1, Cyp2c7, Lefty1, Orm1*	
digestive system process	*Aqp1, Fabp1, Slco1a5, Vsig1*	
modified amino acid transport	*Folr1, Slc7a9, Slco1a5, Ttr*	
metanephric epithelium development	*Adipoq, Aqp1, Cxcr2*	
Molecular Function (MF) GO terms	95 (73.64%)	6 (4.65%)
transferase activity, transferring sulfur-containing groups	*Chst13, Sult1c3, Sult1e1*	
steroid hydroxylase activity	*Cyp17a1, Cyp2c7, Cyp3a23/3a1*	
KEGG terms	51 (39.53%)	14 (10.85%)
Steroid hormone biosynthesis	*Cyp17a1, Cyp2c7, Cyp3a23/3a1, Sult1e1, Ugt1a8, Ugt2b17*	
Bile secretion	*Aqp1, Slc22a7, Slc4a5, Slco1a5*	
Renin secretion	*Aqp1, Clca4, Ppp3r2*	
B cell receptor signaling pathway	*Cd72, Pirb, Ppp3r2*	
Cellular Component terms	106 (82.17%)	4 (3.1%)
brush border membrane	*Aqp1, Folr1, Slc7a9, Slco1a5*	

We also evaluated the transcriptional response of tissues with significant metal content accumulation. According to our results from the ICP-MS analyses these tissues are the pref. cortex and hippocampus of rats dosed with 0.5 and 1 mg/kg B.W. $CoCl_2$ (Fig. 35). Significant DEGs over 2-fold are shown in Fig. 41. Only the genes *Hmgn5*, *Mboat7l1*, *Crnkl1*, *Ly6g6e*, and *Tfap2c* were displayed, therefore we decided to analyse those DEGs expressed over 2-fold without regard for significance levels (no p-value threshold considered). The result of this hierarchical clustering is displayed in Fig. 42. We generated the gene enrichment analysis of these genes with Cytoscape displayed in Table 19 and found several GO terms of importance involved in immunity, and hormone activity similar to those found in Table 18. In addition, the protein-protein interaction (PPI) of DEGs-protein products was created through the STRING webpage (https://string-db.org/) to observe the possible links between the overlapped DEGs (Fig. 43). We can clearly observe the immune axis centered around Interleukin-6 (IL6) separated from other clusters such as related to growth factors and hormone activity, as well as some glucuronosyltransferases, specifically UGT enzymes that are involved in glucuronidation. Other cluster of interest reflected on the PPI is the Glycosylphosphatidylinositol (GPI) anchor biosynthesis.

Additionally, we also analysed the list of pref. cortex and hippocampus DEGs over 2-fold from rats dosed with 0.5 and 1 mg/kg B.W. $CoCl_2$ (Fig. 42) with PathView (https://pathview.uncc.edu/), an online software that allowed us to map the genes of interest over KEGG pathways (Habermann et al., 2015). The "rno00140 Steroid hormone biosynthesis" and "rno04640 Hematopoietic cell lineage" pathways were significantly enriched, and both had corresponding GO terms as obtained by Cytoscape software in Table 19. We added the resulting mapped KEGG pathways to the Appendix D. Four DEGs were emphasised in the mapping of the steroid hormone biosynthesis pathway (Fig. 56 displayed in Appendix D): *Cyp11a1*, *Cyp17a1*, *Cyp3a23/3a1*, and *Ugt1a1*. With regards to the haematopoietic cell lineage pathway the following genes were observed in Fig. 57 displayed in Appendix D: *Cd19*, *Fcer2*, *Cd8a*, *Cd3g*, *Il1r2* and *Il6*.

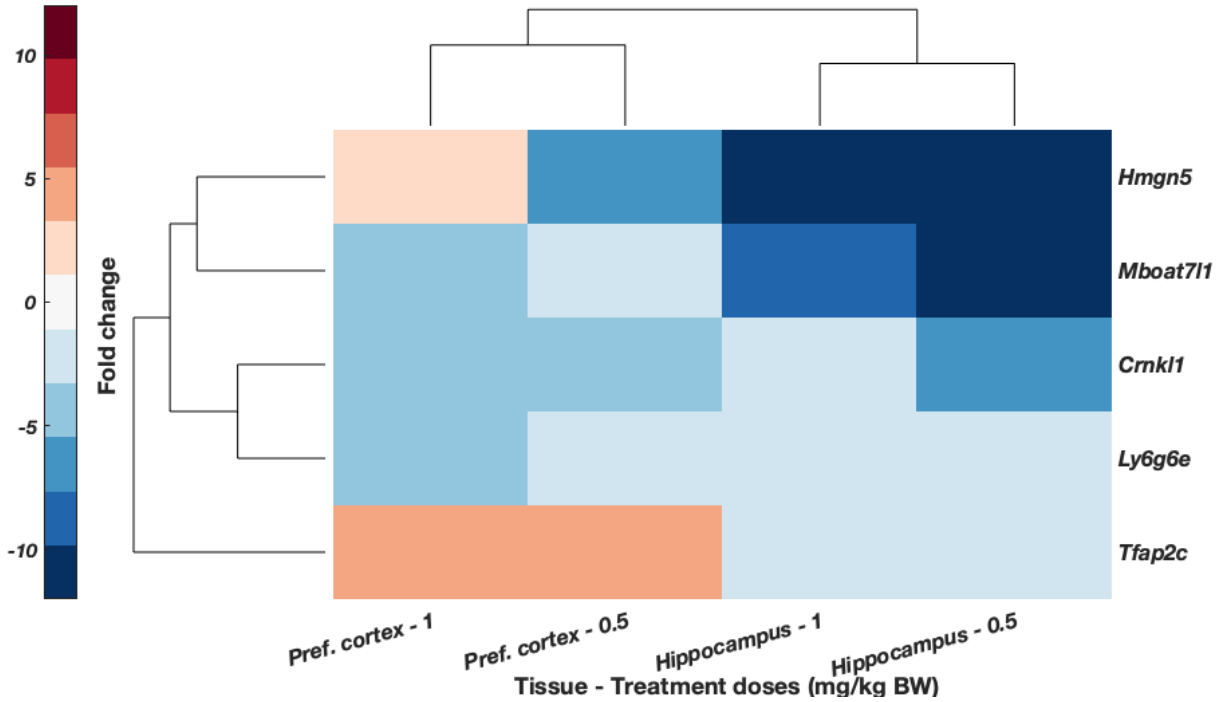

Fig. 41: Hierarchical clustering of DEGs from pref. cortex and hippocampus of rats dosed with 0.5 and 1 mg/kg B.W. $CoCl_2$ compared against control (dH_2O). Conditions applied to DEGS were for the fold change to be over 2 and $p<0.05$. Animals were given daily i.p. injections for 28 days. DEGs were obtained through RNA-Seq analyses. Upregulated genes are displayed in red and downregulated in blue. Hierarchical clustering was carried out according to Euclidian distance. Analysed samples were pooled (n'=1) from n =4 pref. cortex group samples and n = 3 in the case of the hippocampus of rats treated with 0.5 mg/kg B.W. $CoCl_2$, and n =1 for 1 mg/kg B.W. $CoCl_2$. Doses and tissues were selected due to their significant uptake of cobalt (refer to cobalt content results).

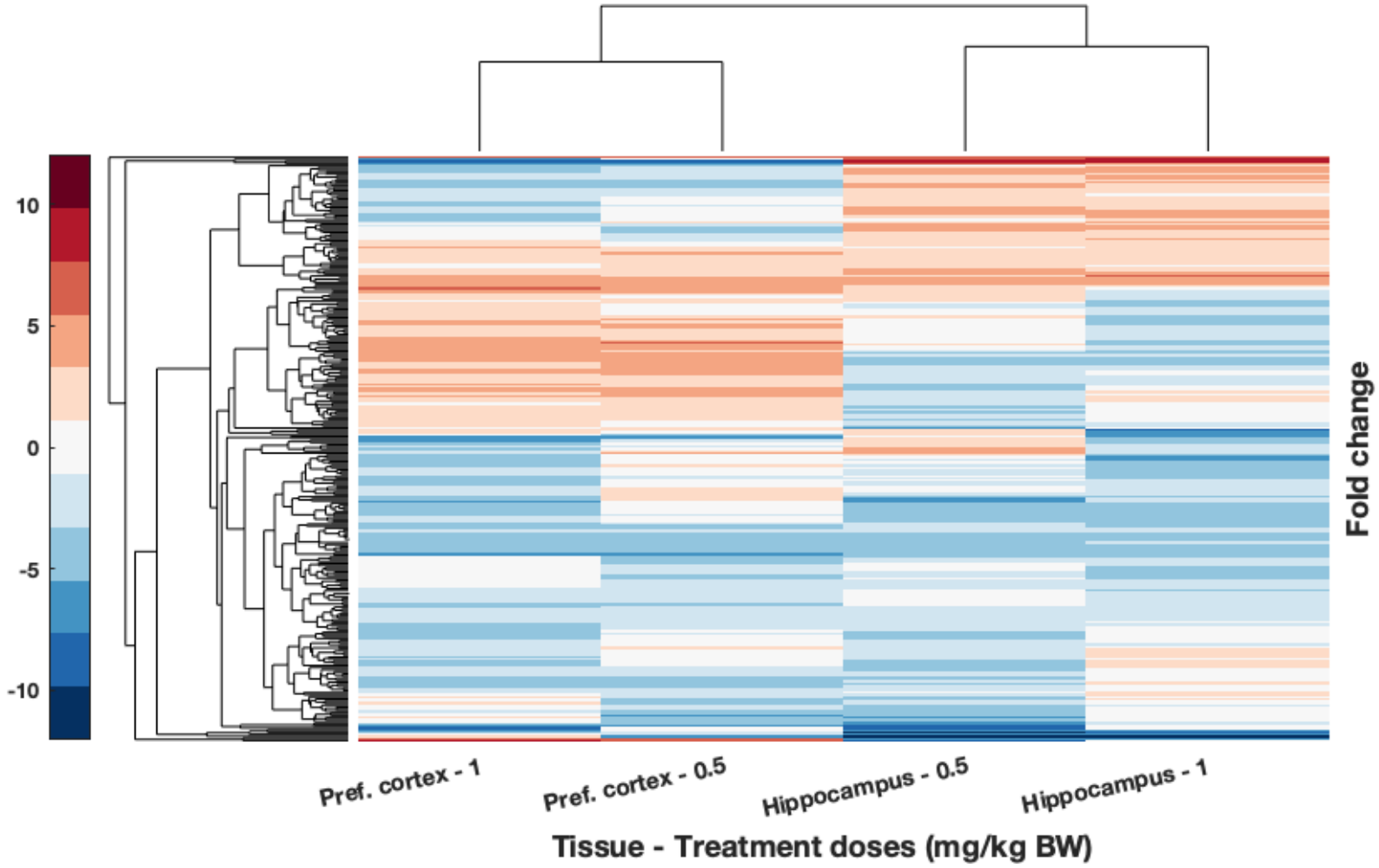
10
5
0
-5
-10
Fold change
Pref. cortex - 1
Pref. cortex - 0.5
Hippocampus - 0.5
Hippocampus - 1
Tissue - Treatment doses (mg/kg BW)

Fig. 42: Hierarchical clustering of DEGs from brain tissues with significant accumulation of cobalt: pref. cortex and hippocampus from rats treated with 0.5 and 1 mg/kg B.W. $CoCl_2$. DEGs were obtained from RNA-Seq comparing the RNA isolated from those tissues with that of controls treated with dH_2O. Condition applied is for fold change to be over 2 (no significance level required). Upregulated genes are shown in red while downregulated are displayed in blue. Hierarchical clustering and resulting dendrogram were generated with Euclidian distance. Samples analysed through RNA-Seq were pooled (n'=1) from n=4 pref. cortex samples, n=3 in hippocampus from 0.5 mg/kg B.W. $CoCl_2$ treatment group, and n=1 from 1 mg/kg B.W. $CoCl_2$ treatment group.

Table 19: Enriched GO terms obtained from DEGs of pref. cortex and hippocampus in response to cobalt treatment with 0.5 and 1 mg/kg B.W. $CoCl_2$ compared to control animals (dH_2O). Rats were dosed for 28 days with i.p. injections. GO terms annotated were significantly enriched with $p<0.05$. GO terms enriched belong to the Molecular Function (MF; 08/04/2016), Biological Process (BP; 08/04/2016), Cellular Component (CC; 08/04/2016) and KEGG (14/06/2016) GO databases.

Gene Ontologies (GO) and GO terms	# genes with annotations in the ontology (%)	# genes represented in GO Terms (%)
Biological Process (BP) GO terms (08/04/2016)	194 (72.12%)	93 (34.57%)
regulation of hormone levels	*Afp, Bco1, Bik, Cga, Cyp11a1, Cyp17a1, Fam3b, Ffar2, Fga, Fgf23, Gh1, Ghrh, Ghrhr, Il6, Nr0b2, Nt5c1b, Pax8, Slc30a8, Slco1a5, Sult1e1*	
response to interleukin-6	*Crp, Fga, Fgf23, Ghrh, Hamp, Il6, Pck1*	
T-helper 17 cell lineage commitment	*Batf, Il6, Ly9*	
response to vitamin	*Cyp11a1, Fgf23, Folr1, Hamp, Orm1, Otc, Sult2a1, Tshb*	
response to pH	*Acer1, Gh1, Gja3, Kcnk18, Pck1*	
response to interleukin-1	*Ccl21, Ccl25, Cyp11a1, Il6, Mmp3, Pck1, Slc30a8*	
cell chemotaxis	*Ccl21, Ccl25, Ccr6, Cxcl13, Cxcl9, Cxcr2, Ffar2, Hrg, Stap1*	
organ formation	*Folr1, Foxh1, Gdnf, Ntf4, Pax8*	
cell fate commitment	*Batf, Elf5, Gata5, Gsx1, Gsx2, Il6, Ly9, Myl2, Ntf4, Olig3, Sostdc1*	
Molecular Function (MF) GO terms (08/04/2016)	185 (68.77%)	60 (22.3%)
cytokine receptor binding	*Bmp10, Ccl21, Ccl25, Cxcl13, Cxcl9, Gh1, Il6, Inhbc, Ntf4, Stap1*	

heparin binding	*Ang2, Comp, Cxcl13, Hrg, Mcpt4, Serpind1, Wisp3*	
growth factor activity	*Areg, Bmp10, Fgf23, Gdnf, Il6, Inhbc, Ntf4*	
steroid binding	*Comp, Crp, Cyp11a1, Fabp1, Sult1e1, Ugt1a1*	
hormone activity	*Bmp10, Cga, Gh1, Ghrh, Gpha2, Hamp, Inhbc, Pyy, Rln3, Tshb*	
KEGG terms (14/06/2016)	97 (36.06%)	29 (10.78%)
Steroid hormone biosynthesis	*Cyp11a1, Cyp17a1, Cyp2c7, Cyp3a23/3a1, Sult1e1, Ugt1a1, Ugt2b17*	
Hematopoietic cell lineage	*Cd19, Cd3g, Cd8a, Fcer2, Il1r2, Il6*	
Cellular Component terms (08/04/2016)	216 (80.3%)	18 (6.69%)
external side of plasma membrane	*Cd19, Cd8a, Cxcl9, Fcer2, Fga, Folr1, Hyal5, Il6, Itgad, Trpm8*	

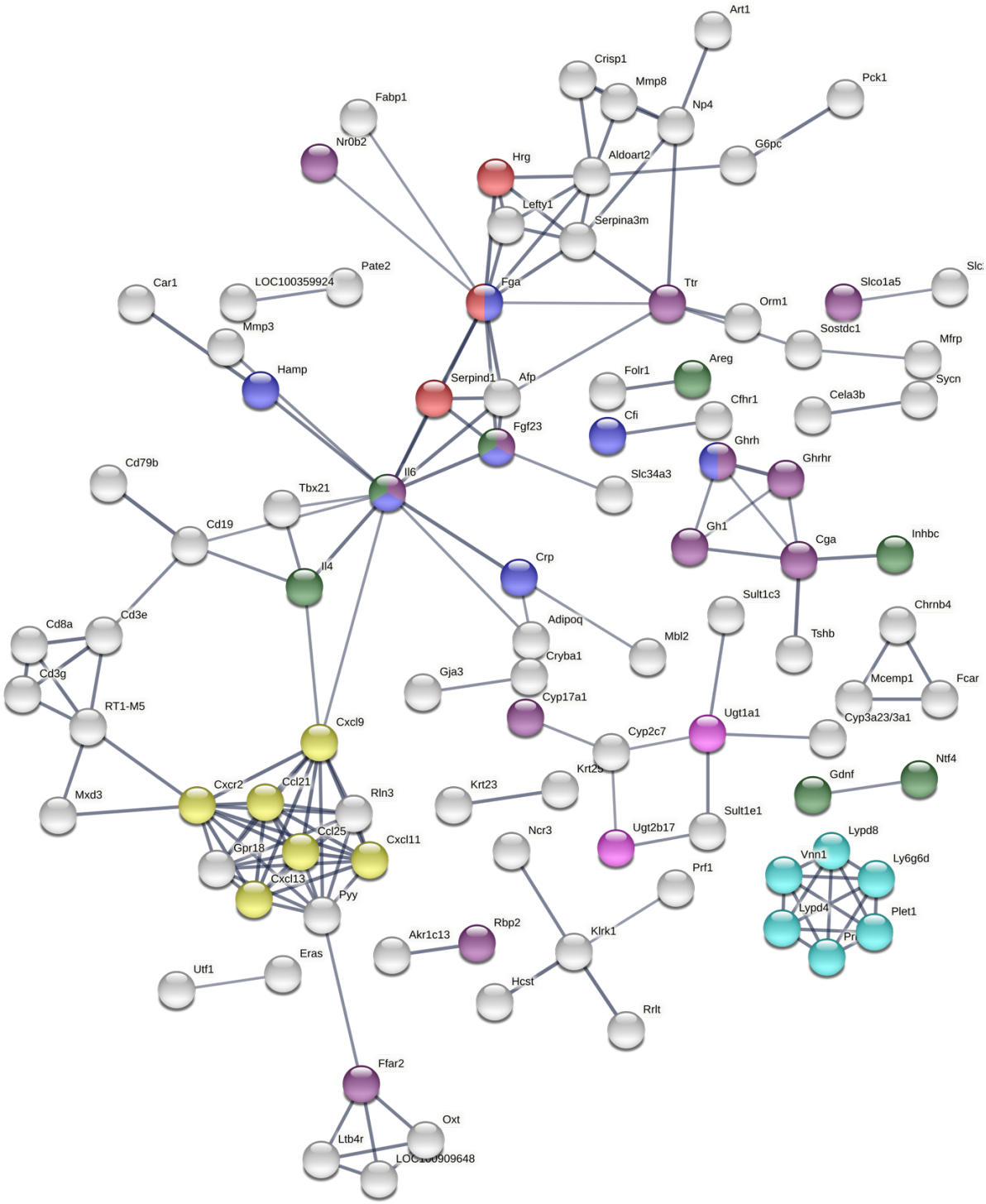

Fig. 43: Protein-protein interaction (PPI) network obtained from STRING web tool (https://string-db.org/) by analysing DEGs as their protein products. DEGs were obtained from RNA-Seq analyses of pref. cortex and hippocampus from rats treated with 0.5 and 1 mg/kg B.W. $CoCl_2$ against controls treated with dH_2O during 28 days of i.p. injections. The following terms/keywords have been highlighted: cellular response to interleukin-6 (blue), regulation of hormone levels (purple), chemokine receptors bind chemokines (yellow), blood coagulation (red), glucuronosyltransferase activity (pink), growth factor activity (green), and post-translational modification: synthesis of GPI-anchored protein (cyan). The thickness of links between nodes represent the confidence in the interaction, only nodes connected with high confidence (0.7) are displayed.

To better observe genes possibly involved in cobalt toxic mechanisms, the DEGs expressed over 2-fold change and with $p<0.05$ from pref. cortex, hippocampus and cerebellum have been plotted on Fig. 44, Fig. 45 and Fig. 46 respectively. They are displayed as arranged by hierarchical clustering analyses of the DEGs (following Euclidian distance, dendrogram not shown). Fig. 44 displays the common genes of pref. cortex across the three doses, and presents several genes whose proteins have a role in inflammation and immunity such as *Crp*, *Tnf*, and *Cxcl13*. *Tnf* was posteriorly inspected in PCR blot and its protein expression evaluated later by Western blot. Fig. 46 shows significant DEGs of the hippocampus over 2-fold change. There are a couple of insulin markers, *Igbp2* and *Igfbp2*, and surprisingly several markers attributed to the choroid plexus such as *Clic6*, *Ttr*, *Kl*, *Col8a1* and others (Lun et al., 2015; Mathew et al., 2016; Sathyanesan et al., 2012). Similarly, some of these choroid plexus markers are also present across doses in the Cerebellum (Fig. 46). In hindsight, the GO term 'brush border membrane' from Table 18 could refer to the brush border of the choroid plexus epithelium.

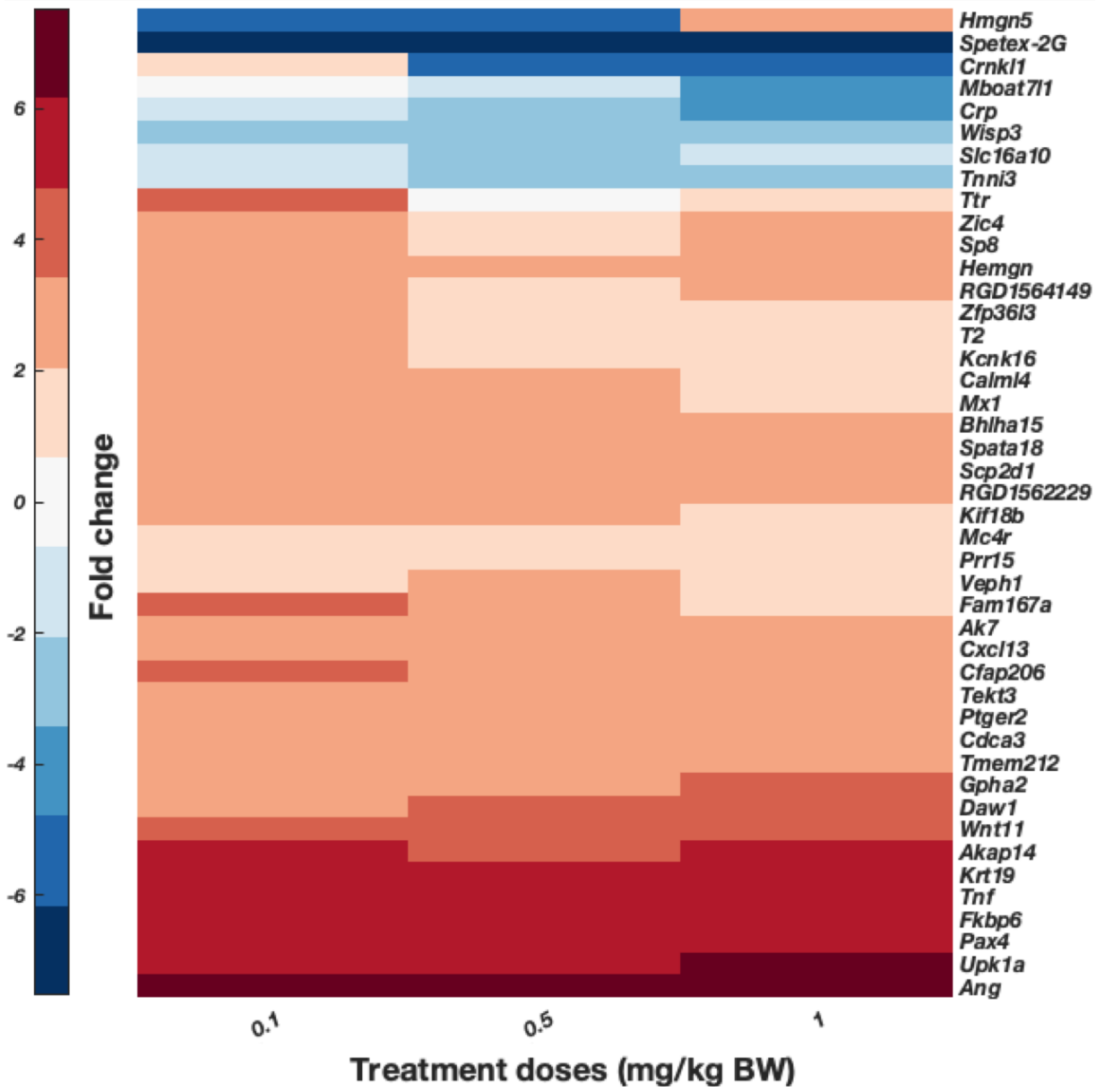

Fig. 44: DEGs obtained from the comparison of pref. cortex from rats dosed with 0.1, 0.5 and 1 mg/kg B.W. $CoCl_2$ against the control group (dH_2O). Animals were treated for 28 days with daily i.p. injections. DEGs displayed were obtained from the RNA-Seq analysis of pooled samples (n'=1 from n=4 samples per group). Fold-change gene expression is indicated by colour as described by the bar in the right side, up-regulated genes are displayed in red while down-regulated are blue. Genes are displayed as determined by the hierarchical clustering performed with the clustergram.m function from MATLAB software of DEGs over 2-fold-change ($p<.05$), dendrogram not shown (Euclidian distance).

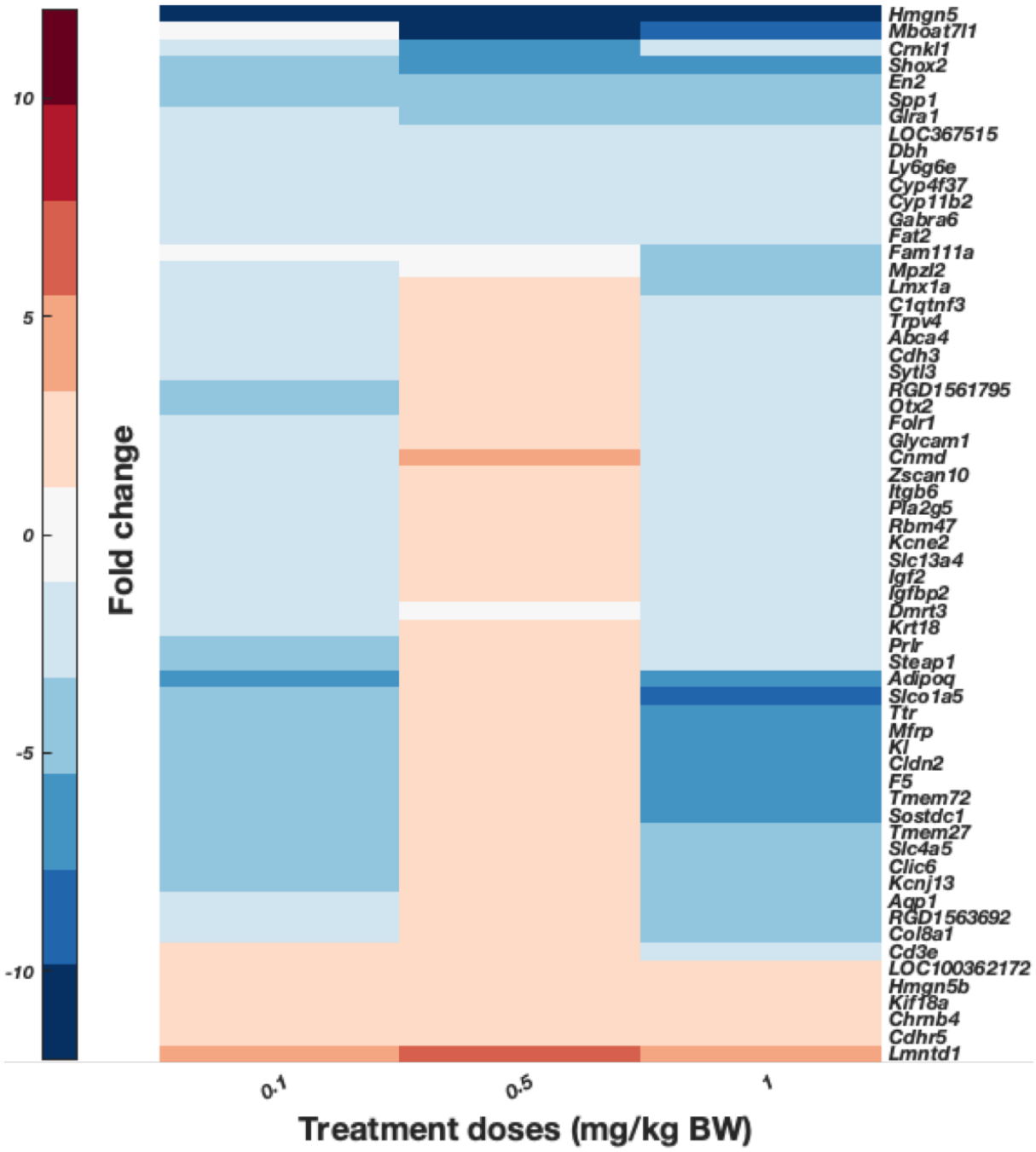

Fig. 45: DEGs expressed in hippocampus of rats treated via i.p. with daily injections of 0.1, 0.5, and 1 mg/kg B.W. $CoCl_2$ or dH_2O (control groups) for 28 days. Pooled samples (n'=1 from n=4 samples in group 0.1 mg/kg B.W. $CoCl_2$, n=3 from 0.5 mg/kg B.W. $CoCl_2$, and n=1 from 1 mg/kg B.W. $CoCl_2$ group) were analysed through RNA-Seq and data are presented as the result of hierarchical clustering performed with MATLAB clustergram.m function. DEGs in the graph are only those with fold-change > 2 and p<.05, dendrogram is not shown. Colour bar presents fold-change: up-regulated genes in red and down-regulated genes in blue.

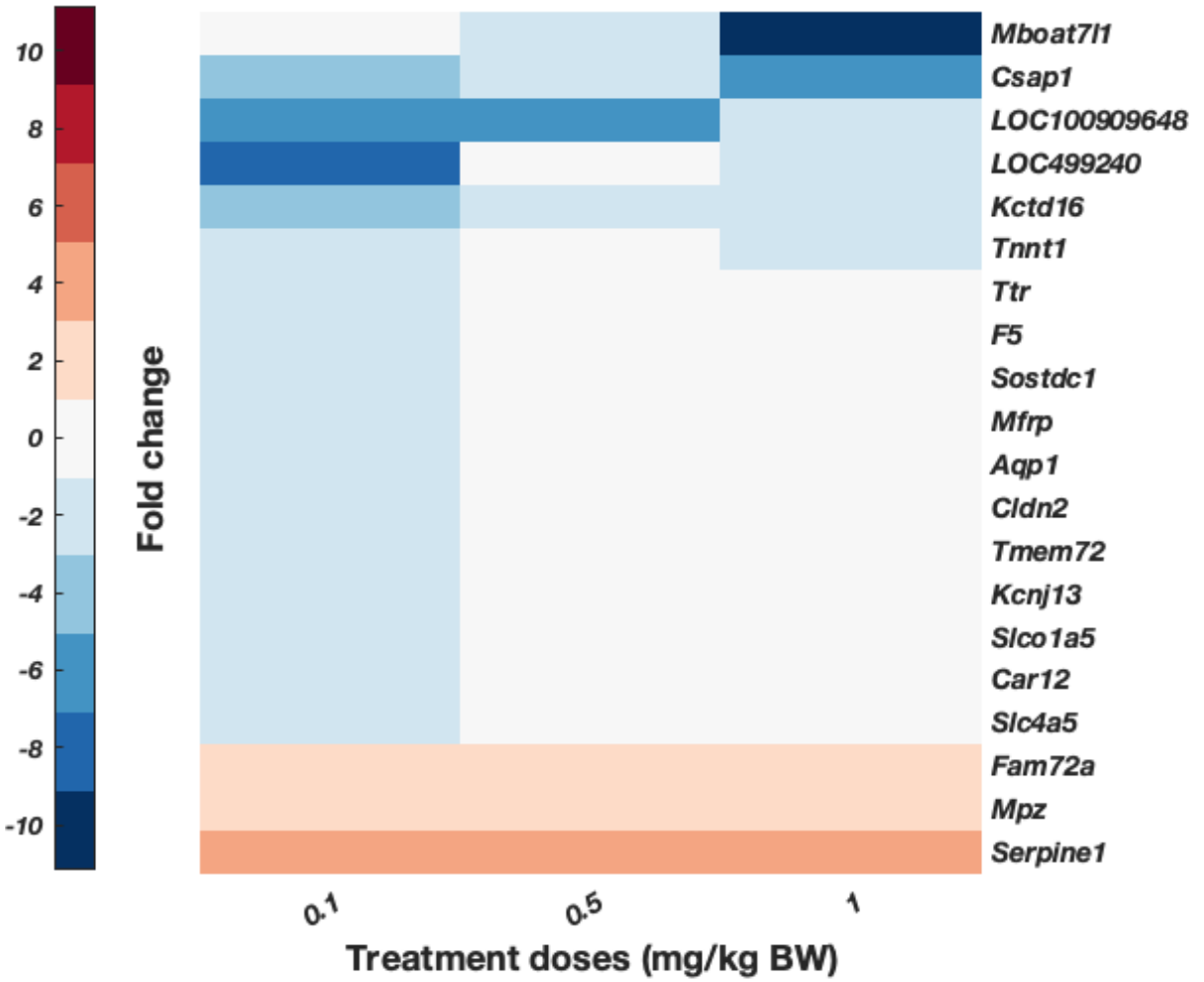

Fig. 46: Gene fold change of cerebellum from rats of $CoCl_2$- treated groups (0.1, 0.5 and 1 mg/kg B.W.) compared with controls (dH_2O). Animals were treated with daily i.p. injections during 28 days. Results show DEGs over 2-fold change and with $p<0.05$ from RNA-Seq analysis organised by hierarchical clustering performed with MATLAB clustergram.m function (Euclidian distance). One sample was analysed per group (n'=1), which was pooled from n=4 samples corresponding to the groups. Colour bar shows upregulated (red) and downregulated (blue) fold changes.

6.2.5. Gene expression validated by RT-qPCR

We selected a few genes to evaluate through RT-qPCR according to their high expression level in RNA-Seq data, as well as their function. Our focus was on the pref. cortex and the hippocampus, the brain areas most responsive to cobalt treatment according to gene expression (Fig. 36 and Fig. 38). The genes selected were *Tnf*, *Spata18*, *Ttr,* and *Akap14* in the pref. cortex and *Kl* in the hippocampus. Transthyretin (*Ttr*) and *Akap14* were chosen as markers of choroid plexus contamination. *Tnf* and *Spata18* are markers of inflammation and mitochondrial damage, respectively. Initially, we selected more genes to validate both in pref. cortex and hippocampus (*Crp*, Cxcl13, *Clic6*, and *Trpv5* among others) but some of the designed primers did not work, and our research was cut short by the COVID-19 lockdown. For the same reason, we only selected the higher dose of cobalt treatment to evaluate gene expression against the control group in these targets.

Fig. 47 shows the fold change according to RT-qPCR and RNA-Seq, which in general are approximatively similar. However, that is not the case for *Tnf* and *Ttr*. Table 20 also describes the fold-changes (before applying the logarithm as described in section 3.7.4. from the *in vitro* methods), with the respective significance. The expression of none of the genes selected was significantly different in the treatment groups from that of the controls. The ΔC_T values shown in Fig. 48 display dissimilar averages in the case of *Spata18*, *Akap14* and *Kl*. However, they are not sufficient to declare statistical significance. For the hippocampus, the fold change of *Kl* for cobalt treatment groups 0.5 and 1 mg/kg B.W. is shown, although only the 0.5 mg/kg B.W. group is displayed as ΔC_T values. That is because we only had one sample available of the hippocampus for the 1 mg/kg B.W. treatment group due to limited tissue availability and dissection difficulties.

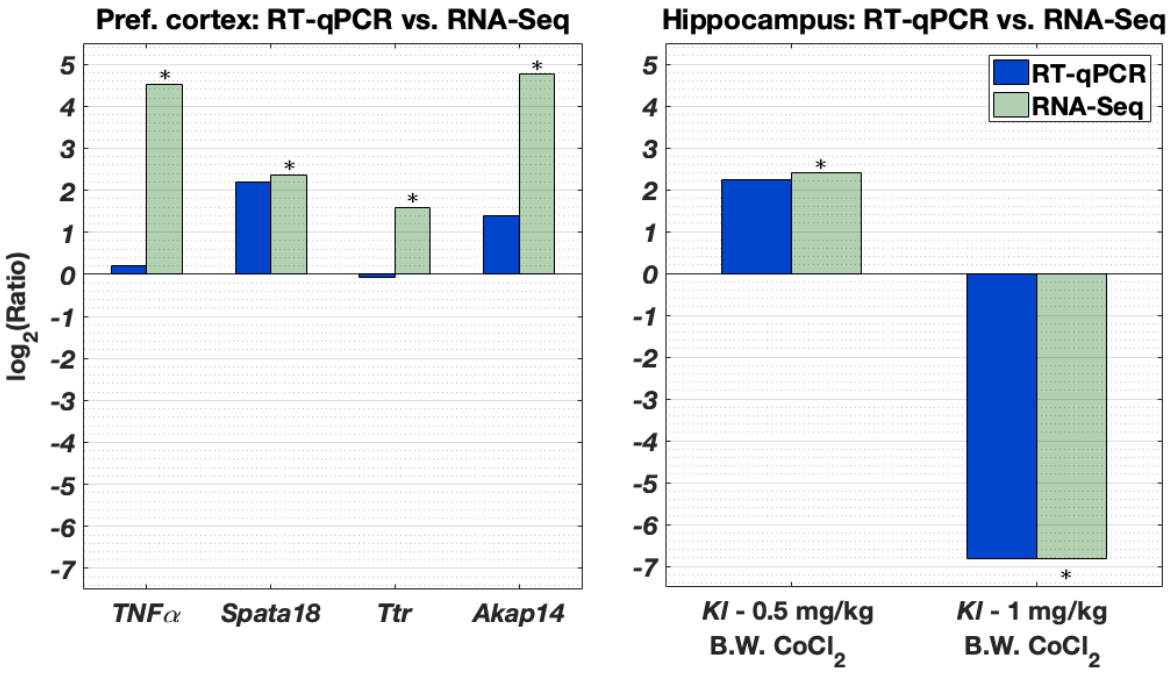

Fig. 47: Fold change mRNA gene expression levels obtained from RNA-Seq (green) and RT-qPCR (blue) of *Tnf*, *Spata18*, *Ttr*, *Akap14* (pref. cortex; n'=1 of n=4 pooled samples) and *Kl* (Klotho; hippocampus; n'=1 from n=4 control group, n=3 in 0.5 mg/kg B.W. $CoCl_2$ treatment group, or n=1 in treatment 1 mg/kg B.W. $CoCl_2$ pooled samples). RT-qPCR normalisation was against *Pes1* in the pref. cortex and *Ywhaz* in the hippocampus. The y-axes show the logarithm of the fold change (aka ratio). * significant difference from the control group at 28 days treatment by independent-samples t-test ($p \leq 0.05$), it does not refer to a significant difference between RT-qPCR and RNA-Seq fold change values.

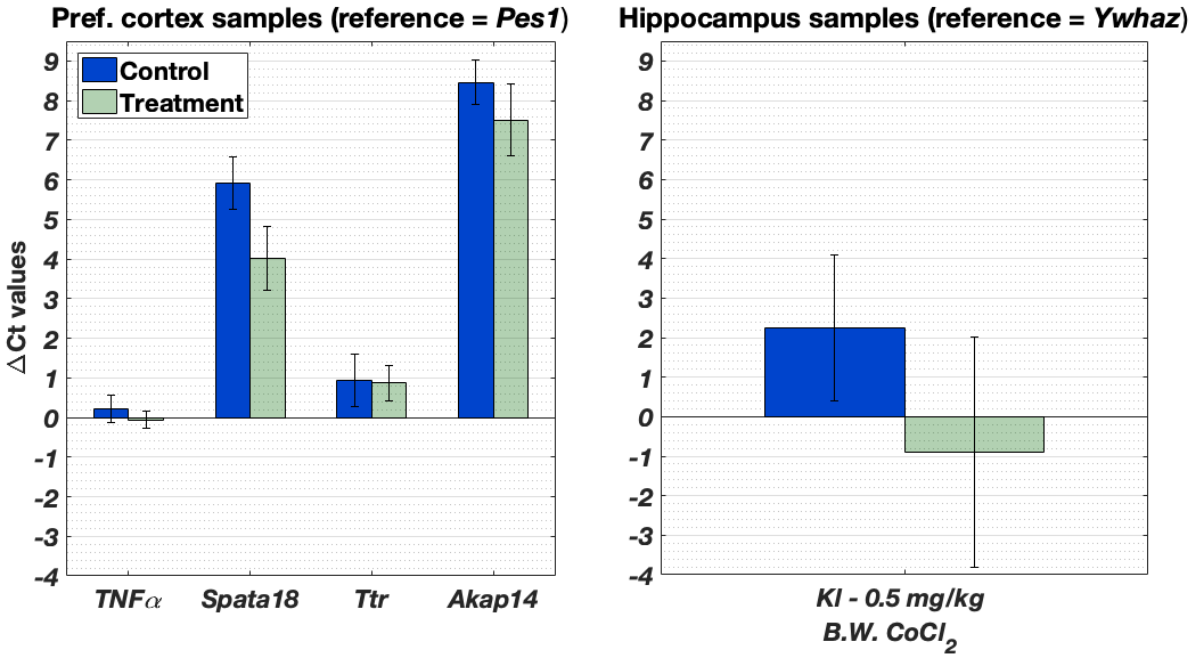

Fig. 48: Quantification of *Tnf*, *Spata18*, *Ttr*, and *Akap14* ΔC_T values (C_T target gene – C_T internal control) in the pref. cortex and *KI* in the hippocampus through RT-qPCR. The internal control for pref. cortex is *Pes1*, and *Ywhaz* for the hippocampus. Data are displayed as mean ± SEM (n=4 for pref. cortex and control group in hippocampus, n=3 for treatment group in hippocampus). * significantly different 0.5 (hippocampus) or 1 (pref. cortex) mg/kg B.W. $CoCl_2$ treatment groups from control group after 28-days i.p. injection treatment by independent-samples t-test ($p \leq 0.05$).

Table 20: Fold change (linear scale) gene expression of treated rats (n=4) compared with control group (n=4; dH_2O) after 28 days cobalt treatment with 1 mg/kg B.W. $CoCl_2$ in the pref. cortex and 0.5 mg/kg B.W. $CoCl_2$ hippocampus. Target genes for the pref. cortex were *Spata18*, *Ttr*, *Akap14*, *Tnf* and *Kl* for the hippocampus. Internal controls were *Pes1* for pref. cortex and *Ywhaz* for hippocampus. P-values were obtained by comparing control and treatment ΔC_T values with independent-samples t-test ($p \leq 0.05$).

Symbol	Pref. cortex		Hippocampus	
	Fold-change	p-Value	Fold-change	p-Value
Spata18	4.56	.115	X	X
Ttr	-1.05	.933	X	X
Akap14	2.65	.412	X	X
TNF-α	1.15	.544	X	X
Klotho (0.5)	X	X	4.68	0.381
Klotho (1)	X	X	-111.87	X

6.2.6. Protein levels of target genes do not change significantly with cobalt treatment

Given the high expression of these and other genes we assessed protein levels of the control group against the treatment group with the highest dose, 1 mg/kg B.W. $CoCl_2$, in the pref. cortex. Although the hippocampus was also a region of interest, it has a small size and there was only enough tissue for metal content and RNA-Seq screening. The cerebellum appeared to be less affected than the pref. cortex (Fig. 36), but some of the genes selected were also highly expressed in the treatment group 1 mg/kg B.W. $CoCl_2$ (data not shown) so we decided to evaluate protein expression in both tissues.

β-Actin was used as the protein control after reviewing that its fold change expression did not vary across doses in the RNA-Seq data (data not shown). The selected antibodies were Spata18 (aka Mieap), involved in mitochondrial ROS and cytosolic vacuolization, tumour necrosis factor (Tnfα), which is a known marker of inflammation, and angiogenin (Ang) indicative of angiogenesis and implicated in neurodegenerative diseases. In addition, given the widespread choroid plexus markers we also selected transthyretin (Ttr), to assess for thyroid binding protein and choroid plexus contamination, as well as A-kinase anchor protein 14 (Akap14 aka Akap28), a protein complex that works synergetically with cAMP and PKA signalling, which are signalling pathways controlling cilia beating in the ventricular ependyma.

Fig. 49 displays the immunoblotting results from Akap-14, Spata18, Angiogenin, and TNF-α proteins in the pref. cortex and cerebellum. In contrast to RNA-Seq gene expression, protein levels were unchanged. The quantification of relative protein can be observed in Fig. 50, and no significant increase or decrease between control and treatment in protein abundance was found in any of these targets ($p < 0.5$).

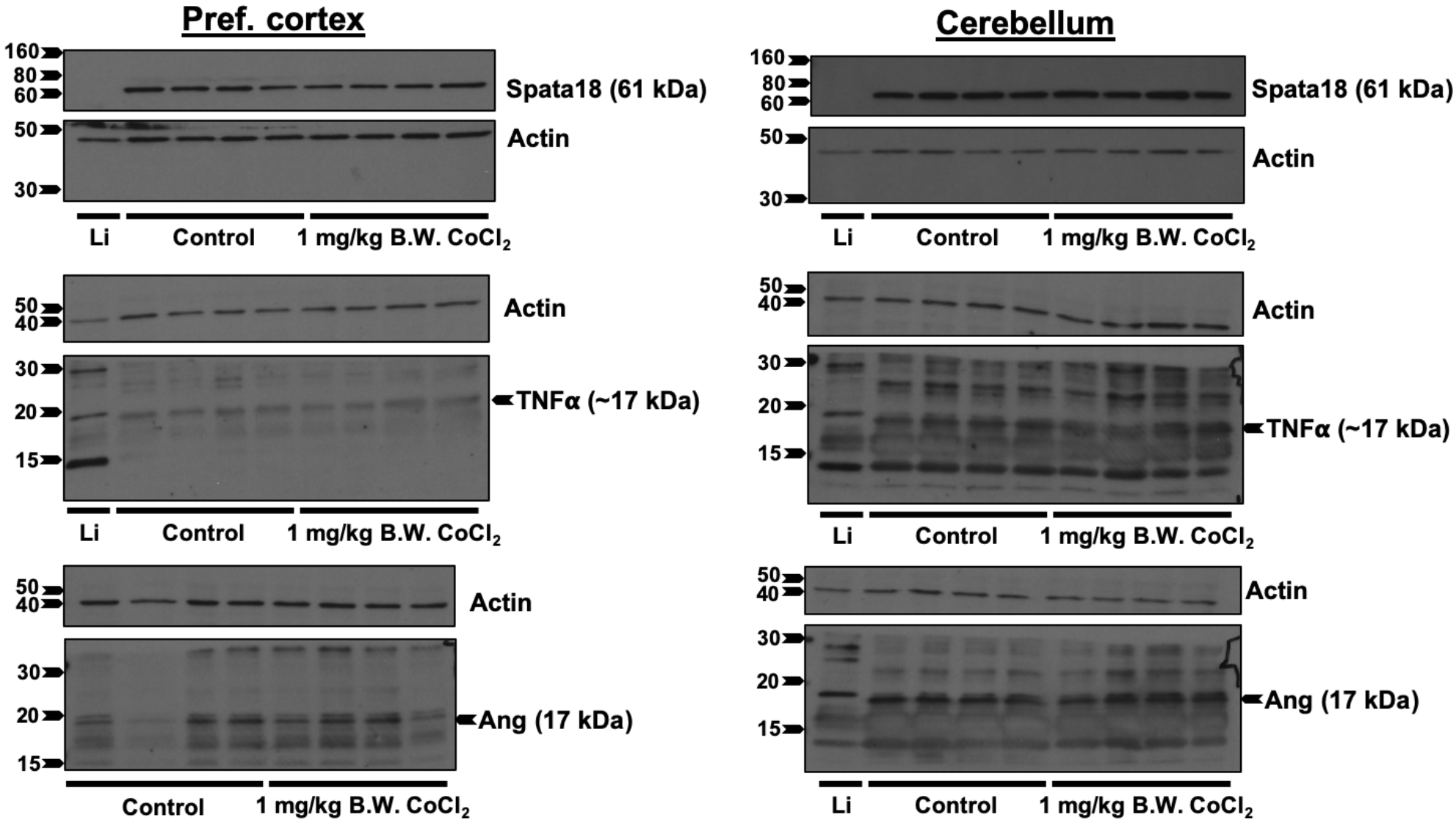
Pref. cortex
160
80
60
Spata18 (61 kDa)
50
30
Actin
Li
Control
1 mg/kg B.W. CoCl2
50
40
Actin
30
20
15
TNFα (~17 kDa)
Li
Control
1 mg/kg B.W. CoCl2
50
40
Actin
30
20
15
Ang (17 kDa)
Control
1 mg/kg B.W. CoCl2
Cerebellum
160
80
60
Spata18 (61 kDa)
50
30
Actin
Li
Control
1 mg/kg B.W. CoCl2
50
40
Actin
30
20
15
TNFα (~17 kDa)
Li
Control
1 mg/kg B.W. CoCl2
50
40
Actin
30
20
15
Ang (17 kDa)
Li
Control
1 mg/kg B.W. CoCl2

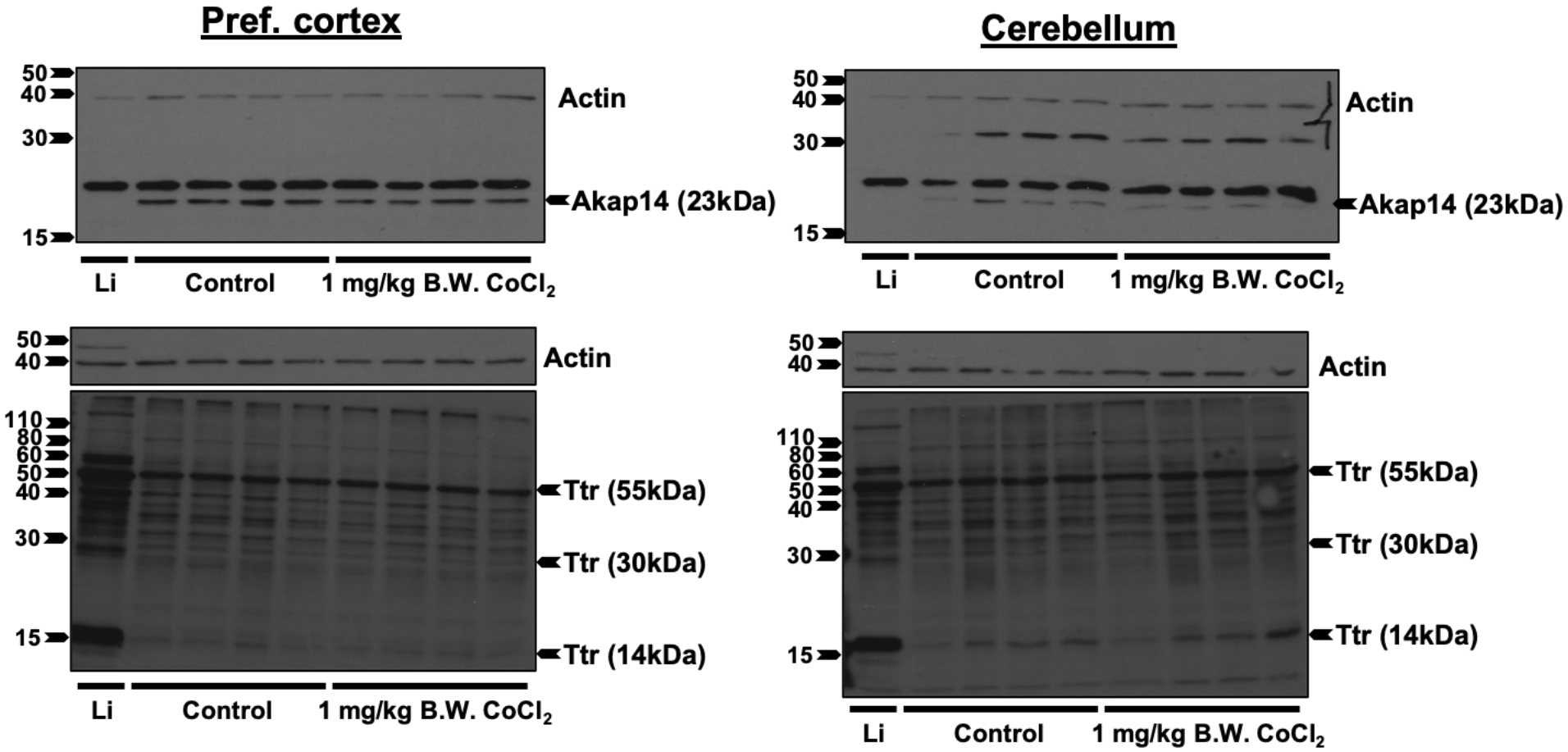

Fig. 49: Immunoblot analyses of target proteins from pref. cortex (left panels) and cerebellum (right panels) tissue homogenates from rats treated with 1 mg/kg B.W. $CoCl_2$ or dH_2O (control). Rats were treated for 28 days with i.p. injections. Target genes were Spata18, Tumour necrosis factor (TNF)-α, Angiogenin (Ang), Akap14 and Transthyretin (Ttr) 50kDa and 14kDa. Relative values were calculated against loading control protein β-Actin. Samples were loaded with 10μg, except for Ttr where 20μg were used. Liver (Li) was used as a control.

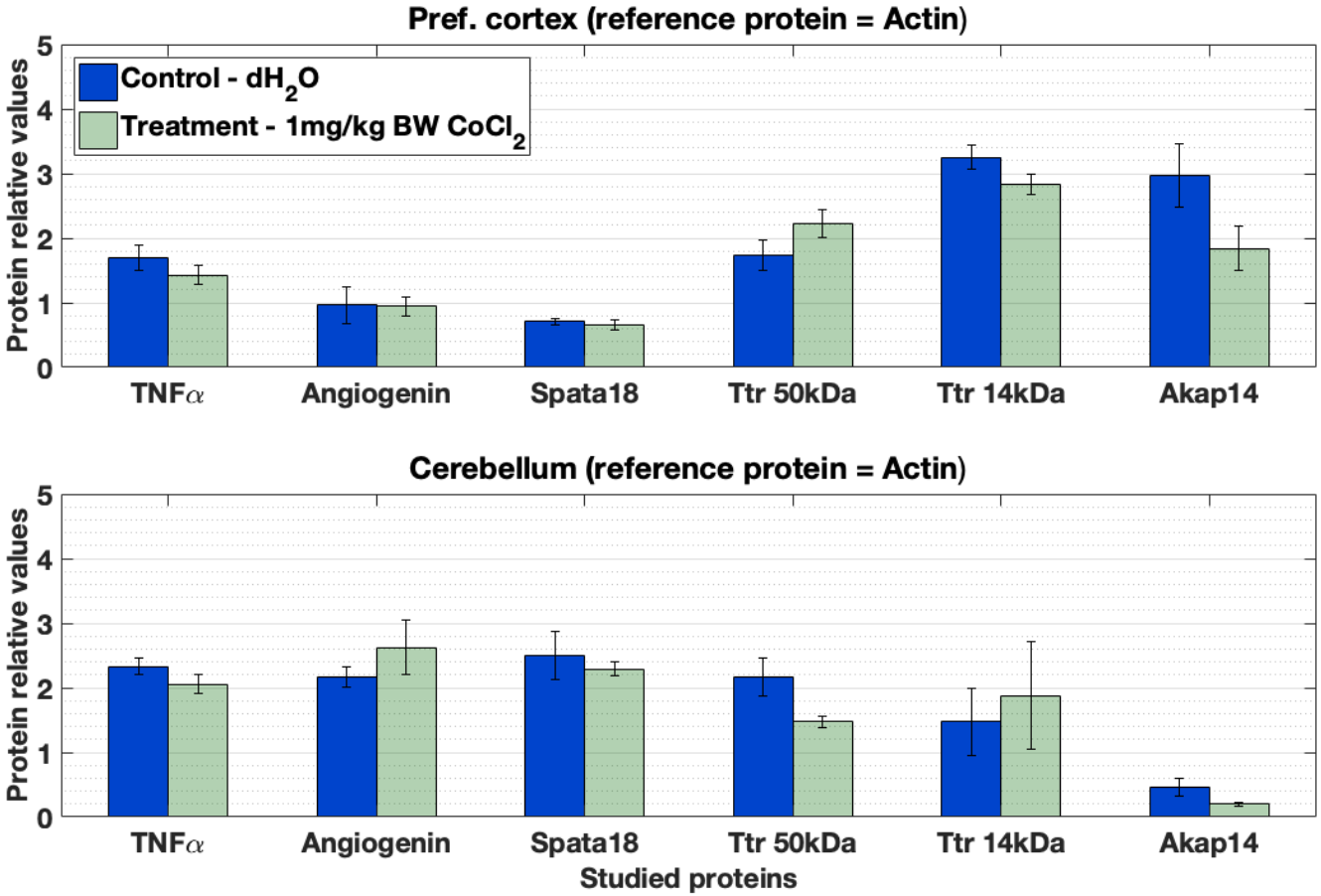

Fig. 50: Relative protein expression of target proteins in pref. cortex (top panel) and cerebellum (lower panel) of rats treated with 1 mg/kg B.W. $CoCl_2$ i.p. injections during 28 days. Controls were treated with dH_2O instead. Target proteins are Spata18, Tumour necrosis factor (TNF)-α, Angiogenin (Ang), Transthyretin (Ttr) 50kDa and 14kDa, as well as Akap14, and relative values were calculated with loading control protein β-Actin after densitometric analysis. Values are mean ± SEM (n=4, except for treatment group in the cerebellum evaluating Akap14 n=3). No significance was found compared with controls with independent t-test ($p<0.05$).

6.3. Discussion

In the previous section, we presented several dose-response outcomes after 28 days cobalt treatment. In summary, we obtained cobalt content of the individual organs and brain parts by ICP-MS, gene expression derived from RNA-Seq and RT-qPCR assays performed on isolated mRNA from the brain, as well as protein levels by immunoblotting. The weight of the animals and of their organs was also measured throughout the experiment to evaluate their general health. These findings are discussed next.

6.3.1. Could cobalt modulate weight gain or loss in patients?

Similar to what was found in the previous chapter, the calculated weight gain rate appears to decrease across the different concentrations of cobalt (Fig. 32). However, the rats' growth is still positive, and these growth rates are not significantly different from the control. As observed in Fig. 30 and Fig. 31, the change in weight acquisition was subtle and went initially unnoticed by us. A recent investigation by Houeto *et al.* compared cobalt and hydroxocobalamin tissue accumulation in dosed rats with 0.75mg/kg B.W. i.p. cobalt injections for three weeks (Houeto et al., 2018). They also detected a significant lower weight in cobalt-treated rats in comparison to controls and animals treated with hydroxocobalamin.

The doses used in our experiments result in low blood cobalt concentrations (<100μg/l) compared to most of the reported cobaltism cases (Fig. 34 and Table 16). Although anorexia has been reported with high blood cobalt concentrations (Gilbert et al., 2013; Zywiel et al., 2013), we wonder if the reduced weight gain seen in our results could have implications for patients with lower cobalt levels in blood, which might also go unnoticed. However, the translation of our results to humans is complicated by the fact that S.D. rats increase their body weight during their lifetimes (Altun et al., 2007) while healthy humans usually plateau during adulthood. We are unaware of studies that monitor the weight of MoM patients and compare it with their cobalt blood levels throughout an extended period of time. Hence, it is unknown whether cobalt could supress weight gain or induce weight loss in otherwise healthy subjects with lower levels of cobalt in blood from our data or other sources in the scientific literature. Nevertheless, our results point to a trend of reduced growth and we know that cobalt

toxicity can induce anorexia at high blood cobalt concentrations, therefore we can hypothesise on the mechanisms behind this effect.

In section 4.3.2. from the Discussion of Chapter 4 we speculated whether cobalt could directly interfere with feeding mechanisms by passing into the CSF from blood and modifying the metabolic activity of tanycytic cells in the hypothalamus. And although it is possible for this to occur, the reduced weight gain could perhaps be explained by more straightforward mechanisms associated to a process of cachexia. Shimada *et al.* recently defined several disease states induced by known liver and kidney toxicants through machine learning algorithms in a transcriptomics database (Shimada and Mitchison, 2019). They discovered that drugs causing organ injury and a new 'drug-induced tolerance' state were characterised by weight loss. The hormones insulin-like growth factor-1 (*Igf1*) and growth differentiation factor-15 (*Gdf15*), as well as its downstream targets, were thought to be causative of the phenotype. Following the hypothesis of Shimada *et al.* we could speculate that cobalt induces tissue injury if not in the brain, in other tissues with higher cobalt concentrations such as the liver, kidney or heart (Fig. 34 and Table 16). Cobalt could also induce a state of tolerance, which was characterised by a transcriptional activation of xenobiotic detoxification and as a transitional state to or from other more severe disease states induced by chemicals. According to Shimada *et al.* both scenarios would lead to secretion of *Gdf15* by the liver, a protein that induces anorexia through the hypothalamus. This would eventually reduce blood glucose, thus modulating insulin and metabolism signalling, and ultimately leading to weight loss and cachexia.

We searched the RNA-Seq data for these markers. Although insulin indicators downstream of *Igf1* can be observed with high fold-change in the hippocampus (*Igf2* and *Igfbp2*; Fig. 45) and are also scattered across RNA-Seq data, the gene expression of *Igf1* itself is not very high for all the tissues analysed as can be observed in Table 21. We also found instances of *Gdf15* in the transcriptomic data which were significantly regulated (Table 22), while its receptor *Gfral* is not significantly or highly regulated in general (Table 23). Thus, it is possible that these pathways are lightly regulated in some of the treated animals, while a few rats could be more affected by cobalt resulting in secretion of *Gdf15*. This is a promising pathway to investigate in future studies of cobalt toxicity.

Table 21: Fold change and p-values of Insulin-like growth factor 1 (*Igf1*) in pref. cortex, hippocampus and cerebellum of 0.1, 0.5 and 1 mg/kg B.W. $CoCl_2$ treated rats. Rats were treated for 28 days via i.p. injections with the mentioned doses or dH_2O in the case of the controls. Gene expression values were obtained from the RNA-Seq data of pooled samples.

Igf1 fold change	Pref. cortex		Hippocampus		Cerebellum	
	Fold-change	p-Value	Fold-change	p-Value	Fold-change	p-Value
0.1 mg/kg B.W.	-0.27	0.25	-0.13	0.60	0.24	0.21
0.5 mg/kg B.W.	-0.66	0.005	-0.39	0.15	0.3	0.10
1 mg/kg B.W.	-0.76	0.003	0.20	0.42	0.43	0.02
1 mg/kg B.W. (1st experiment)	0.15	0.78	X	X	-0.26	0.68

Table 22: Growth Differentiation Factor 15 (*Gdf15*) fold change and p-value across brain parts analysed through RNA-Seq experiments after cobalt treatment: pref. cortex, hippocampus and cerebellum. Rats were dosed daily with i.p. injections of 0.1, 0.5 and 1 mg/kg B.W. $CoCl_2$ or dH_2O (controls) for 28 days. Bold figures display values over 2-fold or significant. RNA from tissues was isolated from pooled samples. RNA-Seq was performed over the pooled RNA samples isolated for each control or treatment group.

Gdf15 fold change	Pref. cortex		Hippocampus		Cerebellum	
	Fold-change	p-Value	Fold-change	p-Value	Fold-change	p-Value
0.1 mg/kg B.W.	-0.67	.66	-1.06	.22	-2.44	.01
0.5 mg/kg B.W.	-0.59	.69	0.70	.29	-1.12	.16
1 mg/kg B.W.	0.74	.51	-3.11	.02	-1.31	.11
1 mg/kg B.W. (1st experiment)	1.04	.59	X	X	4.17	.48

Table 23: GDNF family receptor alpha-like (*Gfral*) fold change and p-values from RNA-Seq data obtained from pref. cortex, cerebellum and hippocampus of rats dosed with i.p. daily injections of 0.1, 0.5 and 1 mg/kg B.W. $CoCl_2$ or dH_2O (controls) during 28 days. In bold are significant figures or fold change over 2-fold.

Gfral fold change	Pref. cortex		Hippocampus		Cerebellum	
	Fold-change	p-Value	Fold-change	p-Value	Fold-change	p-Value
0.1 mg/kg B.W.	-0.43	0.29	0.09	0.76	-0.43	0.53
0.5 mg/kg B.W.	-0.32	0.42	-0.28	0.37	0.38	0.52
1 mg/kg B.W.	-0.44	0.28	-0.27	0.40	-0.32	0.65
1 mg/kg B.W. (1st experiment)	0.53	0.61	X	X	-2.53	0.01

Conversely, the available literature suggests that lowering protein intake could worsen and perhaps trigger some of the severe symptoms of cobaltism. In early studies of cobalt toxicity the researchers observed that protein deficient rats had higher incidence and suffered more severe cardiac effects that normally fed rats (Rona, 1971). This was also noted in Quebec (Morin et al., 1969) and Belgium beer drinkers (Kesteloot et al., 1968), whose beverages also had cobalt additive. The authors of this last study reported that onset of the symptoms appeared to correlate with a period of anorexia. Furthermore, 60% out of 64 beer drinkers with cobalt cardiomyopathy in Omaha had diet alterations two to six months preceding the onset of cardiac symptoms (Sullivan et al., 1969). Other recent cases of cobaltism in patients with hip prosthesis have also reported anorexia (Mao et al., 2011; Zywiel et al., 2013) or significant weight loss (Gilbert et al., 2013).

Previous reviews on cobalt toxicity have hypothesised that the deficient nutrition provoked by cobalt would apparently decrease albumin (hypoalbuminemia), thus raising levels of free cobalt ions in blood (Paustenbach et al., 2013; Zywiel et al., 2016). Indeed, we mentioned in section 4.3.5 that *in vitro* cobalt is sequestered by albumin and histidine in DMEM cell media up to a concentration of 40μM (Sabbioni et al., 2014b), moreover different media compositions produce varying fractions of soluble cobalt (Bresson et al., 2013). However, in spite of this long believed view on albumin production by the body, recent studies on caloric restriction have denied the relationship between blood albumin levels and a deficient diet (Lee et al., 2015). This does not mean albumin is not relevant since inflammation can lower albumin blood content. Furthermore the metal binding ability of albumin is greatly reduced in the case of ischemia modified albumin (IMA), which is precisely measured by the Albumin Cobalt Binding (ACB) assay (Paustenbach et al., 2013).

Certainly, cobalt could exert a dual effect. High cobalt levels could lead to albumin saturation and higher cobalt concentrations in organs, but additionally, further depriving the body of necessary nutrients might precipitate metabolic failure given that cobalt directly affects metabolism. A combination of lack of nutrients and increased free cobalt levels could perhaps explain cobalt susceptibility, which do not seem to correlate clearly with blood or serum cobalt levels (Zywiel et al., 2016). Further research would be needed to understand changes in food intake and prove the role of

cobalt in delayed growth. Nevertheless, it is possible that cobalt could modulate rat feeding behaviour.

6.3.2. The low range cobalt dosage used does not lead to a dose-response

The accumulation of cobalt in most organs appears to be proportional to the dose used (Fig. 34 and Table 16), and this was also the case in the pref. cortex and hippocampus (Fig. 35 and Table 17). We did not observe any apparent or significant changes in any of the organ weights as a result of their cobalt content (Fig. 33). It is known that cobalt can induce cardiomegaly and hepatomegaly (Choi et al., 2019; Sullivan et al., 1969). However, the cobalt blood concentrations obtained here are situated within the lower range in relation to patients with MoM implants (<100μg/l), and normally patients do not seem to demonstrate systemic health issues derived from low blood cobalt levels, although there are exceptions (Mao et al., 2011). Thus, we believe the concentrations used in this study may have a subtle toxic effect, although it is unknown whether the toxicity elicited might lead to more serious effects such as organ hypertrophy over time.

In the brain, the doses with the highest number of DEGs (0.5 and 1 mg/kg B.W. $CoCl_2$; Fig. 36) are those with a significant accumulation of cobalt according to ICP-MS data (Fig. 35 and Table 17). Organ and blood cobalt content at 0.1 mg/kg B.W. are low and not statistically significant compared to the measurements at 0.5 and 1 mg/kg B.W. $CoCl_2$ including in the brain parts. Future research might want to shift the doses studied beyond this concentration. However, the average rat blood cobalt concentration corresponding to 0.1 mg/kg B.W. $CoCl_2$ dosage is 4.4 ± 0.9 μg/l, which is similar to the cobalt levels displayed by many prosthetic patients (Langton et al., 2013). Since the average cobalt in blood is <1 μg/l in unexposed patients, we cannot overlook the response elicited at this concentration in the rat brain. In addition, the fold change of certain DEGs compared to the control group is still very high in the brain even from the 0.1 mg/kg B.W. $CoCl_2$ concentrations (maximum |fold change| = 10; $p<0.5$). Given the demonstrated sensitivity of transcriptomics to detect toxicity in comparison to other more conventional techniques (Joseph, 2017), we decided to also include this concentration as part of our analyses.

To summarise RNA-Seq results, no dose-response was demonstrated either in the number or in the average fold change of DEGs elicited by cobalt treatment (Fig. 36 and Fig. 37). Moreover, we could not find specific DEGs whose fold change followed a dose-response (Fig. 40, and also for pref. cortex Fig. 44, hippocampus Fig. 45, and cerebellum Fig. 46). However, it is also possible for cobalt toxic effects to follow a dose response, but the few concentrations used here do not cover such a range of toxicity.

Furthermore, we do not know which proportion of cobalt corresponds to free ions and which to cobalt-bound to protein complexes as mentioned in the previous section. A few reviews on cobalt have also addressed whether free cobalt ions might be a more relevant metric to evaluate or predict cobalt toxicity instead of whole blood (Kerger et al., 2018; Paustenbach et al., 2013). However, the estimation of cobalt fractions is not straightforward (Kerger et al., 2018; Sabbioni et al., 2014b), and to this date there is not sufficient data covering this issue. In any case, if cobalt is being sequestered by albumin, it is likely that the response to any administered cobalt treatment will be dampened.

Previous studies suggest that the fraction of ionic cobalt remains constant throughout a wide range of cobalt concentrations in blood due to albumin binding capacity (Paustenbach et al., 2013). However, since certain conditions and diseases can modify albumin leading to ischemia-modified albumin (IMA) by decreasing its cobalt binding capacity, the levels of free cobalt could increase. The toxic action of free cobalt ions could in time lead to an underlying state of disease, which potentially could modify albumin binding capacity, i.e. lowering cobalt albumin retention. Eventually, this would allow for more free cobalt ions in blood which would increase cobalt toxicity. Facchin *et al.* researched IMA in a cohort of patients with MoM implants and found that their IMA was elevated, but there was no correlation between cobalt blood levels and IMA (Facchin et al., 2017). Certainly, more research would be needed to understand this matter.

6.3.3. What are the overall transcriptional effects of cobalt?

The genes displayed in the hierarchical clustering analyses of Fig. 39 and Fig. 41 were obtained in a conservative way, only considering significant DEGs ($p<0.05$) over 2-fold change (Zhao et al., 2018). These common DEGs were *Mboatl7* and *Ttr* in Fig. 39, which showed the common genes over all doses and tissues, and *Hmgn5*, *Mboat7l1*, *Crnkl1*, *Ly6g6e* and *Tfap2c,* which were obtained from the pref. cortex and hippocampus of rats dosed with 0.5 and 1 mg/kg B.W. $CoCl_2$ (Fig. 41). The only thing these genes appear to have in common is that they are not well known genes. Their function is still being researched and not a lot of information could be found in the literature about most of them. The fold change and significance conditions for the analysis were imposed to reduce data dimensionality and the number of false positive DEGs (Maleki et al., 2020), but these conditions have proved to be too stringent. We have displayed the number of DEGs for each threshold condition in Appendix E. Although the mentioned genes might have their importance, the reduced number does not allow for a biological interpretation of the effect of cobalt in the brain. Therefore, we removed the requirement for significance for GO enrichment analyses, and focused only in highly expressed DEGs.

Table 18 displays the GO terms from common pref. cortex, hippocampus and cerebellum DEGs over 2-fold change (Fig. 40), while Table 19 shows those DEGs from the pref. cortex and hippocampus of rats dosed with 0.5 and 1 mg/kg B.W. $CoCl_2$ (Fig. 42), which were the doses with significant accumulation of cobalt as can be observed in Fig. 35. The percentage range of annotated genes in the GO ontologies is relatively high (genes recognised by each database): 40-80% in the first enrichment analysis (Table 18) and 36-80% in the second (Table 19) depending on the specific ontology. However, although the analyses with Cytoscape software returned several GO terms with biological importance, the relative number of genes represented in the resulting GOs is not high at all: 3-20% DEGs from all doses/brain parts and 7-35% from pref. cortex and hippocampus of rats treated with 0.5 and 1 mg/kg B.W. $CoCl_2$. In addition, many of the enriched terms contain only 3 genes in Table 18, e.g. ‘response to growth hormone’, ‘metanephric epithelium development’, ‘transferase activity, transferring sulfur-containing groups’, ‘Renin secretion’, and ‘B cell receptor signaling pathway’, or ‘T-helper 17 cell lineage commitment’ in Table 19. Many of these genes included in the

GOs also overlap between terms, and it is possible that some GO terms are functionally related. This points to low representation of the genes from our dataset in the given ontologies. Moreover, many highly expressed and significant DEGs from Fig. 39 and Fig. 41 have not been included in the enrichment. From DEGs common to all the tissues with more constricted conditions (Fig. 39; |fold-change| >2 and $p<0.05$) only transthyretin, *Ttr* is represented in the GO terms of Table 18 and Table 19. It is known that GO annotations are biased towards including a well-known small set of genes that represent only 16% of the human genome (Tomczak et al., 2018). Thus, we should warn about the limitations of our GO enrichment analysis. However, annotations keep evolving so perhaps future revaluations of our data might bring more information about the effect of cobalt in the brain.

Even when the GO enrichment analyses were limited, we found some terms of interest that could be associated with cobalt toxicity. This in the case of 'Steroid hormone biosynthesis' present in both Table 18 and in Table 19, which is comprised by a few genes of the Cytochrome P450 (*Cyp* prefix) family, as well as by a couple UDP-glucuronosyltransferases (*Ugt* prefix) and a sulfotransferase (*Sult* prefix). The protein products of these gene families form part of drug metabolism and detoxification pathways, which would explain why the term 'Bile secretion' is present. These gene families are normally expressed in the liver but the brain also hosts some CYPs (Ferguson and Tyndale, 2011), UGTs (Ouzzine et al., 2014) and SULTs (Asai et al., 2019). Indeed, their functions extend to the clearance of endogenous and exogenous compounds such as bile or urine. UGTs and SULTs can metabolise steroids, thyroid hormones, as well as serotonin and dopamine, although the function of glucuronidated or sulphated neurotransmitters is not understood yet (Di, 2014). Moreover, CYPs are also involved in biosynthesis of serotonin, dopamine (Ferguson and Tyndale, 2011) and steroid hormones (Pikuleva and Waterman, 2013). Genetic polymorphisms of CYPs involved in neurotransmitter synthesis and in the case of steroid hormones such as testosterone and estradiol have been involved in personality traits such as anxiety, impulse control and diminished social traits. Moreover, some CYP genes have been linked with certain cases of Parkinson's disease (Ferguson and Tyndale, 2011). This list of symptoms could be linked to some of those reported by arthroprosthetic cobaltism patients such as increased levels of anxiety, depression, and tremors (Catalani et al., 2012; Gessner et al., 2019; Green et al., 2017). Going back to Chapter

5 section 5.2.7, we suggested that CYPs could be a target of cobalt since they normally bind to heme metal substrate. Some metal ions have been observed to inactivate members of the CYP family, but the evidence is still scarce (Dixit et al., 2020). The implications for impaired function of these proteins is important. They can range from dysregulation of homeostasis of the endocrine system to muscle weakness, and are involved in certain aspects of degenerative diseases (Pikuleva and Waterman, 2013). For example, mutations of *Cyp17a1*, a gene comprised within the GO terms (Table 18 and Table 19), leads to congenital adrenal hyperplasia, which affects the development of the gonads. Many genes obtained through our RNA-Seq experiments puzzlingly referred to spermatocytes, and reproductive organs (data not shown), but it is unclear how interference of cobalt with the protein product of this gene would affect older adults.

Nevertheless, there are other large GO terms linked with hormone homeostasis such as 'hormone metabolic process' in Table 18, or 'regulation of hormone levels', 'steroid binding', and 'hormone activity' in Table 19. Some of these are not directly related to steroid hormones, e.g. essential thyroid related genes (*Tshb*), whose deletion leads to hypothyroidism, and other GO terms such as 'response to retinoic acid'. This evidence together with previous results from the previous chapter (Chapter 5) make us suspect the suggestion that nuclear receptors could be possibly regulated by cobalt due to their metal ion binding activity ('Nuclear, Estrogen and Thyroid receptor superfamily (*Nrxyz, Esr, Thr*)' line in Table from section 5.2.7.; Chapter 5). Nuclear receptors may bind steroids, retinoic acid, or thyroid hormones, and this binding depends on the nuclear receptor zinc finger domain. Given that nuclear receptors control transcriptional regulation in a cell-specific manner and their activity is still not widely understood, it is difficult to relate their possible effects under the influence of cobalt (Sever and Glass, 2013). However, they define cellular identity and they are involved in *in vivo* synapse formation in the brain (Cao et al., 2020), and mitochondria energetics in the heart (Vega and Kelly, 2017) among other functions. We speculate that interference with these targets could lead to loss of function of tissues through interference with differentiation pathways given that some of the GO terms present in Table 19 are 'organ formation' and 'cell fate commitment', which could eventually lead to some of the conditions developed by patients with cobaltism. In addition, we also detected the CYP family to be expressed overall in Chapter 5 results (line 'Cytochromes P450

(*CYP*s)'; Table from section 5.2.7.; Chapter 5). This creates a chicken and egg situation since the CYP family synthesise some of the ligands that the nuclear receptors bind to, and other experiments will have to be performed to ascertain whether cobalt is binding to CYPs or to nuclear receptors and determine the initiating factor (Honkakoski and Negishi, 2000). Thus, the results obtained in this experiment link with those of Chapter 5.

To further understand the relationship between the GO terms we performed a PPI analysis of the genes located in brain parts which had accumulated significant amount of cobalt (pref. cortex and hippocampus at 0.5 and 1 mg/kg B.W. $CoCl_2$) from the hierarchical clustering in Fig. 42. This analysis is displayed in Fig. 43. The PPI displayed regulation of hormone levels consistently with the GO enrichment analysis, as well as a network of drug-metabolizing enzymes consisting of a few *Cyp*, *Ugt* and *Sult* genes. We also found an immune and haematopoietic axis centred around *Il6* with important chemokine presence. This immune response was also reflected in the GO enrichment from Table 19, but not from Table 18. Some of the immune-related GO terms are 'response to interleukin-6', 'T-helper 17 cell lineage commitment', 'response to interleukin-1', 'cell chemotaxis' and 'cytokine receptor binding', which suggest immune cell differentiation, activity and migration. This response might also occur in response to the activation of nuclear receptors, since it has been demonstrated that certain nuclear receptors are involved in the differentiation of T-helper 17 from $CD4^+$ T cells through the regulation of interleukin-1 leading to adaptive immune responses (Tanaka et al., 2018). Other researchers have reported the activation of nuclear receptors by interleukin-6 (IL-6), which resulted in upregulation of hepcidin (Radhakrishnan et al., 2020). The coding gene *Hamp* is also present in the PPI network (Fig. 43) and within the GO terms (Table 19), and it regulates iron homeostasis. Other factors related to blood coagulation such as *Hrg*, *Serpind1* and *Fga* are displayed on Table 19. Activation of the immune system and dysregulation of haematopoietic transcriptional programmes through the activation of nuclear receptors could lead to several autoimmune and blood disease syndromes. Cobalt was a usual treatment of anaemia, and polycythaemia and skin rashes were documented as a sporadic result of cobalt treatment (Paustenbach et al., 2013). The dermatological reactions in cobalt-treated anaemic patients were apparently more frequent in females (Paustenbach et al., 2013) which would agree with the endocrine and autoimmune response character

of nuclear receptor mediation. In addition, it is known that polycythaemia can be concealed when anaemia is present, and increase the risk of myeloid leukaemia (Kambali and Taj, 2018). MoM prostheses have not been found to increase the risk of developing any type of cancer (Brewster et al., 2013). Nevertheless, this relationship is especially worrying since our results suggest that cobalt could also regulate iron levels in parallel through hepcidin.

Finally, the PPI also reported the presence of 'GPI-anchored protein' related transcripts. This is a post-transcriptional modification that occurs mainly in the endoplasmic reticulum, where most glycosylphosphatidylinositol (GPI) synthesis proteins function (Kinoshita, 2020). It allows certain proteins such as enzymes, receptors, immune antigens and complement inhibitors to attach to the extracellular membrane. Thus, some of the functions could overlap with disrupted biological systems in cobaltism. However, the protein products of displayed genes in this group do not bind to metal ions in principle. To our knowledge there is no recognised link between GPI-anchored proteins and nuclear receptors. However, other protein products of the genes from Table 18 and Table 19 are located in the endoplasmic reticulum e.g., CYPs and UGTs, while the nuclear receptors can be outside or inside the nucleus. *In vitro* studies in a few cell lines have determined that cobalt accumulates preferentially in the nucleus and the perinuclear area (Bresson et al., 2013; Ortega et al., 2009; Shah et al., 2015), hence cobalt might affect preferentially metal-binding proteins in the nucleus and the endoplasmic reticulum. Regarding these points, significant highly upregulated DEGs such as *Hmgn5* are located in the heterochromatin supporting the nuclear envelope (Fig. 41), and although the function of *Mboat7l1* is unknown, the protein it takes its name from, *Mboat7*, is situated in the endoplasmic reticulum and modifies phosphatidylinositol in a way which is essential for brain development (Caddeo et al., 2019). We also observed that the protein product of *Mboat7*, as well as the GPI-anchored protein synthesis both depend on phospholipids, while the synthesis of steroid hormones is determined by cholesterol, hence, we suggest that cobalt modulates lipid metabolism.

It is possible that cobalt could modulate lipid metabolism directly as cobalt has been seen to affect the rigidity of lipid membranes such as liposomes (Umbsaar et al., 2018). However, some nuclear receptors such as LXRs and PPARs interact with

phospholipids and can regulate lipid metabolism. Indeed, the complete suppression of NADPH-cytochrome P450 oxidoreductase in the liver altered the expression of CYPs, as well as lipid and sterol metabolism through mediation of androstane and PPARs nuclear receptors, which led to the development of fatty liver and hepatomegaly phenotype (Weng et al., 2005). The expression of NADPH-cytochrome P450 oxidoreductase gene, *Por*, is very low and lacks significance throughout all doses and brain tissues in our results (data not shown). Thus, we do not expect cobalt to induce the exact same reaction. However, there are parallels between the activated transcriptional programs from the hepatic model of Weng and coworkers, and our results (Weng et al., 2005). Cobalt induced lipid and fat droplets, lipofuscin (Alexander, 1972; Auger and Chenard, 1967; Bonenfant, J.L., Miller, G., Roy, 1967; Bonenfant et al., 1969), and high concentrations of free fatty acids in some of the cobalt-containing beer drinkers (Sullivan et al., 1969). Lipid droplets were also present in the spleen of a patient with a CoCr prosthesis (Urban et al., 2004). Moreover, intracytoplasmic lipid and lipofuscin accumulation were found in a recent heart biopsy of a patient with arthroprosthetic cobaltism (Allen et al., 2014). In the same paper they reported that the patient developed cataracts, a common side effect of glucocorticoids, a type of steroid hormone. Another report on cobaltism also mentions cataracts (Apel et al., 2013) but this effect is not widely reported in relation to arthroprosthetic cobaltism.

Whether the initiating factor of toxicity is direct interference of cobalt with nuclear receptors or with Cytochrome P450 (CYPs), it is very likely that the resulting mediated toxicity occurs through the nuclear receptor-mediated toxicity given that the activity of CYPs and nuclear receptors is interconnected. Evidence of this is that our data reveals activation of transcriptional programs as a result of cobalt treatment. This type of toxicity can be compared to that of endocrine disrupting chemicals, where there is no monotonous dose response, because the toxicity is not directly elicited through a target protein, but through receptor-activated signalling, in our case perhaps leading to “transcriptional toxicity”. The dose response would not be deterministic but stochastic (Kanno, 2016). Although a theoretical threshold of 100μg/l cobalt in blood for the development of cobalt systemic toxicity was mentioned in previous chapters, there are patients over that dose with no symptoms, while other cases have reported cobaltism at lower concentrations e.g. Mao *et al.* reported two patients with 410nmol/l (24 μg/l)

and 185 nmol/l (11 μg/l) serum cobalt level with neurotoxicity and other cobalt-derived conditions (Mao et al., 2011).

Kanno hypothesises that these type of receptor-mediated toxicities will lead to 'low frequency of affected subjects among those exposed' (Kanno, 2016), which seems to correspond with the pattern of publications on cobalt toxicity. Cobalt remains in the body of patients for up to years at noticeable concentrations and its actual toxicological importance is currently being discussed. In our opinion, there will be more chances for cobalt ions to interact with CYPs or nuclear receptors if there are higher cobalt concentrations in blood. Nevertheless, the blood cobalt levels obtained for the concentrations used in this experiment here range from 4-38μg/l and may have already resulted in hormone transcriptional activity (Table 18). Significant levels of cobalt in rats' blood, 17.0 ± 2.8 and 38.2 ± 2.1μg/l, may have led to cell fate commitment, as well as the activation of haematopoietic and immune transcriptional programs (Table 19). These levels of cobalt in blood are similar to those found in some asymptomatic MoM patients (Langton et al., 2013). Does this mean that MoM patients within the same cobalt blood range should be further evaluated for systemic cobalt toxicity symptoms? The implications of these results for MoM patients will depend on whether these transcriptional changes extend to the protein domain. Future research would be needed to validate this hypothesis, in the meantime, we should be cautious about pondering the repercussions of these transcriptional results.

To sum up, we found that the common transcriptional response to cobalt involved hormone and drug-metabolising activity, in addition to also describing a powerful immune response perhaps mediated by inteleukin-6 (IL-6). An underlying dysfunction in lipid metabolism is also likely. Through previous results from Chapter 5 section 5.2.7., we hypothesise that these mechanisms have been instigated by the activation of nuclear receptors, perhaps as a consequence of cobalt ion binding and substitution of their native zinc finger domains, or as indirect regulation through their ligand synthesising CYPs. Unfortunately, we did not appreciate this relationship until after the selection of targets for RT-qPCR and immunoblotting, thus future research will have to validate this hypothesis.

Finally, after manual examination of DEGs, we noticed that many of the genes found in the pref. cortex and hippocampus tissues with significant cobalt accumulation (Fig. 42) were characteristic of the choroid plexus: *Cldn2*, *Ttr*, *Slc4a5*, *Aqp1*, *Otx2*, *Clic6*, *Sostdc1*, *Tmem72* among many others. Given that the choroid plexus is a fairly understudied organ, the large presence of its typical genes in our data has likely influenced the low percentage of genes from our dataset represented in the GO Terms (Table 18 and Table 19) since these genes are also less known. If more of these genes were investigated within the context of the choroid plexus we would be able to draw more conclusions about the effect of cobalt in this brain part.

6.3.4. The choroid plexus as a target of cobalt toxicity

We found genetic markers in the pref. cortex (Fig. 44), hippocampus (Fig. 45), and cerebellum (Fig. 46) almost exclusively attributable to the choroid plexus, e.g. *Clic6*, *Klotho* (*Kl*), transthyretin (*Ttr)*, *Veph1*, some cilia markers and *Scl* transporters. The molecular characterisation of the choroid plexus has only been achieved recently (Lun et al., 2015), and unfortunately the GO ontologies have not been adequately updated to report its presence in our data. The function of the protein products from many of these genes is still not well researched. Nevertheless, the appearance of choroid plexus featured genes is widespread. This is especially true in the hippocampus (Fig. 45), while the presence of these markers appears to be less frequent in the pref. cortex.

The choroid plexus is anatomically attached to the hippocampus and its joint dissection can go unnoticed when doing a fast isolation as reported by specialist in the choroid plexus (Mathew et al., 2016; Stankiewicz et al., 2015). In fact, several studies investigating the effect of drugs or other interventions in the hippocampus have knowingly or unwittingly reported choroid plexus markers (Cho et al., 2015; Schneider et al., 2011; Stankiewicz et al., 2015). There are also markers of the choroid plexus such as transthyretin (*Ttr*) and *Akap14* in the pref. cortex, and it is possible that part of the choroid plexus has also been included in other brain samples than the hippocampus since the choroid plexus is distributed through all brain ventricles (Stankiewicz et al., 2015). The choroid plexus transcriptome is heterogeneous across the different ventricles (Lun et al., 2015), which could explain why we find different markers depending on the brain area location. The downside of having choroid plexus

contamination in our data is that we will not be able to ascribe the transcriptomic response to cobalt solely to the hippocampus or pref. cortex, and therefore, we will be unable to understand the full extent of metal toxicity in these brain areas. However, all brain parts were dissected following the same procedure, and we expect the gene expression of the pooled samples to be consistent. Therefore, these results suggest that brain cobalt toxicity might occur early on in the choroid plexus. This is reflected in the fact that we not only find choroid plexus markers, but also many of these choroid plexus genes have been implicated in stress processes in the choroid plexus (Mathew et al., 2016): *Tmem72*, *Sostdc1*, *Cldn2*, *Slc4a5*, *Aqp1*, etc.

Perhaps because of its difficulty of dissection and the scarcity of literature, the choroid plexus has been a neglected target in the field of Toxicology. As we mentioned in in section 4.3.2. from Chapter 4, cobalt has been detected 20-40 times higher in the CSF of prosthetic patients than in non-exposed individuals (Rizzetti et al., 2009; Steens et al., 2006; Tower, 2010). However, different studies reveal that heavy metal preferentially accumulates early on in the choroid plexus. For example, manganese accumulates in the choroid plexus and the anterior pituitary gland after a single dose in contrast to brain areas protected by the blood brain barrier in mice (Watanabe et al., 2002) and humans (Sudarshana et al., 2019). The choroid plexus also seems to accumulate lead in goats (Steuerwald et al., 2014) and humans (Manton et al., 1984), and a recent transcriptomic study on the effect of lead in the hippocampus of rats reported choroid plexus markers unknowingly (Schneider et al., 2011). In rats the choroid plexus retained cadmium from the systemic circulation sealing the brain from the passage of toxins (Takeda et al., 1999). Moreover, pathological changes due to methylmercury dosage in rats' brain matter were not observed until weeks after initial damage to the choroid plexus (Nakamura et al., 2011). Harrison-Brown *et al.* discovered that the penetration of cobalt in the CSF of MoM patients is limited to 15% of the cobalt in plasma (Harrison-Brown et al., 2020). They also found a nonlinear trend with a ceiling effect in the CSF cobalt accumulation in relation to Co plasma levels in blood. Thus, the choroid plexus could function as an absorptive barrier, and early cobalt accumulation and damage in the brain might occur in the choroid plexus. Brain areas such as the hippocampus, the cortex and the cerebellum might endure toxicity after prolonged choroid plexus exposure and filtration of cobalt to the CSF.

Although with our data we cannot investigate the way in which cobalt affects the function of the choroid plexus, we could speculate that some important functions might be affected. For example, it is likely that there will be cobalt competition with calcium. Calcium regulates bicarbonate secretion synergistically with cAMP, which directly impacts fluid production and pH in epithelial cells like those in the choroid plexus (Jung and Lee, 2014). There are also several ciliary markers noted in the RNA-Seq data such as *Akap14, Daw1,* and *Ak7* (Fig. 44). The obliteration of cilia leads to increased levels of cyclic AMP (cAMP) and chloride, ultimately blamed for the increased CSF production in hydrocephalus. Hydrocephalus is a condition that can affect memory, mood and balance but that has very rarely been reported in relationship to metal poisoning (Silva Sieger et al., 2012). Chloride induces the secretion of fluid through the action of cAMP, and this process happens to be regulated by phosphodiesterases in the kidney, particularly *Pde4* (Pinto et al., 2016), which appeared in section 5.3.7. of Chapter 5. Carbonic anhydrases, the other family of genes studied in Chapter 5, are directly involved in the production of CSF by the choroid plexus (Janssen et al., 2013). Metabolic acidosis could be one of the advanced signs of cobalt toxicity (Alexander, 1972), that we previously eluded to a possible dysfunction of carbonic anhydrase in section 5.3.7. of Chapter 5. Moreover, cobalt chloride at concentrations that established hypoxia *in vitro* altered renal epithelial transport, in particular by the direction of sodium secretion, and was also found to alter trans-epithelial permeability (Nag and Resnick, 2017).

Furthermore, in another example in which the effects of cobalt differed from hypoxic conditioning, cobalt obliterated capillary alterations (Peters et al., 2005), in contrast to hypoxia which increased their number. The choroid plexus capillaries are paramount to the production of CSF, and impaired perfusion might lead to intracranial hypotension. The symptoms of this condition are nausea or vomiting, neck pain, tinnitus, other hearing and visual disturbances, cognitive and movement disorders (D'Antona et al., 2021). There are no data referring to the response of the choroid plexus to cobalt, but in the eye, anomalous choroidal perfusion in response to cobalt was noted in angiography experiments, and suspected as the possible cause of retinopathy in cobaltism cases, in addition to dysfunction of the retinal pigment epithelium (Lim et al., 2015). In addition, Klotho (*Kl*) and tight junction marker Claudin-2 (*Cldn2*) gene expression were also present in the data and from the

literature. It is known that Klotho regulates the permeability of the barrier leading to inflammation and immune activation in the choroid plexus (Zhu et al., 2018). Tight junctions seal the unions between choroid plexus epithelial cells (Ghersi-Egea et al., 2018), and chemical hypoxia elicited by cobalt has been shown to disrupt these junctions in an *in vitro* model of brain microvascular ischemia (Page et al., 2016).

In addition, the cachexia-related Gdf15 protein that is normally induced in the liver, has also been found to be produced *in vitro* in choroid plexus cells (Kosa et al., 2020). We wonder whether the choroid plexus could secrete *Gdf15* if cobalt directly damages or modulates the activity of this structure leading to feeding changes. Moreover, very recently, modulation of *Otx2* expression in the choroid plexus has been seen to regulate anxiogenic behaviour in mice (Vincent et al., 2021), and in two studies the choroid plexus transcriptome quickly responded to stress tests in mice (Mathew et al., 2016; Stankiewicz et al., 2015). Given that the choroid plexus has been implicated in depression disorders (Turner et al., 2014), and that some patients with elevated cobalt levels in blood showed signs of neuropsychiatric symptoms such as depression (Green et al., 2017; Tower, 2010), we might speculate that cobalt toxicity in the choroid plexus could impair its function, and contribute towards mood dysregulation.

The choroid plexus is also a place for steroid hormone biosynthesis (Quintela et al., 2013) and it hosts metabolising enzymes to deal with and metabolise xenobiotics (Gradinaru et al., 2009). PathView software detected the steroid hormone biosynthesis pathway as significantly enriched with the following DEGs: *Cyp11a1*, *Cyp17a1*, *Cyp3a23/3a1*, and *Ugt1a1* (Fig. 56 displayed in Appendix D). The protein translated from the gene *Cyp11a1* is located in the inner mitochondrial protein and catalyses the conversion of cholesterol to pregnenolone, which is the precursor of steroid hormones produced in the adrenal cortex, ovaries and testes (Midzak and Papadopoulos, 2016). It is not surprising to find a transcript such as *Cyp11a1* in the data given the functions of the choroid plexus as a steroidogenic and sex hormone regulated organ (Quintela et al., 2013). Since the first steps of steroidogenesis occur in the mitochondria (Midzak and Papadopoulos, 2016), and cobalt is known to induce mitotoxicity, *Cyp11a1* and its translated protein could be used to monitor both mitochondrial function and steroidogenesis in the choroid plexus. The choroid plexus is an important source of cholesterol for the brain (Achariyar et al., 2016; Fujiyoshi et al., 2007), and

pregnenolone has also been detected in the CSF (Santos et al., 2017). After pregnenolone synthesis, the protein produced from *Cyp17a1* subsequently leads the conversion of pregnenolone to androgen precursors and cortisol (Alexander et al., 2011). The function of *Cyp3a23/3a1* is still being researched but *Ugt1a1* metabolises bilirubin and other xenobiotics to ease its excretion, but as other proteins from the UGT family it could also be involved in the glucuronidation of steroid hormones (Mazerska et al., 2016). Metals are known to influence the synthesis of hormones or precursors such as pregnenolone, and cobalt is known to bind with corticosteroids (Stevenson et al., 2019), thus it might be interesting to research whether cobalt interferes with any of these proteins or their synthesised products. The following genes were observed in the haematopoietic cell lineage pathway retrieved by PathView (Fig. 57 displayed in Appendix D): *Cd19*, *Fcer2*, *Cd8a*, *Cd3g*, *Il1r2* and *Il6*. Most of these genes belong to cluster of differentiation (CD) antigens, which are surface markers expressed in cells that allow for the identification of certain cell types mainly of immune origin, and that is the case of lymphoid white blood cells (Christopherson, 2008). We revised the origin and function of these differentiation markers through the NCBI Entrez gene database (Gene [Internet]. NCBI Entrez Gene Database, 2004), and they correspond to B (*Cd19* and *Fcer2*) and T-lymphocyte (*Cd8a* and *Cd3g*) antigens. The brain parenchyma is thought to be an "immune-privileged site" since apart from microglia it is, in general, devoid of cells from the adaptive immune system (Ghersi-Egea et al., 2018). However, many immune cells are resident in the choroid plexus, which works as the site for immune trafficking with the brain (Ghersi-Egea et al., 2018). B and T lymphocytes can infiltrate the choroid plexus and affect its function under certain challenges, thus leading to inflammation (Baruch et al., 2013; Stock et al., 2019; Zhu et al., 2018). The presence of these CD markers together with other genes involved in cytokine activity such as interleukin 1 receptor type 2, *Il1r2,* and interleukin 6, *Il6*, might be indicative of inflammation within the choroid plexus in response to cobalt. Moreover, looking at Table 19 we found parallel GO terms retrieved by the Cytoscape software such as 'cell chemotaxis' and 'cytokine receptor binding' which contain some of these genes in addition to other DEGs of interest. In particular, the 'cell chemotaxis' GO term includes *Cxcl13* a chemokine that recruits B lymphocytes, and it has been involved in lymphoid infiltration in the choroid plexus in a mouse model of neuropsychiatric lupus (Stock et al., 2019). We previously mentioned that activation of the nuclear receptors might affect each tissue differently. It is possible that the activation of nuclear receptors would

have triggered haematopoietic and immune responses specifically in the choroid plexus because it is the niche for immune cells in the CNS and it is naturally enriched for genes involved in heparin binding (Lun et al., 2015). In the future, researchers might want to consider evaluating the markers of inflammation and lymphoid cell activation emphasised by PathView, as well as the steroidogenic activity in the choroid plexus in response to cobalt.

In summary, though hydrocephalus would be very unlikely to occur in response to cobalt poisoning, cobalt toxicity in the choroid plexus could modulate CSF secretion and be implicated in some of the symptoms reported by arthroprosthetic cobaltism patients such as anorexia, irritability, and loss of memory. The inclusion of the choroid plexus inadvertently during dissection of the brain tissues could have interfered with the interpretation of the overall transcriptional changes. Conversely, given that the choroid plexus partially shares hepatic and kidney detoxification functions (Johanson et al., 2011; Sathyanesan et al., 2012), and that as a capillary network it becomes the first point of contact of cobalt with CNS tissue, we could argue that not incorporating the choroid plexus during dissection would have made the identification of mechanisms for cobalt toxicity more difficult in the CNS.

6.3.5. Validation of protein and gene expression in response to cobalt

Previous research investigating validation of RNA-Seq gene expression has shown 100% RT-qPCR confirmation rate on those genes that were both statistically significant and had high fold change in the RNA-Seq data (Black et al., 2014). These were also our conditions to select DEGs of interest in the pref. cortex and hippocampus: $|\text{fold change}|>2$ and $p<0.05$. However, as can be observed from our RT-qPCR results (Fig. 47) the fold-change values do not always correspond with those obtained from the RNA-Seq data, especially in the case of *Tnf* and *Ttr* in the pref. cortex. We looked back at the original RT-qPCR files and did not find any evidence that the designed primers were not working correctly. It is known that a few genes will produce inconsistent results across RT-qPCR and RNA-Seq platforms (Everaert et al., 2017). However, it is possible that improved primer design would retrieve inconsistent changes, and we should be cautious to extract conclusions about the validity of RNA-Seq data based on limited RT-qPCR results.

Fig. 48 shows that the ΔC_T values of individual samples are within a broad range and the standard errors of the mean (SEMs) are wide, particularly for the hippocampus samples. As a result, none of the genes selected for RT-qPCR screening had significant changes in transcript levels (Table 20). However, the ΔC_T mean and SEM also indicate a biological change in the amount of target mRNA transcripts in the case of *Spata18* and *Akap14*, although these changes are not significant. The example of *Kl* is not at all clear because of the wide SEM compared to the ΔC_T mean. This lack of significance has its roots in the technical differences between RT-qPCR and RNA-Seq, the low number of replicates used (n=4), and the consequences of using pooled samples in our research design setting.

For example, normalisation techniques are not the same for RNA-Seq and RT-qPCR. RT-qPCR is taken as the gold standard for quantification of mRNA levels but the stability of housekeeping genes might affect the resulting gene expression, while the normalisation method has an important impact on RNA-Seq fold change and statistical significance (Black et al., 2014). Moreover, although the sample evaluated was the same, there could be variations in the sample preparation after RNA isolation. The method of pooling would have averaged the within-group variability of the final analysed sample and reduced the level of transcriptional noise of DEGs with very low fold changes (Takele Assefa et al., 2020). This method allowed us to detect the effect of cobalt in the transcriptome with n'=1, which we did, and we could also confirm the absence of a dose response, as well as a possible mechanism of cobalt toxicity within the cobalt range used, all with a limited budget. However, this procedure also meant that the individual variations of DEGs were not considered. In the case of tissue samples, the composition of the tissues might vary between samples, which is especially relevant in our case since we did not take into account the inclusion of the choroid plexus. Moreover, the response to cobalt appears to be subtle and in humans is nevertheless very heterogenous. Thus, individual sample variability is a natural consequence of the research design and perhaps future research with similar requirements might need to increase the number of samples to account for it, as well as to counteract outliers. However, this solution will considerably increase the costs of the RNA-Seq analysis. The price of sending samples to be analysed is lowering each year and more laboratories are opting to analyse individual samples. Despite the lack

of significance, the fold expression of evaluated DEGs from RNA-Seq and RT-qPCR in this chapter as well as those in section 5.2.8. from the time-response experiment presented in Chapter 5 do correlate in general. This is consistent with previous high-throughput comparison between the two technologies (Everaert et al., 2017). Thus, the selected genes could have a significant function in the etiology of cobalt toxicity.

Although we were also interested in the hippocampus, there was not enough tissue to carry out Western blots in this brain part after we assigned it for metal content and RNA analysis. We selected TNF-α, Spata18, Angiogenin, transthyretin (Ttr), and Akap14 from pref. cortex due to their high expression and statistical significance across doses in the brain area. We also evaluated these targets by immunoblotting in the cerebellum because some were moderately expressed at 1 mg/kg B.W. $CoCl_2$ cobalt dosage (data not shown), which is the concentration chosen for RT-qPCR and immunoblotting testing.

TNF-α is a widely acknowledged role player in inflammation and apoptosis in the brain. However, its homeostatic function is also seen as essential in the brain by its involvement in the formation of synapses, myelin regeneration and in granting neuroprotection over toxic and traumatic injuries (Probert, 2015). Although TNF-α is generated basally by brain cells such as neurons and glia, it is normally assumed to be produced by immune cells (Probert, 2015). The concept of immune privilege in the brain has been refuted in recent years, and it is now acknowledged that both immune and CNS systems are connected. Indeed, the choroid plexus hosts immune cells and acts as an immune cell gatekeeper to the brain (Zhu et al., 2018). The presence of immune markers such as *Tnf* indicates that neuroinflammation could be occurring in response to cobalt toxicity either in the pref. cortex or the choroid plexus. For example, TNF-α is highly up-regulated in the choroid plexus of the brains of patients with Alzheimer's disease (Steeland et al., 2018). However, gene and protein expression results are discordant in our study.

In addition, we also evaluated the protein expression of Angiogenin (*Ang*). This gene is also implicated in inflammation, but it is mainly known for inducing angiogenesis and regulating metabolism (Sheng and Xu, 2016). In that regard, the choroid plexus contains a network of capillaries, which might show angiogenic activities (Lun et al.,

2015), while cobalt has been implicated in obliteration of small capillaries (Peters et al., 2005). Due to COVID-19 lockdown pressures, we did not have enough time to order and utilise a primer set to evaluate the RT-qPCR gene expression, but the protein expression was not significant.

Mitochondrial damage was a feature of cobalt toxicity in the Quebec Beer Drinkers, together with ER stress and myofibril damage. These findings have also been reported in recent years in papers about MoM patients (Allen et al., 2014; Choi et al., 2019; Goode et al., 2012). The protein product of *Spata18* aka mitochondria-eating protein (Mieap) has been implicated in the quality control of mitochondria. As its name indicates it removes damaged mitochondria, therefore reducing ROS levels. Contrary to the RNA-Seq results, neither gene expression by RT-qPCR nor protein expression were significantly up- or down- regulated. However, RT-qPCR gene expression correlated with that of RNA-Seq results.

Transthyretin is involved in the transport of thyroid hormones and retinol, and its widespread expression across the data could perhaps be indicative of a problem with its secretion by the choroid plexus (Fig. 39). The 'response to retinoic acid' GO term was present in Table 18 associated with DEGs across all doses and brain parts. The impairment of thyroid function has also been reported as a symptom of cobalt toxicity in the cases of Quebec Beer Drinkers (Alexander, 1972; Bonenfant, J.L., Miller, G., Roy, 1967; Bonenfant et al., 1969), and is also cited with high prevalence in patients with arthroprosthetic cobaltism (Gessner et al., 2019). Moreover, previous studies in rats have shown that direct cobalt application in the brain increases the level of transthyretin (Kajiwara et al., 2008). In addition, we also evaluated protein expression of Akap14, a highly expressed gene in the pref. cortex (Fig. 44), related to cilia function (Kultgen et al., 2002), which could potentially alter CSF circulation and cAMP levels (Banizs et al., 2005). It has appeared in a previous study of the choroid plexus (Bowyer et al., 2013). However, neither of these markers reported significant changes in protein expression (Fig. 49 and Fig. 50).

There could be a few reasons behind the incongruity between gene and protein expression. The simplest explanation is that, although during dissection we took brain parts from the same brain area for analysis, the pieces of tissue destined for gene

expression and immunoblotting evaluation would have been adjacent regions within the same brain area. Thus, the high gene expression could correspond to a specific location that was not present or dominant in the region utilised for protein expression evaluation. The brain is a highly regionalised area with important cellular diversity, and gene expression might vary greatly across cellular subpopulations (Sugino et al., 2019).

Furthermore, the high fold-change of choroid plexus markers indicate that it is somehow greatly impacted by the effects of cobalt. Since we did not account for contamination of this brain area in our samples, it could have been inconsistently included in different tissue sections resulting in different gene and protein expression. Whether these markers belong to the choroid plexus should be investigated further in the future. New research might take these possibilities into consideration, and double the number of animals to parallel gene and protein expression analyses. Microdissection or microscopy techniques could be a useful tool to respectively select or identify the same areas with precision.

Other factors different from technical issues might contribute, e.g. previous *in vitro* research indicated that cobalt might not be a good model for retinal ischemia in contrast to hypoxic atmospheres because gene and protein expression were discordant, although results agreed *in vivo* (Tang et al., 2017). Some groups have already reported the presence of highly expressed transcripts without corresponding translated protein after comparing RNA-Seq data with high-throughput protein detection methods (Denninger et al., 2020). Presently, there is an agreement on our limited understanding about the relationship between the regulation in the transcriptome and the resulting protein synthesis (Liu et al., 2016). Thus, many factors could be implicated in the disagreement between gene and protein expression, from technical issues, the direct effect of cobalt, or the relationship between transcriptional and translational layers.

6.3.6. The nucleus, a besieged organelle?

Although we did not have time to assess all the interesting genes through RT-qPCR and immunoblotting, we found certain markers *a posteriori* in the RNA-Seq that deserve attention. A common gene appearing in the DEG lists across different brain tissues is High Mobility Group Nucleosome Binding Domain 5 (*Hmgn5*) aka Nucleosome-Binding Protein 1 (*Nsbp1*), which was also present in the results of the time-response experiments in Chapter 5 (section 5.2.4.). This gene also arose in RNA-Seq data from the hearts of cobalt-treated rats in the study of one of our colleagues (unpublished PhD thesis, S. Laovitthayanggoon, 2018, University of Strathclyde) with the following fold changes: 8.31-fold change at 7 days treatment, and 8.79-fold change after 28 days of cobalt exposure (1 mg/kg B.W. $CoCl_2$, following the same procedures as in the current study). In contrast with the heart, the expression of *Hmgn5* in the brain was generally highly down-regulated (Table 24). Although *Hmgn5* appears up-regulated in the higher cobalt dosage: 1 mg/kg BW. It is possible that *Hmgn5* is homeostatically controlled and changes its regulation at higher doses. Through ICP-MS cobalt content analysis in organs, we know that cobalt in the heart is higher than in any of the brain areas (Fig. 34). It is conceivable to think that at higher cobalt levels the expression of certain genes might be reversed. This effect has been observed in transcriptomic studies when comparing sub-toxic and toxic concentrations of manganese *in vitro* (Fernandes et al., 2019). In the case of cobalt, more doses and higher concentrations would be needed to test this hypothesis.

Table 24: *Hmgn5* (p<0.05) fold change in the pref. cortex, cerebellum and hippocampus of rats dosed during 28 days with i.p. injections of 0.1, 0.5, and 1 mg/kg B.W. $CoCl_2$ or dH_2O (controls). Overexpression is indicated in bold. The origin of the *Hmgn5* gene expression from the first experiment refers to the values obtained in the time-response study described in Chapter 5 (section 5.2.4.).

Hmgn5 fold change	Dose (mg/kg B.W.)			
	0.1	0.5	1	1 (1st experiment)
Hippocampus	- 10.0	- 10.0	- 10.0	-
Pref. cortex	- 6.1	- 6.1	**3.0**	- 8.1
Cerebellum	- 7.5	- 7.5	**0.2**	**7.0**

Bustin *et al.* overexpressed *Hmgn5 in vitro* and *in vivo* (Furusawa et al., 2015). The main result of *Hmgn5* overexpression was the decompaction of heterochromatin with corresponding weakening of the nuclear envelope lamina, and loss of nuclear rigidity. Overall, they found misshapen and enlarged nuclei with little or no heterochromatin. At birth the studied mice were healthy, however, adults showed heart hypertrophy and cardiac function worsened over time.

Apart from Quebec, cobalt beer poisoning also occurred in Belgium, Omaha, and Minneapolis. The clinicians from Omaha comprehensibly analysed several cases of cobaltism finding ubiquitous extreme cardiomegaly, which most times was generalised across the heart chambers or, in fewer instances, exaggerated in the left ventricle, and occasionally accompanied by pericardial effusion (Sullivan et al., 1969). These findings support the previous reports from Quebec (Barborik and Dusek, 1972; Bonenfant, J.L., Miller, G., Roy, 1967; Morin et al., 1969), Belgium (Kesteloot et al., 1968), and Minneapolis (Alexander, 1972), as well as recent papers of patients affected by cobaltism due to metallic hip prostheses (Allen et al., 2014; Choi et al., 2019; Gilbert et al., 2013; Machado et al., 2012; Zywiel et al., 2013). Also, hepatomegaly was found in a few reports (Bonenfant, J.L., Miller, G., Roy, 1967; Morin et al., 1969; Sullivan et al., 1969), as well as occasional distention of veins and arteries (Morin et al., 1969), and sometimes capillaries (Bonenfant, J.L., Miller, G., Roy, 1967). Although the latter indications could also result as a consequence of the accompanying heart condition. Loss of cell wall integrity would also explain the pleural, pericardial and peritoneal effusions (Alexander, 1972; Bonenfant, J.L., Miller, G., Roy, 1967; Morin et al., 1969; Sullivan et al., 1969), as well as the oedema or mural thrombi (Alexander, 1972; Barborik and Dusek, 1972; Bonenfant, J.L., Miller, G., Roy, 1967; Morin et al., 1969). The aetiology of cobaltism is unique and unusual with regards to common diseases, being more suggestive of rather rare conditions such as capillary leak syndrome (Kapoor et al., 2010) or thiamine deficiency, also known as beriberi.

The reason behind the high expression of *Hmgn5* could involve cobalt uptake. A few *in vitro* studies have determined that cobalt accumulates in the nucleus of osteoblasts (Shah et al., 2015), keratinocytes (Ortega et al., 2009), and lung epithelial cells (Bresson et al., 2013), as well as in the perinuclear area of keratinocytes and osteoblasts. The endoplasmic and sarcoplasmic reticulum are continuous with the

nuclear envelope, and calcium fluctuations extend from one structure to the other (Subramanian and Meyer, 1997; Wu and Bers, 2006). Several reports mention the sarcoplasmic reticulum to be severely dilated by cobalt (Alexander, 1972; Auger and Chenard, 1967; Bonenfant et al., 1969; Knieriem and Herbertz, 1969; Rona, 1971; Zadnipryany et al., 2017), sometimes with the presence of odd whorled vesicles in its lumen (Auger and Chenard, 1967), while the Golgi apparatus, the sarcoplasmic membranes and most of the nuclei remained intact (Auger and Chenard, 1967; Bonenfant et al., 1969). In brain tissue, Caltana *et al.* found enlarged endoplasmic reticulum after direct cobalt hemisphere injection, as well as oedematous perinuclear areas (Caltana et al., 2009). Misshapen mitochondria and nuclei were also found. In previous chapters we discussed the role of calcium in mitochondria homeostasis. However, both the sarcoplasmic reticulum in myocytes and endoplasmic reticulum in other cells, as well as the nuclear envelope function are regarded as important calcium stores (Mauger, 2012). We have mentioned before that calcium signalling appears to be impaired in models of cobalt toxicity (Karovic et al., 2007; Shah et al., 2017). Moreover, heterochromatin can modulate nuclear stiffness quickly through calcium in response to tissue stretching so as to protect nuclear integrity (Nava et al., 2020). In contrast, heterochromatin can also harden the nucleus to facilitate cell migration (Gerlitz, 2020). Extracellular divalent ions have also been seen to increase heterochromatin levels by its interaction with mechanosensitive ion channels in a variety of cells (Stephens et al., 2019). Hence, it is possible that cobalt interference with calcium limits the ability of cells to withstand mechanical stress though the modulation of heterochromatin compaction. Other possibility is that cobalt interference with lipid metabolism could affect the double lipid bilayer of the nuclear envelope, which is more elastic than the plasma membrane through an increased composition of phosphatidylinositol (PI) lipids and cholesterol (Dazzoni et al., 2020). *Hmgn5* expression changes could represent a homeostatic mechanism to control the nucleus mechanical characteristics through heterochromatin. Cobalt has been shown to affect the mechanical rigidity of lipid membranes (Umbsaar et al., 2018), and we have previously discussed other genes involved in lipid metabolism present in the RNA-Seq data such as *Cyp11a1*, *Mboat7* and those related to GPI-anchored protein synthesis.

Strangely, some macrophages obtained from MoM periprosthetic tissue revealed a distorted membrane conformation in which the outer nuclear membrane was separated

from the inner membrane (Goode et al., 2012). Osteocytes exposed to cobalt and chromium *in vitro* also had impaired responses to shear stress (Shah et al., 2017). Different cell types endure unique mechanical strains that impact their nucleus (Jahed and Mofrad, 2019), for example, by cells being squeezed during diapedesis or immune cell extravasation, as well as through shear stress in epithelial, endothelial and bone cells, or myofibril contraction in muscle. Perhaps the unique mechanical strains that cell types endure could lead to distinct damage and impairment features if the nuclear membrane was weakened.

Furusawa *et al.* showed that *Hmgn5* is also strongly expressed in the brain (Furusawa et al., 2015). It is difficult to imagine the effect that loss or gain of heterochromatin would have on the mechanics of brain cells since they are not thought of as being mechanically active during adulthood. There are only a few examples of osmotically active neurons and microglia which have been studied in this regard (Bollmann et al., 2015; Prager-Khoutorsky, 2017). Of course, the choroid plexus is a tissue that endures different mechanical strains, and CSF circulation will have a mechanical impact in brain cells. However, chromatin decompaction by Hmgn5 not only has an effect in the mechanical characteristics of the cell, it also adjusts cell-type transcription fidelity, thus modifying the transcriptional profile of cells with unknown consequences (Kugler et al., 2013; Rochman et al., 2009). Moreover, in brain cells Hmgn5 facilitates neurite outgrowth and is transported from the nucleus to the growth cones (Moretti et al., 2015), but whether cobalt affects synaptogenesis is unknown. In any case, these studies in Hmgn5 suggest that there may be a layer of epigenetic modifications underlying cobalt toxicity, and further studies might be warranted to investigate this aspect.

Furthermore, activation of nuclear receptor transcriptional programmes needs to be investigated first by altering chromatin states (Biddie and John, 2014). It is unknown whether Hmgn5 is part of the molecular machinery utilised by nuclear receptors to regulate transcription. In theory, heterochromatin modification is a possible mode of transcriptional regulation for nuclear receptors (Sharma et al., 2014), and glucocorticoid steroid hormones have also been observed to increase H3K27me3, a mark of heterochromatin, in the nuclear periphery of macrophages (Misale et al.,

2018). This is a far-fetched hypothesis, but it would be interesting to study considering the plausible implication of nuclear receptors in cobalt toxicity.

In Quebec Beer Drinkers, the predominant histological features appeared to be the disintegration of myofibrils and contractile elements, distorted mitochondria, and dilated sarcoplasmic reticulum (Alexander, 1972; Auger and Chenard, 1967; Bonenfant, J.L., Miller, G., Roy, 1967; Bonenfant et al., 1969), similar to what occurred in rat models of cobalt toxicity (Knieriem and Herbertz, 1969; Rona, 1971; Zadnipryany et al., 2017). This peculiar characteristic was also present in the heart of a patient with a DePuy ASR prosthesis (Allen et al., 2014). Additionally, also excessive glycogen and vacuolation of the cytoplasm were reported (Bonenfant, J.L., Miller, G., Roy, 1967), as well as damage to other muscle contractile elements (Alexander, 1972). Damage to nuclei was not considered pronounced and, in some cases discarded as an important factor of cobalt toxicity as there were no apparent changes in the majority of the nuclei (Auger and Chenard, 1967; Bonenfant et al., 1969). In the few cobalt-histological papers available from the Quebec Beer Drinker cases other nuclear findings were reported, such as nuclei swelling (Bonenfant, J.L., Miller, G., Roy, 1967), and exaggerated folding of some of the nuclear membranes in heart muscle (Auger and Chenard, 1967). A more recent paper also stated remarkable nuclear indentations in brain cortical tissue after direct cobalt injection into one of the brain hemispheres (Caltana et al., 2009).

Hyperchromatic or densely stained nuclei were also observed with the intake of high levels of cobalt in Quebec Beer Drinkers (Alexander, 1972; Bonenfant, J.L., Miller, G., Roy, 1967), and also in a rat model of cobaltism more recently (Zadnipryany et al., 2017). *In vitro*, several authors have reported nuclei with condensed chromatin after cobalt exposure in brain and stem cells, which they considered a marker of apoptosis (Jung et al., 2007, 2008; Jung and Kim, 2004; Karovic et al., 2007; J.-H. Lee et al., 2013; Li et al., 2015). In nervous tissues, rabbits treated with high levels of cobalt also displayed ganglion cells with pyknotic nuclei and shrunken cytoplasm (Apostoli et al., 2013). Nuclear condensation and cellular shrinkage also occurred in explant tissue from the cochlea after cobalt exposure (Li et al., 2015). These cases could simply point towards cobalt-induced apoptosis *in vivo*, rather than an alternative mechanism of chromatin condensation induced by divalent ions (Stephens et al., 2019).

A recent rat model of cobaltism showed not only pyknotic nuclei, but also particular changes in the chromatin, such as disintegration and disarranged patterns, although the authors only described these phenomena in the text (Zadnipryany et al., 2017). The authors of this paper pointed out that nuclear alterations occurred concurrently with the changes in the myocyte cytoplasm (sarcoplasm), and that the myofibrils in the perinuclear area seemed more affected by the effect of cobalt than those in the periphery. Bonenfant *et al.* also noted that myofibrils tended to be situated near the peripheral sarcoplasmic membrane but could not find an explanation for this phenomenon (Bonenfant, J.L., Miller, G., Roy, 1967). Our colleague S. Laovitthayanggoon reported breakage of actin filaments after low cobalt concentration treatment (5μM) for 3 weeks *in vitro* (unpublished PhD thesis, S. Laovitthayanggoon, 2018, University of Strathclyde). She described that phalloidin-stained actin location had moved away from the nucleus to the cell membrane border. This suggested that the actin cap, which is connected to the nuclear envelope, had become disrupted (Khatau et al., 2009). These cells were cultured in a stationary medium, hence for cells subjected to mechanical strains *in vivo* the disruption of the actin cap might lead to further structural damage (Kim et al., 2017).

We should take into consideration that the histological reports from the Quebec Beer Drinkers are old (1967-1972) and therefore limited by the technology available at the time, and from variations derived from sample preservation and processing, as well as fixation techniques (Auger and Chenard, 1967). In addition, it is unclear which results come from biopsies or autopsies, and the individual levels of cobalt they represented were unknown. However, this is the most thorough source of histological information available on cobalt toxicity. Two of the three cobalt cardiotoxicity animal models were published around the same time as the Quebec Beer Drinker problems, and the authors found similar microscopic features i.e. mitochondrial damage, sarcoplasmic reticulum dilation, and myofibril dismantling (Knieriem and Herbertz, 1969; Rona, 1971; Zadnipryany et al., 2017). We lack more up-to-date data to further contrast these results and newer and more detailed histological research in cobalt models would be needed to observe phenotypical changes. Specifically, new research will need to extend the research to other organs such as nervous and thyroid tissue, or liver and kidney.

In summary, cobalt could be interfering with the calcium flux of the endoplasmic reticulum and by extension the nuclear envelope. It is clear that heterochromatin plays an important role in the mechanical stability of the nucleus as well as in transcriptional control, and that the overall expression of *Hmgn5* indicates some level of epigenetic regulation. However, we do not know whether *Hmgn5* is homeostatically regulated e.g. by nuclear receptors or another mechanism such as a homeostatic response to the loss of lipid integrity in the nuclear envelope, or whether it is actually a target of cobalt toxicity from this data. Most importantly, the presence of this marker in response to cobalt should be validated by RT-qPCR and other techniques as a priority.

6.3.7. What we could not find: hypoxia and mitochondrial markers

Although the effect of cobalt in mitochondria is well known both in arthroprosthetic patients (Allen et al., 2014), Quebec Beer Drinkers (Alexander, 1972; Auger and Chenard, 1967) or more recent *in vivo* (Caltana et al., 2009) and *in vitro* assays (Karovic et al., 2007), we did not find major clues regarding mitotoxicity in the RNA-Seq data. Still, gene functions continue to be annotated and investigated, thus it is possible that future reanalysis will shed more light into whether mitochondria damage plays a role in cobalt toxicity in the brain at the concentrations used.

Furthermore, the data does not appear to indicate the presence of hypoxia in the response to cobalt. We presented the RNA-Seq fold change values and significance of Hypoxia-inducible factor 1-α (*Hif1a*) in Table 25 across tissues and doses. The fold changes of *Hif1a* are very low, thus we decided not to evaluate its protein expression. Cobalt is known to upregulate Hif-1α *in vitro* within a few hours of 100-300μM $CoCl_2$ application (Muñoz-Sánchez and Chánez-Cárdenas, 2019), but very few papers have dealt with whether cobalt elicits hypoxia *in vivo*. Very high concentrations of cobalt (20 mg/kg B.W. of $CoCl_2$) via oral dosing (gavage) during 15 days led to significant expression of Hif-1α in the brain of mice (Rani and Prasad, 2014). However, the authors did not report cobalt blood levels or what the overall health consequences were in the rats. Consequently, it is difficult to compare their research with our results or patients' outcomes. Nevertheless, our highest concentration is 1 mg/kg B.W. of $CoCl_2$, and we speculate that our setup will likely result in blood levels much inferior to

the ones obtained by Rani *et al.* or the *in vitro* doses used to elicit hypoxia. Therefore, it is unknown whether further accumulation of cobalt over time at our concentrations might lead to hypoxia induction in the brain. Since the heart, kidney and liver accumulate more cobalt (Fig. 34), they would theoretically reach the required cobalt concentrations to induce hypoxia first. Thus, future research into the effect of cobalt in these organs should consider whether Hif-1α protein expression is being induced. With regard to patients, it is difficult to tell whether Hif-1α is an important factor in cobalt toxicity. Metabolic failure and severe acidosis endured by some of the Quebec Beer Drinkers could have corresponded to a state of tissue hypoxia, although other explanations were offered at the time such as hepatic failure (Sullivan et al., 1969).

However, *Hmgn5* has recently been linked with hypoxia (Xu et al., 2019), and the peripheral margination of chromatin to the periphery was also found to be an early marker of hypoxia (Dehghani et al., 2018). Whether *Hmgn5* is an early marker of hypoxia in the brain tissue could be studied in the future.

Table 25: Hypoxia-inducible factor 1-α (*Hif1a*) fold change and p-value in the pref. cortex, cerebellum and hippocampus of rats dosed during 28 days with i.p. injections of 0.1, 0.5 and 1 mg/kg B.W. $CoCl_2$ or dH_2O (controls).

Hif1a fold change	Pref. cortex		Hippocampus		Cerebellum	
	Fold-change	p-Value	Fold-change	p-Value	Fold-change	p-Value
0.1 mg/kg B.W.	-0.14	0.02	-0.07	0.21	-0.04	0.33
0.5 mg/kg B.W.	-0.14	0.02	0.05	0.51	-0.09	0.02
1 mg/kg B.W.	-0.30	0.00	-0.03	0.38	-0.02	0.65
1 mg/kg B.W. (1st experiment)	0.93	0.00	X	X	-0.16	0.01

6.3.8. Future work and recommendations

Due to choroid plexus contamination, we have focused on the overall transcriptional effects of cobalt in the brain, rather than on how cobalt could affect brain parts differently. Fig. 38 shows that each brain part has tissue-specific DEGs. Therefore, future research might want to understand what the effects of cobalt are in the individual brain areas without having the interference of the choroid plexus. However, since cobalt appears to have a particular impact in the choroid plexus, it would be interesting to produce similar metal content and transcriptional experiments but investigating this brain area. *In vitro* models of the choroid plexus are imperfect, and they are still being developed but they might be useful to perform functional assays.

In general, it is recommended that a comprehensive histological study of cobalt should be performed in different organs. Specifically, new research will need to extend the research to organs other than cardiac tissue such as nervous and thyroid tissue, or liver and kidney. It might be necessary to use higher concentrations than the dosage used here to observe a histological effect in certain tissues with lower cobalt concentrations, since as we know, RNA-Seq is more sensitive than other established techniques, and we are unsure whether the transcriptional changes would actually get translated to morphological changes.

More precise dissection techniques might help determine the relationship between gene and protein expression. For example, techniques such as immunofluorescence microscopy or in situ hybridisation to observe a few targets in defined brain locations. In addition, high-throughput mass spectrometry can detect overall protein expression, and it could help determine whether cobalt is directly interfering with protein expression when comparing its output to that of RNA-Seq. This could be especially relevant if cobalt was mediating toxicity through nuclear receptors given that the probable nature of the binding and the wide extent of transcription might prove elusive.

We did not have time to confirm the gene expression of nuclear receptors, *Cyp* genes or *Hmgn5* in our samples. RT-qPCR could be easily used to validate the fold change of these genes. Validating the nuclear receptor hypothesis would need interdisciplinary techniques. It is unclear whether cobalt would act as an agonist or antagonist of

nuclear receptors, but *in vitro* cell culture with simultaneous application of steroid hormones that activate known receptors and cobalt might shed some light on whether the given activation of the nuclear receptor pathway is changed. Higher resolution and more precise techniques should be used to determine whether there is direct damage to the heterochromatin or the nuclear lamina, or changes in the lipid profile of the nuclear envelope, which might be the reason behind the high expression of *Hmgn5*. In that regard, *in vitro* work in which the cells are not mechanically disturbed while being exposed to cobalt might not represent a good model of cobalt toxicity. Adding mechanical challenges during cobalt treatment could provide a better model to observe whether cells are challenged by the presence of cobalt in the medium.

We concluded that the doses used here appear to relate to early cobalt damage at least in the brain. However, heart and liver receive a greater portion of the cobalt dose administered, and it might be possible therefore to find markers of mitochondrial damage at the doses used here. No histology has been done in the brain of patients with arthroprosthetic cobaltism, thus we do not know the extent to which they could be affected *in vivo*. However, mitochondrial damage might never occur in the brain of patients with high cobalt levels since it could be a tissue specific reaction.

We also searched for RNA-Seq markers that would make a good loading control for immunoblotting. We found that the gene coding for β-Actin, *Actb*, was stable under cobalt treatment. Our recommendation would be to avoid β-Actin protein as loading control because of potential cobalt damage to cytoskeleton. The blot bands retrieved for β-Actin were homogeneous after normalisation with the Lowry protein assay results as can be observed in Fig. 49. Thus, we do not believe that variations in β-Actin expression as a consequence of cobalt could have an effect in the quantification of the bands resulting from our samples at the doses used.

Finally, the possibility exists that local or compartmentalised immune reactions to cobalt in the synovial membrane and the local prosthetic area (Langton et al., 2018) could lead to a systemic immune response in patients which, in turn, could affect distant tissues such as the brain or the heart. Epidemiological studies are increasingly showing the prevalence of comorbidities in the context of conditions driven by chronic allergic inflammation such as atopic dermatitis (Andersen et al., 2017), asthma (Su et

al., 2016), or allergic rhinitis (Cingi et al., 2017). Given that our experimental set-up did not rely on inducing local inflammation around the joint area, as well as the systemic streaming of cobalt through blood, and that the choroid plexus is a blood-exposed brain part which seems to be the most affected based on the RNA-Seq data, we think it is the direct interaction of cobalt with the barrier that induces the inflammatory markers. Whether persistent inflammatory activity at a distant site such as the hip joint or the synovial membrane indirectly triggers cardiac or neural immune reactions is outside the reach of our current study. Nevertheless, given the continuous inflammatory conditions around failed prostheses (Langton et al., 2018), the issue of systemic chronic inflammation (Furman et al., 2019) could become very relevant for prosthetic patients. Thus, such studies would be very beneficial to the understanding of systemic cobalt and potentially chromium toxicity.

The large effusions observed in the synovial fluid of patients with MoM implants (Langton et al., 2018) are reminiscent of the pericardial effusions seen in patients with MoM implants, as well as those of cobalt beer drinkers (Alexander, 1972; Kesteloot et al., 1968), which also mentioned pleural effusions (Sullivan et al., 1969). It is possible that both Co and Cr ions damage solute barriers, which in turn could impair metal clearance and exacerbate Co and Cr concentrations leading to more severe immunological reactions. Langton *et al.* hypothesised that the excess cobalt and albumin concentration in synovial effusions was indicative of impaired synovial membrane permeability and was either the cause or the consequence of ALVAL (Langton et al., 2018). Given than the choroid plexus is a solute barrier, it is possible that accumulation of Co and Cr ions in the brain-CSF barrier could replicate these conditions and, if not leading to hydrocephalus, at least disturbing the balance of electrolytes and nutrients in the CSF. Therefore, the immune reaction transcripts obtained through RNA-Seq technology could be associated with immune reactivity within the choroid plexus caused by a similar process to that described by Langton *et al*. There is little evidence of this process on the literature, however, transthyretin, a protein solely produced in the choroid plexus, was found to be upregulated after direct brain cobalt injection (Kajiwara et al., 2008). This is a protein known to transport thyroid hormones and retinol proteins, and the effect might be indicative of impaired protein transport. Further studying the transport of proteins across barriers in the presence of cobalt might potentially answer whether cobalt affects the physiology of barriers.

6.4. Conclusion

We have investigated the effect of cobalt brain accumulation across three cobalt doses: 0.1, 0.5, and 1 mg/kg B.W. $CoCl_2$. The doses were administered via i.p. injections for 28 days, and the controls were given dH_2O. The parameters we investigated were cobalt accumulation through ICP-MS, gene expression via RNA-Seq and RT-qPCR, and protein levels through Western blot. The following conclusions were drawn from our results:

- Cobalt at the concentrations used might impair weight gain in rats. However, the overall differences in growth rate are not significant compared to the controls. Longer exposure times and higher n number might be needed to prove this effect.
- Organ weight ratios appear not to change with the cobalt dosage and length of treatment used in this study.
- Cobalt organ content rises as a result of all cobalt treatments, and its accumulation following doses of between 0.5 and 1 mg/kg B.W. $CoCl_2$ leads to significant levels of cobalt in most organs, including the brain.
- Consistently with previous results, kidney, liver, and heart in that order contain more cobalt than other organs after cobalt treatment, while the metal accumulated in pref. cortex, cerebellum and hippocampus regions of the brain is comparatively lower, but still significant, compared with the control group.
- Blood cobalt levels as a result of the doses administered are within the 4-38μg/l range which, in terms of systemic toxicity, include part of the low (<20μg/l) to moderate (<100μg/l) spectrum of MoM patients with raised levels of cobalt that could induced systemic toxicity.
- Cobalt does not appear to elicit a transcriptional dose-response in the pref. cortex and cerebellum with the doses used neither in fold change gene expression, nor in number of DEGs.
- The overall transcriptional changes indicate a disruption or activation of hormone and steroid metabolising activity, as well as lipid metabolism. Immune and haematopoietic transcriptional programmes were also disrupted. This transcriptional response was elicited at cobalt concentrations in blood similar to those found in some MoM patients.

- Given the outcomes of Chapter 5, we hypothesise that the transcriptional changes occur as a result of cobalt interfering with the metal binding of cytochrome P450 enzymes (CYPs) or nuclear receptors. This hypothesis requires validation.
- The presence of choroid plexus gene expression and transcriptional markers was widespread throughout doses and tissues. This indicates tissue contamination, but also might indicate preferential toxicity of cobalt in the rat blood-CSF barrier within the doses and duration of our cobalt treatment.
- RNA-Seq and RT-qPCR gene expression correlated for *Spata18*, *Akap14*, *Kl* targets, but *Tnf* and *Ttr* did not. Improvement of primer design might produce better results. In general, RT-qPCR validated RNA-Seq findings.
- Protein levels of Spata18, Tumour necrosis factor (TNF)-α, Angiogenin (Ang), Transthyretin (Ttr) and Akap14 do not change significantly with cobalt treatment. Since the choroid plexus was unknowingly included in the tissues it is possible that the selected targets are all expressed in the choroid plexus and the regional localisation of gene expression might not correlate.
- We found that *Hmgn5*, a gene whose protein product is involved in chromatin state modification, is highly expressed in our RNA-Seq results. This might indicate a layer of epigenetic modification as a consequence of cobalt toxicity. *Hmgn5* gene and protein expression also require further validation.

In the next section we will summarise the findings highlighted throughout this PhD thesis, and suggest future work on the evaluation of cobalt toxicity.

7. SUMMARY OF RESULTS AND FUTURE RESEARCH

7.1. Main *in vitro* and *in vivo* findings on cobalt toxicity in this thesis.

The principal aim of this work was to find mechanisms responsible for cobalt toxicity that could affect brain function, and by extension the function of other organs involved in arthroprosthetic cobaltism, such as the heart or the liver. To obtain a broader vision of the subject, we set up different research workflows *in vitro* and *in vivo*. We specifically relied on cell viability assays, the quantification of cobalt content in cells and tissues through ICP-MS, as well as RNA-Seq, a hypothesis-free technique that allows for the screening of differentially expressed genes (DEGs). RT-qPCR was used to validate RNA-Seq results, and translation of the differential expression of mRNAs to the protein domain was studied by Western blotting. We will describe the main findings of the thesis in this section, followed by a brief review of the overall limitations of our research, and the possible impact in patients with MoM implants.

7.1.1. *In vitro* findings on brain cells exposed to cobalt

To investigate the direct response of cells to cobalt we treated two brain cell lines, astrocytoma (U-373) and neuroblastoma (SH-SY5Y), with cobalt chloride ($CoCl_2$) concentrations ranging from 0 to 500μM. We found that:

- Cobalt lowers cell proliferation and depresses cell metabolism at high concentrations (>100μM) after treatment for 24-72h as indicated by BrdU tests (proliferation) and MTT and NR (metabolism and viability) assays. Reduced DNA synthesis preceded metabolic decline according to the IC50s obtained via BrdU, MTT and NR tests with neuroblastoma and astrocytoma cells.
- Life epifluorescence microscopy confirmed that cobalt induced abnormal changes in cell morphology such as cytoplasmic vacuolisation and cell shrinking at high concentrations *in vitro*, while brightfield microscopy revealed a considerable degree of cell blebbing suggestive of cell death.

- Lower concentrations of cobalt appear to stimulate metabolic drive as shown by MTT assay, although this effect was inconsistent across concentrations and time-points.
- Cellular cobalt content measured by ICP-MS was concentration-dependent in both brain derived cell lines.
- Viability (MTT and NR) and proliferation assays (BrdU) demonstrate that neuroblastoma cells are more susceptible than astrocytoma cells to cobalt ions. Astrocytoma cells, despite showing greater resistance to cobalt toxicity, appear to demonstrate increased cobalt uptake.

A full description of these results is in **Chapter 4-An *in vitro* study into cobalt toxicity in brain cells (section 4.2.)**. The outcomes of this *in vitro* study were recently published in the Toxicology *in Vitro* scientific journal (Gómez-Arnaiz et al., 2020).

7.1.2. *In vivo* findings from time and dose-response rodent models of cobalt toxicity

In order to uncover mechanisms of cobalt toxicity, we used a rodent model of cobalt exposure in which rats were dosed daily by i.p. injections as described previously by Laovitthayanggoon *et al*. (Laovitthayanggoon et al., 2019). Initially, we performed a two time point exposure during 7 and 28 days with a fixed concentration of 1 mg/kg B.W. $CoCl_2$. We analysed the metal content of samples by ICP-MS, and gene expression at 28 days exposure via RNA-Seq and RT-qPCR. In the subsequent dose-response experiment, 0.1, 0.5 and 1 mg/kg B.W. $CoCl_2$ concentrations were used to dose rats for 28 days. We obtained metal content and gene expression of brain tissue, as well as protein levels in the pref. cortex and cerebellum at the highest cobalt concentration: 1 mg/kg B.W. $CoCl_2$. The following points illustrate our main findings from the time and dose-response experiments:

- Cobalt treatment for 28 days appeared to impact weight gain at all concentrations used, however, the decline in growth rate was still not significantly different from that of the dH_2O-treated controls.
- Relative organ weights did not vary with cobalt treatment as compared with controls.
- Kidney, liver and heart, in that order, received most of the cobalt at any time point and dosage as measured by ICP-MS in both time and dose-dependent experiments.
- Only 0.5 and 1 mg/kg B.W. $CoCl_2$ dosage samples contained significant concentrations of accumulated cobalt in all organs after 28 days treatment compared with controls. Pref. cortex and hippocampus had significantly elevated cobalt at these concentrations after 28 days.
- Blood, liver, kidney and spleen also had significantly elevated levels of cobalt after 7 days treatment with 1 mg/kg B.W. $CoCl_2$. Unfortunately, the offset of the controls introduced by an ICP-MS artefact did not allow us to extend the significance to other tissues such as heart and brain parts.
- Blood Co levels were elevated within the range 4-38μg/l as compared with control animals treated with dH_2O only, which had 1μg/l approximately. These moderately elevated levels of cobalt in blood correspond to part of the spectrum

of concentrations observed in patients with MoM. Thus, the rodent model used is clinically relevant to the study of systemic cobaltism in patients.

- Gene expression evaluated through RNA-Seq of pref. cortex and cerebellum pooled samples from rats treated with 1 mg/kg B.W. $CoCl_2$ during 28 days revealed possible metal dysregulation, specifically in transcripts of protein products that bind to zinc, calcium and magnesium. Several protein families that normally bind metal ions were also present throughout the RNA-Seq data e.g. carbonic anhydrases, phosphodiesterases, nuclear receptors, cytochromes P450 (CYPs) and synaptotagmin among others.
- The gene expression of carbonic anhydrase and phosphodiesterase families were evaluated through RT-qPCR and correlated with that of RNA-Seq from the time-response experiment. *Spata18*, *Akap14* and *Kl* genes also validated RNA-Seq results from the dose-response experiment, in contrast to *Tnf* and *Ttr* genes, the PCR fold changes of which did not correlate.
- Dose-response experiments revealed that neither the number nor the fold change of the Differentially Expressed Genes (DEGs) of pref. cortex and hippocampus followed a dose response.
- Highly expressed DEGs observed in pref. cortex, cerebellum and hippocampus corresponded to the choroid plexus indicating tissue contamination. But it also indicates that cobalt toxicity affects primarily the choroid plexus.
- GO enrichment analyses of DEGs present across dose-response outcomes point towards a change in hormone and lipid metabolism. The transcriptional changes in these programmes could be originated by cobalt binding to native metal sites of cytochrome P450 enzymes (CYPs) or nuclear receptors, which appeared as possible metal binding targets in the time-response experiment. Other possibility is that cobalt impacts lipid profiles first, and CYPs and nuclear receptors are affected in a downstream fashion.
- GO enrichment analyses in the dose-response experiment also identified immune and haematopoietic transcriptional activation possibly mediated by interleukin-6 (IL-6). The high expression of *Hmgn5* gene could signal changes in chromatin accessibility and thus, gene expression.
- Protein levels of highly expressed genes did not change significantly in the pref. cortex and cerebellum with cobalt treatment at the highest dose used (1 mg/kg B.W. $CoCl_2$). These proteins were Spata18, TNF-α, Angiogenin, Transthyretin

and Akap14. We suggest that the markers chosen from the RNA-Seq data could indeed belong to the choroid plexus, which could have influenced this outcome given the highly specialised protein localisation in brain tissue and that the tissue destined for protein and mRNA isolation did not coincide spatially.

These results are presented in both Chapter 5. *In vivo* time-response investigation into cobalt toxicity (section 5.2.) and Chapter 6. *In vivo* dose-response investigation into cobalt toxicity (section 6.2.). A scheme of the proposed mechanism of cobalt toxicity is presented in Fig. 51. We will now discuss briefly the limitations encountered during this research, and what we could have carried out better with the benefit of hindsight. After this discussion, we suggest future investigations that could arise from the work.

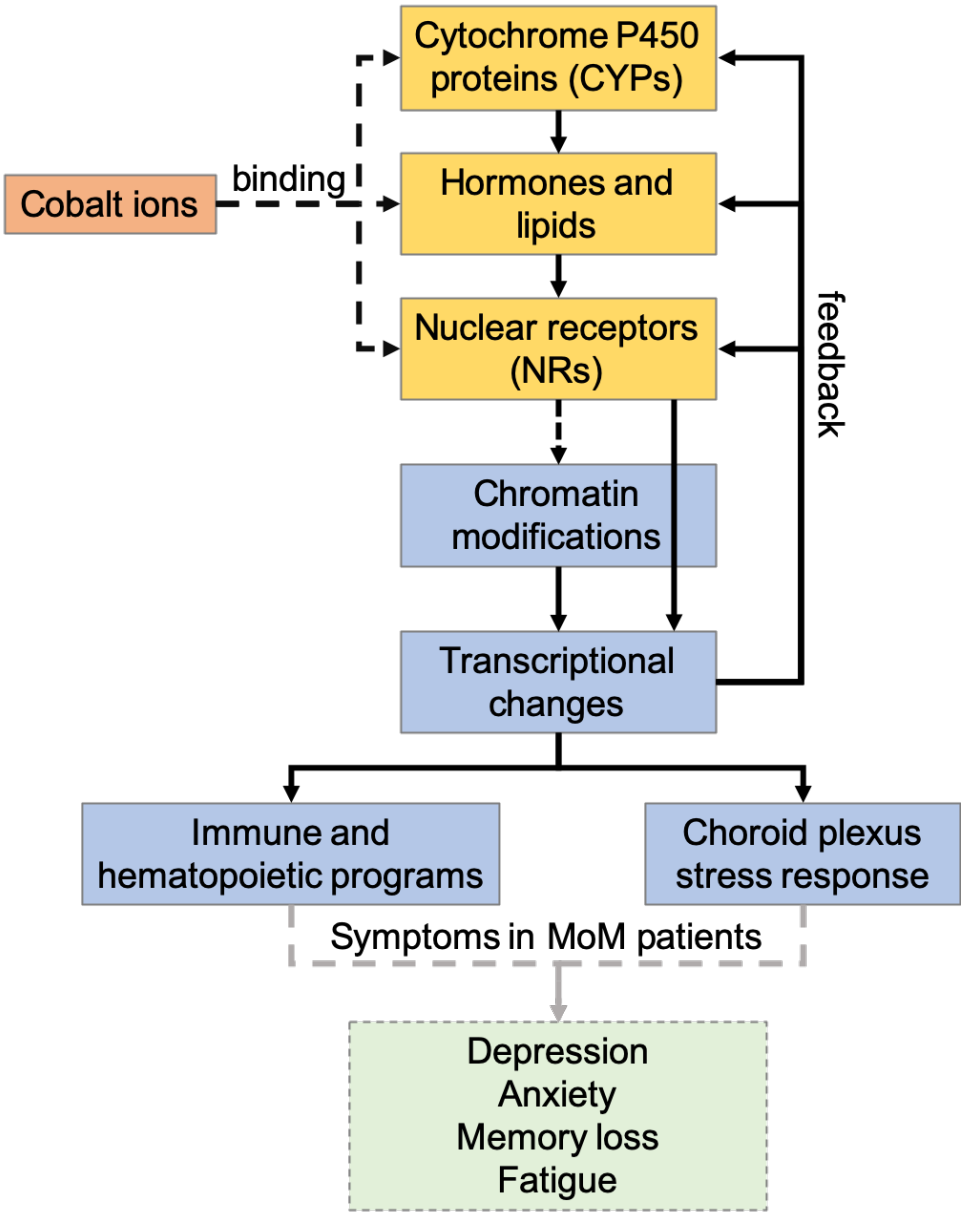

Fig. 51: Proposed mechanism of cobalt toxicity in the brain obtained from the RNA-Seq data of time and dose-response in vivo experiments in a rodent model of i.p. cobalt exposure. Cobalt ions might directly bind to either CYP proteins, hormones or nuclear receptors (NR), which are part of the same pathway. Interference with any of these factors will modify the activity of nuclear receptors leading to transcriptional changes, perhaps through altering chromatin state via Hmgn5. We mainly observed transcripts associated with the choroid plexus and its stress response, as well as many DEGs involved in immune and haematopoietic programmes. These transcriptional changes could potentially lead to neurological symptoms, although there is not enough evidence to confirm if the transcriptional programmes shown here could lead to the symptoms described by MoM patients with cobaltism e.g. depression, memory loss, anxiety or fatigue. Arrows indicate direct relationship through the research we carried out or the scientific literature while dotted arrows point towards lower levels of evidence, and grey dotted arrows indicate weak evidence of a relationship between modules.

7.2. Limitations of our research on systemic cobalt toxicity, and future directions.

The compiled results offer possible mechanisms of cobalt toxicity in the brain and point towards metal dysregulation, specific cobalt targets such as hormone and lipid metabolism, as well as disrupted nuclear receptor signalling and transcriptional changes, in addition to the considerable implication of the involvement of the choroid plexus (Fig. 51). Therefore, we have provided an explanation for cobalt toxicity, which was the main aim of this work. However, due to time and cost limitations we were restricted in our ability to validate the proposed hypothesis. Several aspects of cobalt toxicity have also remained unexplored in our investigations. We will describe some of our limitations and suggest future lines of research in the following paragraphs.

Due to the limited time available, we primarily focused on well-researched genes involved in inflammation, stress, and hormonal responses. However, these common genes could well be nonspecific given that they appear differentially expressed in transcriptional studies researching diverse conditions (Crow et al., 2019). These generic DEGs are important for the development of pathology (Crow et al., 2019), however, they may also distract from the study of markers which could be specifically associated with cobalt toxicity. The bias towards commonly studied genes is further strengthened by DEG enrichment engines, which are based on gene annotations, and that we have used to process the data. Less than 20% of coding-protein genes in humans are thoroughly annotated, but a third of them still lack annotations (Tomczak et al., 2018). Stoeger *et al.* found that redundant focus on certain genes could be attributed to endogenous gene characteristics but, more importantly, to whether a gene had been previously well-studied (Stoeger et al., 2018). Microarray technology has been used to study gene expression in response to cobalt *in vitro* in human pulmonary cells (Malard et al., 2007) and rat liver cell lines (Permenter et al., 2013), and while it offers interesting results the pre-selection of gene panels imposes a bias towards previously well-studied genes. Due to this and the different nature of our work, *in vitro* versus *in vivo*, the use of different tissues, we could not find many common genes in between studies. Thus, prior knowledge is an important factor on the selection of targets within a list of competing genes that generally blocks research into new targets. In our study, the genes *Mboat7L1* and *Hmgn5* appeared in the DEG top hit list across tissues and dosages, and while we did not focus on them due to the little scientific

literature available during our research, both genes could potentially be important in the development of cobalt poisoning.

For example, *Mboat7l1*, aka *Mboat7* or *Lpiat1*, is necessary for brain development and its deletion leads to disarranged cortical lamination, atrophy of the cerebral cortex and hippocampus, as well as early postnatal death (Lee et al., 2012). Severely enlarged ventricles associated with hydrocephalus have also been reported in the *Mboat7*-knockout mouse model (Vogel et al., 2012). Patients with mutations in this gene suffer primarily from intellectual disability, but they may additionally present with epilepsy and autism (Johansen et al., 2016), in addition to motor incoordination, self-harming behaviour and refusal to feed (Sun et al., 2020). *Mboat7* is a phospholipid acyltransferase responsible for transferring arachidonic acid from arachidonoyl-CoA to lysophosphatidylinositol, which changes the acyl-chain composition of these phospholipids via the Lands' cycle and influences their properties (Caddeo et al., 2021). More importantly, it has recently been found a culprit of non-alcoholic fatty liver disease (NAFLD), a condition that shows as build-up of fat in liver tissue (Tanaka et al., 2021). Tanaka *et al.* were able to avoid postnatal lethal defects of *Mboat7*-knockout mice by generating a tamoxifen-inducible *Mboat7*-knockout mouse line which showed lipid accumulation and, surprisingly, normal brain histology. Although we did not find articles about cobalt toxicity that reported lipid accumulation in the liver, the pathology is reminiscent of the lipid deposits found in prosthetic patients' cardiac tissue (Allen et al., 2014), and the hearts of Quebec Beer drinkers (Alexander, 1972; Auger and Chenard, 1967; Bonenfant, J.L., Miller, G., Roy, 1967; Bonenfant et al., 1969). *Mboat7*-knockout mice also developed a fibrotic phenotype driven by a high-fat diet (Tanaka et al., 2021; Thangapandi et al., 2021). In line with this, inadequate nutrition was suspected to correlate with the severity of pathology in cobalt-adulterated beer drinkers (Kesteloot et al., 1968; Rona, 1971; Sullivan et al., 1969). Moreover, both diacylglycerol kinase and phospholipase C, which bind to calcium ions, appeared as potential metalloprotein families targeted by cobalt in our previous results (Table 13)**.** Phospholipase C is known to degrade phospholipids into diacylglycerol, which is later used to produce triglycerides, and it is involved in the increased phospholipid turnover observed in the *Mboat7*-knockout mice (Tanaka et al., 2021). Finally, *in vitro* studies in macrophages have observed a tight relationship between the expression of *Mboat7*,

phospholipase C and calcium oscillations (Takemasu et al., 2019), which the authors suggested could play a role in liver inflammation and the development of fibrosis.

The pathology of NAFLD has also been recently linked to a disruption of lipid metabolism within the nuclear envelope, which is structurally connected with the endoplasmic reticulum, the main site of lipid synthesis (Östlund et al., 2020). The nuclear envelope is composed by an inner and an outer bilayer nuclear membrane. Thus, changes in their lipid composition due to a change in their metabolism could potentially alter the structural stability of the nucleus, and cobalt is known to change the fluidity of cell-like membranes (Umbsaar et al., 2018). As we have previously discussed, *Hmgn5* appears to be important for the mechanical stability of the nucleus by modifying the compaction of heterochromatin (Furusawa et al., 2015), as well as for the regulation of gene expression (Kugler et al., 2013; Rochman et al., 2009). Thus, *Hmgn5* expression could be a homeostatic response to structural changes in the nuclear envelope in order to preserve transcriptional stability and nuclear integrity. The nuclear membranes also hold several hormonal and vitamin receptors which, if disturbed, might lead to changes in gene expression (Garcia-Gil and Albi, 2017). Research on the relationship between genome integrity and nuclear lipid composition can be considered a newly founded field (Moriel-Carretero, 2021). However, this link could explain part of the transcriptional response to cobalt which we showed in this thesis. Moreover, one of our colleagues studied the effect of cobalt in neuronal cell lines *in vitro* through liquid chromatography-mass spectrometry (LC-MS) (Alanazi, 2019). Alanazi suggested that cobalt induced an alteration of methylation pathways, which could potentially correspond to widespread changes in gene expression. We initially planned to carry out a metabolomic study in *in vivo* samples from the cobalt dose-response experiment, however, we run out of time to analyse these results, which would require intensive labour. Further studying these data might give information on the lipid composition and metabolic changes in the brain as a result of cobalt interaction and offer an explanation for the gene expression patterns seen in response to cobalt.

Moreover, both *Hmgn5* and *Mboat7* were downregulated in the hippocampus. We found a particular gene expression landscape in this brain part compared to the prefrontal cortex and cerebellum in that its gene expression pattern seemed homogeneous across doses and that there were a few DEGs with elevated fold

changes (Fig. 40). We can speculate about the reason why the hippocampus could be particularly affected by cobalt given its proximity with the choroid plexus since it could be the choroid plexus response that it is actually being displayed due to dissection issues. Nevertheless, we should also note other highly downregulated genes in the hippocampus which might be linked with the activity of *Hmgn5* and *Mboat7* (Fig. 45): *Crnkl1*, *En2* and *Lmntd1*. *Crnkl1* regulates the nuclear export of spliced mRNA to the cytoplasm (Xiao et al., 2021). Moreover, lipids are also involved in the transport of *En2* across the plasma membrane (Amblard et al., 2020), and the over-expressed gene *Lmntd1* has its protein located on the nuclear envelope and it is known to be expressed in the brain (Wang et al., 2005). The function of these genes is starting to be studied but, all together, they start to portray a relationship between lipid metabolism, transcriptional regulation and cellular structural stability which could be an issue in cobalt toxicity. We do not know if the proteins from these genes bind to metal ions. However, the possibility exists that cobalt could bind to proteins with native zinc or calcium such as phospholipase C, but that their gene expression would not be as disturbed as expected. Rather, the downstream or upstream targets of these protein might be up or downregulated reflecting compensatory changes in gene expression (Jakutis and Stainier, 2021). We hope that further research will shed light into our own hypotheses about cobalt toxicity.

Mitochondrial damage was not directly reflected in the RNA-Seq data or by any of the methods employed. However, several papers attest to cobalt inducing mitochondrial toxicity *in vitro*, *in vivo* and in patients. It is possible that the specific techniques used in this research are not sensitive enough to detect mitotoxicity, or that the doses and exposure times used here cannot be used to indicate mitochondrial damage in the brain, or even that the brain responds to cobalt in different ways than the heart and does not produce mitochondrial toxicity at the doses used. Future research employing mitochondrial specific tests might be needed to explain this matter.

From the literature and from our data, cobalt appears to induce metal dysregulation. Further assays *in vitro* could elucidate how cobalt interferes directly with calcium and zinc handling, and how this impacts on cell function. Screening of metal transporters and identification of subcellular compartments containing cobalt in several cell types could provide insight into the mechanisms of cobalt toxicity in different organs. In

addition, pre-selection of the cell types most affected by cobalt *in vivo* would make this research far more relevant for patients with MoM implants. In our work, we identified organs that accumulated systemic cobalt, more specifically kidney, liver and heart received the highest quantity. Silver staining or other metal imaging techniques could help determine cell populations with high cobalt uptake. Current *in vitro* research is constrained to a few cell types, however, the impact of cobalt in thyroid and sensory tissues is well known, and we also found a strong response of the choroid plexus, which has not been suggested before. Diversifying the number and relevance of cell types studied would support our knowledge on the effect of cobalt in different tissues.

Furthermore, it is difficult to rationally parallel *in vitro* concentrations in cellular systems with cobalt levels in MoM patients' blood. As mentioned in the *in vitro* experiments chapter (section 4.1.), the differences between the cobalt range used in our *in vitro* experiments are very pronounced: 25-500μM theoretically compares to 1,473–29,465 μg/l levels of cobalt in blood (Co MW=58.93). While the maximum cobalt level in blood detected is 6,521μg/l (Zywiel et al., 2013), the majority of patients, and even those with higher values, will have under 300 μg/l cobalt in blood (Langton et al., 2013; Sidaginamale et al., 2013). Comparisons are complicated by the fact that cobalt binds to albumin and other molecular components added to cell media in a non-physiological fashion, which will likely affect the amount of free ionic cobalt taken up by cells. We detected signs of mild toxicity in the *in vivo* RNA-Seq data meaning that we did not find indications of cell death in contrast to our *in vitro* model. The levels of cobalt seen in tissues and blood might equate to the lower concentrations used *in vitro* (<100μM). This sparks other questions, e.g. could the decrease in cell proliferation or the inconsistent increase in glycolysis at lower concentrations *in vitro* be mediated by activation of CYPs and nuclear receptors? A link between nuclear receptors and glycolysis has already been described in the literature (Baba et al., 2014), and if the metabolic regulation of the cells was to fail due to cobalt interfering with CYPs and nuclear receptors, this effect could potentially activate glycolysis and impair cell proliferation in the long term. The probabilistic binding of cobalt to receptors and CYPs would explain inconsistent increase in glycolysis at lower concentrations across doses and time points. The success of future *in vitro* models to evaluate cobalt toxicity will depend on the adjustment of concentrations e.g. by matching the observed effects in MoM patients with *in vitro* cobalt toxicity modes. Finally, some of the proposed

hypotheses extracted from RNA-Seq data could be easily evaluated *in vitro*, thus limiting the use of research animals.

Our hypothesis of cobalt toxicity involved the displacement of native metal ligands by cobalt, which could modify enzyme or protein activity. We identified several protein families that could potentially bind to cobalt due to their presence in the RNA-Seq data. Although in a first moment we focused in phosphodiesterases (Pde) and carbonic anhydrase (Car) metal binding families, we found from the dose-response RNA-Seq experiment that the disturbance of cytochrome P450 enzymes (CYPs) and nuclear receptors could also underlie relevant transcriptional changes in hormone metabolism. The advantage of high-throughput techniques such as RNA-Seq is that it allows for the exploration of multiple research avenues, however the sheer amount of data produced and the variety of analysis modes makes it difficult to decide what to prioritise. For our research, it meant that we could not fully validate our hypotheses, but nonetheless we were able to gain a perspective on possibly the most relevant modes of action at the resulting moderate cobalt blood levels. Thus, we defined plausible hypotheses about the mechanisms of cobalt toxicity that can be further evaluated *in vitro* and *in vivo*. In the future, other researchers would also have the opportunity to review the RNA-Seq data and extract more valuable information about cobalt effects in the brain e.g. by relaxing the criteria for the selection of DEGs such as fold-change values or using new or updated Gene Ontology (GO) databases. Moreover, as the number of transcriptomic studies increases, our ability to interpret these sort of data will improve. This is likely to happen with other diseases and even well-known toxins as they are being evaluated with new High-throughput technologies.

Although we established the important emergence of choroid plexus markers, it was not possible to detect the tissue-specific effects of cobalt in the individual brain parts precisely due to the considerable presence of the brain-CSF barrier markers. Future research might want to study the effect of cobalt in the isolated pref. cortex, cerebellum and hippocampus without the contribution of the choroid plexus. In addition, the specific stress response of the choroid plexus could have contributed towards the interpretation of the proposed mechanism of cobalt toxicity. Further studies in isolated brain areas, heart and other tissues affected by systemic cobalt toxicity will result in more robust analyses.

Protein and gene expression could be partially used for the validation of our hypotheses. RT-qPCR could quickly validate the gene expression of *Cyp* family and *Hmgn5* genes. Given that our difficulties to observe protein expression might be due to the use of uncorrelated tissue for gene and protein expression, other techniques that allow spatial tissue localisation such as in situ hybridisation, immunofluorescence microscopy or even histology, could be helpful and used to observe the localised effects of cobalt. If co-localization of gene and protein expression does still not occur, the comparison of RNA-Seq outcomes with other methods such as high-throughput mass spectrometry might establish which mRNAs are being translated to protein.

We also propose that the integration of protein structure information and transcriptomic data could be a useful premise for the discovery of toxicity mechanisms. Fortunately, metal binding information has already been integrated in the Gene Ontology (GO) databases through the Molecular Function GO ontology, which has simplified our research. For other toxins, the integration of protein structural information might not be as straightforward. Nevertheless, whether cobalt interferes directly with CYPs or nuclear receptors remains to be tested. Due to the probabilistic nature of receptor binding and signal activation, the individual response of the animals rather than pooled samples should also be taken into consideration. Moreover, it is known that nuclear receptors and hormones play an important role in heart (Vega and Kelly, 2017) and bone remodelling (Bae et al., 2020). Thus, it would be beneficial to find out if this hypothesis also translates to tissues such as heart or bone e.g. in the development of heart disease, pseudotumous and osteolysis by patients with CoCr prostheses (Bijukumar et al., 2018).

Finally, cost limitations impacted on the study design with regards to the number of rats per group (n=4). This led to the choice of only male rats to reduce housing cost and, we thought, hormonal variability. Selecting only male rodents is a common practice in neuroscience (Will et al., 2017). However, the decision not to use female rats is part of a wider culture in which they tend to be excluded due to the misconception that the estrous cycle induces variability. The assumption that hormone fluctuations will reduce statistical power has been refuted in a study of the literature that evaluated neuroscience research looking at rat behaviour, histology,

electrophysiology, and neurochemistry independently of the estrous cycle (Becker et al., 2016). Sex differences were obvious regarding body and organ weights, which we documented in our *in vivo* studies. Unfortunately, the implication of this bias is poorer treatment outcomes for women because of overlooked sex-specific adverse responses (Mauvais-Jarvis et al., 2021). Women could have a more reactive immune system (Desai and Brinton, 2019) and they tend to show worse prosthetic outcomes (Haughom et al., 2015; Inacio et al., 2013). If only male patients or animal models are used to research cobalt toxicity the indicated safe metal levels in blood for women could be misleading, and clinicians might miss preventable cases of toxicity. Therefore, given the available evidence today, future research teams might want to focus solely on female animals, which might endure more obvious responses, or further investigate sex differences to cobalt exposure.

7.3. Significance of our research for patients with MoM implants and arthroprosthetic cobaltism

We concluded that, in a rodent model with moderate levels of cobalt in blood similar to those seen in patients (average range: 17-38μg/l), cobalt accumulated significantly in brain parts leading to transcriptional effects in the brain that could go as far as chromatin remodelling. These transcriptional changes occur before the accumulation of cobalt is statistically significant in these brain areas e.g. with 0.1 mg/kg B.W. $CoCl_2$ dosage (average cobalt in blood: 4μg/l). Moreover, we identified a possible disruption of hormone, steroid and lipid synthesis by cobalt, which we suggest could be initiated by cobalt interfering with metal-binding cytochrome P450 proteins (CYPs) and nuclear receptors (Fig. 51). In our research, although cobalt appeared to accumulate in a dose and time-response fashion in blood and tissue, we could not detect a dose-response relationship in terms of the number or the fold change of transcripts. Increasing the number of concentrations and time points evaluated would provide further insight since we used a limited number of doses and time points. However, we proposed that the probabilistic nature of nuclear receptor activation could lead to a stochastic dose response rather than to a linear deterministic dose response (Kanno, 2016). This conclusion offers an explanation as to why the systemic effects of cobalt do not appear to follow a straightforward dose-response in patients meaning that while some patients with considered low levels of cobalt develop systemic toxicity (Mao et al., 2011), other patients with very high cobalt levels appear asymptomatic (Ho et al., 2017). In the cited

references Mao *et al.* report symptoms around 10-25μg/l (Mao et al., 2011), and so does Ho *et al.* who, in addition, did not observe a correlation of systemic effects in MoM patients with cobalt serum levels even in patients with concentrations of cobalt over 100μg/l (Ho et al., 2017).

Problems in the synthesis and signalling of hormones and nuclear hormone receptors are likely to be dependent on gender. Moreover, cobalt can bind to steroid hormones (Stevenson et al., 2019), and has been exceptionally used in combination with hormone replacement therapy to reduce estrogen levels in menopausal women (Wright, 2005). Thus, cobalt systemic effects could be different and more pronounced in females. There is a plethora of cofounding factors such as implant head size, and a few other studies have found contradicting results (Donahue et al., 2018; Renner et al., 2016) but, in the cobalt literature, it is suspected that females present a higher incidence of pseudotumors, osteolysis and hip failure (Haughom et al., 2015; Van Der Straeten et al., 2020). It has been shown that women with total joint replacements are more prone than men to develop metal sensitivity and to experience aseptic pain and be positive for metal sensitivity testing as measured by lymphocyte transformation test (LTT) (Caicedo et al., 2017). The authors stated that this increased metal sensitivity in females could be associated with the reported higher failure rates presented by women with MoM hip resurfacing arthroplasties (Haughom et al., 2015) and unilateral THR (Inacio et al., 2013). A recent study tested this hypotheses in rodents and confirmed that young female mice showed increased DTH responses to wear debris (Samelko et al., 2021). Women are at higher risk of autoimmune diseases such as multiple sclerosis, lupus or rheumatoid arthritis due to the endocrine transitions they endure during their lifetime, and the interplay between the endocrine and the immune system (Desai and Brinton, 2019). The results by Samelko *et al.* and Caicedo *et al.* suggest that the modulatory effect of hormones in a challenged immune system is at play, apparently increasing women's susceptibility to metallic wear (Caicedo et al., 2017; Samelko et al., 2021). However, given the sparse number of case reports it is difficult to make similar statements regarding systemic cobalt toxicity (Zywiel et al., 2016). Whether cobalt could also be a causative factor of differential gender effects through cobalt affecting sex-specific hormones differently could be of interest to other research groups. There are several hormone level tests either in blood or urine that could help

establish whether cobalt interferes with any of these hormones in patients with MoM implants.

We also face certain difficulties with the interpretation of these results. One of them is that we cannot establish that conditions such as depression, anxiety, and memory loss are induced by cobalt in the research animals due to the inherent difficulty to translate these complex issues to a rodent model. Thus, even when our data shows clear transcriptional effects in the brain, we cannot assume that the transcriptomic effects observed in our *in vivo* experiments are the cause of the symptoms described by some patients with cobaltism. Nevertheless, hormonal fluctuations are known to lead to mood changes (Dwyer et al., 2020), the choroid plexus is involved in anxiety behaviours (Vincent et al., 2021), and nuclear receptors regulate the formation of synapses (Cao et al., 2020) which modulate learning and memory. Previous epidemiological research has suggested that screening of patients with MoM implants for cardiac effects should be introduced to investigate the effects of subtle pathological changes (Lassalle et al., 2018; Lodge et al., 2018). Further research in this area would be needed to evaluate the impact of cobalt exposure on the brain and to determine whether a screening programme for systemic symptoms in patients with MoM implants is needed.

We consider that the results described here pave the way to new research in cobalt toxicity. Our investigation defines a new plausible mechanism of cobalt toxicity that might eventually lead to serious neurological health issues. Just as the doctors from the Quebec Beer Drinkers case were unable to identify the symptoms displayed by the patients with any previous established heart diseases, such as beriberi or alcoholic cardiomyopathy (Alexander, 1972), the current transcriptomic results cannot be completely assimilated to other datasets or previous studies as revealed by GO enrichment and PPI network analysis. The clues shown here point towards a new aetiology and less known mechanism of metal toxicity, which does not primarily involve ROS or other gene expression patterns previously identified in cobalt toxicity and instead appears to be related with metal endocrine disruption (Stevenson et al., 2019), changes in the lipidome and adaptive immunological responses at least throughout the concentrations used. Thus, our findings have important implications for patients with

MoM implants both by providing a mechanism of cobalt toxicity and an explanation for the non-deterministic dose response seen in patients.

References

Abdel-Gadir, A., Berber, R., Porter, J.B., Quinn, P.D., Suri, D., Kellman, P., Hart, A.J., Moon, J.C., Manisty, C., Skinner, J.A., 2016. Detection of metallic cobalt and chromium liver deposition following failed hip replacement using T2∗ and R2 magnetic resonance. J. Cardiovasc. Magn. Reson. 18, 29. https://doi.org/10.1186/s12968-016-0248-z

Abdülkadir Coban, T., Beydemir, Ş., Gücin, İ., Ekinci, D., Innocenti, A., Vullo, D., Supuran, C.T., 2009. Sildenafil is a strong activator of mammalian carbonic anhydrase isoforms I–XIV. Bioorg. Med. Chem. 17, 5791–5795. https://doi.org/10.1016/j.bmc.2009.07.019

Achariyar, T.M., Li, B., Peng, W., Verghese, P.B., Shi, Y., McConnell, E., Benraiss, A., Kasper, T., Song, W., Takano, T., Holtzman, D.M., Nedergaard, M., Deane, R., 2016. Glymphatic distribution of CSF-derived apoE into brain is isoform specific and suppressed during sleep deprivation. Mol. Neurodegener. 11, 74. https://doi.org/10.1186/s13024-016-0138-8

Ackermann, T., Tardito, S., 2019. Cell Culture Medium Formulation and Its Implications in Cancer Metabolism. Trends in Cancer 5, 329–332. https://doi.org/10.1016/j.trecan.2019.05.004

Adams, T.N., Butt, Y.M., Batra, K., Glazer, C.S., 2017. Cobalt related interstitial lung disease. Respir. Med. 129, 91–97. https://doi.org/10.1016/j.rmed.2017.06.008

Afolaranmi, G., Akbar, M., Brewer, J., Grant, M., 2012. Distribution of metal released from cobalt–chromium alloy orthopaedic wear particles implanted into air pouches in mice. J Biomed Mater Res A 100, 1529–1538. https://doi.org/10.1002/jbm.a.34091

Afolaranmi, G.A., Henderson, C., Grant, M.H., 2011. Effect of chromium and cobalt ions on phase I and phase II enzymatic activities in vitro in freshly isolated rat hepatocytes. Toxicol. Vitr. 25, 125–130. https://doi.org/10.1016/j.tiv.2010.10.003

Akbar, M., Brewer, J.M., Grant, M.H., 2011. Effect of chromium and cobalt ions on primary human lymphocytes in vitro. J. Immunotoxicol. 8, 140–149. https://doi.org/10.3109/1547691X.2011.553845

Aki, T., Nara, A., Uemura, K., 2012. Cytoplasmic vacuolization during exposure to drugs and other substances. Cell Biol. Toxicol. 28, 125–131.

https://doi.org/10.1007/s10565-012-9212-3

Al-abcha, A., Wang, L., Reilly, M.J., Rosenman, K.D., 2020. Work-related asthma in cobalt-exposed workers. J. Asthma 1–10. https://doi.org/10.1080/02770903.2020.1759090

Al-Mehdi, A.-B., Pastukh, V.M., Swiger, B.M., Reed, D.J., Patel, M.R., Bardwell, G.C., Pastukh, V. V., Alexeyev, M.F., Gillespie, M.N., 2012. Perinuclear Mitochondrial Clustering Creates an Oxidant-Rich Nuclear Domain Required for Hypoxia-Induced Transcription. Sci. Signal. 5, ra47–ra47. https://doi.org/10.1126/scisignal.2002712

Alanazi, I.M., 2019. Evaluation of the mechanisms of neurotoxicity using metabolomic strategies. University of Strathclyde.

Alexander, C.S., 1972. Cobalt-beer cardiomyopathy. A clinical and pathologic study of twenty-eight cases. Am. J. Med. 53, 395–417. https://doi.org/10.1016/0002-9343(72)90136-2

Alexander, S., Mathie, A., Peters, J., 2011. Guide to Receptors and Channels (GRAC), 5th edition. Br. J. Pharmacol. 164, S1–S2. https://doi.org/10.1111/j.1476-5381.2011.01649_1.x

Allen, L.A., Ambardekar, A. V., Devaraj, K.M., Maleszewski, J.J., Wolfel, E.E., 2014. Missing elements of the history. N. Engl. J. Med. 370, 559–566. https://doi.org/10.1056/NEJMcps1213196

Altun, M., Bergman, E., Edström, E., Johnson, H., Ulfhake, B., 2007. Behavioral impairments of the aging rat. Physiol. Behav. 92, 911–923. https://doi.org/10.1016/j.physbeh.2007.06.017

Amblard, I., Dupont, E., Alves, I., Miralvès, J., Queguiner, I., Joliot, A., 2020. Bidirectional transfer of Engrailed homeoprotein across the plasma membrane requires PIP2. J. Cell Sci. 133. https://doi.org/10.1242/jcs.244327

Andersen, Y.M.F., Egeberg, A., Skov, L., Thyssen, J.P., 2017. Comorbidities of Atopic Dermatitis: Beyond Rhinitis and Asthma. Curr. Dermatol. Rep. 6, 35–41. https://doi.org/10.1007/s13671-017-0168-7

Andrews, R.E., Shah, K.M., Wilkinson, J.M., Gartland, A., 2011. Effects of cobalt and chromium ions at clinically equivalent concentrations after metal-on-metal hip replacement on human osteoblasts and osteoclasts: Implications for skeletal health. Bone 49, 717–723. https://doi.org/10.1016/j.bone.2011.06.007

Antunes, M., Chelminski, D.S., Jr, F.B., 2013. Phosphodiesterase Type 5 Inhibitors

and sudden sensorineural hearing loss. Braz. J. Otorhinolaryngol. 79, 727–733. https://doi.org/10.5935/1808-8694.20130133

Apel, W., Stark, D., Stark, A., O'Hagan, S., Ling, J., 2013. Cobalt-chromium toxic retinopathy case study. Doc. Ophthalmol. 126, 69–78. https://doi.org/10.1007/s10633-012-9356-8

Apostoli, P., Catalani, S., Zaghini, A., Mariotti, A., Poliani, P.L., Vielmi, V., Semeraro, F., Duse, S., Porzionato, A., Macchi, V., Padovani, A., Rizzetti, M.C., De Caro, R., 2013. High doses of cobalt induce optic and auditory neuropathy. Exp. Toxicol. Pathol. 65, 719–727. https://doi.org/10.1016/j.etp.2012.09.006

Asai, Y., Sakakibara, Y., Kondo, M., Nadai, M., Katoh, M., 2019. Expression and activities of sulfotransferase in rat brain. Xenobiotica 49, 270–275. https://doi.org/10.1080/00498254.2018.1440656

Astashkina, A., Mann, B., Grainger, D.W., 2012. A critical evaluation of in vitro cell culture models for high-throughput drug screening and toxicity. Pharmacol. Ther. 134, 82–106. https://doi.org/10.1016/j.pharmthera.2012.01.001

Auger, C., Chenard, J., 1967. Quebec beer-drinkers' cardiomyopathy: ultrastructural changes in one case. Can. Med. Assoc. J. 97, 916–921.

Aurousseau, M.R.P., Osswald, I.K., Bowie, D., 2012. Thinking of Co2+-staining explant tissue or cultured cells? How to make it reliable and specific. Eur. J. Neurosci. 35, 1201–1207. https://doi.org/10.1111/j.1460-9568.2012.08042.x

Averaimo, S., Nicol, X., 2014. Intermingled cAMP, cGMP and calcium spatiotemporal dynamics in developing neuronal circuits. Front. Cell. Neurosci. 8, 376. https://doi.org/10.3389/fncel.2014.00376

Baba, T., Otake, H., Sato, T., Miyabayashi, K., Shishido, Y., Wang, C.-Y., Shima, Y., Kimura, H., Yagi, M., Ishihara, Y., Hino, S., Ogawa, H., Nakao, M., Yamazaki, T., Kang, D., Ohkawa, Y., Suyama, M., Chung, B.-C., Morohashi, K.-I., 2014. Glycolytic genes are targets of the nuclear receptor Ad4BP/SF-1. Nat. Commun. 5, 3634. https://doi.org/10.1038/ncomms4634

Bae, S., Zeng, S., Park-Min, K.-H., 2020. Nuclear receptors in osteoclasts. Curr. Opin. Pharmacol. 53, 8–17. https://doi.org/10.1016/j.coph.2020.03.002

Banizs, B., Pike, M., Millican, C., Ferguson, W., Komlosi, P., Sheetz, J., Bell, P., Schwiebert, E., Yoder, B., 2005. Dysfunctional cilia lead to altered ependyma and choroid plexus function, and result in the formation of hydrocephalus. Development 132, 5329–5339. https://doi.org/10.1242/dev.02153

Banza Lubaba Nkulu, C., Casas, L., Haufroid, V., De Putter, T., Saenen, N.D., Kayembe-Kitenge, T., Musa Obadia, P., Kyanika Wa Mukoma, D., Lunda Ilunga, J.-M., Nawrot, T.S., Luboya Numbi, O., Smolders, E., Nemery, B., 2018. Sustainability of artisanal mining of cobalt in DR Congo. Nat. Sustain. 1, 495–504. https://doi.org/10.1038/s41893-018-0139-4

Barborik, M., Dusek, J., 1972. Cardiomyopathy accompaning industrial cobalt exposure. Br. Heart J. 34, 113–116. https://doi.org/10.1136/hrt.34.1.113

Barbosa, D.J., Capela, J.P., de Lourdes Bastos, M., Carvalho, F., 2015. In vitro models for neurotoxicology research. Toxicol. Res. (Camb). 4, 801–842. https://doi.org/10.1039/C4TX00043A

Bardsley, E.N., Davis, H., Ajijola, O.A., Buckler, K.J., Ardell, J.L., Shivkumar, K., Paterson, D.J., 2018. RNA Sequencing Reveals Novel Transcripts from Sympathetic Stellate Ganglia During Cardiac Sympathetic Hyperactivity. Sci. Rep. 8, 8633. https://doi.org/10.1038/s41598-018-26651-7

Baruch, K., Ron-Harel, N., Gal, H., Deczkowska, A., Shifrut, E., Ndifon, W., Mirlas-Neisberg, N., Cardon, M., Vaknin, I., Cahalon, L., Berkutzki, T., Mattson, M.P., Gomez-Pinilla, F., Friedman, N., Schwartz, M., 2013. CNS-specific immunity at the choroid plexus shifts toward destructive Th2 inflammation in brain aging. Proc. Natl. Acad. Sci. 110, 2264–2269. https://doi.org/10.1073/pnas.1211270110

Bathgate, R.A.D., Samuel, C.S., Burazin, T.C.D., Gundlach, A.L., Tregear, G.W., 2003. Relaxin: New peptides, receptors and novel actions. Trends Endocrinol. Metab. 14, 207–213. https://doi.org/10.1016/S1043-2760(03)00081-X

Battaglia, V., Compagnone, A., Bandino, A., Bragadin, M., Rossi, C.A., Zanetti, F., Colombatto, S., Grillo, M.A., Toninello, A., 2009. Cobalt induces oxidative stress in isolated liver mitochondria responsible for permeability transition and intrinsic apoptosis in hepatocyte primary cultures. Int. J. Biochem. Cell Biol. 41, 586–594. https://doi.org/10.1016/j.biocel.2008.07.012

Becker, J.B., Prendergast, B.J., Liang, J.W., 2016. Female rats are not more variable than male rats: a meta-analysis of neuroscience studies. Biol. Sex Differ. 7, 34. https://doi.org/10.1186/s13293-016-0087-5

Berg, J.M., Tymoczko, J.L., Stryer, L., 2015. Biochemistry, 8th edition. W. H. Freeman and Company.

Biddie, S.C., John, S., 2014. Minireview: Conversing With Chromatin: The Language of Nuclear Receptors. Mol. Endocrinol. 28, 3–15.

https://doi.org/10.1210/me.2013-1247

Bijukumar, D.R., Segu, A., Souza, J.C.M., Li, X.J., Barba, M., Mercuri, L.G., J. Jacobs, J., Mathew, M.T., 2018. Systemic and local toxicity of metal debris released from hip prostheses: A review of experimental approaches. Nanomedicine Nanotechnology, Biol. Med. 14, 951–963. https://doi.org/10.1016/j.nano.2018.01.001

Black, M.B., Parks, B.B., Pluta, L., Chu, T.-M., Allen, B.C., Wolfinger, R.D., Thomas, R.S., 2014. Comparison of Microarrays and RNA-Seq for Gene Expression Analyses of Dose-Response Experiments. Toxicol. Sci. 137, 385–403. https://doi.org/10.1093/toxsci/kft249

Bollmann, L., Koser, D.E., Shahapure, R., Gautier, H.O.B., Holzapfel, G.A., Scarcelli, G., Gather, M.C., Ulbricht, E., Franze, K., 2015. Microglia mechanics: immune activation alters traction forces and durotaxis. Front. Cell. Neurosci. 9, 363. https://doi.org/10.3389/fncel.2015.00363

Bonenfant, J.L., Miller, G., Roy, P.., 1967. Quebec beer-drinkers' cardiomyopathy: pathological studies. Can. Med. Assoc. J. 97, 910–916.

Bonenfant, J.L., Auger, C., Miller, G., Chenard, J., Roy, P.E., 1969. Quebec beer-drinkers' myocardosis: pathological aspects. Ann. New York Acad. Sci. 156, 577–582.

Böttcher, M., Müller-Fielitz, H., Sundaram, S.M., Gallet, S., Neve, V., Shionoya, K., Zager, A., Quan, N., Liu, X., Schmidt-Ullrich, R., Haenold, R., Wenzel, J., Blomqvist, A., Engblom, D., Prevot, V., Schwaninger, M., 2020. NF-κB signaling in tanycytes mediates inflammation-induced anorexia. Mol. Metab. 39, 101022. https://doi.org/10.1016/j.molmet.2020.101022

Bowyer, J.F., Patterson, T.A., Saini, U.T., Hanig, J.P., Thomas, M., Camacho, L., George, N.I., Chen, J.J., 2013. Comparison of the global gene expression of choroid plexus and meninges and associated vasculature under control conditions and after pronounced hyperthermia or amphetamine toxicity. BMC Genomics 14, 147. https://doi.org/10.1186/1471-2164-14-147

Bresson, C., Darolles, C., Carmona, A., Gautier, C., Sage, N., Roudeau, S., Ortega, R., Ansoborlo, E., Malard, V., 2013. Cobalt chloride speciation, mechanisms of cytotoxicity on human pulmonary cells, and synergistic toxicity with zinc. Metallomics 5, 133. https://doi.org/10.1039/c3mt20196a

Brewster, D.H., Stockton, D.L., Reekie, A., Ashcroft, G.P., Howie, C.R., Porter, D.E.,

Black, R.J., 2013. Risk of cancer following primary total hip replacement or primary resurfacing arthroplasty of the hip: a retrospective cohort study in Scotland. Br. J. Cancer 108, 1883–1890. https://doi.org/10.1038/bjc.2013.129

Bridges, R.L., Cho, C.S., Beck, M.R., Gessner, B.D., Tower, S.S., 2020. F-18 FDG PET brain imaging in symptomatic arthroprosthetic cobaltism. Eur. J. Nucl. Med. Mol. Imaging 47, 1961–1970. https://doi.org/10.1007/s00259-019-04648-2

Brini, M., Calì, T., Ottolini, D., Carafoli, E., 2014. Neuronal calcium signaling: Function and dysfunction. Cell. Mol. Life Sci. 71, 2787–2814. https://doi.org/10.1007/s00018-013-1550-7

Bustin, S.A., Benes, V., Garson, J.A., Hellemans, J., Huggett, J., Kubista, M., Mueller, R., Nolan, T., Pfaffl, M.W., Shipley, G.L., Vandesompele, J., Wittwer, C.T., 2009. The MIQE Guidelines: Minimum Information for Publication of Quantitative Real-Time PCR Experiments. Clin. Chem. 55, 611–622. https://doi.org/10.1373/clinchem.2008.112797

Cabrera-Pastor, A., Malaguarnera, M., Taoro-Gonzalez, L., Llansola, M., Felipo, V., 2016. Extracellular cGMP Modulates Learning Biphasically by Modulating Glycine Receptors, CaMKII and Glutamate-Nitric Oxide-cGMP Pathway. Sci. Rep. 6, 1–13. https://doi.org/10.1038/srep33124

Cabrera-Pastor, A., Taoro-González, L., Cuñat, A.N., Canet-López, D., Balzano, T., Felipo, V., 2017. Extracellular Cyclic GMP Modulates Membrane Expression of the GluA1 and GluA2 Subunits of AMPA Receptor in Cerebellum: Molecular Mechanisms Involved. Sci. Rep. 7, 1–13. https://doi.org/10.1038/s41598-017-18024-3

Caddeo, A., Hedfalk, K., Romeo, S., Pingitore, P., 2021. LPIAT1/MBOAT7 contains a catalytic dyad transferring polyunsaturated fatty acids to lysophosphatidylinositol. Biochim. Biophys. Acta - Mol. Cell Biol. Lipids 1866, 158891. https://doi.org/10.1016/j.bbalip.2021.158891

Caddeo, A., Jamialahmadi, O., Solinas, G., Pujia, A., Mancina, R.M., Pingitore, P., Romeo, S., 2019. MBOAT7 is anchored to endomembranes by six transmembrane domains. J. Struct. Biol. 206, 349–360. https://doi.org/10.1016/j.jsb.2019.04.006

Cai, G., Zhu, J., Shen, C., Cui, Y., Du, J., Chen, X., 2012. The Effects of Cobalt on the Development, Oxidative Stress, and Apoptosis in Zebrafish Embryos. Biol. Trace Elem. Res. 150, 200–207. https://doi.org/10.1007/s12011-012-9506-6

Caicedo, M.S., Solver, E., Coleman, L., Jacobs, J.J., Hallab, N.J., 2017. Females with Unexplained Joint Pain Following Total Joint Arthroplasty Exhibit a Higher Rate and Severity of Hypersensitivity to Implant Metals Compared with Males. J. Bone Jt. Surg. 99, 621–628. https://doi.org/10.2106/JBJS.16.00720

Caltana, L., Merelli, A., Lazarowski, A., Brusco, A., 2009. Neuronal and Glial Alterations Due to Focal Cortical Hypoxia Induced by Direct Cobalt Chloride (CoCl2) Brain Injection. Neurotox. Res. 15, 348–358. https://doi.org/10.1007/s12640-009-9038-9

Campbell, P., Takamura, K., 2020. Local and systemic consequences of metal-on-metal hip resurfacing implants. Ann. Jt. 5. https://doi.org/10.21037/aoj.2019.10.01

Canto de Souza, L., Provensi, G., Vullo, D., Carta, F., Scozzafava, A., Costa, A., Schmidt, S.D., Passani, M.B., Supuran, C.T., Blandina, P., 2017. Carbonic anhydrase activation enhances object recognition memory in mice through phosphorylation of the extracellular signal-regulated kinase in the cortex and the hippocampus. Neuropharmacology 118, 148–156. https://doi.org/10.1016/j.neuropharm.2017.03.009

Cao, H., Li, M.-Y., Li, G., Li, S.-J., Wen, B., Lu, Y., Yu, X., 2020. Retinoid X Receptor α Regulates DHA-Dependent Spinogenesis and Functional Synapse Formation In Vivo. Cell Rep. 31, 107649. https://doi.org/10.1016/j.celrep.2020.107649

Catalani, S., Rizzetti, M., Padovani, A., Apostoli, P., 2012. Neurotoxicity of cobalt. Hum. Exp. Toxicol. 31, 421–437. https://doi.org/10.1177/0960327111414280

Chandel, N.S., Maltepe, E., Goldwasser, E., Mathieu, C.E., Simon, M.C., Schumacker, P.T., 1998. Mitochondrial reactive oxygen species trigger hypoxia-induced transcription. Proc. Natl. Acad. Sci. 95, 11715–11720. https://doi.org/10.1073/pnas.95.20.11715

Cheung, A.C., Banerjee, S., Cherian, J.J., Wong, F., Butany, J., Gilbert, C., Overgaard, C., Syed, K., Zywiel, M.G., J, J.J., A., M.M., Zywiel, M.G., Cherian, J.J., Banerjee, S., Cheung, A.C., Wong, F., Butany, J., Gilbert, C., Overgaard, C., Syed, K., Jacobs, J.J., Mont, M.A., 2016. Systemic cobalt toxicity from total hip arthroplasties: review of a rare condition Part 1—History, mechanism, measurements, and pathophysiology. Bone Joint J. 98-B, 6–13. https://doi.org/10.1302/0301-620X.98B1.36374

Chimeh, U., Zimmerman, M.A., Gilyazova, N., Li, P.A., 2018. B355252, a novel small molecule, confers neuroprotection against cobalt chloride toxicity in mouse

hippocampal cells through altering mitochondrial dynamics and limiting autophagy induction. Int. J. Med. Sci. 15, 1384–1396. https://doi.org/10.7150/ijms.24702

Cho, J., Yu, N.-K., Choi, J.-H., Sim, S.-E., Kang, S.J., Kwak, C., Lee, S.-W., Kim, J., Choi, D. Il, Kim, V.N., Kaang, B.-K., 2015. Multiple repressive mechanisms in the hippocampus during memory formation. Science (80-.). 350, 82–87. https://doi.org/10.1126/science.aac7368

Choi, H.I., Hong, J.A., Kim, M.S., Lee, S.E., Jung, S.H., Yoon, P.W., Song, J.S., Kim, J.J., 2019. Severe Cardiomyopathy Due to Arthroprosthetic Cobaltism: Report of Two Cases with Different Outcomes. Cardiovasc. Toxicol. 19, 82–89. https://doi.org/10.1007/s12012-018-9480-0

Christensen, J.M., Poulsen, O.M., 1994. A 1982–1992 surveillance programme on Danish pottery painters. Biological levels and health effects following exposure to soluble or insoluble cobalt compounds in cobalt blue dyes. Sci. Total Environ. 150, 95–104. https://doi.org/10.1016/0048-9697(94)90134-1

Christopherson, R.I., 2008. CD Antigens, in: Encyclopedia of Cancer. Springer Berlin Heidelberg, Berlin, Heidelberg. https://doi.org/10.1007/978-3-540-47648-1_947

Ciavardelli, D., Consalvo, A., Caldaralo, V., Di Vacri, M.L., Nisi, S., Corona, C., Frazzini, V., Sacchetta, P., Urbani, A., Di Ilio, C., Sensi, S.L., 2012. Characterisation of element profile changes induced by long-term dietary supplementation of zinc in the brain and cerebellum of 3xTg-AD mice by alternated cool and normal plasma ICP-MS. Metallomics 4, 1321–1332. https://doi.org/10.1039/c2mt20162c

Cingi, C., Gevaert, P., Mösges, R., Rondon, C., Hox, V., Rudenko, M., Muluk, N.B., Scadding, G., Manole, F., Hupin, C., Fokkens, W.J., Akdis, C., Bachert, C., Demoly, P., Mullol, J., Muraro, A., Papadopoulos, N., Pawankar, R., Rombaux, P., Toskala, E., Kalogjera, L., Prokopakis, E., Hellings, P.W., Bousquet, J., 2017. Multi-morbidities of allergic rhinitis in adults: European Academy of Allergy and Clinical Immunology Task Force Report. Clin. Transl. Allergy 7, 17. https://doi.org/10.1186/s13601-017-0153-z

Cirla, A.M., 1994. Cobalt-related asthma: clinical and immunological aspects. Sci. Total Environ. 0.

Clark, M.J., Prentice, J.R., Hoggard, N., Paley, M.N., Hadjivassiliou, M., Wilkinson, J.M., 2014. Brain Structure and Function in Patients after Metal-on-Metal Hip Resurfacing. Am. J. Neuroradiol. 35, 1753–1758.

https://doi.org/10.3174/ajnr.A3922

Cohen, D., 2011. Out of joint: The story of the ASR. BMJ 342:d2905. https://doi.org/10.1136/bmj.d2905

Crow, M., Lim, N., Ballouz, S., Pavlidis, P., Gillis, J., 2019. Predictability of human differential gene expression. Proc. Natl. Acad. Sci. 116, 6491–6500. https://doi.org/10.1073/pnas.1802973116

D'Antona, L., Jaime Merchan, M.A., Vassiliou, A., Watkins, L.D., Davagnanam, I., Toma, A.K., Matharu, M.S., 2021. Clinical Presentation, Investigation Findings, and Treatment Outcomes of Spontaneous Intracranial Hypotension Syndrome. JAMA Neurol. 78, 329–337. https://doi.org/10.1001/jamaneurol.2020.4799

Dalman, M.R., Deeter, A., Nimishakavi, G., Duan, Z.-H., 2012. Fold change and p-value cutoffs significantly alter microarray interpretations. BMC Bioinformatics 13, S11. https://doi.org/10.1186/1471-2105-13-S2-S11

Danial, N.N., Gramm, C.F., Scorrano, L., Zhang, C.-Y., Krauss, S., Ranger, A.M., Robert Datta, S., Greenberg, M.E., Licklider, L.J., Lowell, B.B., Gygi, S.P., Korsmeyer, S.J., 2003. BAD and glucokinase reside in a mitochondrial complex that integrates glycolysis and apoptosis. Nature 424, 952–956. https://doi.org/10.1038/nature01825

Daniel, J., Ziaee, H., Pradhan, C., McMinn, D.J.W., 2009. Six-year results of a prospective study of metal ion levels in young patients with metal-on-metal hip resurfacings. J. Bone Joint Surg. Br. 91-B, 176–179. https://doi.org/10.1302/0301-620X.91B2.21654

Daniel, J., Ziaee, H., Pradhan, C., Pynsent, P.B., McMinn, D.J.W., 2010. Renal Clearance of Cobalt in Relation to the Use of Metal-on-Metal Bearings in Hip Arthroplasty. J. Bone Jt. Surgery-American Vol. 92, 840–845. https://doi.org/10.2106/JBJS.H.01821

Dazzoni, R., Grélard, A., Morvan, E., Bouter, A., Applebee, C.J., Loquet, A., Larijani, B., Dufourc, E.J., 2020. The unprecedented membrane deformation of the human nuclear envelope, in a magnetic field, indicates formation of nuclear membrane invaginations. Sci. Rep. 10, 5147. https://doi.org/10.1038/s41598-020-61746-0

DeFelipe, J., 2011. The Evolution of the Brain, the Human Nature of Cortical Circuits, and Intellectual Creativity. Front. Neuroanat. 5, 29. https://doi.org/10.3389/fnana.2011.00029

Dehaine, Q., Tijsseling, L.T., Glass, H.J., Törmänen, T., Butcher, A.R., 2021.

Geometallurgy of cobalt ores: A review. Miner. Eng. 160, 106656. https://doi.org/10.1016/j.mineng.2020.106656

Dehghani, A., Karatas, H., Can, A., Erdemli, E., Yemisci, M., Eren-Kocak, E., Dalkara, T., 2018. Nuclear expansion and pore opening are instant signs of neuronal hypoxia and can identify poorly fixed brains. Sci. Rep. 8, 14770. https://doi.org/10.1038/s41598-018-32878-1

Deitmer, J.W., Theparambil, S.M., Ruminot, I., Noor, S.I., Becker, H.M., 2019. Energy Dynamics in the Brain: Contributions of Astrocytes to Metabolism and pH Homeostasis. Front. Neurosci. 13, 1–7. https://doi.org/10.3389/fnins.2019.01301

Denisov, W., Strong, W., Walder, M., Gingrich, J., Wintz, H., 2008. Development and Validation of RQI: An RNA Quality Indicator for the Experion Automated Electrophoresis System. Bio-Rad Bull.

Denninger, J.K., Chen, X., Turkoglu, A.M., Sarchet, P., Volk, A.R., Rieskamp, J.D., Yan, P., Kirby, E.D., 2020. Defining the adult hippocampal neural stem cell secretome: In vivo versus in vitro transcriptomic differences and their correlation to secreted protein levels. Brain Res. 1735, 146717. https://doi.org/10.1016/j.brainres.2020.146717

Desai, M.K., Brinton, R.D., 2019. Autoimmune Disease in Women: Endocrine Transition and Risk Across the Lifespan. Front. Endocrinol. (Lausanne). 10, 265. https://doi.org/10.3389/fendo.2019.00265

Di, L., 2014. The role of drug metabolizing enzymes in clearance. Expert Opin. Drug Metab. Toxicol. 10, 379–393. https://doi.org/10.1517/17425255.2014.876006

Di Laura, A., Quinn, P.D., Panagiotopoulou, V.C., Hothi, H.S., Henckel, J., Powell, J.J., Berisha, F., Amary, F., Mosselmans, J.F.W., Skinner, J.A., Hart, A.J., 2017. The Chemical Form of Metal Species Released from Corroded Taper Junctions of Hip Implants: Synchrotron Analysis of Patient Tissue. Sci. Rep. 7, 10952. https://doi.org/10.1038/s41598-017-11225-w

Diamond, J.S., 2011. Calcium-Permeable AMPA Receptors in the Retina. Front. Mol. Neurosci. 4, 1–5. https://doi.org/10.3389/fnmol.2011.00027

Díaz-García, C.M., Mongeon, R., Lahmann, C., Koveal, D., Zucker, H., Yellen, G., 2017. Neuronal Stimulation Triggers Neuronal Glycolysis and Not Lactate Uptake. Cell Metab. 26, 361-374.e4. https://doi.org/10.1016/j.cmet.2017.06.021

Díaz, D., Bartolo, R., Delgadillo, D.M., Higueldo, F., Gomora, J.C., 2005. Contrasting effects of Cd2+ and Co2+ on the blocking/unblocking of human Cav3 channels. J.

Membr. Biol. 207, 91–105. https://doi.org/10.1007/s00232-005-0804-1

Distler, J.H.W., Györfi, A.-H., Ramanujam, M., Whitfield, M.L., Königshoff, M., Lafyatis, R., 2019. Shared and distinct mechanisms of fibrosis. Nat. Rev. Rheumatol. 15, 705–730. https://doi.org/10.1038/s41584-019-0322-7

Dixit, V.A., Warwicker, J., Visser, S.P., 2020. How Do Metal Ions Modulate the Rate-Determining Electron-Transfer Step in Cytochrome P450 Reactions? Chem. – A Eur. J. 26, 15270–15281. https://doi.org/10.1002/chem.202003024

Donahue, G.S., Lindgren, V., Galea, V.P., Madanat, R., Muratoglu, O.K., Malchau, H., 2018. Risk factors for mid-term revision surgery in patients with articular surface replacement total hip arthroplasty. HIP Int. 28, 44–49. https://doi.org/10.5301/hipint.5000524

Dörrbaum, A.R., Kochen, L., Langer, J.D., Schuman, E.M., 2018. Local and global influences on protein turnover in neurons and glia. Elife 7, e34202. https://doi.org/10.7554/eLife.34202

Dwyer, J.B., Aftab, A., Radhakrishnan, R., Widge, A., Rodriguez, C.I., Carpenter, L.L., Nemeroff, C.B., McDonald, W.M., Kalin, N.H., 2020. Hormonal Treatments for Major Depressive Disorder: State of the Art. Am. J. Psychiatry 177, 686–705. https://doi.org/10.1176/appi.ajp.2020.19080848

Ebramzadeh, E., Campbell, P., Tan, T.L., Nelson, S.D., Sangiorgio, S.N., 2015. Can Wear Explain the Histological Variation Around Metal-on-metal Total Hips? Clin. Orthop. Relat. Res. 473, 487–494. https://doi.org/10.1007/s11999-014-3874-5

ECACC, 2021. ECACC General Cell Collection: U-373 MG (Uppsala) [WWW Document]. URL https://www.phe-culturecollections.org.uk/products/celllines/generalcell/detail.jsp?refId=08061901&collection=ecacc_gc

Ellenbroek, B., Youn, J., 2016. Rodent models in neuroscience research: is it a rat race? Dis. Model. Mech. 9, 1079–1087. https://doi.org/10.1242/dmm.026120

Engelhardt, B., Vajkoczy, P., Weller, R.O., 2017. The movers and shapers in immune privilege of the CNS. Nat. Immunol. 18, 123–131. https://doi.org/10.1038/ni.3666

Evans, J.T., Evans, J.P., Walker, R.W., Blom, A.W., Whitehouse, M.R., Sayers, A., 2019. How long does a hip replacement last? A systematic review and meta-analysis of case series and national registry reports with more than 15 years of follow-up. Lancet 393, 647–654. https://doi.org/10.1016/S0140-6736(18)31665-9

Everaert, C., Luypaert, M., Maag, J.L. V., Cheng, Q.X., Dinger, M.E., Hellemans, J.,

Mestdagh, P., 2017. Benchmarking of RNA-sequencing analysis workflows using whole-transcriptome RT-qPCR expression data. Sci. Rep. 7, 1559. https://doi.org/10.1038/s41598-017-01617-3

Eybalin, M., Caicedo, A., Renard, N., Ruel, J., Puel, J.L., 2004. Transient Ca2+-permeable AMPA receptors in postnatal rat primary auditory neurons. Eur. J. Neurosci. 20, 2981–2989. https://doi.org/10.1111/j.1460-9568.2004.03772.x

Facchin, F., Catalani, S., Bianconi, E., Pasquale, D. De, Stea, S., Toni, A., Canaider, S., Beraudi, A., 2017. Albumin as marker for susceptibility to metal ions in metal-on-metal hip prosthesis patients. Hum. Exp. Toxicol. 36, 319–327. https://doi.org/10.1177/0960327116650011

Fang, D., Li, Z., Zhong-ming, Q., Mei, W.X., Ho, Y.W., Yuan, X.W., Ya, K., 2008. Expression of bystin in reactive astrocytes induced by ischemia/reperfusion and chemical hypoxia in vitro. Biochim. Biophys. Acta 1782, 658–663. https://doi.org/10.1016/j.bbadis.2008.09.007

Ferguson, C.S., Tyndale, R.F., 2011. Cytochrome P450 enzymes in the brain: emerging evidence of biological significance. Trends Pharmacol. Sci. 32, 708–714. https://doi.org/10.1016/j.tips.2011.08.005

Fernandes, J., Chandler, J.D., Lili, L.N., Uppal, K., Hu, X., Hao, L., Go, Y.-M., Jones, D.P., 2019. Transcriptome Analysis Reveals Distinct Responses to Physiologic versus Toxic Manganese Exposure in Human Neuroblastoma Cells. Front. Genet. 10, 676. https://doi.org/10.3389/fgene.2019.00676

Finley, B., Scott, P.K., Glynn, M.E., Paustenbach, D., Donovan, E., Thuett, K.A., 2017. Chromium speciation in the blood of metal-on-metal hip implant patients. Toxicol. Environ. Chem. 99, 48–64. https://doi.org/10.1080/02772248.2016.1148904

Fisher, J.W., 1998. A quest for erythropoietin over nine decades. Annu. Rev. Pharmacol. Toxicol. 38, 1–20. https://doi.org/10.1146/annurev.pharmtox.38.1.1

Fleming, T.J., Kavanagh, A., Duggan, G., 2020. The effect of melt temperature on the mechanical properties of cast ASTM F75 CoCrMo alloy as explained by nitrogen and oxygen content. J. Mater. Res. Technol. 9, 9479–9486. https://doi.org/10.1016/j.jmrt.2020.06.079

Forster, J.I., Köglsberger, S., Trefois, C., Boyd, O., Baumuratov, A.S., Buck, L., Balling, R., Antony, P.M.A., 2016. Characterization of Differentiated SH-SY5Y as Neuronal Screening Model Reveals Increased Oxidative Vulnerability. J. Biomol. Screen. 21, 496–509. https://doi.org/10.1177/1087057115625190

Foster, A.W., Osman, D., Robinson, N.J., 2014. Metal preferences and metallation. J. Biol. Chem. 289, 28095–28103. https://doi.org/10.1074/jbc.R114.588145

Fox, D.A., He, L., Poblenz, A.T., Medrano, C.J., Blocker, Y.S., Srivastava, D., 1998. Lead-induced alterations in retinal cGMP phosphodiesterase trigger calcium overload , mitochondrial dysfunction and rod photoreceptor apoptosis 359–361.

Fujiyoshi, M., Ohtsuki, S., Hori, S., Tachikawa, M., Terasaki, T., 2007. 24 S - hydroxycholesterol induces cholesterol release from choroid plexus epithelial cells in an apical- and apoE isoform-dependent manner concomitantly with the induction of ABCA1 and ABCG1 expression. J. Neurochem. 100, 968–978. https://doi.org/10.1111/j.1471-4159.2006.04240.x

Fung, E.S., Monnot, A., Kovochich, M., Unice, K.M., Tvermoes, B.E., Galbraith, D., Finley, B.L., Paustenbach, D.J., 2018. Characteristics of Cobalt-Related Cardiomyopathy in Metal Hip Implant Patients: An Evaluation of 15 Published Reports. Cardiovasc. Toxicol. 18, 206–220. https://doi.org/10.1007/s12012-017-9433-z

Fung, F.K.C., Law, B.Y.K., Lo, A.C.Y., 2016. Lutein Attenuates Both Apoptosis and Autophagy upon Cobalt (II) Chloride-Induced Hypoxia in Rat Műller Cells. PLoS One 11, e0167828. https://doi.org/10.1371/journal.pone.0167828

Furman, D., Campisi, J., Verdin, E., Carrera-Bastos, P., Targ, S., Franceschi, C., Ferrucci, L., Gilroy, D.W., Fasano, A., Miller, G.W., Miller, A.H., Mantovani, A., Weyand, C.M., Barzilai, N., Goronzy, J.J., Rando, T.A., Effros, R.B., Lucia, A., Kleinstreuer, N., Slavich, G.M., 2019. Chronic inflammation in the etiology of disease across the life span. Nat. Med. 25, 1822–1832. https://doi.org/10.1038/s41591-019-0675-0

Furusawa, T., Rochman, M., Taher, L., Dimitriadis, E.K., Nagashima, K., Anderson, S., Bustin, M., 2015. Chromatin decompaction by the nucleosomal binding protein HMGN5 impairs nuclear sturdiness. Nat. Commun. 6, 6138. https://doi.org/10.1038/ncomms7138

Furuta, T., Ohishi, A., Nagasawa, K., 2019. Intracellular labile zinc is a determinant of vulnerability of cultured astrocytes to oxidative stress. Neurosci. Lett. 707, 134315. https://doi.org/10.1016/j.neulet.2019.134315

Gadagkar, S.R., Call, G.B., 2015. Computational tools for fitting the Hill equation to dose-response curves. J. Pharmacol. Toxicol. Methods 71, 68–76. https://doi.org/10.1016/j.vascn.2014.08.006

García-Cáceres, C., Balland, E., Prevot, V., Luquet, S., Woods, S.C., Koch, M., Horvath, T.L., Yi, C.-X., Chowen, J.A., Verkhratsky, A., Araque, A., Bechmann, I., Tschöp, M.H., 2019. Role of astrocytes, microglia, and tanycytes in brain control of systemic metabolism. Nat. Neurosci. 22, 7–14. https://doi.org/10.1038/s41593-018-0286-y

Garcia-Gil, M., Albi, E., 2017. Nuclear Lipids in the Nervous System: What they do in Health and Disease. Neurochem. Res. 42, 321–336. https://doi.org/10.1007/s11064-016-2085-8

García, F., Ortega, A., Domingo, J.L., Corbella, J., 2001. Accumulation of metals in autopsy tissues of subjects living in Tarragona County, Spain. J. Environ. Sci. Heal. Part A 36, 1767–1786. https://doi.org/10.1081/ESE-100106258

Garoui, E., Amara, I. Ben, Driss, D., Elwej, A., Chaabouni, S.E., Boudawara, T., Zeghal, N., 2013. Effects of Cobalt on Membrane ATPases, Oxidant, and Antioxidant Values in the Cerebrum and Cerebellum of Suckling Rats. Biol. Trace Elem. Res. 154, 387–395. https://doi.org/10.1007/s12011-013-9746-0

Gene [Internet]. NCBI Entrez Gene Database, 2004. National Center for Biotechnology Information (NCBI) [WWW Document]. URL https://www.ncbi.nlm.nih.gov/gene/

Gerhard, D.M., Wohleb, E.S., Duman, R.S., 2016. Emerging treatment mechanisms for depression: Focus on glutamate and synaptic plasticity. Drug Discov. Today 21, 454–464. https://doi.org/10.1016/j.drudis.2016.01.016

Gerhardsson, L., Lundh, T., Minthon, L., Londos, E., 2008. Metal concentrations in plasma and cerebrospinal fluid in patients with Alzheimer's disease. Dement. Geriatr. Cogn. Disord. 25, 508–515. https://doi.org/10.1159/000129365

Gerlitz, G., 2020. The Emerging Roles of Heterochromatin in Cell Migration. Front. Cell Dev. Biol. 8, 394. https://doi.org/10.3389/fcell.2020.00394

Gessner, B.D., Steck, T., Woelber, E., Tower, S.S., 2019. A Systematic Review of Systemic Cobaltism After Wear or Corrosion of Chrome-Cobalt Hip Implants. J. Patient Saf. 15, 97–104. https://doi.org/10.1097/PTS.0000000000000220

Ghersi-Egea, J.-F., Strazielle, N., Catala, M., Silva-Vargas, V., Doetsch, F., Engelhardt, B., 2018. Molecular anatomy and functions of the choroidal blood-cerebrospinal fluid barrier in health and disease. Acta Neuropathol. 135, 337–361. https://doi.org/10.1007/s00401-018-1807-1

Gibb, A.A., Lazaropoulos, M.P., Elrod, J.W., 2020. Myofibroblasts and Fibrosis. Circ. Res. 127, 427–447. https://doi.org/10.1161/CIRCRESAHA.120.316958

Gilbert, C.J., Cheung, A., Butany, J., Zywiel, M.G., Syed, K., McDonald, M., Wong, F., Overgaard, C., 2013. Hip Pain and Heart Failure: The Missing Link. Can. J. Cardiol. 29, 639.e1-639.e2. https://doi.org/10.1016/j.cjca.2012.10.015

Giorgi, C., Marchi, S., Pinton, P., 2018. The machineries, regulation and cellular functions of mitochondrial calcium. Nat. Rev. Mol. Cell Biol. 19, 713–730. https://doi.org/10.1038/s41580-018-0052-8

Gómez-Arnaiz, S., Tate, R.J., Grant, M.H., 2020. Cytotoxicity of cobalt chloride in brain cell lines - a comparison between astrocytoma and neuroblastoma cells. Toxicol. Vitr. 68, 104958. https://doi.org/10.1016/j.tiv.2020.104958

Goode, A.E., Perkins, J.M., Sandison, A., Karunakaran, C., Cheng, H., Wall, D., Skinner, J. a., Hart, A.J., Porter, A.E., McComb, D.W., Ryan, M.P., 2012. Chemical speciation of nanoparticles surrounding metal-on-metal hips. Chem. Commun. 48, 8335. https://doi.org/10.1039/c2cc33016d

Goyer, R.A., Clarkson, T.W., 2008. Toxic Effects of Metals, in: Klaassen, C.D. (Ed.), Casarett & Doull's Toxicology: The Basic Science of Poisons. McGraw-Hill, London, pp. 931–979.

Gradinaru, D., Minn, A.-L., Artur, Y., Minn, A., Heydel, J.-M., 2009. Drug metabolizing enzyme expression in rat choroid plexus: effects of in vivo xenobiotics treatment. Arch. Toxicol. 83, 581–586. https://doi.org/10.1007/s00204-008-0386-7

Green, B., Griffiths, E., Almond, S., 2017. Neuropsychiatric symptoms following metal-on-metal implant failure with cobalt and chromium toxicity. BMC Psychiatry 17, 33. https://doi.org/10.1186/s12888-016-1174-1

Habermann, B., Villaveces, J., Koti, P., 2015. Tools for visualization and analysis of molecular networks, pathways, and -omics data. Adv. Appl. Bioinforma. Chem. 8, 11–22. https://doi.org/10.2147/AABC.S63534

Hailer, Y.D., Kärrholm, J., Eriksson, N., Holmberg, L., Hailer, N.P., 2022. Similar risk of cancer in patients younger than 55 years with or without a total hip arthroplasty (THA): a population- based cohort study on 18,771 exposed to THA and 87,683 controls. Acta Orthop. 93, 317–326. https://doi.org/10.2340/17453674.2022.2044

Hallab, N., 2017. Diagnosis of Metal Hypersensitivity in Orthopedics. Oper. Tech. Orthop. 27, 168–177. https://doi.org/10.1053/j.oto.2017.05.005

Hallab, N.J., Jacobs, J.J., 2017. Chemokines Associated with Pathologic Responses to Orthopedic Implant Debris. Front. Endocrinol. (Lausanne). 8, 5. https://doi.org/10.3389/fendo.2017.00005

Hamamura, M., Oshikata, T., Katoku, K., Tsuchitani, M., Yamaguchi, R., 2017. Two types of deposits, hyaline droplets and eosinophilic bodies, associated with α_{2u}-globulin accumulation in the rat kidney. J. Toxicol. Pathol. 30, 275–282. https://doi.org/10.1293/tox.2017-0023

Harrison-Brown, M., Scholes, C., Field, C., McQuilty, R., Farah, S.B., Nizam, I., Kerr, D., Kohan, L., 2020. Limited penetration of cobalt and chromium ions into the cerebrospinal fluid following metal on metal arthroplasty: a cross-sectional analysis. Clin. Toxicol. 58, 233–240. https://doi.org/10.1080/15563650.2019.1636993

Hart, A.J., Quinn, P.D., Sampson, B., Sandison, A., Atkinson, K.D., Skinner, J.A., Powell, J.J., Mosselmans, J.F.W., 2010. The chemical form of metallic debris in tissues surrounding metal-on-metal hips with unexplained failure. Acta Biomater. 6, 4439–4446. https://doi.org/10.1016/j.actbio.2010.06.006

Hart, A.J., Sandison, A., Quinn, P., Sampson, B., Atkinson, K.D., Skinner, J.A., Goode, A., Powell, J.J., Mosselmans, J.F.W., 2009. Microfocus study of metal distribution and speciation in tissue extracted from revised metal on metal hip implants. J. Phys. Conf. Ser. 190, 012208. https://doi.org/10.1088/1742-6596/190/1/012208

Hartwig, K., Fackler, V., Jaksch-Bogensperger, H., Winter, S., Furtner, T., Couillard-Despres, S., Meier, D., Moessler, H., Aigner, L., 2014. Cerebrolysin protects PC12 cells from CoCl2 -induced hypoxia employing GSK3β signaling. Int. J. Dev. Neurosci. 38, 52–58. https://doi.org/10.1016/j.ijdevneu.2014.07.005

Haughom, B.D., Erickson, B.J., Hellman, M.D., Jacobs, J.J., 2015. Do Complication Rates Differ by Gender After Metal-on-metal Hip Resurfacing Arthroplasty? A Systematic Review. Clin. Orthop. Relat. Res. 473, 2521–2529. https://doi.org/10.1007/s11999-015-4227-8

He, Y., Sun, B., Li, S., Sun, X., Guo, Y., Zhao, H., Wang, Y., Jiang, G., Xing, M., 2016. Simultaneous analysis 26 mineral element contents from highly consumed cultured chicken overexposed to arsenic trioxide by inductively coupled plasma mass spectrometry. Environ. Sci. Pollut. Res. 23, 21741–21750. https://doi.org/10.1007/s11356-016-7318-5

Heckman, P.R.A., Blokland, A., Bollen, E.P.P., Prickaerts, J., 2018. Phosphodiesterase inhibition and modulation of corticostriatal and hippocampal circuits: Clinical overview and translational considerations. Neurosci. Biobehav. Rev. 87, 233–254. https://doi.org/10.1016/j.neubiorev.2018.02.007

Heinloth, A.N., Irwin, R.D., Boorman, G.A., Nettesheim, P., Fannin, R.D., Sieber, S.O., Snell, M.L., Tucker, C.J., Li, L., Travlos, G.S., Vansant, G., Blackshear, P.E., Tennant, R.W., Cunningham, M.L., Paules, R.S., 2004. Gene Expression Profiling of Rat Livers Reveals Indicators of Potential Adverse Effects. Toxicol. Sci. 80, 193–202. https://doi.org/10.1093/toxsci/kfh145

Ho, J.H., Leikin, J.B., Dargan, P.I., Archer, J.R.H., Wood, D.M., Brent, J., 2017. Metal-on-Metal Hip Joint Prostheses: a Retrospective Case Series Investigating the Association of Systemic Toxicity with Serum Cobalt and Chromium Concentrations. J. Med. Toxicol. 13, 321–328. https://doi.org/10.1007/s13181-017-0629-1

Hodge, R.D., Bakken, T.E., Miller, J.A., Smith, K.A., Barkan, E.R., Graybuck, L.T., Close, J.L., Long, B., Johansen, N., Penn, O., Yao, Z., Eggermont, J., Höllt, T., Levi, B.P., Shehata, S.I., Aevermann, B., Beller, A., Bertagnolli, D., Brouner, K., Casper, T., Cobbs, C., Dalley, R., Dee, N., Ding, S.-L., Ellenbogen, R.G., Fong, O., Garren, E., Goldy, J., Gwinn, R.P., Hirschstein, D., Keene, C.D., Keshk, M., Ko, A.L., Lathia, K., Mahfouz, A., Maltzer, Z., McGraw, M., Nguyen, T.N., Nyhus, J., Ojemann, J.G., Oldre, A., Parry, S., Reynolds, S., Rimorin, C., Shapovalova, N. V., Somasundaram, S., Szafer, A., Thomsen, E.R., Tieu, M., Quon, G., Scheuermann, R.H., Yuste, R., Sunkin, S.M., Lelieveldt, B., Feng, D., Ng, L., Bernard, A., Hawrylycz, M., Phillips, J.W., Tasic, B., Zeng, H., Jones, A.R., Koch, C., Lein, E.S., 2019. Conserved cell types with divergent features in human versus mouse cortex. Nature 573, 61–68. https://doi.org/10.1038/s41586-019-1506-7

Hoffmanová, I., Sánchez, D., 2018. Metabolic acidosis and anaemia associated with dorzolamide in a patient with impaired renal function. Br J Clin Pharmacol. 84, 796–799. https://doi.org/10.1111/bcp.13499

Honkakoski, P., Negishi, M., 2000. Regulation of cytochrome P450 (CYP) genes by nuclear receptors. Biochem. J. 347, 321–37. https://doi.org/10.1042/0264-6021:3470321

Houeto, P., Houzé, P., Baud, F.J., 2018. Comparative study of the tissue distribution of equimolar repeated doses of hydroxocobalamin and cobalt chloride in the rats. Ann. Biol. Clin. (Paris). 76, 179–184. https://doi.org/10.1684/abc.2017.1318

Hu, J., Yao, H., Gan, F., Tokarski, A., Wang, Y., 2012. Interaction of OKL38 and p53 in regulating mitochondrial structure and function. PLoS One 7. https://doi.org/10.1371/journal.pone.0043362

Hunt, L.P., Whitehouse, M.R., Beswick, A., Porter, M.L., Howard, P., Blom, A.W., 2018. Implications of Introducing New Technology: Comparative Survivorship Modeling of Metal-on-Metal Hip Replacements and Contemporary Alternatives in the National Joint Registry. J. Bone Jt. Surg. 100, 189–196. https://doi.org/10.2106/JBJS.17.00039

Ilo, K.C., Aboelmagd, K., Hothi, H.S., Asaad, A., Skinner, J.A., Hart, A.J., 2021. Does modularity of metal-on-metal hip implants increase cobalt: chromium ratio? HIP Int. 31, 109–114. https://doi.org/10.1177/1120700019873637

Inacio, M.C.S., Ake, C.F., Paxton, E.W., Khatod, M., Wang, C., Gross, T.P., Kaczmarek, R.G., Marinac-Dabic, D., Sedrakyan, A., 2013. Sex and Risk of Hip Implant Failure. JAMA Intern. Med. 173, 435–41. https://doi.org/10.1001/jamainternmed.2013.3271

Jahed, Z., Mofrad, M.R., 2019. The nucleus feels the force, LINCed in or not! Curr. Opin. Cell Biol. 58, 114–119. https://doi.org/10.1016/j.ceb.2019.02.012

Jakutis, G., Stainier, Di.Y.R., 2021. Genotype–Phenotype Relationships in the Context of Transcriptional Adaptation and Genetic Robustness. Annu. Rev. Genet. 55, 71–91. https://doi.org/10.1146/annurev-genet-071719-020342

Janssen, S.F., Van Der Spek, S.J.F., Ten Brink, J.B., Essing, A.H.W., Gorgels, T.G.M.F., Van Der Spek, P.J., Jansonius, N.M., Bergen, A.A.B., 2013. Gene expression and functional annotation of the human and mouse choroid plexus epithelium. PLoS One 8. https://doi.org/10.1371/journal.pone.0083345

Jensen, P.J., Gitlin, J.D., Carayannopoulos, M.O., 2006. GLUT1 Deficiency Links Nutrient Availability and Apoptosis during Embryonic Development. J. Biol. Chem. 281, 13382–13387. https://doi.org/10.1074/jbc.M601881200

Jiang, X., Weng, Y., Wu, X., Cui, J., Lyu, H., Jiang, J., Song, G., Jin, H., Qin, D., Wang, C., 2020. Early globalized industrial chain revealed by residual submicron pigment particles in Chinese imperial blue-and-white porcelains. Proc. Natl. Acad. Sci. 117, 6446–6452. https://doi.org/10.1073/pnas.1916630117

Johansen, A., Rosti, R.O., Musaev, D., Sticca, E., Harripaul, R., Zaki, M., Çağlayan, A.O., Azam, M., Sultan, T., Froukh, T., Reis, A., Popp, B., Ahmed, I., John, P., Ayub, M., Ben-Omran, T., Vincent, J.B., Gleeson, J.G., Abou Jamra, R., 2016. Mutations in MBOAT7 , Encoding Lysophosphatidylinositol Acyltransferase I, Lead to Intellectual Disability Accompanied by Epilepsy and Autistic Features. Am. J. Hum. Genet. 99, 912–916. https://doi.org/10.1016/j.ajhg.2016.07.019

Johanson, C., Stopa, E., McMillan, P., Roth, D., Funk, J., Krinke, G., 2011. The Distributional Nexus of Choroid Plexus to Cerebrospinal Fluid, Ependyma and Brain. Toxicol. Pathol. 39, 186–212. https://doi.org/10.1177/0192623310394214

Jones, S.M., Novak, A.E., Elliott, J.P., 2013. The role of HIF in cobalt-induced ischemic tolerance. Neuroscience 252, 420–430. https://doi.org/10.1016/j.neuroscience.2013.07.060

Joseph, P., 2017. Transcriptomics in toxicology. Food Chem. Toxicol. 109, 650–662. https://doi.org/10.1016/j.fct.2017.07.031

Jung, J.-Y., Kim, W.-J., 2004. Involvement of mitochondrial- and Fas-mediated dual mechanism in CoCl2-induced apoptosis of rat PC12 cells. Neurosci. Lett. 371, 85–90. https://doi.org/10.1016/j.neulet.2004.06.069

Jung, J.-Y., Mo, H.-C., Yang, K.-H., Jeong, Y.-J., Yoo, H.-G., Choi, N.-K., Oh, W.-M., Oh, H.-K., Kim, S.-H., Lee, J.-H., Kim, H.-J., Kim, W.-J., 2007. Inhibition by epigallocatechin gallate of CoCl2-induced apoptosis in rat PC12 cells. Life Sci. 80, 1355–1363. https://doi.org/10.1016/j.lfs.2006.11.033

Jung, J., Lee, M.G., 2014. Role of calcium signaling in epithelial bicarbonate secretion. Cell Calcium 55, 376–384. https://doi.org/10.1016/j.ceca.2014.02.002

Jung, J.Y., Roh, K.H., Jeong, Y.J., Kim, S.H., Lee, E.J., Kim, M.S., Oh, W.M., Oh, H.K., Kim, W.J., 2008. Estradiol protects PC12 cells against CoCl2-induced apoptosis. Brain Res. Bull. 76, 579–585. https://doi.org/10.1016/j.brainresbull.2008.04.006

Kajiwara, K., Sunaga, K., Tsuda, T., Sugaya, A., Sugaya, E., Kimura, M., 2008. Peony root extract upregulates transthyretin and phosphoglycerate mutase in mouse cobalt focus seizure. Biochem. Biophys. Res. Commun. 371, 375–379. https://doi.org/10.1016/j.bbrc.2008.04.094

Kambali, S., Taj, A., 2018. Polycythemia vera masked due to severe iron deficiency anemia. Hematol. Oncol. Stem Cell Ther. 11, 38–40. https://doi.org/10.1016/j.hemonc.2016.08.007

Kanno, J., 2016. Introduction to the concept of signal toxicity. J. Toxicol. Sci. 41, SP105–SP109. https://doi.org/10.2131/jts.41.SP105

Kapoor, P., Greipp, P.T., Schaefer, E.W., Mandrekar, S.J., Kamal, A.H., Gonzalez-Paz, N.C., Kumar, S., Greipp, P.R., 2010. Idiopathic Systemic Capillary Leak Syndrome (Clarkson's Disease): The Mayo Clinic Experience. Mayo Clin. Proc. 85, 905–912. https://doi.org/10.4065/mcp.2010.0159

Karovic, O., Tonazzini, I., Rebola, N., Edström, E., Lövdahl, C., Fredholm, B.B., Daré,

E., 2007. Toxic effects of cobalt in primary cultures of mouse astrocytes. Similarities with hypoxia and role of HIF-1α. Biochem. Pharmacol. 73, 694–708. https://doi.org/10.1016/j.bcp.2006.11.008

Kavanagh, K.T., Kraman, S.S., Kavanagh, S.P., 2018. An Analysis of the FDA MAUDE Database and the Search for Cobalt Toxicity in Class 3 Johnson & Johnson/DePuy Metal-on-Metal Hip Implants. J. Patient Saf. 14, e89–e96. https://doi.org/10.1097/PTS.0000000000000534

Kayembe-Kitenge, T., Manyong'a Kadiamba, V., Luca, C., Musa Obadia, P., Kasamba Ilunga, E., Mbuyi-Musanzayi, S., Nawrot, T., Lubaba Nkulu, C.B., Nemery, B., Devriendt, K., 2020. Agnathia otocephaly: A case from the Katanga Copperbelt. Birth Defects Res. 112, 1287–1291. https://doi.org/10.1002/bdr2.1758

Kelly, M.P., Adamowicz, W., Bove, S., Hartman, A.J., Mariga, A., Pathak, G., Reinhart, V., Romegialli, A., Kleiman, R.J., 2014. Select 3′,5′-cyclic nucleotide phosphodiesterases exhibit altered expression in the aged rodent brain. Cell. Signal. 26, 383–397. https://doi.org/10.1016/j.cellsig.2013.10.007

Kerger, B.D., Gerads, R., Gurleyuk, H., Tsuji, J.A., 2018. Metals Measurements in Body Tissues and Fluids: Toxicological and Clinical Importance of Standardizing Quality Analytical Methods for Differentiating Cobalt Partitioning on a Molecular Level, in: Beyond the Implant: Retrieval Analysis Methods for Implant Surveillance. ASTM International, 100 Barr Harbor Drive, PO Box C700, West Conshohocken, PA 19428-2959, pp. 229–244. https://doi.org/10.1520/STP160620170034

Kesteloot, H., Roelandt, J., Willems, J., Claes, J.H., Joossens, J. V., 1968. An Enquiry into the Role of Cobalt in the Heart Disease of Chronic Beer Drinkers. Circulation 37, 854–864. https://doi.org/10.1161/01.CIR.37.5.854

Khan, A.H., Verma, R., Bajpai, A., Mackey-Bojack, S., 2015. Unusual Case of Congestive Heart Failure. Circ. Cardiovasc. Imaging 8, e003352. https://doi.org/10.1161/CIRCIMAGING.115.003352

Khatau, S.B., Hale, C.M., Stewart-Hutchinson, P.J., Patel, M.S., Stewart, C.L., Searson, P.C., Hodzic, D., Wirtz, D., 2009. A perinuclear actin cap regulates nuclear shape. Proc. Natl. Acad. Sci. 106, 19017–19022. https://doi.org/10.1073/pnas.0908686106

Khrustalev, V.V., Khrustaleva, T.A., Poboinev, V.V., Karchevskaya, C.I., Shablovskaya, E.A., Terechova, T.G., 2019. Cobalt(II) cation binding by proteins.

Metallomics 11, 1743–1752. https://doi.org/10.1039/C9MT00205G

Kikuchi, S., Ninomiya, T., Kohno, T., Kojima, T., Tatsumi, H., 2018. Cobalt inhibits motility of axonal mitochondria and induces axonal degeneration in cultured dorsal root ganglion cells of rat. Cell Biol. Toxicol. 34, 93–107. https://doi.org/10.1007/s10565-017-9402-0

Kim, J.-K., Louhghalam, A., Lee, G., Schafer, B.W., Wirtz, D., Kim, D.-H., 2017. Nuclear lamin A/C harnesses the perinuclear apical actin cables to protect nuclear morphology. Nat. Commun. 8, 2123. https://doi.org/10.1038/s41467-017-02217-5

Kinoshita, T., 2020. Biosynthesis and biology of mammalian GPI-anchored proteins. Open Biol. 10, 190290. https://doi.org/10.1098/rsob.190290

Kirkland, D., Brock, T., Haddouk, H., Hargeaves, V., Lloyd, M., Mc Garry, S., Proudlock, R., Sarlang, S., Sewald, K., Sire, G., Sokolowski, A., Ziemann, C., 2015. New investigations into the genotoxicity of cobalt compounds and their impact on overall assessment of genotoxic risk. Regul. Toxicol. Pharmacol. 73, 311–338. https://doi.org/10.1016/j.yrtph.2015.07.016

Klionsky, D.J., Al., E., 2016. Guidelines for the use and interpretation of assays for monitoring autophagy (3rd edition). Autophagy 12, 1–222. https://doi.org/10.1080/15548627.2015.1100356

Knieriem, H.J., Herbertz, G., 1969. Elektronemikroskopische Befunde sowie photometrische und aktivierungsanalytische Ergebnisse bei experimenteller Herzinsuffizienz durch Kobaltchlorid [Electron-microscopic findings, and photometric and activation-analytical results in experimental caridac . Virchows Arch. B, Cell Pathol. 2, 32–46. https://doi.org/10.1007/BF02889568

Knoop, A., Planitz, P., Wüst, B., Thevis, M., 2020. Analysis of cobalt for human sports drug testing purposes using ICP- and LC-ICP-MS. Drug Test. Anal. 12, 1666–1672. https://doi.org/10.1002/dta.2962

Köhler, K., Hillebrecht, A., Schulze Wischeler, J., Innocenti, A., Heine, A., Supuran, C.T., Klebe, G., 2007. Saccharin Inhibits Carbonic Anhydrases: Possible Explanation for its Unpleasant Metallic Aftertaste. Angew. Chemie Int. Ed. 46, 7697–7699. https://doi.org/10.1002/anie.200701189

Koronfel, M.A., Goode, A.E., Weker, J.N., Tay, S.E.R., Stitt, C.A., Simoes, T.A., Mosselmans, J.F.W., Quinn, P., Brydson, R., Hart, A., Toney, M.F., Porter, A.E., Ryan, M.P., 2018. Understanding the reactivity of CoCrMo-implant wear particles. npj Mater. Degrad. 2, 8. https://doi.org/10.1038/s41529-018-0029-2

Kosa, P., Wu, T., Phillips, J., Leinonen, M., Masvekar, R., Komori, M., Wichman, A., Sandford, M., Bielekova, B., 2020. Idebenone does not inhibit disability progression in primary progressive MS. Mult. Scler. Relat. Disord. 45, 102434. https://doi.org/10.1016/j.msard.2020.102434

Kotake-Nara, E., Saida, K., 2007. Characterization of CoCl2-induced reactive oxygen species (ROS): Inductions of neurite outgrowth and endothelin-2/vasoactive intestinal contractor in PC12 cells by CoCl2 are ROS dependent, but those by MnCl2 are not. Neurosci. Lett. 422, 223–227. https://doi.org/10.1016/j.neulet.2007.06.026

Kovochich, M., Finley, B.L., Novick, R., Monnot, A.D., Donovan, E., Unice, K.M., Fung, E.S., Fung, D., Paustenbach, D.J., 2018. Understanding outcomes and toxicological aspects of second generation metal-on-metal hip implants: a state-of-the-art review. Crit Rev Toxicol 48, 853–901. https://doi.org/10.1080/10408444.2018.1563048

Kugler, J.E., Horsch, M., Huang, D., Furusawa, T., Rochman, M., Garrett, L., Becker, L., Bohla, A., Hölter, S.M., Prehn, C., Rathkolb, B., Racz, I., Aguilar-Pimentel, J.A., Adler, T., Adamski, J., Beckers, J., Busch, D.H., Eickelberg, O., Klopstock, T., Ollert, M., Stöger, T., Wolf, E., Wurst, W., Yildirim, A.Ö., Zimmer, A., Gailus-Durner, V., Fuchs, H., Hrabě de Angelis, M., Garfinkel, B., Orly, J., Ovcharenko, I., Bustin, M., 2013. High Mobility Group N Proteins Modulate the Fidelity of the Cellular Transcriptional Profile in a Tissue- and Variant-specific Manner. J. Biol. Chem. 288, 16690–16703. https://doi.org/10.1074/jbc.M113.463315

Kultgen, P.L., Byrd, S.K., Ostrowski, L.E., Milgram, S.L., 2002. Characterization of an A-Kinase Anchoring Protein in Human Ciliary Axonemes. Mol. Biol. Cell 13, 4156–4166. https://doi.org/10.1091/mbc.e02-07-0391

Lakics, V., Karran, E.H., Boess, F.G., 2010. Quantitative comparison of phosphodiesterase mRNA distribution in human brain and peripheral tissues. Neuropharmacology 59, 367–374. https://doi.org/10.1016/j.neuropharm.2010.05.004

Langlet, F., 2014. Tanycytes: A Gateway to the Metabolic Hypothalamus. J. Neuroendocrinol. 26, 753–760. https://doi.org/10.1111/jne.12191

Langton, D.J., Natu, S., Harrington, C.F., Bowsher, J.G., Nargol, A.V.F., 2019. Is the synovial fluid cobalt-to-chromium ratio related to the serum partitioning of metal debris following metal-on-metal hip arthroplasty? Bone Joint Res. 8, 146–155.

https://doi.org/10.1302/2046-3758.83.BJR-2018-0049.R1

Langton, D.J., Sidaginamale, R.P., Joyce, T.J., Bowsher, J.G., Holland, J.P., Deehan, D., Nargol, A.V.F., Natu, S., 2018. Aseptic lymphocyte-dominated vasculitis-associated lesions are related to changes in metal ion handling in the joint capsules of metal-on-metal hip arthroplasties. Bone Joint Res. 7, 388–396. https://doi.org/10.1302/2046-3758.76.BJR-2018-0037

Langton, D.J., Sidaginamale, R.P., Joyce, T.J., Natu, S., Blain, P., Jefferson, R.D., Rushton, S., Nargol, A.V.F., 2013. The clinical implications of elevated blood metal ion concentrations in asymptomatic patients with MoM hip resurfacings: a cohort study. BMJ Open 3, 1–10. https://doi.org/10.1136/bmjopen-2012-001541

Laovitthayanggoon, S., Henderson, C.J., McCluskey, C., MacDonald, M., Tate, R.J., Grant, M.H., Currie, S., 2019. Cobalt Administration Causes Reduced Contractility with Parallel Increases in TRPC6 and TRPM7 Transporter Protein Expression in Adult Rat Hearts. Cardiovasc. Toxicol. 19, 276–286. https://doi.org/10.1007/s12012-018-9498-3

Lassalle, M., Colas, S., Rudnichi, A., Zureik, M., Dray-Spira, R., 2018. Is There a Cardiotoxicity Associated With Metallic Head Hip Prostheses? A Cohort Study in the French National Health Insurance Databases. Clin. Orthop. Relat. Res. 476, 1441–1451. https://doi.org/10.1097/01.blo.0000533617.64678.69

Le Merre, P., Ährlund-Richter, S., Carlén, M., 2021. The mouse prefrontal cortex: Unity in diversity. Neuron. https://doi.org/10.1016/j.neuron.2021.03.035

Learmonth, I.D., Young, C., Rorabeck, C., 2007. The operation of the century: total hip replacement. Lancet 370, 1508–1519. https://doi.org/10.1016/S0140-6736(07)60457-7

Lee, H.-C., Inoue, T., Sasaki, J., Kubo, T., Matsuda, S., Nakasaki, Y., Hattori, M., Tanaka, F., Udagawa, O., Kono, N., Itoh, T., Ogiso, H., Taguchi, R., Arita, M., Sasaki, T., Arai, H., 2012. LPIAT1 regulates arachidonic acid content in phosphatidylinositol and is required for cortical lamination in mice. Mol. Biol. Cell 23, 4689–4700. https://doi.org/10.1091/mbc.e12-09-0673

Lee, J.-H., Choi, S.-H., Baek, M.-W., Kim, M.-H., Kim, H.-J., Kim, S.-H., Oh, S.-J., Park, H.-J., Kim, W.-J., Jung, J.-Y., 2013. CoCl2 induces apoptosis through the mitochondria- and death receptor-mediated pathway in the mouse embryonic stem cells. Mol. Cell. Biochem. 379, 133–140. https://doi.org/10.1007/s11010-013-1635-5

Lee, J.L., Oh, E.S., Lee, R.W., Finucane, T.E., 2015. Serum Albumin and Prealbumin in Calorically Restricted, Nondiseased Individuals: A Systematic Review. Am. J. Med. 128, 1023.e1-1023.e22. https://doi.org/10.1016/j.amjmed.2015.03.032

Lee, M., Kang, H., Jang, S.-W., 2013. CoCl2 induces PC12 cells apoptosis through p53 stability and regulating UNC5B. Brain Res. Bull. 96, 19–27. https://doi.org/10.1016/j.brainresbull.2013.04.007

Lehtovirta, L., Reito, A., Lainiala, O., Parkkinen, J., Hothi, H., Henckel, J., Hart, A., Eskelinen, A., 2019. Host-specific factors affect the pathogenesis of adverse reaction to metal debris. BMC Musculoskelet. Disord. 20, 195. https://doi.org/10.1186/s12891-019-2578-0

Leikin, J.B., Karydes, H.C., Whiteley, P.M., Wills, B.K., Cumpston, K.L., Jacobs, J.J., 2013. Outpatient toxicology clinic experience of patients with hip implants. Clin. Toxicol. 51, 230–236. https://doi.org/10.3109/15563650.2013.768343

Leyssens, L., Vinck, B., Van Der Straeten, C., De Smet, K., Dhooge, I., Wuyts, F.L., Keppler, H., Degeest, S., Valette, R., Lim, R., Maes, L., 2020. The Ototoxic Potential of Cobalt From Metal-on-Metal Hip Implants. Ear Hear. 41, 217–230. https://doi.org/10.1097/AUD.0000000000000747

Li, P., Ding, D., Salvi, R., Roth, J.A., 2015. Cobalt-Induced Ototoxicity in Rat Postnatal Cochlear Organotypic Cultures. Neurotox. Res. 28, 209–221. https://doi.org/10.1007/s12640-015-9538-8

Li, Y., Jiao, Q., Xu, H., Du, X., Shi, L., Jia, F., Jiang, H., 2017. Biometal Dyshomeostasis and Toxic Metal Accumulations in the Development of Alzheimer's Disease. Front. Mol. Neurosci. 10, 339. https://doi.org/10.3389/fnmol.2017.00339

Liberti, M. V., Locasale, J.W., 2016. The Warburg Effect: How Does it Benefit Cancer Cells? Trends Biochem. Sci. 41, 211–218. https://doi.org/10.1016/j.tibs.2015.12.001

Lim, C.A., Khan, J., Chelva, E., Khan, R., Unsworth-Smith, T., 2015. The effect of cobalt on the human eye. Doc. Ophthalmol. 130, 43–48. https://doi.org/10.1007/s10633-014-9469-3

Lindsay, D., Kerr, W., 2011. Cobalt close-up. Nat. Chem. 3, 494–494. https://doi.org/10.1038/nchem.1053

Linna, A., Uitti, J., Oksa, P., Toivio, P., Virtanen, V., Lindholm, H., Halkosaari, M., Sauni, R., 2020. Effects of occupational cobalt exposure on the heart in the

production of cobalt and cobalt compounds: a 6-year follow-up. Int. Arch. Occup. Environ. Health 93, 365–374. https://doi.org/10.1007/s00420-019-01488-3

Lionetto, M.G., Caricato, R., Giordano, M.E., Schettino, T., 2016. The Complex Relationship between Metals and Carbonic Anhydrase : New Insights and Perspectives. https://doi.org/10.3390/ijms17010127

Liu, Y., Beyer, A., Aebersold, R., 2016. On the Dependency of Cellular Protein Levels on mRNA Abundance. Cell 165, 535–550. https://doi.org/10.1016/j.cell.2016.03.014

Lodge, F., Khatun, R., Lord, R., John, A., Fraser, A.G., Yousef, Z., 2018. Prevalence of subclinical cardiac abnormalities in patients with metal-on-metal hip replacements. Int. J. Cardiol. 271, 274–280. https://doi.org/10.1016/j.ijcard.2018.05.047

Low, A.K., Matharu, G.S., Ostlere, S.J., Murray, D.W., Pandit, H.G., 2016. How Should We Follow-Up Asymptomatic Metal-on-Metal Hip Resurfacing Patients? A Prospective Longitudinal Cohort Study. J. Arthroplasty 31, 146–151. https://doi.org/10.1016/j.arth.2015.08.007

Lowry, O.H., Rosebrough, N.J., Farr, A.L., Randall, R.J., 1951. Protein measurement with the folin phenol reagent. J. Biol. Chem. 193, 265–75.

Lü, L., Zhang, L., Wai, M.S.M., Yew, D.T.W., Xu, J., 2012. Exocytosis of MTT formazan could exacerbate cell injury. Toxicol Vitr. 26, 636–644. https://doi.org/10.1016/j.tiv.2012.02.006

Lun, M.P., Johnson, M.B., Broadbelt, K.G., Watanabe, M., Kang, Y. -j., Chau, K.F., Springel, M.W., Malesz, A., Sousa, A.M.M., Pletikos, M., Adelita, T., Calicchio, M.L., Zhang, Y., Holtzman, M.J., Lidov, H.G.W., Sestan, N., Steen, H., Monuki, E.S., Lehtinen, M.K., 2015. Spatially Heterogeneous Choroid Plexus Transcriptomes Encode Positional Identity and Contribute to Regional CSF Production. J. Neurosci. 35, 4903–4916. https://doi.org/10.1523/JNEUROSCI.3081-14.2015

Luo, W., Pant, G., Bhavnasi, Y.K., Blanchard, S.G., Brouwer, C., 2017. Pathview Web: user friendly pathway visualization and data integration. Nucleic Acids Res. 45, W501–W508. https://doi.org/10.1093/nar/gkx372

Machado, C., Appelbe, A., Wood, R., 2012. Arthroprosthetic Cobaltism and Cardiomyopathy. Hear. Lung Circ. 21, 759–760. https://doi.org/10.1016/j.hlc.2012.03.013

Madl, A.K., Kovochich, M., Liong, M., Finley, B.L., Paustenbach, D.J., Oberdörster, G., 2015. Toxicology of wear particles of cobalt-chromium alloy metal-on-metal hip implants Part II: Importance of physicochemical properties and dose in animal and in vitro studies as a basis for risk assessment. Nanomedicine Nanotechnology, Biol. Med. 11, 1285–1298. https://doi.org/10.1016/j.nano.2015.02.006

Magistretti, P.J., Allaman, I., 2015. A Cellular Perspective on Brain Energy Metabolism and Functional Imaging. Neuron 86, 883–901. https://doi.org/10.1016/j.neuron.2015.03.035

Malard, V., Berenguer, F., Prat, O., Ruat, S., Steinmetz, G., Quemeneur, E., 2007. Global gene expression profiling in human lung cells exposed to cobalt. BMC Genomics 8, 1–13. https://doi.org/10.1186/1471-2164-8-147

Maleki, F., Ovens, K., Hogan, D.J., Kusalik, A.J., 2020. Gene Set Analysis: Challenges, Opportunities, and Future Research. Front. Genet. 11, 654. https://doi.org/10.3389/fgene.2020.00654

Manton, W.I., Kirkpatrick, J.B., Cook, J.D., 1984. Does the choroid plexus really protect the brain from lead? Lancet 324, 351. https://doi.org/10.1016/S0140-6736(84)92719-3

Mao, X., Wong, A. a, Crawford, R.W., 2011. Cobalt toxicity--an emerging clinical problem in patients with metal-on-metal hip prostheses? Med. J. Aust. 194, 649–651. https://doi.org/10.5694/j.1326-5377.2011.tb03151.x

Markwardt, M.L., Seckinger, K.M., Rizzo, M.A., 2016. Regulation of Glucokinase by Intracellular Calcium Levels in Pancreatic β Cells. J. Biol. Chem. 291, 3000–3009. https://doi.org/10.1074/jbc.M115.692160

Martin, J.R., Spencer-Gardner, L., Camp, C.L., Stulak, J.M., Sierra, R.J., 2015. Cardiac cobaltism: A rare complication after bilateral metal-on-metal total hip arthroplasty. Arthroplast. Today 1, 99–102. https://doi.org/10.1016/j.artd.2015.10.002

Matharu, G.S., Judge, A., Pandit, H.G., Murray, D.W., 2018. Follow-up for patients with metal-on-metal hip replacements: Are the new MHRA recommendations justified? BMJ 360:k566. https://doi.org/10.1136/bmj.k566

Mathew, R.S., Mullan, H., Blusztajn, J.K., Lehtinen, M.K., 2016. Comment on “Multiple repressive mechanisms in the hippocampus during memory formation.” Science (80-.). 353, 453. https://doi.org/10.1126/science.aaf1288

Mathieu, E., Gupta, N., Ahari, A., Zhou, X., Hanna, J., Yücel, Y.H., 2017. Evidence for Cerebrospinal Fluid Entry Into the Optic Nerve via a Glymphatic Pathway. Investig.

Opthalmology Vis. Sci. 58, 4784–4791. https://doi.org/10.1167/iovs.17-22290

Mauger, J.-P., 2012. Role of the nuclear envelope in calcium signalling. Biol. Cell 104, 70–83. https://doi.org/10.1111/boc.201100103

Mauvais-Jarvis, F., Berthold, H.K., Campesi, I., Carrero, J.-J., Dhakal, S., Franconi, F., Gouni-Berthold, I., Heiman, M.L., Kautzky-Willer, A., Klein, S.L., Murphy, A., Regitz-Zagrosek, V., Reue, K., Rubin, J.B., 2021. Sex- and Gender-Based Pharmacological Response to Drugs. Pharmacol. Rev. 73, 730–762. https://doi.org/10.1124/pharmrev.120.000206

Maywald, M., Wessels, I., Rink, L., 2017. Zinc Signals and Immunity. Int. J. Mol. Sci. 18, 2222. https://doi.org/10.3390/ijms18102222

Mazerska, Z., Mróz, A., Pawłowska, M., Augustin, E., 2016. The role of glucuronidation in drug resistance. Pharmacol. Ther. 159, 35–55. https://doi.org/10.1016/j.pharmthera.2016.01.009

McMullen, P.D., Pendse, S.N., Black, M.B., Mansouri, K., Haider, S., Andersen, M.E., Clewell, R.A., 2019. Addressing systematic inconsistencies between in vitro and in vivo transcriptomic mode of action signatures. Toxicol. Vitr. 58, 1–12. https://doi.org/10.1016/j.tiv.2019.02.014

MDA/2010/033, 2010. Medical Device Alert. All metal-on-metal (MoM) hip replacements. http://www.mhra.gov.uk/. MHRA Database.

MDA/2017/018, 2017. Medical Device Alert. All metal-on-metal (MoM) hip replacements: updated advice for follow-up of patients. http://www.mhra.gov.uk/.

Meier, B., 2010. The Implants Loophole. New York Times Section B, Page 1.

Merritt, K., Brown, S.A., 1995. Release of hexavalent chromium from corrosion of stainless steel and cobalt?chromium alloys. J. Biomed. Mater. Res. 29, 627–633. https://doi.org/10.1002/jbm.820290510

Midzak, A., Papadopoulos, V., 2016. Adrenal Mitochondria and Steroidogenesis: From Individual Proteins to Functional Protein Assemblies. Front. Endocrinol. (Lausanne). 7, 106. https://doi.org/10.3389/fendo.2016.00106

Misale, M.S., Witek Janusek, L., Tell, D., Mathews, H.L., 2018. Chromatin organization as an indicator of glucocorticoid induced natural killer cell dysfunction. Brain. Behav. Immun. 67, 279–289. https://doi.org/10.1016/j.bbi.2017.09.004

Mitterdorfer, J., Bean, B.P., 2002. Potassium currents during the action potential of hippocampal CA3 neurons. J. Neurosci. 22, 10106–10115. https://doi.org/22/23/10106 [pii]

Mobasheri, A., Proudman, C.J., 2015. Cobalt chloride doping in racehorses: Concerns over a potentially lethal practice. Vet. J. 205, 335–338. https://doi.org/10.1016/j.tvjl.2015.04.005

Moretti, F., Rolando, C., Winker, M., Ivanek, R., Rodriguez, J., Von Kriegsheim, A., Taylor, V., Bustin, M., Pertz, O., 2015. Growth Cone Localization of the mRNA Encoding the Chromatin Regulator HMGN5 Modulates Neurite Outgrowth. Mol. Cell. Biol. 35, 2035–2050. https://doi.org/10.1128/MCB.00133-15

Moriel-Carretero, M., 2021. The Many Faces of Lipids in Genome Stability (and How to Unmask Them). Int. J. Mol. Sci. 22, 12930. https://doi.org/10.3390/ijms222312930

Morin, Y., Tětu, A., Mercier, G., 1969. Québec beer-drinkers' cardiomyopathy: clinical and hemodynamic aspects. Ann. N. Y. Acad. Sci. 156, 566–576. https://doi.org/10.1111/j.1749-6632.1969.tb16751.x

Morita, S., Furube, E., Mannari, T., Okuda, H., Tatsumi, K., Wanaka, A., Miyata, S., 2016. Heterogeneous vascular permeability and alternative diffusion barrier in sensory circumventricular organs of adult mouse brain. Cell Tissue Res. 363, 497–511. https://doi.org/10.1007/s00441-015-2207-7

Morrell, A.P., Floyd, H., W. Mosselmans, J.F., Grover, L.M., Castillo-Michel, H., Davis, E.T., Parker, J.E., Martin, R.A., Addison, O., 2019. Improving our understanding of metal implant failures: Multiscale chemical imaging of exogenous metals in ex-vivo biological tissues. Acta Biomater. 98, 284–293. https://doi.org/10.1016/j.actbio.2019.05.071

Morrison, J.P., Sharma, A.K., Rao, D., Pardo, I.D., Garman, R.H., Kaufmann, W., Bolon, B., 2015. Fundamentals of Translational Neuroscience in Toxicologic Pathology. Toxicol. Pathol. 43, 132–139. https://doi.org/10.1177/0192623314558306

Mosier, B.A., Maynard, L., Sotereanos, N.G., Sewecke, J.J., 2016. Progressive Cardiomyopathy in a Patient With Elevated Cobalt Ion Levels and Bilateral Metal-on-Metal Hip Arthroplasties. Am. J. Orthop. 45, E132-5.

Mou, Y.H., Yang, J.Y., Cui, N., Wang, J.M., Hou, Y., Song, S., Wu, C.F., 2012. Effects of cobalt chloride on nitric oxide and cytokines/chemokines production in microglia. Int. Immunopharmacol. 13, 120–125. https://doi.org/10.1016/j.intimp.2012.03.017

Muñoz-Sánchez, J., Chánez-Cárdenas, M.E., 2019. The use of cobalt chloride as a

chemical hypoxia model. J. Appl. Toxicol. 39, 556–570. https://doi.org/10.1002/jat.3749

Mushak, P., 2013. How prevalent is chemical hormesis in the natural and experimental worlds? Sci. Total Environ. 443, 573–581. https://doi.org/10.1016/j.scitotenv.2012.11.028

Nag, S., Resnick, A., 2017. Stabilization of hypoxia inducible factor by cobalt chloride can alter renal epithelial transport. Physiol. Rep. 5, e13531. https://doi.org/10.14814/phy2.13531

Nakamura, M., Yasutake, A., Fujimura, M., Hachiya, N., Marumoto, M., 2011. Effect of methylmercury administration on choroid plexus function in rats. Arch. Toxicol. 85, 911–918. https://doi.org/10.1007/s00204-010-0623-8

National Joint Registry, 2020. National Joint Registry. 17th Annual Report. http://www.njrcentre.org.uk.

National Joint Registry, 2016. National Joint Registry for England and Wales. 13th Annual report. http://www.njrcentre.org.uk.

Natu, S., Sidaginamale, R.P., Gandhi, J., Langton, D.J., Nargol, A.V.F., 2012. Adverse reactions to metal debris: histopathological features of periprosthetic soft tissue reactions seen in association with failed metal on metal hip arthroplasties. J. Clin. Pathol. 65, 409–418. https://doi.org/10.1136/jclinpath-2011-200398

Nava, M.M., Miroshnikova, Y.A., Biggs, L.C., Whitefield, D.B., Metge, F., Boucas, J., Vihinen, H., Jokitalo, E., Li, X., García Arcos, J.M., Hoffmann, B., Merkel, R., Niessen, C.M., Dahl, K.N., Wickström, S.A., 2020. Heterochromatin-Driven Nuclear Softening Protects the Genome against Mechanical Stress-Induced Damage. Cell 181, 800-817.e22. https://doi.org/10.1016/j.cell.2020.03.052

Naves, T., Jawhari, S., Jauberteau, M.-O., Ratinaud, M.-H., Verdier, M., 2013. Autophagy takes place in mutated p53 neuroblastoma cells in response to hypoxia mimetic CoCl2. Biochem. Pharmacol. 85, 1153–1161. https://doi.org/10.1016/j.bcp.2013.01.022

Neumaier, F., Dibué-Adjei, M., Hescheler, J., Schneider, T., 2015. Voltage-gated calcium channels: Determinants of channel function and modulation by inorganic cations. Prog. Neurobiol. 129, 1–36. https://doi.org/10.1016/j.pneurobio.2014.12.003

Newton, A.W., Ranganath, L., Armstrong, C., Peter, V., Roberts, N.B., 2012. Differential distribution of cobalt, chromium, and nickel between whole blood,

plasma and urine in patients after metal-on-metal (MoM) hip arthroplasty. J. Orthop. Res. 30, 1640–1646. https://doi.org/10.1002/jor.22107

Ng, C.T., Tang, F.M.A., Li, J.J., Ong, C., Yung, L.L.Y., Bay, B.H., 2015. Clathrin-Mediated Endocytosis of Gold Nanoparticles In Vitro. Anat. Rec. 298, 418–427. https://doi.org/10.1002/ar.23051

Nousiainen, T., Palosaari, S., Peräniemi, S., Tervahauta, A., Niinimäki, J., Leppilahti, J., Lehenkari, P., 2020. Retention of metals in periprosthetic tissues of patients with metal-on-metal total hip arthroplasty is reflected in the synovial fluid to blood cobalt transfer ratio in the presence of a pseudotumour. BMC Musculoskelet. Disord. 21, 610. https://doi.org/10.1186/s12891-020-03636-0

Ortega, R., Bresson, C., Fraysse, A., Sandre, C., Devès, G., Gombert, C., Tabarant, M., Bleuet, P., Seznec, H., Simionovici, A., Moretto, P., Moulin, C., 2009. Cobalt distribution in keratinocyte cells indicates nuclear and perinuclear accumulation and interaction with magnesium and zinc homeostasis. Toxicol. Lett. 188, 26–32. https://doi.org/10.1016/j.toxlet.2009.02.024

Osman, D., Foster, A.W., Chen, J., Svedaite, K., Steed, J.W., Lurie-Luke, E., Huggins, T.G., Robinson, N.J., 2017. Fine control of metal concentrations is necessary for cells to discern zinc from cobalt. Nat. Commun. 8. https://doi.org/10.1038/s41467-017-02085-z

Östlund, C., Hernandez-Ono, A., Shin, J.-Y., 2020. The Nuclear Envelope in Lipid Metabolism and Pathogenesis of NAFLD. Biology (Basel). 9, 338. https://doi.org/10.3390/biology9100338

Ouzzine, M., Gulberti, S., Ramalanjaona, N., Magdalou, J., Fournel-Gigleux, S., 2014. The UDP-glucuronosyltransferases of the blood-brain barrier: their role in drug metabolism and detoxication. Front. Cell. Neurosci. 8, 349. https://doi.org/10.3389/fncel.2014.00349

Packer, M., 2016. Cobalt Cardiomyopathy: A Critical Reappraisal in Light of a Recent Resurgence. Circ. Hear. Fail. 9, e003604. https://doi.org/10.1161/CIRCHEARTFAILURE.116.003604

Page, S., Munsell, A., Al-Ahmad, A.J., 2016. Cerebral hypoxia/ischemia selectively disrupts tight junctions complexes in stem cell-derived human brain microvascular endothelial cells. Fluids Barriers CNS 13, 16. https://doi.org/10.1186/s12987-016-0042-1

Pandit, H., Glyn-Jones, S., McLardy-Smith, P., Gundle, R., Whitwell, D., Gibbons,

C.L.M., Ostlere, S., Athanasou, N., Gill, H.S., Murray, D.W., 2008. Pseudotumours associated with metal-on-metal hip resurfacings. J. Bone Joint Surg. Br. 90-B, 847–851. https://doi.org/10.1302/0301-620X.90B7.20213

Paustenbach, D.J., Tvermoes, B.E., Unice, K.M., Finley, B.L., Kerger, B.D., 2013. A review of the health hazards posed by cobalt. Crit. Rev. Toxicol. 43, 316–362. https://doi.org/10.3109/10408444.2013.779633

Pelizzoni, I., Zacchetti, D., Campanella, A., Grohovaz, F., Codazzi, F., 2013. Iron uptake in quiescent and inflammation-activated astrocytes: A potentially neuroprotective control of iron burden. Biochim. Biophys. Acta 1832, 1326–1333. https://doi.org/10.1016/j.bbadis.2013.04.007

Perino, G., De Martino, I., Zhang, L., Xia, Z., Gallo, J., Natu, S., Langton, D., Huber, M., Rakow, A., Schoon, J., Gomez-Barrena, E., Krenn, V., 2021. The contribution of the histopathological examination to the diagnosis of adverse local tissue reactions in arthroplasty. EFORT Open Rev. 6, 399–419. https://doi.org/10.1302/2058-5241.6.210013

Permenter, M.G., Dennis, W.E., Sutto, T.E., Jackson, D.A., Lewis, J.A., Stallings, J.D., 2013. Exposure to cobalt causes transcriptomic and proteomic changes in two rat liver derived cell lines. PLoS One 8. https://doi.org/10.1371/journal.pone.0083751

Peters, K., Schmidt, H., Unger, R.E., Kamp, G., Pröls, F., Berger, B.J., Kirkpatrick, C.J., 2005. Paradoxical effects of hypoxia-mimicking divalent cobalt ions in human endothelial cells in vitro. Mol. Cell. Biochem. 270, 157–166. https://doi.org/10.1007/s11010-005-4504-z

Pezzini, F., Bettinetti, L., Di Leva, F., Bianchi, M., Zoratti, E., Carrozzo, R., Santorelli, F.M., Delledonne, M., Lalowski, M., Simonati, A., 2017. Transcriptomic Profiling Discloses Molecular and Cellular Events Related to Neuronal Differentiation in SH-SY5Y Neuroblastoma Cells. Cell. Mol. Neurobiol. 37, 665–682. https://doi.org/10.1007/s10571-016-0403-y

Phatak, V.M., Muller, P.A.J., 2015. Metal toxicity and the p53 protein: an intimate relationship. Toxicol. Res. (Camb). 4, 576–591. https://doi.org/10.1039/C4TX00117F

Pikuleva, I.A., Waterman, M.R., 2013. Cytochromes P450: Roles in Diseases. J. Biol. Chem. 288, 17091–17098. https://doi.org/10.1074/jbc.R112.431916

Pinto, C.S., Raman, A., Reif, G.A., Magenheimer, B.S., White, C., Calvet, J.P., Wallace, D.P., 2016. Phosphodiesterase Isoform Regulation of Cell Proliferation

and Fluid Secretion in Autosomal Dominant Polycystic Kidney Disease. J. Am. Soc. Nephrol. 27, 1124–1134. https://doi.org/10.1681/ASN.2015010047

Podda, M.V., Grassi, C., 2014. New perspectives in cyclic nucleotide-mediated functions in the CNS : the emerging role of cyclic nucleotide-gated (CNG) channels 1241–1257. https://doi.org/10.1007/s00424-013-1373-2

Posada, O.M., Gilmour, D., Tate, R.J., Grant, M.H., 2014. CoCr wear particles generated from CoCr alloy metal-on-metal hip replacements, and cobalt ions stimulate apoptosis and expression of general toxicology-related genes in monocyte-like U937 cells. Toxicol. Appl. Pharmacol. 281, 125–135. https://doi.org/10.1016/j.taap.2014.09.010

Posada, O.M., Tate, R.J., Grant, M.H., 2015. Effects of CoCr metal wear debris generated from metal-on-metal hip implants and Co ions on human monocyte-like U937 cells. Toxicol. Vitr. 29, 271–280. https://doi.org/10.1016/j.tiv.2014.11.006

Prager-Khoutorsky, M., 2017. Mechanosensing in hypothalamic osmosensory neurons. Semin. Cell Dev. Biol. 71, 13–21. https://doi.org/10.1016/j.semcdb.2017.06.006

Probert, L., 2015. TNF and its receptors in the CNS: The essential, the desirable and the deleterious effects. Neuroscience 302, 2–22. https://doi.org/10.1016/j.neuroscience.2015.06.038

Provensi, G., Carta, F., Nocentini, A., Supuran, C.T., Casamenti, F., Passani, M.B., Fossati, S., 2019. A New Kid on the Block? Carbonic Anhydrases as Possible New Targets in Alzheimer's Disease. Int. J. Mol. Sci. 20, 4724. https://doi.org/10.3390/ijms20194724

Quintela, T., Gonçalves, I., Carreto, L.C., Santos, M.A.S., Marcelino, H., Patriarca, F.M., Santos, C.R.A., 2013. Analysis of the Effects of Sex Hormone Background on the Rat Choroid Plexus Transcriptome by cDNA Microarrays. PLoS One 8, e60199. https://doi.org/10.1371/journal.pone.0060199

Radhakrishnan, K., Kim, Y.-H., Jung, Y.S., Kim, J., Kim, D.-K., Cho, S.J., Lee, I.-K., Dooley, S., Lee, C.-H., Choi, H.-S., 2020. Orphan Nuclear Receptor ERRγ Is a Novel Transcriptional Regulator of IL-6 Mediated Hepatic BMP6 Gene Expression in Mice. Int. J. Mol. Sci. 21, 7148. https://doi.org/10.3390/ijms21197148

Rana, S.V.S., 2008. Metals and apoptosis: Recent developments. J. Trace Elem. Med. Biol. 22, 262–284. https://doi.org/10.1016/j.jtemb.2008.08.002

Rani, A., Prasad, S., 2014. CoCl2-Induced Biochemical Hypoxia Down Regulates

Activities and Expression of Super Oxide Dismutase and Catalase in Cerebral Cortex of Mice. Neurochem. Res. 39, 1787–1796. https://doi.org/10.1007/s11064-014-1388-x

Rao, D.B., Little, P.B., Sills, R.C., 2014. Subsite Awareness in Neuropathology Evaluation of National Toxicology Program (NTP) Studies: a review of select neuroanatomical structures with their functional significance in rodents. Toxicol. Pathol. 42, 487–509. https://doi.org/10.1177/0192623313501893

Ratinaud, M.-H., 2011. The cell death response to the ROS inducer, cobalt chloride, in neuroblastoma cell lines according to p53 status. Int. J. Oncol. 39, 601–609. https://doi.org/10.3892/ijo.2011.1083

Renner, L., Schmidt-Braekling, T., Faschingbauer, M., Boettner, F., 2016. Do cobalt and chromium levels predict osteolysis in metal-on-metal total hip arthroplasty? Arch. Orthop. Trauma Surg. 136, 1657–1662. https://doi.org/10.1007/s00402-016-2565-y

Repetto, G., del Peso, A., Zurita, J.L., 2008. Neutral red uptake assay for the estimation of cell viability/cytotoxicity. Nat. Protoc. 3, 1125–1131. https://doi.org/10.1038/nprot.2008.75

Reyes, J., Lahav, G., 2018. Leveraging and coping with uncertainty in the response of individual cells to therapy. Curr. Opin. Biotechnol. 51, 109–115. https://doi.org/10.1016/j.copbio.2017.12.007

Rizzetti, M.C., Liberini, P., Zarattini, G., Catalani, S., Pazzaglia, U., Apostoli, P., Padovani, A., 2009. Loss of sight and sound. Could it be the hip? Lancet 373, 1052. https://doi.org/10.1016/S0140-6736(09)60490-6

Rochman, M., Postnikov, Y., Correll, S., Malicet, C., Wincovitch, S., Karpova, T.S., McNally, J.G., Wu, X., Bubunenko, N.A., Grigoryev, S., Bustin, M., 2009. The Interaction of NSBP1/HMGN5 with Nucleosomes in Euchromatin Counteracts Linker Histone-Mediated Chromatin Compaction and Modulates Transcription. Mol. Cell 35, 642–656. https://doi.org/10.1016/j.molcel.2009.07.002

Rona, G., 1971. Experimental aspects of cobalt cardiomyopathy. Br. Heart J. 33, 171–174. https://doi.org/10.1136/hrt.33.Suppl.171

Sabbioni, E., Fortaner, S., Farina, M., Del Torchio, R., Olivato, I., Petrarca, C., Bernardini, G., Mariani-Costantini, R., Perconti, S., Di Giampaolo, L., Gornati, R., Di Gioacchino, M., 2014a. Cytotoxicity and morphological transforming potential of cobalt nanoparticles, microparticles and ions in Balb/3T3 mouse fibroblasts: an

in vitro model. Nanotoxicology 8, 455–464. https://doi.org/10.3109/17435390.2013.796538

Sabbioni, E., Fortaner, S., Farina, M., Del Torchio, R., Petrarca, C., Bernardini, G., Mariani-Costantini, R., Perconti, S., Di Giampaolo, L., Gornati, R., Di Gioacchino, M., 2014b. Interaction with culture medium components, cellular uptake and intracellular distribution of cobalt nanoparticles, microparticles and ions in Balb/3T3 mouse fibroblasts. Nanotoxicology 8, 88–99. https://doi.org/10.3109/17435390.2012.752051

Sadiq, S., Ghazala, Z., Chowdhury, A., Büsselberg, D., 2012. Metal Toxicity at the Synapse: Presynaptic, Postsynaptic, and Long-Term Effects. J. Toxicol. 2012, 132671. https://doi.org/10.1155/2012/132671

Salloum, Z., Lehoux, E.A., Harper, M., Catelas, I., 2021. Effects of cobalt and chromium ions on glycolytic flux and the stabilization of hypoxia-inducible factor-1α in macrophages in vitro. J. Orthop. Res. 39, 112–120. https://doi.org/10.1002/jor.24758

Samelko, L., Caicedo, M., McAllister, K., Jacobs, J., Hallab, N.J., 2021. Metal-induced delayed type hypersensitivity responses potentiate particle induced osteolysis in a sex and age dependent manner. PLoS One 16, e0251885. https://doi.org/10.1371/journal.pone.0251885

Samelko, L., Caicedo, M.S., Jacobs, J., Hallab, N.J., 2019. Transition from metal-DTH resistance to susceptibility is facilitated by NLRP3 inflammasome signaling induced Th17 reactivity: Implications for orthopedic implants. PLoS One 14, e0210336. https://doi.org/10.1371/journal.pone.0210336

Samelko, L., Landgraeber, S., McAllister, K., Jacobs, J., Hallab, N.J., 2016. Cobalt Alloy Implant Debris Induces Inflammation and Bone Loss Primarily through Danger Signaling, Not TLR4 Activation: Implications for DAMP-ening Implant Related Inflammation. PLoS One 11, e0160141. https://doi.org/10.1371/journal.pone.0160141

Sanders, N.M., Dunn-Meynell, A.A., Levin, B.E., 2004. Third Ventricular Alloxan Reversibly Impairs Glucose Counterregulatory Responses. Diabetes 53, 1230–1236. https://doi.org/10.2337/diabetes.53.5.1230

Santos, C.R.A., Duarte, A.C., Quintela, T., Tomás, J., Albuquerque, T., Marques, F., Palha, J.A., Gonçalves, I., 2017. The choroid plexus as a sex hormone target: Functional implications. Front. Neuroendocrinol. 44, 103–121.

https://doi.org/10.1016/j.yfrne.2016.12.002

Sathyanesan, M., Girgenti, M.J., Banasr, M., Stone, K., Bruce, C., Guilchicek, E., Wilczak-Havill, K., Nairn, A., Williams, K., Sass, S., Duman, J.G., Newton, S.S., 2012. A molecular characterization of the choroid plexus and stress-induced gene regulation. Transl. Psychiatry 2, e139. https://doi.org/10.1038/tp.2012.64

Scharf, B., Clement, C.C., Zolla, V., Perino, G., Yan, B., Elci, S.G., Purdue, E., Goldring, S., Macaluso, F., Cobelli, N., Vachet, R.W., Santambrogio, L., 2014. Molecular analysis of chromium and cobalt-related toxicity. Sci. Rep. 4, 5729. https://doi.org/10.1038/srep05729

Schmidt, S.D., Costa, A., Rani, B., Godfried Nachtigall, E., Passani, M.B., Carta, F., Nocentini, A., de Carvalho Myskiw, J., Furini, C.R.G., Supuran, C.T., Izquierdo, I., Blandina, P., Provensi, G., 2020. The role of carbonic anhydrases in extinction of contextual fear memory. Proc. Natl. Acad. Sci. 117, 16000–16008. https://doi.org/10.1073/pnas.1910690117

Schmitt, C., Strazielle, N., Richaud, P., Bouron, A., Ghersi-Egea, J.-F., 2011. Active transport at the blood-CSF barrier contributes to manganese influx into the brain. J. Neurochem. 117, no-no. https://doi.org/10.1111/j.1471-4159.2011.07246.x

Schmittgen, T.D., Livak, K.J., 2008. Analyzing real-time PCR data by the comparative CT method. Nat. Protoc. 3, 1101–1108. https://doi.org/10.1038/nprot.2008.73

Schneider, J.S., Anderson, D.W., Sonnenahalli, H., Vadigepalli, R., 2011. Sex-based differences in gene expression in hippocampus following postnatal lead exposure. Toxicol. Appl. Pharmacol. 256, 179–190. https://doi.org/10.1016/j.taap.2011.08.008

Schwarz, E.R., Kapur, V., Rodriguez, J., Rastogi, S., Rosanio, S., 2007. The effects of chronic phosphodiesterase-5 inhibitor use on different organ systems. Int J Impot Res. 19, 139–148. https://doi.org/10.1038/sj.ijir.3901491

Schwarz, G., Droogmans, G., Nilius, B., 1990. Characterization of two components of the N-like, high-threshold-activated calcium channel current in differentiated SH-SY5Y cells. Pflugers Arch. 421, 394–96.

Schwindinger, W.F., Betz, K.S., Giger, K.E., Sabol, A., Bronson, S.K., Robishaw, J.D., 2003. Loss of G protein gamma 7 alters behavior and reduces striatal alpha(olf) level and cAMP production. J. Biol. Chem. 278, 6575–6579. https://doi.org/10.1074/jbc.M211132200

Sebastian, K., Detro-Dassen, S., Rinis, N., Fahrenkamp, D., Müller-Newen, G., Merk,

H.F., Schmalzing, G., Zwadlo-Klarwasser, G., Baron, J.M., 2013. Characterization of SLCO5A1/OATP5A1, a solute carrier transport protein with non-classical function. PLoS One 8, e83257. https://doi.org/10.1371/journal.pone.0083257

Seghizzi, P., D'Adda, F., Borleri, D., Barbic, F., Mosconi, G., 1994. Cobalt myocardiopathy. A critical review of literature. Sci. Total Environ. 150, 105–109. https://doi.org/10.1016/0048-9697(94)90135-X

Sever, R., Glass, C.K., 2013. Signaling by Nuclear Receptors. Cold Spring Harb. Perspect. Biol. 5, a016709–a016709. https://doi.org/10.1101/cshperspect.a016709

Shah, K.M., Orton, P., Mani, N., Wilkinson, J.M., Gartland, A., 2017. Osteocyte physiology and response to fluid shear stress are impaired following exposure to cobalt and chromium: Implications for bone health following joint replacement. J. Orthop. Res. 35, 1716–1723. https://doi.org/10.1002/jor.23449

Shah, K.M., Quinn, P.D., Gartland, A., Wilkinson, J.M., 2015. Understanding the tissue effects of tribo-corrosion: Uptake, distribution, and speciation of cobalt and chromium in human bone cells. J. Orthop. Res. 33, 114–121. https://doi.org/10.1002/jor.22729

Sharma, Y., Chilamakuri, C.S.R., Bakke, M., Lenhard, B., 2014. Computational Characterization of Modes of Transcriptional Regulation of Nuclear Receptor Genes. PLoS One 9, e88880. https://doi.org/10.1371/journal.pone.0088880

Sheng, J., Xu, Z., 2016. Three decades of research on angiogenin: a review and perspective. Acta Biochim. Biophys. Sin. (Shanghai). 48, 399–410. https://doi.org/10.1093/abbs/gmv131

Shimada, K., Mitchison, T.J., 2019. Unsupervised identification of disease states from high-dimensional physiological and histopathological profiles. Mol. Syst. Biol. 15, e8636. https://doi.org/10.15252/msb.20188636

Sidaginamale, R.P., Joyce, T.J., Bowsher, J.G., Lord, J.K., Avery, P.J., Natu, S., Nargol, A.V.F., Langton, D.J., 2016. The clinical implications of metal debris release from the taper junctions and bearing surfaces of metal-on-metal hip arthroplasty. Bone Joint J. 98-B, 925–933. https://doi.org/10.1302/0301-620X.98B7.37029

Sidaginamale, R.P., Joyce, T.J., Lord, J.K., Jefferson, R., Blain, P.G., Nargol, A.V.F., Langton, D.J., 2013. Blood metal ion testing is an effective screening tool to identify poorly performing metal-on-metal bearing surfaces. Bone Joint Res. 2,

84–95. https://doi.org/10.1302/2046-3758.25.2000148

Silva Sieger, F.A., Díaz Silva, G.A., Ardila, G.P., García, R.G., 2012. Mercury chronic toxicity might be associated to some cases of hydrocephalus in adult humans? Med. Hypotheses 79, 13–16. https://doi.org/10.1016/j.mehy.2012.03.022

Simões, R.F., Ferrão, R., Silva, M.R., Pinho, S.L.C., Ferreira, L., Oliveira, P.J., Cunha-Oliveira, T., 2021. Refinement of a differentiation protocol using neuroblastoma SH-SY5Y cells for use in neurotoxicology research. Food Chem. Toxicol. 149, 111967. https://doi.org/10.1016/j.fct.2021.111967

Simonsen, L.O., Brown, A.M., Harbak, H., Kristensen, B.I., Bennekou, P., 2011a. Cobalt uptake and binding in human red blood cells. Blood Cells, Mol. Dis. 46, 266–276. https://doi.org/10.1016/j.bcmd.2011.02.009

Simonsen, L.O., Harbak, H., Bennekou, P., 2012a. Cobalt metabolism and toxicology-A brief update. Sci. Total Environ. 432, 210–215. https://doi.org/10.1016/j.scitotenv.2012.06.009

Simonsen, L.O., Harbak, H., Bennekou, P., 2012b. Cobalt metabolism and toxicology—A brief update. Sci. Total Environ. 432, 210–215. https://doi.org/10.1016/j.scitotenv.2012.06.009

Simonsen, L.O., Harbak, H., Bennekou, P., 2011b. Passive transport pathways for Ca2+ and Co2+ in human red blood cells. 57Co2+ as a tracer for Ca2+ influx. Blood Cells, Mol. Dis. 47, 214–225. https://doi.org/10.1016/j.bcmd.2011.09.002

Sjöstedt, E., Zhong, W., Fagerberg, L., Karlsson, M., Mitsios, N., Adori, C., Oksvold, P., Edfors, F., Limiszewska, A., Hikmet, F., Huang, J., Du, Y., Lin, L., Dong, Z., Yang, L., Liu, X., Jiang, H., Xu, X., Wang, J., Yang, H., Bolund, L., Mardinoglu, A., Zhang, C., von Feilitzen, K., Lindskog, C., Pontén, F., Luo, Y., Hökfelt, T., Uhlén, M., Mulder, J., 2020. An atlas of the protein-coding genes in the human, pig, and mouse brain. Science (80-.). 367, eaay5947. https://doi.org/10.1126/science.aay5947

Stankiewicz, A.M., Goscik, J., Majewska, A., Swiergiel, A.H., Juszczak, G.R., 2015. The Effect of Acute and Chronic Social Stress on the Hippocampal Transcriptome in Mice. PLoS One 10, e0142195. https://doi.org/10.1371/journal.pone.0142195

Steeland, S., Gorlé, N., Vandendriessche, C., Balusu, S., Brkic, M., Van Cauwenberghe, C., Van Imschoot, G., Van Wonterghem, E., De Rycke, R., Kremer, A., Lippens, S., Stopa, E., Johanson, C.E., Libert, C., Vandenbroucke, R.E., 2018. Counteracting the effects of TNF receptor-1 has therapeutic potential

in Alzheimer's disease. EMBO Mol. Med. 10, e8300. https://doi.org/10.15252/emmm.201708300

Steens, W., Von Foerster, G., Katzer, A., 2006. Severe cobalt poisoning with loss of sight after ceramic-metal pairing in a hip - a case report. Acta Orthop. 77, 830–832. https://doi.org/10.1080/17453670610013079

Stephens, A.D., Liu, P.Z., Kandula, V., Chen, H., Almassalha, L.M., Herman, C., Backman, V., O'Halloran, T., Adam, S.A., Goldman, R.D., Banigan, E.J., Marko, J.F., 2019. Physicochemical mechanotransduction alters nuclear shape and mechanics via heterochromatin formation. Mol. Biol. Cell 30, 2320–2330. https://doi.org/10.1091/mbc.E19-05-0286

Stepien, K.M., Abidin, Z., Lee, G., Cullen, R., Logan, P., Pastores, G.M., 2018. Metallosis mimicking a metabolic disorder: a case report. Mol. Genet. Metab. Reports 17, 38–41. https://doi.org/10.1016/j.ymgmr.2018.09.005

Steuerwald, A.J., Blaisdell, F.S., Geraghty, C.M., Parsons, P.J., 2014. Regional Distribution and Accumulation of Lead in Caprine Brain Tissues Following a Long-Term Oral Dosing Regimen. J. Toxicol. Environ. Heal. Part A 77, 663–678. https://doi.org/10.1080/15287394.2014.880328

Stevenson, M.J., Uyeda, K.S., Harder, N.H.O., Heffern, M.C., 2019. Metal-dependent hormone function: the emerging interdisciplinary field of metalloendocrinology. Metallomics 11, 85–110. https://doi.org/10.1039/C8MT00221E

Stock, A.D., Der, E., Gelb, S., Huang, M., Weidenheim, K., Ben-Zvi, A., Putterman, C., 2019. Tertiary lymphoid structures in the choroid plexus in neuropsychiatric lupus. JCI Insight 4. https://doi.org/10.1172/jci.insight.124203

Stockert, J.C., Horobin, R.W., Colombo, L.L., Blázquez-Castro, A., 2018. Tetrazolium salts and formazan products in Cell Biology: Viability assessment, fluorescence imaging, and labeling perspectives. Acta Histochem. 120, 159–167. https://doi.org/10.1016/j.acthis.2018.02.005

Stoeger, T., Gerlach, M., Morimoto, R.I., Nunes Amaral, L.A., 2018. Large-scale investigation of the reasons why potentially important genes are ignored. PLOS Biol. 16, e2006643. https://doi.org/10.1371/journal.pbio.2006643

Strange, B.A., Witter, M.P., Lein, E.S., Moser, E.I., 2014. Functional organization of the hippocampal longitudinal axis. Nat. Rev. Neurosci. 15, 655–669. https://doi.org/10.1038/nrn3785

Su, X., Ren, Y., Li, M., Zhao, X., Kong, L., Kang, J., 2016. Prevalence of Comorbidities

in Asthma and Nonasthma Patients. Medicine (Baltimore). 95, e3459. https://doi.org/10.1097/MD.0000000000003459

Subramanian, K., Meyer, T., 1997. Calcium-Induced Restructuring of Nuclear Envelope and Endoplasmic Reticulum Calcium Stores. Cell 89, 963–971. https://doi.org/10.1016/S0092-8674(00)80281-0

Sudarshana, D.M., Nair, G., Dwyer, J.T., Dewey, B., Steele, S.U., Suto, D.J., Wu, T., Berkowitz, B.A., Koretsky, A.P., Cortese, I.C.M., Reich, D.S., 2019. Manganese-enhanced MRI of the brain in healthy volunteers. Am. J. Neuroradiol. 40, 1309–1316. https://doi.org/10.3174/ajnr.A6152

Sugino, K., Clark, E., Schulmann, A., Shima, Y., Wang, L., Hunt, D.L., Hooks, B.M., Tränkner, D., Chandrashekar, J., Picard, S., Lemire, A.L., Spruston, N., Hantman, A.W., Nelson, S.B., 2019. Mapping the transcriptional diversity of genetically and anatomically defined cell populations in the mouse brain. Elife 8, e38619. https://doi.org/10.7554/eLife.38619

Sullivan, J., Parker, M., Carson, S., 1968. Tissue cobalt content in “beer drinkers’’ myocardiopathy".” J. Lab. Clin. Med. 71, 893–911.

Sullivan, J.F., Egan, J.D., George, R.P., 1969. A distinctive myocardiopathy occurring in Omaha, Nebraska: clinical aspects. Ann. N. Y. Acad. Sci. 156, 526–543. https://doi.org/10.1111/j.1749-6632.1969.tb16749.x

Sun, L., Khan, A., Zhang, H., Han, S., Habulieti, X., Wang, R., Zhang, X., 2020. Phenotypic Characterization of Intellectual Disability Caused by MBOAT7 Mutation in Two Consanguineous Pakistani Families. Front. Pediatr. 8, 585053. https://doi.org/10.3389/fped.2020.585053

Swiatkowska, I., Mosselmans, J.F.W., Geraki, T., Wyles, C.C., Maleszewski, J.J., Henckel, J., Sampson, B., Potter, D.B., Osman, I., Trousdale, R.T., Hart, A.J., 2018. Synchrotron analysis of human organ tissue exposed to implant material. J. Trace Elem. Med. Biol. 46, 128–137. https://doi.org/10.1016/j.jtemb.2017.12.007

Szklarczyk, D., Gable, A.L., Nastou, K.C., Lyon, D., Kirsch, R., Pyysalo, S., Doncheva, N.T., Legeay, M., Fang, T., Bork, P., Jensen, L.J., von Mering, C., 2021. The STRING database in 2021: customizable protein–protein networks, and functional characterization of user-uploaded gene/measurement sets. Nucleic Acids Res. 49, D605–D612. https://doi.org/10.1093/nar/gkaa1074

Takeda, A., Takefuta, S., Ijiro, H., Okada, S., Oku, N., 1999. ^{109}Cd transport in rat brain. Brain Res. Bull. 49, 453–457. https://doi.org/10.1016/S0361-9230(99)00080-5

Takele Assefa, A., Vandesompele, J., Thas, O., 2020. On the utility of RNA sample pooling to optimize cost and statistical power in RNA sequencing experiments. BMC Genomics 21, 312. https://doi.org/10.1186/s12864-020-6721-y

Takemasu, S., Ito, M., Morioka, S., Nigorikawa, K., Kofuji, S., Takasuga, S., Eguchi, S., Nakanishi, H., Matsuoka, I., Sasaki, J., Sasaki, T., Hazeki, K., 2019. Lysophosphatidylinositol-acyltransferase-1 is involved in cytosolic Ca 2+ oscillations in macrophages. Genes to Cells 24, 366–376. https://doi.org/10.1111/gtc.12681

Tallquist, M.D., Molkentin, J.D., 2017. Redefining the identity of cardiac fibroblasts. Nat. Rev. Cardiol. 14, 484–491. https://doi.org/10.1038/nrcardio.2017.57

Tanaka, K., Martinez, G.J., Yan, X., Long, W., Ichiyama, K., Chi, X., Kim, B.-S., Reynolds, J.M., Chung, Y., Tanaka, S., Liao, L., Nakanishi, Y., Yoshimura, A., Zheng, P., Wang, X., Tian, Q., Xu, J., O'Malley, B.W., Dong, C., 2018. Regulation of Pathogenic T Helper 17 Cell Differentiation by Steroid Receptor Coactivator-3. Cell Rep. 23, 2318–2329. https://doi.org/10.1016/j.celrep.2018.04.088

Tanaka, Y., Shimanaka, Y., Caddeo, A., Kubo, T., Mao, Y., Kubota, T., Kubota, N., Yamauchi, T., Mancina, R.M., Baselli, G., Luukkonen, P., Pihlajamäki, J., Yki-Järvinen, H., Valenti, L., Arai, H., Romeo, S., Kono, N., 2021. LPIAT1/MBOAT7 depletion increases triglyceride synthesis fueled by high phosphatidylinositol turnover. Gut 70, 180–193. https://doi.org/10.1136/gutjnl-2020-320646

Tang, M., Yang, Y., Yu, J., Wu, N., Chen, P., Xu, L., Wang, Q., Xu, Z., Ge, J., Yu, K., Zhuang, J., 2017. Discordant mRNA and protein expression of CXCR4 under in vitro CoCl2-induced hypoxic conditions. Biochem. Biophys. Res. Commun. 484, 285–291. https://doi.org/10.1016/j.bbrc.2017.01.102

Taylor, S., Wakem, M., Dijkman, G., Alsarraj, M., Nguyen, M., 2010. A practical approach to RT-qPCR—Publishing data that conform to the MIQE guidelines. Methods 50, S1–S5. https://doi.org/10.1016/j.ymeth.2010.01.005

Thangapandi, V.R., Knittelfelder, O., Brosch, M., Patsenker, E., Vvedenskaya, O., Buch, S., Hinz, S., Hendricks, A., Nati, M., Herrmann, A., Rekhade, D.R., Berg, T., Matz-Soja, M., Huse, K., Klipp, E., Pauling, J.K., Wodke, J.A.H., Miranda Ackerman, J., Bonin, M. von, Aigner, E., Datz, C., von Schönfels, W., Nehring, S., Zeissig, S., Röcken, C., Dahl, A., Chavakis, T., Stickel, F., Shevchenko, A., Schafmayer, C., Hampe, J., Subramanian, P., 2021. Loss of hepatic Mboat7 leads to liver fibrosis. Gut 70, 940–950. https://doi.org/10.1136/gutjnl-2020-320853

The UniProt Consortium, 2017. UniProt: the universal protein knowledgebase. Nucleic Acids Res. 45, D158–D169. https://doi.org/10.1093/nar/gkw1099

Timerman, D., Yeung, C.M., 2014. Identity confusion of glioma cell lines. Gene 536, 221–222. https://doi.org/10.1016/j.gene.2013.11.096

Tomczak, A., Mortensen, J.M., Winnenburg, R., Liu, C., Alessi, D.T., Swamy, V., Vallania, F., Lofgren, S., Haynes, W., Shah, N.H., Musen, M.A., Khatri, P., 2018. Interpretation of biological experiments changes with evolution of the Gene Ontology and its annotations. Sci. Rep. 8, 5115. https://doi.org/10.1038/s41598-018-23395-2

Tower, S.S., 2010. Arthroprosthetic Cobaltism: Neurological and Cardiac Manifestations in Two Patients with Metal-on-Metal Arthroplasty: A Case Report. J Bone Jt. Surg Am 92, 2847–51. https://doi.org/10.2106/JBJS.J.00125

Tresguerres, M., Levin, L.R., Buck, J., 2011. Intracellular cAMP signaling by soluble adenylyl cyclase. Kidney Int. 79, 1277–1288. https://doi.org/10.1038/ki.2011.95

Tsui, H.-C., Decaesteker, T., Jonckheere, A.-C., Vande Velde, G., Cremer, J., Verbeken, E., Hoet, P.H.M., Nemery, B., Vanoirbeek, J.A.J., 2020. Cobalt exposure via skin alters lung immune cells and enhances pulmonary responses to cobalt in mice. Am. J. Physiol. Cell. Mol. Physiol. 319, L641–L651. https://doi.org/10.1152/ajplung.00265.2020

Turner, C.A., Thompson, R.C., Bunney, W.E., Schatzberg, A.F., Barchas, J.D., Myers, R.M., Akil, H., Watson, S.J., 2014. Altered choroid plexus gene expression in major depressive disorder. Front. Hum. Neurosci. 8, 238. https://doi.org/10.3389/fnhum.2014.00238

Umbsaar, J., Kerek, E., Prenner, E.J., 2018. Cobalt and nickel affect the fluidity of negatively-charged biomimetic membranes. Chem. Phys. Lipids 210, 28–37. https://doi.org/10.1016/j.chemphyslip.2017.11.016

Unsworth-Smith, T., Khan, J.C., Khan, R.J.K., Chelva, E., Lim, C.A., Haebich, S., Trevenen, M.L., 2017. Impact of Raised Serum Cobalt Levels From Recalled Articular Surface Replacement Hip Prostheses on the Visual Pathway. J. Arthroplasty 32, 3147–3151. https://doi.org/10.1016/j.arth.2017.04.064

Urban, R M, Jacobs, J.J., Tomlinson, M.J., Gavrilovic, J., Black, J., Peoc'h, M., 2000. Dissemination of wear particles to the liver, spleen, and abdominal lymph nodes of patients with hip or knee replacement. J. Bone Joint Surg. Am. 82, 457–476. https://doi.org/10.2106/00004623-200004000-00002

Urban, R.M., Jacobs, J.J., Tomlinson, M.J., Gavrilovic, J., Black, J., Peoc'h, M., 2000. Dissemination of wear particles to the liver, spleen, and abdominal lymph nodes of patients with hip or knee replacement. J. bone Jt. Surg. 82, 457.

Urban, R.M., Tomlinson, M.J., Hall, D.J., Jacobs, J.J., 2004. Accumulation in liver and spleen of metal particles generated at nonbearing surfaces in hip arthroplasty. J. Arthroplasty 19, 94–101. https://doi.org/10.1016/j.arth.2004.09.013

Vaishnavi, S.N., Vlassenko, A.G., Rundle, M.M., Snyder, A.Z., Mintun, M.A., Raichle, M.E., 2010. Regional aerobic glycolysis in the human brain. Proc. Natl. Acad. Sci. U. S. A. 107, 17757–17762. https://doi.org/10.1073/pnas.1010459107

Valko, M., Jomova, K., Rhodes, C.J., Kuča, K., Musílek, K., 2016. Redox- and non-redox-metal-induced formation of free radicals and their role in human disease. Arch. Toxicol. 90, 1–37. https://doi.org/10.1007/s00204-015-1579-5

Van Brusselen, D., Kayembe-Kitenge, T., Mbuyi-Musanzayi, S., Lubala Kasole, T., Kabamba Ngombe, L., Musa Obadia, P., Kyanika wa Mukoma, D., Van Herck, K., Avonts, D., Devriendt, K., Smolders, E., Nkulu, C.B.L., Nemery, B., 2020. Metal mining and birth defects: a case-control study in Lubumbashi, Democratic Republic of the Congo. Lancet Planet. Heal. 4, e158–e167. https://doi.org/10.1016/S2542-5196(20)30059-0

Van Der Straeten, C., Calistri, A., Grammatopoulos, G., De Smet, K., 2020. Radiographic evaluation of hip resurfacing: the role of x-rays in the diagnosis of a problematic resurfaced hip. HIP Int. 30, 167–175. https://doi.org/10.1177/1120700019836373

van Lingen, C.P., Ettema, H.B., Van Der Straeten, C., Kollen, B.J., Verheyen, C.C.P.M., 2014. Self-Reported Neurological Clinical Manifestations of Metal Toxicity in Metal-on-Metal Hip Arthroplasty. HIP Int. 24, 568–574. https://doi.org/10.5301/hipint.5000179

Vega, R.B., Kelly, D.P., 2017. Cardiac nuclear receptors: architects of mitochondrial structure and function. J. Clin. Invest. 127, 1155–1164. https://doi.org/10.1172/JCI88888

Verstraelen, S., Remy, S., Casals, E., De Boever, P., Witters, H., Gatti, A., Puntes, V., Nelissen, I., 2014. Gene expression profiles reveal distinct immunological responses of cobalt and cerium dioxide nanoparticles in two in vitro lung epithelial cell models. Toxicol. Lett. 228, 157–169. https://doi.org/10.1016/j.toxlet.2014.05.006

Vincent, C., Gilabert-Juan, J., Gibel-Russo, R., Alvarez-Fischer, D., Krebs, M.-O., Le Pen, G., Prochiantz, A., Di Nardo, A.A., 2021. Non-cell-autonomous OTX2 transcription factor regulates anxiety-related behavior in the mouse. Mol. Psychiatry. https://doi.org/10.1038/s41380-021-01132-y

Vogel, P., Read, R.W., Hansen, G.M., Payne, B.J., Small, D., Sands, A.T., Zambrowicz, B.P., 2012. Congenital Hydrocephalus in Genetically Engineered Mice. Vet. Pathol. 49, 166–181. https://doi.org/10.1177/0300985811415708

Wa, W., 2001. Zn 2 + and Cd 2 + increase the cyclic GMP level in PC12 cells by inhibition of the cyclic nucleotide phosphodiesterase 157, 167–175.

Waldron, K.J., Rutherford, J.C., Ford, D., Robinson, N.J., 2009. Metalloproteins and metal sensing. Nature 460, 823–830. https://doi.org/10.1038/nature08300

Walters, G.I., Robertson, A.S., Moore, V.C., Burge, P.S., 2014. Cobalt asthma in metalworkers from an automotive engine valve manufacturer. Occup. Med. (Chic. Ill). 64, 358–364. https://doi.org/10.1093/occmed/kqu043

Wang, C., Gong, B., Bushel, P.R., Thierry-Mieg, J., Thierry-Mieg, D., Xu, J., Fang, H., Hong, H., Shen, J., Su, Z., Meehan, J., Li, X., Yang, L., Li, H., Łabaj, P.P., Kreil, D.P., Megherbi, D., Gaj, S., Caiment, F., van Delft, J., Kleinjans, J., Scherer, A., Devanarayan, V., Wang, J., Yang, Y., Qian, H.-R., Lancashire, L.J., Bessarabova, M., Nikolsky, Y., Furlanello, C., Chierici, M., Albanese, D., Jurman, G., Riccadonna, S., Filosi, M., Visintainer, R., Zhang, K.K., Li, J., Hsieh, J.-H., Svoboda, D.L., Fuscoe, J.C., Deng, Y., Shi, L., Paules, R.S., Auerbach, S.S., Tong, W., 2014. The concordance between RNA-seq and microarray data depends on chemical treatment and transcript abundance. Nat. Biotechnol. 32, 926–932. https://doi.org/10.1038/nbt.3001

Wang, M., Futamura, M., Wang, Y., You, M., 2005. Pas1c1 is a candidate for the mouse pulmonary adenoma susceptibility 1 locus. Oncogene 24, 1958–1963. https://doi.org/10.1038/sj.onc.1208295

Wang, P., Li, L., Zhang, Z., Kan, Q., Chen, S., Gao, F., 2016. Time-dependent homeostasis between glucose uptake and consumption in astrocytes exposed to CoCl2 treatment. Mol. Med. Rep. 13, 2909–2917. https://doi.org/10.3892/mmr.2016.4873

Watanabe, T., Natt, O., Boretius, S., Frahm, J., Michaelis, T., 2002. In vivo 3D MRI staining of mouse brain after subcutaneous application of $MnCl_2$. Magn. Reson. Med. 48, 852–859. https://doi.org/10.1002/mrm.10276

Weiss, J.H., Sensi, S.L., 2000. Ca2+-Zn2+permeable AMPA or kainate receptors: Possible key factors in selective neurodegeneration. Trends Neurosci. 23, 365–371. https://doi.org/10.1016/S0166-2236(00)01610-6

Weng, Y., DiRusso, C.C., Reilly, A.A., Black, P.N., Ding, X., 2005. Hepatic Gene Expression Changes in Mouse Models with Liver-specific Deletion or Global Suppression of the NADPH-Cytochrome P450 Reductase Gene. J. Biol. Chem. 280, 31686–31698. https://doi.org/10.1074/jbc.M504447200

Will, T.R., Proaño, S.B., Thomas, A.M., Kunz, L.M., Thompson, K.C., Ginnari, L.A., Jones, C.H., Lucas, S.-C., Reavis, E.M., Dorris, D.M., Meitzen, J., 2017. Problems and Progress regarding Sex Bias and Omission in Neuroscience Research. eNeuro 4, ENEURO.0278-17.2017. https://doi.org/10.1523/ENEURO.0278-17.2017

Wright, J. V., 2005. Bio-Identical Steroid Hormone Replacement: Selected Observations from 23 Years of Clinical and Laboratory Practice. Ann. N. Y. Acad. Sci. 1057, 506–524. https://doi.org/10.1196/annals.1356.039

Wu, X., Bers, D.M., 2006. Sarcoplasmic reticulum and nuclear envelope are one highly interconnected Ca2+ store throughout cardiac myocyte. Circ. Res. 99, 283–291. https://doi.org/10.1161/01.RES.0000233386.02708.72

Wyles, C.C., Wright, T.C., Bois, M.C., Amin, S., Fayyaz, A., Jenkins, S.M., Wyles, S.P., Day, P.L., Murray, D.L., Trousdale, R.T., Anavekar, N.S., Edwards, W.D., Maleszewski, J.J., 2017. Myocardial cobalt levels are elevated in the setting of total hip arthroplasty. J. Bone Jt. Surg. Am 99, e118. https://doi.org/10.2106/JBJS.17.00159

Xia, Z., Ricciardi, B.F., Liu, Z., von Ruhland, C., Ward, M., Lord, A., Hughes, L., Goldring, S.R., Purdue, E., Murray, D., Perino, G., 2017. Nano-analyses of wear particles from metal-on-metal and non-metal-on-metal dual modular neck hip arthroplasty. Nanomedicine Nanotechnology, Biol. Med. 13, 1205–1217. https://doi.org/10.1016/j.nano.2016.11.003

Xiao, H., Wyler, E., Milek, M., Grewe, B., Kirchner, P., Ekici, A., Silva, A.B.O.V., Jungnickl, D., Full, F., Thomas, M., Landthaler, M., Ensser, A., Überla, K., 2021. CRNKL1 Is a Highly Selective Regulator of Intron-Retaining HIV-1 and Cellular mRNAs. MBio 12, 1–24. https://doi.org/10.1128/mBio.02525-20

Xie, F., Xiao, P., Chen, D., Xu, L., Zhang, B., 2012. miRDeepFinder: a miRNA analysis tool for deep sequencing of plant small RNAs. Plant Mol. Biol. 80, 75–84.

https://doi.org/10.1007/s11103-012-9885-2

Xu, E., Ji, Z., Jiang, H., Lin, T., Ma, J., Zhou, X., 2019. Hypoxia-Inducible Factor 1A Upregulates HMGN5 by Increasing the Expression of GATA1 and Plays a Role in Osteosarcoma Metastasis. Biomed Res. Int. 2019, 5630124. https://doi.org/10.1155/2019/5630124

Yang, M.T., Chien, W.L., Lu, D.H., Liou, H.C., Fu, W.M., 2013. Acetazolamide impairs fear memory consolidation in rodents. Neuropharmacology 67, 412–418. https://doi.org/10.1016/j.neuropharm.2012.11.031

Yao, H., Li, P., Venters, B.J., Zheng, S., Thompson, P.R., Pugh, B.F., Wang, Y., 2008. Histone Arg modifications and p53 regulate the expression of OKL38, a mediator of apoptosis. J. Biol. Chem. 283, 20060–20068. https://doi.org/10.1074/jbc.M802940200

Zadnipryany, I., Tretiakova, O., Sataieva, T., Zukow, W., 2017. Experimental review of cobalt induced cardiomyopathy. Russ. Open Med. J. 6, e0103. https://doi.org/10.15275/rusomj.2017.0103

Zare, E.N., Zheng, X., Makvandi, P., Gheybi, H., Sartorius, R., Yiu, C.K.Y., Adeli, M., Wu, A., Zarrabi, A., Varma, R.S., Tay, F.R., 2021. Nonspherical Metal-Based Nanoarchitectures: Synthesis and Impact of Size, Shape, and Composition on Their Biological Activity. Small 17, 2007073. https://doi.org/10.1002/smll.202007073

Zhang, R., Wang, L., Zhao, J., Wang, C., Bao, J., Li, J., 2016. Effects of Selenium and Cadmium on Ion Profiles in the Brains of Chickens. Biol. Trace Elem. Res. 174, 218–225. https://doi.org/10.1007/s12011-016-0693-4

Zhao, B., Erwin, A., Xue, B., 2018. How many differentially expressed genes: A perspective from the comparison of genotypic and phenotypic distances. Genomics 110, 67–73. https://doi.org/10.1016/j.ygeno.2017.08.007

Zheng, M., Marron, R.M., Sehgal, S., 2020. Hard Metal Lung Disease: Update in Diagnosis and Management. Curr. Pulmonol. Reports 9, 37–46. https://doi.org/10.1007/s13665-020-00247-x

Zhu, H., Liu, Y., Hong, H., Wang, W., Liu, F., 2017. Protective effects of Zn2+ against cobalt nanoparticles and cobalt chloride-induced cytotoxicity of RAW 264.7cells via ROS pathway. Biochem. Biophys. Res. Commun. 486, 357–363. https://doi.org/10.1016/j.bbrc.2017.03.045

Zhu, L., Stein, L.R., Kim, D., Ho, K., Yu, G.-Q., Zhan, L., Larsson, T.E., Mucke, L.,

2018. Klotho controls the brain–immune system interface in the choroid plexus. Proc. Natl. Acad. Sci. 115, E11388–E11396. https://doi.org/10.1073/pnas.1808609115

Zhu, X., Zhou, W., Cui, Y., Zhu, L., Li, J., Xia, Z., Shao, B., Wang, H., Chen, H., 2009. Muscarinic activation attenuates abnormal processing of β-amyloid precursor protein induced by cobalt chloride-mimetic hypoxia in retinal ganglion cells. Biochem. Biophys. Res. Commun. 384, 110–113. https://doi.org/10.1016/j.bbrc.2009.04.080

Zhu, Y., Costa, M., 2020. Metals and molecular carcinogenesis. Carcinogenesis 41, 1161–1172. https://doi.org/10.1093/carcin/bgaa076

Zou, Q., Jin, J., Xiao, Y., Hu, H., Zhou, X., Jie, Z., Xie, X., Li, J.Y.H., Cheng, X., Sun, S.-C., 2015. T cell development involves TRAF3IP3-mediated ERK signaling in the Golgi. J. Exp. Med. 212, 1323–1336. https://doi.org/10.1084/jem.20150110

Zou, W., Zeng, J., Zhuo, M., Xu, W., Sun, L., Wang, J., Liu, X., 2002. Involvement of caspase-3 and p38 mitogen-activated protein kinase in cobalt chloride-induced apoptosis in PC12 cells. J. Neurosci. Res. 67, 837–843. https://doi.org/10.1002/jnr.10168

Zywiel, M.G., Brandt, J.M., Overgaard, C.B., Cheung, A.C., Turgeon, T.R., Syed, K.A., 2013. Fatal cardiomyopathy after revision total hip replacement for fracture of a ceramic liner. Bone Jt. J. 95-B, 31–37. https://doi.org/10.1302/0301-620X.95B1.30060

Zywiel, M.G., Cherian, J.J., Banerjee, S., Cheung, A.C., Wong, F., Butany, J., Gilbert, C., Overgaard, C., Syed, K., Jacobs, J.J., Mont, M.A., 2016. Systemic cobalt toxicity from total hip arthroplasties Part 2—measurement, risk factors, and step-wise approach to treatment. Bone Jt. J. 98-B, 14–20. https://doi.org/10.1302/0301-620X.98B1.36712

Appendices

Appendix A: RNA quality of samples obtained from brain tissue

This appendix provides the information about the quality of the RNA samples used for RNA-Seq and RT-qPCR experiments shown in this thesis. The parameters evaluated are the concentration of RNA, and the ratios of absorbance found at 260 nm and 280 nm (260/280), and at 260nm and 230 nm (260/230) with the Nanodrop spectrophotometer. These ratios indicate the purity of nucleic acid, and lowered values may point towards the presence of contaminants. The ribosomal RNA 28S/18S ratio and the RNA quality indicator (RQI) value are estimations of the integrity of the samples obtained through Experion automated electrophoresis system. Lower 28S/18S ratio and RQI values could indicate that the RNA has been degraded. The accepted parameter values for RNA are: [260/280]~2; [260/230]>2; [28S/18S]>0.7; RQI>7.

Table 26 and Table 27 display the information about the cerebellum and the pref. cortex from the *in vivo* time-response. The quality check of samples from the dose-response experiment in the pref. cortex are in Table 28, values from the cerebellum are in Table 29, and for hippocampus in Table 30. The parameters were also measured in the pooled samples before being sent for RNA-Seq analyses.

Table 26: Quality check of RNA samples from the cerebellum tissue obtained from the *in vivo* time-response experiments (Chapter 5). Parameters shown are RNA concentration (ng/μl), and ratios [260/280] and [260/230] indicating RNA purity, in addition to ratio [28S/18S] and RQI indicating RNA integrity. The bottom part of the table shows the pooled samples. 'Crbm X.Y' abbreviation refers to cerebellum sample number Y from group X (group 4; control group which had dH_2O i.p. injection treatment, and group 5; treatment group which had 1 mg/kg B.W $CoCl_2$ daily i.p. injections for 28 days). There are n = 3 samples per each control or treatment group, each group was later pooled into a single sample for RNA-Seq evaluation.

Quality check of RNA samples from the cerebellum					
Samples	**RNA concentration (ng/μl)**	**Ratio [260/280]**	**Ratio [260/230]**	**Ratio [28S/18S]**	**RQI**
Cerebellum Control (Crbm 4.1)	442.2	2.07	2.26	-	-
Cerebellum Control (Crbm 4.2)	407.1	2.07	2.19	-	-
Cerebellum Control (Crbm 4.3)	478.1	2.07	2.23	-	-
Cerebellum Treatment (Crbm 5.1)	368.2	2.04	2.13	-	-
Cerebellum Treatment (Crbm 5.2)	380.8	2.06	2.20	-	-
Cerebellum Treatment (Crbm 5.3)	499.2	2.00	2.00	-	-
Pooled samples					
Cerebellum Control (Crbm 4)	433.4	2.08	2.07	1.37	9.7
Cerebellum Treatment (Crbm 5)	385.4	2.07	2.16	1.32	9.4

Table 27: Quality check of RNA samples from the pref. cortex tissue obtained from the *in vivo* time-response experiments (Chapter 5). Parameters shown are RNA concentration (ng/μl), and ratios [260/280] and [260/230] indicating RNA purity, in addition to ratio [28S/18S] and RQI indicating RNA integrity. The bottom part of the table shows the pooled samples. 'Crtx X.Y' abbreviation refers to pref. cortex sample number Y from group X (group 4, control group which had dH_2O treatment; and group 5, treatment group which had 1 mg/kg B.W $CoCl_2$ daily i.p. injections for 28 days). There are n = 3 samples per each control or treatment group, each group was later pooled into a single sample for RNA-Seq evaluation.

Quality check of RNA samples from the pref. cortex					
Samples	**RNA concentration (ng/μl)**	**Ratio [260/280]**	**Ratio [260/230]**	**Ratio [28S/18S]**	**RQI**
Pref. cortex Control (Crtx 4.1)	288.3	2.07	2.19	-	-
Pref. cortex Control (Crtx 4.2)	456.9	2.01	2.01	-	-
Pref. cortex Control (Crtx 4.3)	345.1	2.03	2.03	-	-
Pref. cortex Treatment (Crtx 5.1)	412.3	2.07	2.20	-	-
Pref. cortex Treatment (Crtx 5.2)	474.1	2.05	2.19	-	-
Pref. cortex Treatment (Crtx 5.3)	581.1	2.08	2.27	-	-
Pooled samples					
Pref. cortex Control (Crtx 4)	347.7	2.06	2.18	1.01	9
Pref. cortex Treatment (Crtx 5)	488.8	2.08	2.12	1.27	9.5

Table 28: Quality check of RNA samples from the pref. cortex tissue obtained from the dose-response *in vivo* experiments (Chapter 6). Parameters shown are RNA concentration (ng/μl), and ratios [260/280] and [260/230] indicating RNA purity, in addition to ratio [28S/18S] and RQI indicating RNA integrity. The bottom part of the table shows the pooled samples. 'Crtx X.Y' abbreviation refers to pref. cortex sample number Y from group X (group 1 is the control group which had daily dH_2O i.p. injection treatment; 2, 3 and 4 treatment groups had 0.1, 0.5 and 1 mg/kg B.W $CoCl_2$ daily i.p. injections for 28 days respectively). There are n = 4 samples per each control or treatment group, each group was later pooled into a single sample for RNA-Seq evaluation.

Quality check of RNA samples from the pref. cortex					
Samples	**RNA concentration (ng/μl)**	**Ratio [260/280]**	**Ratio [260/230]**	**Ratio [28S/18S]**	**RQI**
Pref. cortex Control (Crtx 1.1)	237.3	2.08	2.16	1.30	9.4
Pref. cortex Control (Crtx 1.2)	309.3	2.08	2.30	1.59	9.6
Pref. cortex Control (Crtx 1.3)	208.9	2.06	2.27	1.39	9.7
Pref. cortex Control (Crtx 1.4)	278.0	2.07	2.25	1.34	9.7
Pref. cortex 0.1 mg/kg BW (Crtx 2.1)	410.8	2.08	2.24	1.30	9.3
Pref. cortex 0.1 mg/kg BW (Crtx 2.2)	178.0	2.07	2.02	1.53	9.2
Pref. cortex 0.1 mg/kg BW (Crtx 2.3)	375.2	2.09	2.21	1.53	9.4
Pref. cortex 0.1 mg/kg BW (Crtx 2.4)	437.9	2.09	2.26	1.17	8.9
Pref. cortex 0.5 mg/kg BW (Crtx 3.1)	260.2	2.06	2.29	1.31	9.3
Pref. cortex 0.5 mg/kg BW (Crtx 3.2)	256.6	2.09	2.20	1.35	9.2

Pref. cortex 0.5 mg/kg BW (Crtx 3.3)	291.0	2.07	2.24	1.42	9.5
Pref. cortex 0.5 mg/kg BW (Crtx 3.4)	293.0	2.09	2.25	1.54	9.5
Pref. cortex 1 mg/kg BW (Crtx 4.1)	282.7	2.07	2.27	1.34	9.7
Pref. cortex 1 mg/kg BW (Crtx 4.2)	279.2	2.09	1.98	1.43	9.3
Pref. cortex 1mg/kg BW (Crtx 4.3)	308.9	2.11	1.32	1.47	9.3
Pref. cortex 1 mg/kg BW (Crtx 4.4)	352.4	2.06	2.18	1.58	9.7
Pooled samples					
Pref. cortex Control	252.1	2.06	2.22	1.38	9.5
Pref. cortex 0.1 mg/kg BW Treatment	280.7	2.06	2.15	1.41	9.0
Pref. cortex 0.5 mg/kg BW Treatment	272.2	2.06	2.22	1.25	8.5
Pref. cortex 1 mg/kg BW Treatment	260.4	2.06	1.90	1.34	9.5

Table 29: Quality check of RNA samples from the cerebellum tissues obtained from the *in vivo* dose-response experiments (Chapter 6). Parameters shown are RNA concentration (ng/μl), and ratios [260/280] and [260/230] indicating RNA purity, in addition to ratio [28S/18S] and RQI indicating RNA integrity. The bottom part of the table shows the pooled samples. 'Crbm X.Y' abbreviation refers to cerebellum sample number Y from group X (group 1 is the control group with daily i.p injections of dH_2O; and 2, 3 and 4 treatment groups had 0.1, 0.5 and 1 mg/kg B.W $CoCl_2$ daily i.p. injections for 28 days respectively). There are n = 4 samples per each control or treatment group, each group was later pooled into a single sample for RNA-Seq evaluation. Some of the samples could not be obtained and less samples than n=4 were pooled.

Quality check of RNA samples from the cerebellum					
Samples	**RNA concentration (ng/μl)**	**Ratio [260/280]**	**Ratio [260/230]**	**Ratio [28S/18S]**	**RQI**
Cerebellum Control (Crbm 1.1)	199.8	2.06	2.24	1.44	9.7
Cerebellum Control (Crbm 1.2)	360.8	2.10	2.31	1.64	9.9
Cerebellum Control (Crbm 1.3)	307.8	2.08	2.13	1.45	9.6
Cerebellum Control (Crbm 1.4)	303.9	2.08	2.30	1.45	9.7
Cerebellum 0.1 mg/kg BW (Crbm 2.1)	365.6	2.03	2.21	1.46	9.7
Cerebellum 0.1 mg/kg BW (Crbm 2.2)	366.4	2.07	2.25	1.59	9.9
Cerebellum 0.1 mg/kg BW (Crbm 2.3)	351.2	2.09	2.28	1.49	9.3
Cerebellum 0.1 mg/kg BW (Crbm 2.4)	283.6	2.06	2.22	1.48	9.8

Cerebellum 0.5 mg/kg BW (Crbm 3.1)	330.2	2.09	2.32	1.55	9.6
Cerebellum 0.5 mg/kg BW (Crbm 3.2)	354.6	2.09	2.29	1.66	9.8
Cerebellum 0.5 mg/kg BW (Crbm 3.3)	388.9	2.09	2.24	1.57	9.8
Cerebellum 0.5 mg/kg BW (Crbm 3.4)	221.3	2.06	2.28	1.74	8.3
Cerebellum 1 mg/kg BW (Crbm 4.1)	454.5	2.09	2.25	1.38	9.1
Cerebellum 1 mg/kg BW (Crbm 4.2)	372.7	2.09	2.31	1.41	9.7
Cerebellum 1mg/kg BW (Crbm 4.3)	345.3	2.10	1.88	1.58	9.8
Cerebellum 1 mg/kg BW (Crbm 4.4)	534.3	2.09	2.31	1.49	9.6
Pooled samples					
Cerebellum Control	278.7	2.07	2.22	1.35	-
Cerebellum 0.1 mg/kg BW Treatment	309.5	2.08	2.25	1.43	9.4
Cerebellum 0.5 mg/kg BW Treatment	300.8	2.08	2.25	1.53	9.8
Cerebellum 1 mg/kg BW Treatment	401.1	2.08	2.14	1.52	9.6

Table 30: Quality check of RNA samples from the hippocampus tissues obtained from the *in vivo* dose-response experiments (Chapter 6). Parameters shown are RNA concentration (ng/μl), and ratios [260/280] and [260/230] indicating RNA purity, in addition to ratio [28S/18S] and RQI indicating RNA integrity. The bottom part of the table shows the pooled samples. 'Hppc X.Y' abbreviation refers to hippocampus sample number Y from group X (group 1 is the control group which had daily i.p. injections of dH_2O; and 2, 3 and 4 treatment groups which had 0.1, 0.5 and 1 mg/kg B.W $CoCl_2$ daily i.p. injections for 28 days respectively). There are n = 4 samples per each control or treatment group, each group was later pooled into a single sample for RNA-Seq evaluation. Some of the samples could not be obtained and less samples than n=4 were pooled.

Quality check of RNA samples from the hippocampus					
Samples	**RNA concentration (ng/μl)**	**Ratio [260/280]**	**Ratio [260/230]**	**Ratio [28S/18S]**	**RQI**
Hippocampus Control (Hppc 1.1)	184.4	2.1	2.18	1.41	9.6
Hippocampus Control (Hppc 1.2)	158.6	2.08	1.56	1.50	9.4
Hippocampus Control (Hppc 1.3)	372.6	2.08	2.28	1.13	9.3
Hippocampus Control (Hppc 1.4)	154.1	2.04	2.18	1.22	9.5
Hippocampus 0.1 mg/kg BW (Hppc 2.1)	109.2	2.05	2.15	1.24	9.3
Hippocampus 0.2 mg/kg BW (Hppc 2.2)	89.3	2.03	1.95	1.21	8.2
Hippocampus 0.2 mg/kg BW (Hppc 2.3)	-	-	-	-	-
Hippocampus 0.2 mg/kg BW (Hppc 2.4)	207.7	2.07	1.98	1.51	9.6
Hippocampus 0.5 mg/kg BW (Hppc 3.1)	-	-	-	-	-
Hippocampus 0.5 mg/kg BW (Hppc 3.2)	141.9	1.97	1.87	1.56	9.8

Hippocampus 0.5 mg/kg BW (Hppc 3.3)	174.2	2.07	2.27	1.61	9.7
Hippocampus 0.5 mg/kg BW (Hppc 3.4)	227.9	2.07	2.31	1.27	8.9
Hippocampus 1 mg/kg BW (Hppc 4.1)	-	-	-	-	-
Hippocampus 1 mg/kg BW (Hppc 4.2)	286.5	2.08	2.20	1.44	9.2
Hippocampus 1mg/kg BW (Hppc 4.3)	-	-	-	-	-
Hippocampus 1 mg/kg BW (Hppc 4.4)	-	-	-	-	-
Pooled samples					
Hippocampus Control	185.0	2.06	1.97	1.30	9.6
Hippocampus 0.1 mg/kg BW Treatment	115.3	2.04	1.99	1.31	9.7
Hippocampus 0.5 mg/kg BW Treatment	153.0	2.05	2.24	1.36	9.6
Hippocampus 1 mg/kg BW Treatment	260.0	2.06	2.20	1.43	9.4

Appendix B: Selection of reference genes for the normalisation of target gene expression through RT-qPCR

The selection of appropriate reference genes is vital in order to calculate relative gene expression accurately (Bustin et al., 2009). For the selection, we measured the Ct values of all the reference genes from all the control and treatment samples and used RefFinder software to determine the most stable gene for RT-qPCR calculations (https://www.heartcure.com.au/reffinder/). RefFinder is a robust software tool that compares the variability of Ct results from reference genes within certain experimental conditions and ranks them from more to less stable (Xie et al., 2012). The candidate reference genes for normalisation of gene expression data were *Ywhaz*, *Pes* and *Tbp*. Fig. 52 and Fig. 53 present the RefFinder ranking of most stable genes for the time-response experiment in the pref. cortex and the cerebellum respectively, the results of which were presented in Chapter 5. *Ywhaz* was selected as the most stable reference gene for the pref. cortex, while *Tbp* was preferred for the cerebellum. RefFinder results corresponding to the dose-response experiment presented in Chapter 6 were also calculated. Fig. 54 shows the RefFinder ranking results for the pref. cortex tissue from the dose-response experiment while Fig. 55 shows the results for the hippocampus. *Pes1* gene was selected for the pref. cortex and *Ywhaz* for the hippocampus.

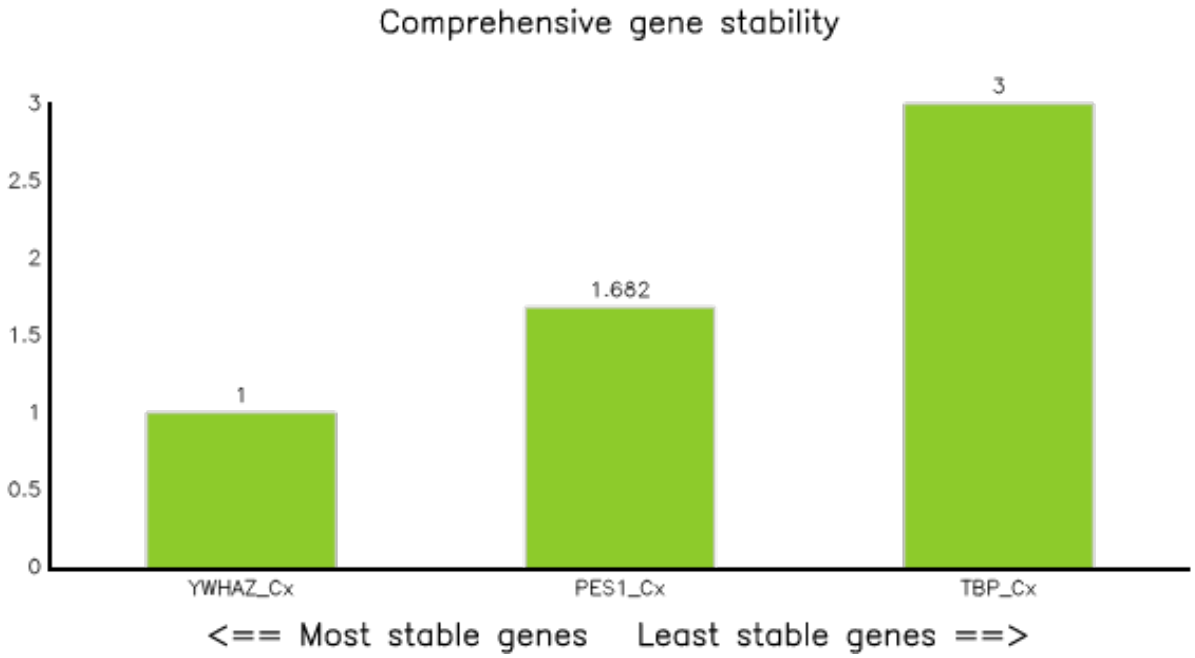

Fig. 52: RefFinder ranking of three reference genes Ct values in pref. cortex samples from the *in vivo* time-response experiment. Only the samples from the rats dosed with i.p. injections for 28 days with dH_20 (controls) and 1mg/kg B.W. $CoCl_2$ (treatment group) were analysed. The candidate reference genes were *Ywhaz*, *Pes1* and *Tbp*. The most stable and gene selected for further RT-qPCR assays in the pref. cortex samples of the time-response experiment is *Ywhaz* (Chapter 5).

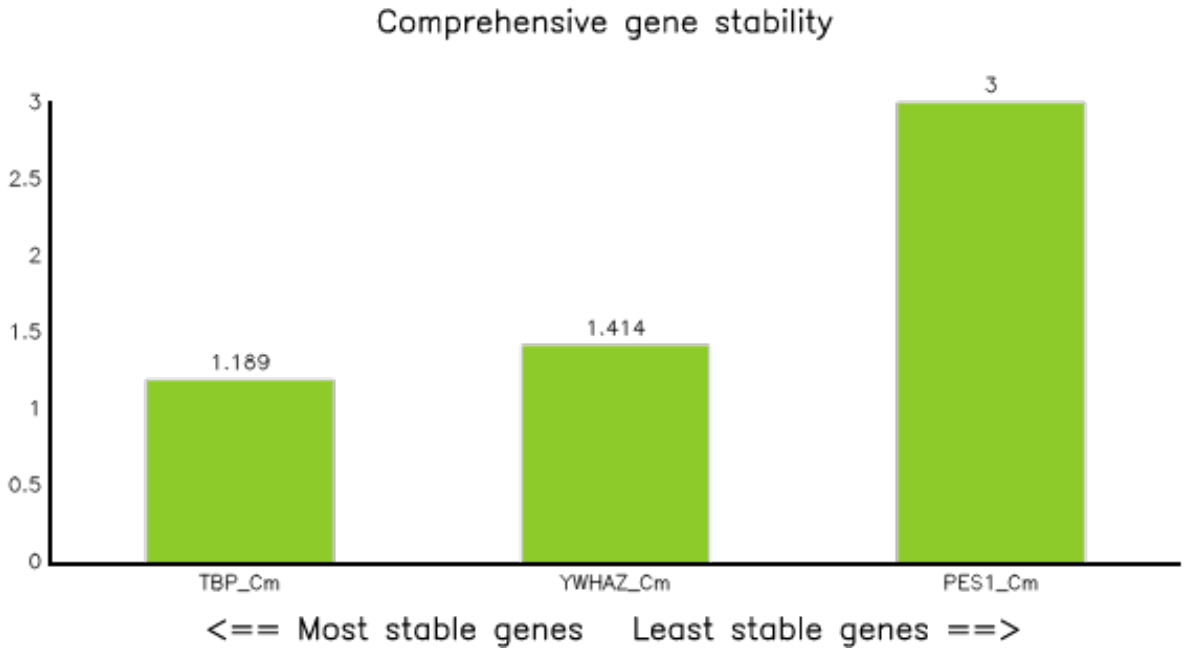

Fig. 53: RefFinder ranking of three reference genes Ct values in cerebellum samples from the *in vivo* time-response experiment. Only the samples from the rats dosed with i.p. injections for 28 days with dH_20 (controls) and 1mg/kg B.W. $CoCl_2$ (treatment group) were analysed. The candidate reference genes were *Ywhaz*, *Pes1* and *Tbp*. The most stable and gene selected for further RT-qPCR assays in the cerebellum samples of the time-response experiment is *Tbp* (Chapter 5).

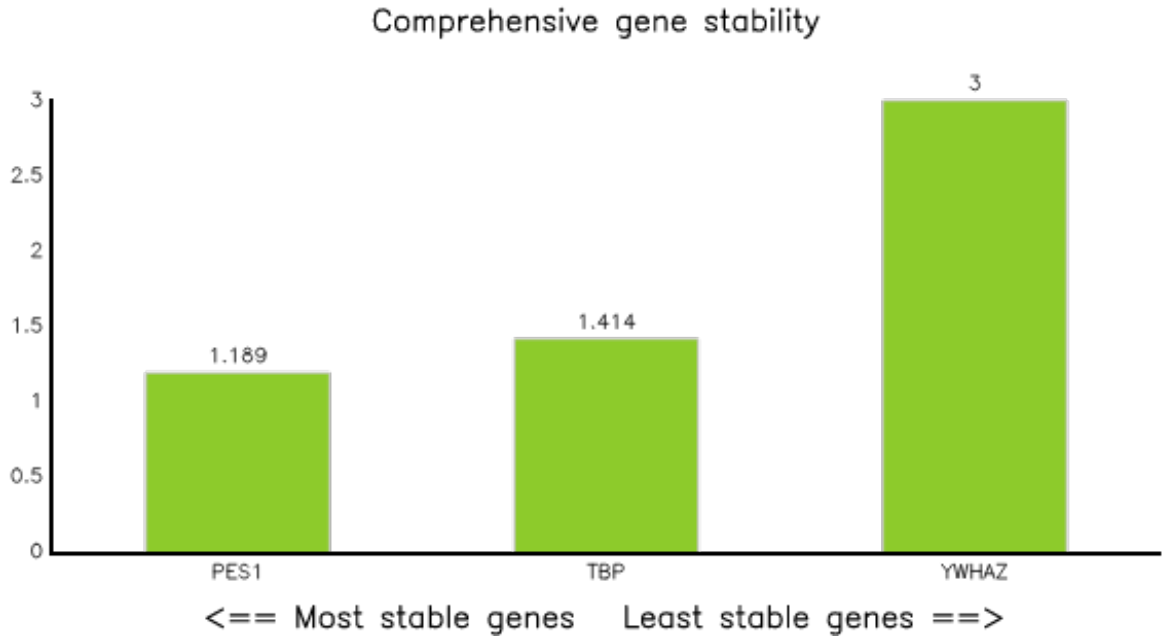

Fig. 54: RefFinder ranking of three reference genes Ct values in pref. cortex samples from the *in vivo* dose-response experiment. Only the samples from the rats dosed with i.p. injections for 28 days with dH_20 (controls) and 1mg/kg B.W. $CoCl_2$ (treatment group) were analysed. The candidate reference genes were *Ywhaz*, *Pes1* and *Tbp*. The most stable and gene selected for further RT-qPCR assays in the pref. cortex samples of the time-response experiment is *Pes1* (Chapter 6).

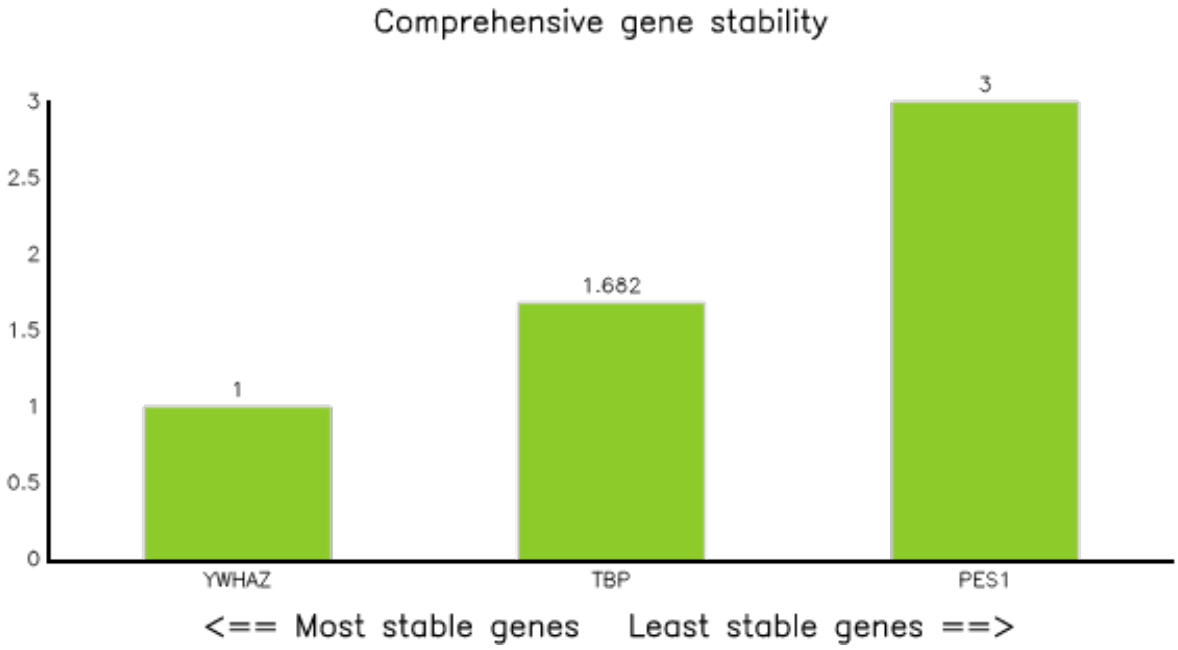

Fig. 55: RefFinder ranking of three reference genes Ct values in hippocampus samples from the *in vivo* dose-response experiment. Only the samples from the rats dosed with i.p. injections for 28 days with dH_20 (controls) and 1mg/kg B.W. $CoCl_2$ (treatment group) were analysed. The candidate reference genes were *Ywhaz*, *Pes1* and *Tbp*. The most stable and gene selected for further RT-qPCR assays in the hippocampus samples of the time-response experiment is *Ywhaz* (Chapter 6).

Appendix C: MIQE checklist

Table 31: MIQE checklist from the MIQE guidelines (Bustin et al., 2009) for reproducibility and assessment of experimental RT-qPCR conditions. Essential information must be made available in the manuscript (E) while desirable information (D) is only made available if possible. Unless indicated otherwise, the protocol details required in the checklist have been presented in Chapter 3, where we described the materials and methods for the *in vivo* work.

Item to check		Checklist
Experimental Design		
Definition of experimental and control groups	E	Yes
Number within each group	E	Yes
Assay carried out by the core or investigator's laboratory?	D	Yes
Acknowledgement of authors' contributions	D	-
Sample		
Description	E	Yes
Volume/mass of sample processed	D	Yes
Microdissection or macrodissection	E	Yes
Processing procedure	E	Yes
If frozen, how and how quickly?	E	Dissected samples were immediately submerged in RNALater and incubated at 4^{o}C overnight. The day after, RNALater was removed and samples were frozen at -80^{o}C
If fixed, with what, how quickly?	E	Not applicable
Sample storage conditions and duration especially for formalin-fixed, paraffin-embedded (FFPE) samples	E	Yes
Nucleic Acid Extraction		
Procedure and/or instrumentation	E	Yes
Name of kit and details of any modifications	E	Yes

Source of additional reagents used	D	Yes
Details of DNase or RNAse treatment	E	Not needed due to the presence of gDNA Eliminator Solution in the isolation kit (RNeasy Plus Universal Midi Kit (Qiagen, UK))
Contamination assessment (DNA or RNA)	E	No-reverse transcription (RT-) and no-template controls (NTC) were included
Nucleic acid quantification	E	Yes, through Nanodrop-2000c spectrophotometer
Instrument and method	E	Yes
Purity (A260/A280)	D	Yes (provided in Appendix A)
Yield	D	Yes (provided in Appendix A)
RNA integrity method/instrument	E	Yes, via Experion Automated Electrophoresis System
RNA integrity number/RNA quality indicator (RIN/RQI) or Cq of 3' and 5' transcripts	E	Yes (provided in Appendix A)
Electrophoresis traces	D	No
Inhibition testing (Cq dilutions, spike or other)	E	No, we used new reagents and the company's recommended concentrations
Reverse Transcription		
Complete reaction conditions	E	Yes
Amount of RNA and reaction volume	E	Yes
Priming oligonucleotide if using gene-specific priming (GSP) and concentration	E	Yes
Reverse transcriptase and concentration	E	Yes
Temperature and time	E	Yes
Manufacturer of reagents and catalogue numbers	D	Manufacturer is provided, but not the catalogue numbers.
Cqs with and without reverse transcription	D	Yes
Storage conditions of cDNA	D	Synthesised cDNA was kept at -20°C
qPCR Target Information		
Gene symbol	E	Yes
Sequence accession number	E	Yes
Location of amplicon	D	Yes
Amplicon length	E	Yes
In silico specificity screen (BLAST, and so on)	E	Yes
Pseudogenes, retropseudogenes or other homologs?	D	Primers retrieving pseudogenes from the target gene were used when there were no more options

Sequence alignment	D	No
Secondary structure analysis of amplicon	D	No
Location of each primer by exon or intron (if applicable)	E	No
What splice variants are targeted?	E	No
qPCR Oligonucleotides		
Primer sequences	E	Yes
RTPrimerDB Identification Number	D	No
Probe sequences	D	No
Location and identity of any modifications	E	Not applicable
Manufacturer of oligonucleotides	D	Yes, Integrated DNA Technologies (IDT, Belgium)
Purification method	D	No
qPCR Protocol		
Complete reaction conditions	E	Yes
Reaction volume and amount of cDNA/DNA	E	Yes
Primer, (probe), Mg++ and deoxynucleoside triphosphate (dNTP) concentrations	E	Yes
Polymerase identity and concentration	E	Yes
Buffer/kit identity and manufacturer	E	Yes
Exact chemical constitution of the buffer	D	No (not provided by manufacturer)
Additives (SYBR Green I, DMSO, and so forth)	E	No
Manufacturer of plates/tubes and catalog number	D	Yes
Complete thermocycling parameters	E	Yes
Reaction setup (manual/robotic)	D	Manual setup
Manufacturer of qPCR instrument	E	Yes
qPCR Validation		
Evidence of optimisation (from gradients)	D	No
Specificity (gel, sequence, melt, or digest)	E	Yes, melt curve

For SYBR Green I, Cq of the NTC	E	Yes
Calibration/Standard curves with slope and y intercept	E	No
PCR efficiency calculated from slope	E	PCR efficiencies were calculated but not applied due to the limited range of the standard curve for some primers meaning that the Cts from the most diluted samples of the 5-fold serial dilution (Ct>26) were close to the reliable limit of quantification (Ct~40) in the case of low copy number genes.
Confidence interval (CI) for PCR efficiency or standard error (SE)	D	No
r2 of standard curve	E	No
Linear dynamic range	E	No
Cq variation at lower limit	E	No
Confidence intervals throughout range	D	No
Evidence for limit of detection (LOD)	E	No
If multiplex, efficiency and LOD of each assay.	E	Not applicable
Data Analysis		
qPCR analysis program (source, version)	E	Yes
Cq method determination	E	Yes
Outlier identification and disposition	E	No data points were excluded as outliers
Results of NTCs	E	Cts of non-template controls were labelled as 'Undetermined' by the software meaning that they were below the detection limit.
Justification of number and choice of reference genes	E	Yes (provided in Appendix B)
Description of normalisation method	E	Yes
Number and concordance of biological replicates	D	Yes
Number and stage (RT or qPCR) of technical replicates	E	Yes
Repeatability (intra-assay variation)	E	Yes
Reproducibility (inter-assay variation, %CV)	D	No
Power analysis	D	Not applicable
Statistical methods for result significance	E	Yes

Software (source, version)	E	Yes
Cq or raw data submission using RDML	D	No

Appendix D: Pathway mapping of genes obtained with PathView software

We mapped the DEGs from the pref. cortex and hippocampus in response to cobalt treatment with 0.5 and 1 mg/kg B.W. $CoCl_2$ compared to control animals (dH_2O) to biological pathways with PathView software (https://pathview.uncc.edu/) (Habermann et al., 2015). The software identified two significantly enriched pathways "rno00140 Steroid hormone biosynthesis" (q-value = 0.01) and "rno04640 Hematopoietic cell lineage" (q-value = 0.046). Fig. 56 shows the steroid hormone biosynthesis pathway, and Fig. 57 displays the KEGG pathway with the haematopoietic cell lineage pathway. The red numbered squares represent mapped genes. The names of these genes have been indicated in the captions.

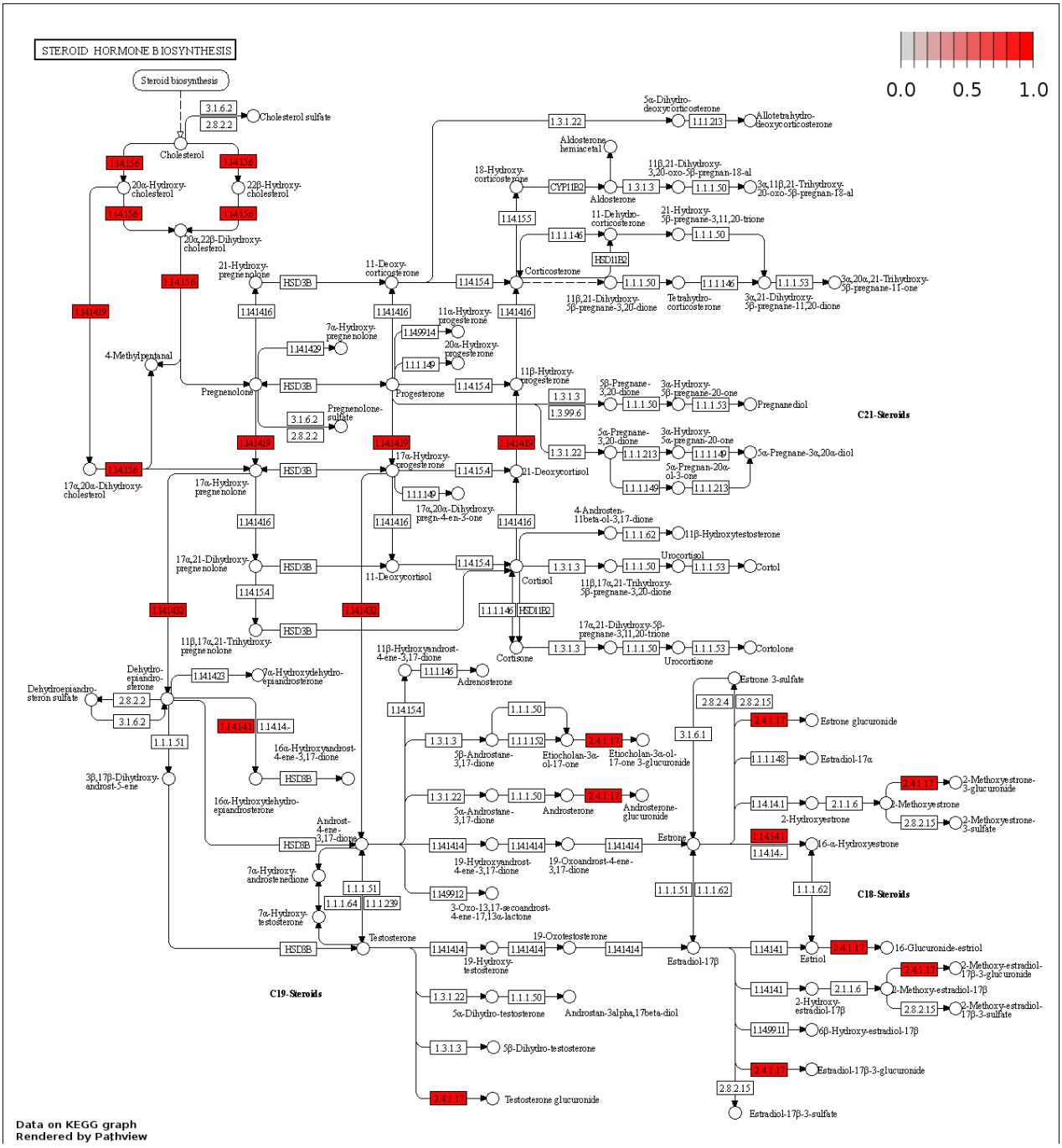

Fig. 56: Mapped 'rno00140 Steroid hormone biosynthesis' pathway with common DEGs from the pref. cortex and hippocampus in response to cobalt treatment with 0.5 and 1 mg/kg B.W. $CoCl_2$ compared to the control samples from rats treated with dH_2O. Rats were dosed for 28 days with i.p. injections and brain tissues were obtained for posterior RNA isolation and RNA-Seq analysis. The red squares represent genes present on the data with the following numeration: 1.14.14.32 and 1.14.14.19 is *Cyp17a*, 1.14.15.6 is *Cyp11a1*, 1.14.14.1 is *Cyp3a23/3a1*, and 2.4.1.17 represents *Ugt1a1*.

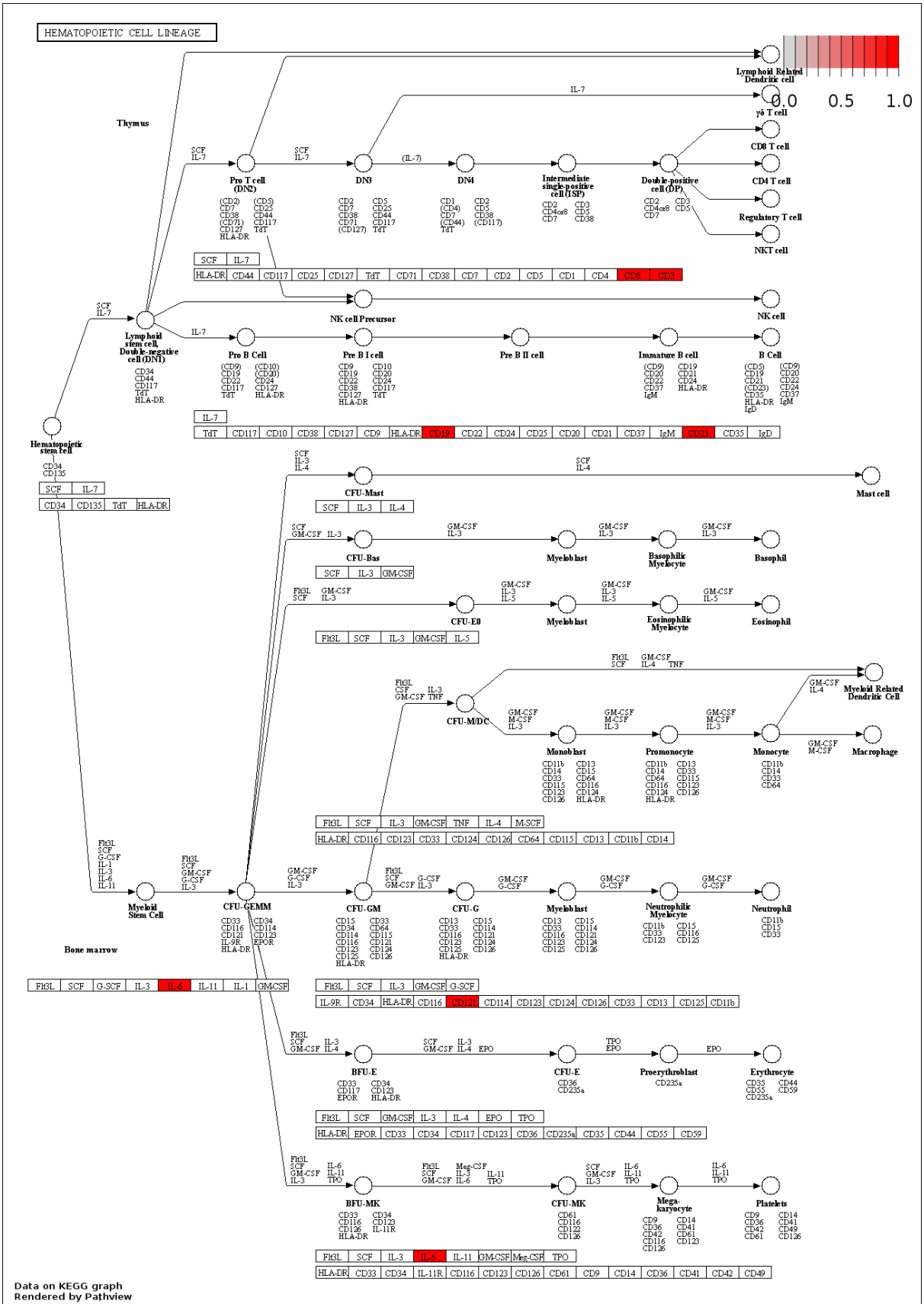

Fig. 57: Mapped 'rno04640 Hematopoietic cell lineage' pathway with common DEGs from the pref. cortex and hippocampus in response to cobalt treatment with 0.5 and 1 mg/kg B.W. $CoCl_2$ compared to the control samples from rats

treated with dH_2O. Rats were dosed for 28 days with i.p. injections and brain tissues were obtained for posterior RNA isolation and RNA-Seq analysis. The genes in red squares are differentially expressed in the RNA-Seq data: *Cd8a* corresponding to Cd8, *Cd3g* corresponding to Cd3, *Cd19*, *Fcer2* corresponding to Cd23, *Il1r2* corresponding to Cd121, and *Il6*.

Appendix E: Comparison of number of DEGs with different cutoff values

We obtained the number of DEGs from the dose-response *in vivo* treatment (Chapter 6) according to the different fold change and p-value cutoffs. Animals were dosed for 28 days with i.p. injections of $CoCl_2$ at three different concentrations: 0.1, 0.5 and 1mg/kg B.W. The control group was treated equally with only dH_2O. The RNA isolated from the brain samples was pooled in a single sample per group to be analysed through RNA-Seq (n'=1). Fold change over 2 is an arbitrary cutoff value widely used in RNA-Seq and microarray analyses (Maleki et al., 2020; Zhao et al., 2018). The number of DEGs resulting from the conditions |fold change|> 2 and p <0.05 is presented in Fig. 58 , while the number of DEGs after applying a |fold change|> 2 cutoff is displayed Fig. 59. The number of DEGs resulting from applying |fold change|> 2 and p <0.05 conditions is lower (range: 51-151) than when only applying a |fold change|> 2 cutoff (range: 703-823), thus the former condition is more stringent.

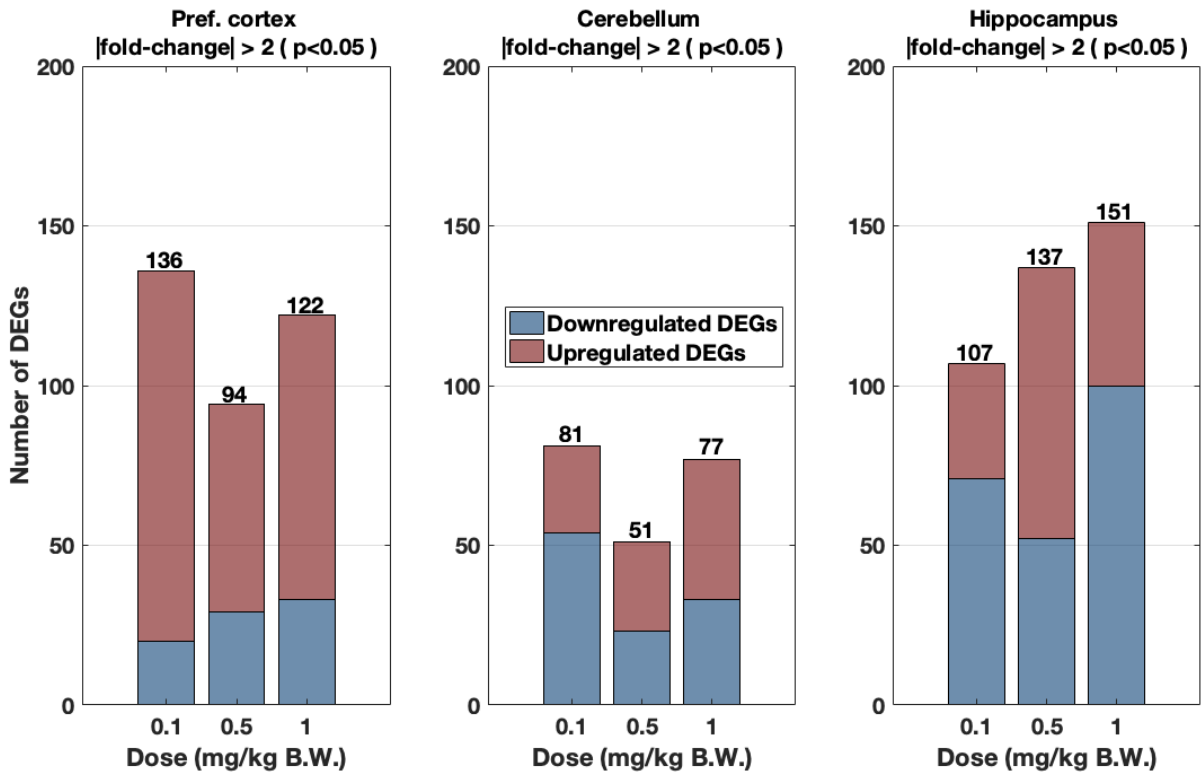

Fig. 58: Number of up-regulated (red) and down-regulated (blue) DEGs (cutoff |fold change|>2 and p<0.05) in pref. cortex, cerebellum and hippocampus according to cobalt dose treatment: 0.1, 0.5 and 1 mg/kg B.W. $CoCl_2$. Animals were dosed i.p. daily, for 28 days with those doses or dH_2O. Data were extracted from RNA-Seq experiments in which n=4 samples were pooled to get n'=1, except in the case of the hippocampus treatment group 0.5 mg/kg B.W. $CoCl_2$ where n'=n=3, as well as for 1 mg/kg B.W. $CoCl_2$ where n'=n=1.

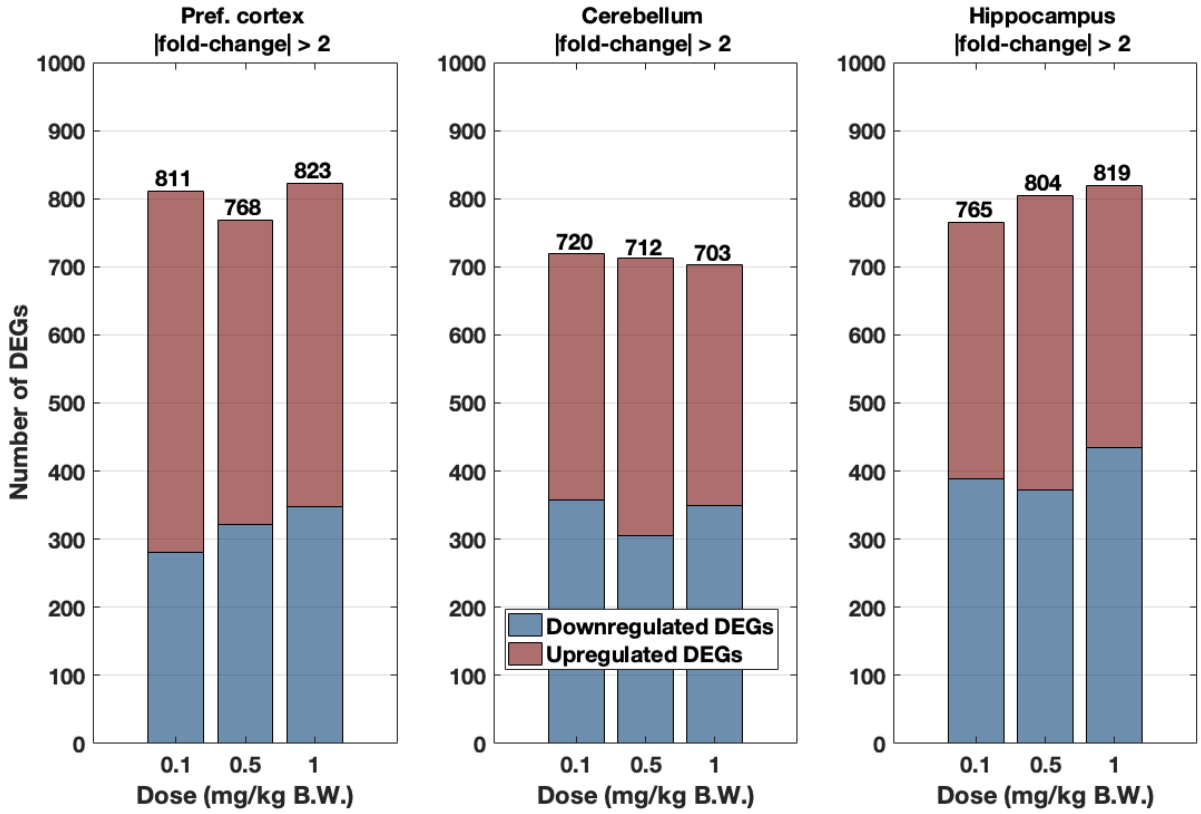

Fig. 59: Number of up-regulated (red) and down-regulated (blue) DEGs (cutoff |fold change|>2 only) in pref. cortex, cerebellum and hippocampus according to cobalt dose treatment: 0.1, 0.5 and 1 mg/kg B.W. $CoCl_2$. Animals were dosed i.p. daily, for 28 days with those doses or dH_2O. Data were extracted from RNA-Seq experiments in which n=4 samples were pooled to get n'=1, except in the case of the hippocampus treatment group 0.5 mg/kg B.W. $CoCl_2$ where n'=n=3, as well as for 1 mg/kg B.W. $CoCl_2$ where n'=n=1.